

# UC Merced

## UC Merced Electronic Theses and Dissertations

### Title

Applications of Uncertainty Quantification to Coagulation Biology

### Permalink

<https://escholarship.org/uc/item/0cf8q8ph>

### Author

Stobb, Michael T.

### Publication Date

2019

Peer reviewed|Thesis/dissertation



UNIVERSITY OF CALIFORNIA, MERCED

DISSERTATION

**Applications of Uncertainty  
Quantification to Coagulation  
Biology**

by

Michael T. Stobb

A technical report submitted  
in partial fulfillment of the requirements for the degree of

Doctor of Philosophy in Applied Mathematics

2019

Committee Members:

Professor Karin Leiderman, Co-Chair

Professor Suzanne Sindi, Co-Chair

Professor Harish Bhat

Professor Noemi Petra

Chapter 2 ©2019 Elsevier  
Chapter 3 ©2018 PloS  
All other Chapters ©2019 Michael T. Stobb  
All rights reserved

UNIVERSITY OF CALIFORNIA, MERCED  
Graduate Division

This is to certify that I have examined a copy of a technical report by

Michael T. Stobb

and found it satisfactory in all respects, and that any and all revisions  
required by the examining committee have been made.

Committee Chairs:

---

Professor Karin Leiderman

---

Professor Suzanne S. Sindi

Committee Member:

---

Professor Harish S. Bhat

Committee Member:

---

Professor Noemi Petra

---

Date

## Acknowledgments

I would like to acknowledge my full committee, Professors Karin Leiderman, Suzanne Sindi, Harish Bhat, and Noemi Petra, for their help and support in the dissertation writing process. Thanks to DESCARTES, the NSF, and the US Army for funding me during my years of research: DMS-1331109, R01HL120728, and ARO-12369656.

My name may be the only one listed on the degree, but there were countless people who poured into me that made it possible. First among them are my research advisors, without whom this work would never have happened. Professor Leiderman has pushed, pulled, and prodded me into becoming a better writer, mathematician, and scientist; for this guidance I am extremely grateful. Her unwavering diligence to see me succeed has frequently been the motivation I needed to try one more time. Likewise, Professor Sindi has been a source of constant support over the many years. Her seemingly bottomless supply of optimism is something I came to count upon, especially when it all felt for naught.

The Applied Math Department at UC Merced has become my second family, and I am deeply indebted to the many individuals within it that were willing to spend the shocking amounts of time necessary - in coffee hours, “mid-semester receptions”, and general discussion - in our pursuit of truth. In the end, I believe we did determine what *is* and *is not* a sandwich.

A deep thanks to my fellow graduate students: Mario Banuelos, Jason and Julia Dark, Omar DeGuchy, and many more. You have been great friends and colleagues. Our fun conversations over the years have been a refuge from the worst of the work and the first place for me to rejoice in success.

Finally, I must thank my wife, Megan. She encouraged me to seek higher education, believed I could do it, and loved me throughout, even when it became difficult. Truly *I* am the lucky one.

# Contents

|                                                                                                   |           |
|---------------------------------------------------------------------------------------------------|-----------|
| Signature Page . . . . .                                                                          | iii       |
| Acknowledgments . . . . .                                                                         | iv        |
| Abstract . . . . .                                                                                | viii      |
| List of Figures . . . . .                                                                         | ix        |
| List of Tables . . . . .                                                                          | xvii      |
| <b>1 Introduction</b>                                                                             | <b>1</b>  |
| 1.1 Background on Uncertainty Quantification . . . . .                                            | 2         |
| Classification of Uncertainty . . . . .                                                           | 2         |
| 1.1.1 Forward UQ . . . . .                                                                        | 3         |
| Monte-Carlo Approach . . . . .                                                                    | 3         |
| Surrogate Models . . . . .                                                                        | 4         |
| 1.1.2 Parameter Estimation . . . . .                                                              | 4         |
| Maximum Likelihood Methods . . . . .                                                              | 5         |
| Bayesian . . . . .                                                                                | 5         |
| 1.1.3 Sensitivity Analysis . . . . .                                                              | 8         |
| Local Sensitivity Analysis . . . . .                                                              | 8         |
| Global Sensitivity Analysis . . . . .                                                             | 9         |
| 1.2 Applications . . . . .                                                                        | 11        |
| 1.2.1 Blood Coagulation . . . . .                                                                 | 12        |
| Static Vs Flow-Mediated Coagulation . . . . .                                                     | 12        |
| Mathematical Models of Coagulation . . . . .                                                      | 13        |
| Coagulopathies . . . . .                                                                          | 13        |
| 1.2.2 Static Clotting Assays: Chromogenic Substrates . . . . .                                    | 15        |
| Bibliography . . . . .                                                                            | 17        |
| <b>2 Assessing the Significance of Product Inhibition In Chromogenic Assays (Journal Article)</b> | <b>24</b> |
| 2.1 Abstract . . . . .                                                                            | 24        |
| 2.2 Introduction . . . . .                                                                        | 25        |
| 2.3 Materials and Methods . . . . .                                                               | 27        |
| 2.3.1 Experimental Procedures . . . . .                                                           | 27        |
| Standard chromogenic assay . . . . .                                                              | 27        |
| Antithrombin inhibition assay . . . . .                                                           | 27        |
| 2.3.2 Conversion of Absorbance to Concentration . . . . .                                         | 28        |
| 2.3.3 Kinetic Schemes . . . . .                                                                   | 28        |
| Naive Model . . . . .                                                                             | 28        |

|          |                                                                                                                                                  |           |
|----------|--------------------------------------------------------------------------------------------------------------------------------------------------|-----------|
|          | The Null Model: Incorporating Uncertainty . . . . .                                                                                              | 29        |
|          | The Alternative Model: Incorporating Product Inhibition . . . . .                                                                                | 30        |
| 2.3.4    | Uncertainty Propagation . . . . .                                                                                                                | 31        |
| 2.3.5    | MCMC Estimation of Parameters . . . . .                                                                                                          | 31        |
|          | Prior Distributions for Uncertain Parameters . . . . .                                                                                           | 32        |
|          | Sampling the Posterior Distributions . . . . .                                                                                                   | 33        |
|          | Model Selection . . . . .                                                                                                                        | 33        |
| 2.4      | Results and Discussion . . . . .                                                                                                                 | 33        |
| 2.4.1    | Naive Model Does Not Quantitatively Agree with CS Assay . . . . .                                                                                | 33        |
| 2.4.2    | Null Model: Introducing Uncertainty . . . . .                                                                                                    | 34        |
| 2.4.3    | Alternative Model: Including Product Inhibition . . . . .                                                                                        | 37        |
| 2.4.4    | Alternative Model with Production Inhibition is Experimentally Val-<br>idated . . . . .                                                          | 38        |
| 2.4.5    | Further Impact of Product Inhibition: A Theoretical Investigation . . . . .                                                                      | 38        |
| 2.5      | Conclusion . . . . .                                                                                                                             | 41        |
|          | Bibliography . . . . .                                                                                                                           | 44        |
| <b>3</b> | <b>A local and global sensitivity analysis of a mathematical model of coagu-<br/>lation and platelet deposition under flow (Journal Article)</b> | <b>48</b> |
| 3.1      | Abstract . . . . .                                                                                                                               | 48        |
| 3.2      | Introduction . . . . .                                                                                                                           | 49        |
|          | 3.2.1 Mathematical model of coagulation under flow . . . . .                                                                                     | 51        |
|          | 3.2.2 Uncertainty and sensitivity analyses . . . . .                                                                                             | 54        |
| 3.3      | Materials and methods . . . . .                                                                                                                  | 57        |
|          | 3.3.1 Local Sensitivity Analysis . . . . .                                                                                                       | 58        |
|          | 3.3.2 Morris Method . . . . .                                                                                                                    | 59        |
|          | 3.3.3 Global Sensitivity Analysis . . . . .                                                                                                      | 61        |
|          | 3.3.4 Robustness to Shear Rate . . . . .                                                                                                         | 62        |
| 3.4      | Results . . . . .                                                                                                                                | 63        |
|          | 3.4.1 Varying Plasma Levels . . . . .                                                                                                            | 63        |
|          | 3.4.2 Varying Kinetic Rate Constants . . . . .                                                                                                   | 65        |
|          | Local Sensitivity Analysis . . . . .                                                                                                             | 65        |
|          | Method of Morris . . . . .                                                                                                                       | 66        |
|          | Global Sensitivity Analysis . . . . .                                                                                                            | 66        |
|          | 3.4.3 Varying Platelet Characteristics . . . . .                                                                                                 | 67        |
|          | 3.4.4 Varying All Model Parameters . . . . .                                                                                                     | 68        |
|          | Conditional Input Distributions for Fast/Slow Thrombin Production . . . . .                                                                      | 70        |
|          | 3.4.5 Varying Flow . . . . .                                                                                                                     | 72        |
| 3.5      | Discussion . . . . .                                                                                                                             | 73        |
|          | 3.5.1 Plasma levels . . . . .                                                                                                                    | 73        |
|          | 3.5.2 Platelet characteristics . . . . .                                                                                                         | 73        |
|          | 3.5.3 Kinetic rate constants . . . . .                                                                                                           | 74        |
|          | 3.5.4 Varying all parameter classes . . . . .                                                                                                    | 74        |
|          | 3.5.5 Flow . . . . .                                                                                                                             | 75        |
|          | 3.5.6 Limitations of our methodology . . . . .                                                                                                   | 75        |
|          | 3.5.7 Local versus global analysis: what have we learned? . . . . .                                                                              | 76        |

|                                                                                                                                  |            |
|----------------------------------------------------------------------------------------------------------------------------------|------------|
| Bibliography . . . . .                                                                                                           | 88         |
| 3.6 Supplement . . . . .                                                                                                         | 93         |
| <b>4 A mathematical model of coagulation under flow identifies factor V as a modifier of thrombin generation in hemophilia A</b> | <b>116</b> |
| 4.1 Abstract . . . . .                                                                                                           | 116        |
| 4.2 Introduction . . . . .                                                                                                       | 117        |
| 4.2.1 Brief overview of clotting . . . . .                                                                                       | 118        |
| 4.2.2 Tissue factor density distributions for normal and FVIII-deficient plasma . . . . .                                        | 120        |
| 4.2.3 GSA identifies FV as a modifier of thrombin generation in hemophilia A . . . . .                                           | 120        |
| 4.2.4 Exploration of Mechanism: The competition for FXa . . . . .                                                                | 121        |
| 4.2.5 Partial inhibition of FV enhances fibrin deposition in FVIII-deficient blood under flow . . . . .                          | 123        |
| 4.2.6 Low FV and partial inhibition of FV enhances thrombin generation in FVIII-inhibited or FVIII-deficient plasma . . . . .    | 125        |
| 4.3 Discussion . . . . .                                                                                                         | 125        |
| Bibliography . . . . .                                                                                                           | 128        |
| 4.4 Supplement . . . . .                                                                                                         | 132        |
| 4.4.1 Mathematical Model Description . . . . .                                                                                   | 132        |
| 4.4.2 Global Sensitivity Analysis . . . . .                                                                                      | 134        |
| 4.4.3 Variations in Kinetic Rate Constants . . . . .                                                                             | 134        |
| 4.4.4 Affect of APC & Thrombin-mediate FV/FVIII Activation . . . . .                                                             | 134        |
| 4.4.5 Race to Tenase Formation . . . . .                                                                                         | 135        |
| 4.4.6 Materials . . . . .                                                                                                        | 135        |
| 4.4.7 Tissue factor vesicles . . . . .                                                                                           | 136        |
| 4.4.8 Subject recruitment and blood collection . . . . .                                                                         | 136        |
| 4.4.9 Subject clinical categorization . . . . .                                                                                  | 136        |
| 4.4.10 Whole blood flow assays . . . . .                                                                                         | 136        |
| 4.4.11 Determination of TF surface concentration . . . . .                                                                       | 137        |
| 4.4.12 Image Acquisition and Analysis . . . . .                                                                                  | 137        |
| 4.4.13 Calibrated automated thrombography . . . . .                                                                              | 138        |
| 4.4.14 Statistical analysis . . . . .                                                                                            | 138        |
| Bibliography . . . . .                                                                                                           | 150        |
| <b>5 Conclusions &amp; Future Work</b>                                                                                           | <b>151</b> |
| 5.1 Conclusions . . . . .                                                                                                        | 151        |
| 5.2 Full Progress Curves of Chromogenic Substrates Provide Evidence for Two Step Inactivation of FXa by AT . . . . .             | 152        |
| 5.2.1 Kinetic Schemes . . . . .                                                                                                  | 152        |
| One-Step Inactivation . . . . .                                                                                                  | 153        |
| Two-Step Inactivation . . . . .                                                                                                  | 154        |
| Preliminary Results . . . . .                                                                                                    | 155        |
| Ongoing Work . . . . .                                                                                                           | 156        |
| 5.3 Global Sensitivity of Coagulopathies . . . . .                                                                               | 156        |
| Bibliography . . . . .                                                                                                           | 160        |

# Applications of Uncertainty Quantification to Coagulation Biology

by

Michael T. Stobb

Doctorate in Applied Mathematics

Karin Leiderman, Co-Chair

Suzanne Sindi, Co-Chair

University of California, Merced

2019

## Abstract

Blood coagulation is a complex system comprised of numerous biochemical reactions. Due to this complexity, mathematical modeling has been used to increase the overall understanding of the system as a whole, determine previously unknown mechanisms, and to predict system responses. These models, however, may involve uncertainty in both parameter values and kinetic schemes that describe the reactions; this dissertation examines two such ideas. First, we examine the interactions between a specific coagulation factor, FXa, and an experimental tool designed to measure its action, a chromogenic substrate. Second, we examine a more complex mathematical model in regards to its parametric uncertainty. Chapter 1 gives a background on the mathematical tools used in this dissertation and necessary for uncertainty quantification (UQ) and an overview of the two aforementioned systems. In Chapter 2 we demonstrate how an application of UQ identifies a new model for product inhibition between FXa and its chromogenic substrate, which is validated experimentally. In Chapter 3 we conduct an extensive local and global sensitivity analysis for a mathematical model of flow-mediated blood coagulation. We determined that for many cases a local analysis is sufficient to understand the uncertainty in the model's output, but that for certain cases there are classes of parameters that exhibit strong synergistic behavior, and so a global method that is capable of resolving interaction effects is necessary. These results motivated the work in Chapter 4 where we used global sensitivity analysis on a mathematical model to identify a novel mechanism for recovering a normal clotting response in hemophilia A; the potential mechanism was further supported by experimental validation. Chapter 5 summarizes the conclusions from the preceding chapters and presents ongoing work relating to the two projects.

# List of Figures

|     |                                                                                                                                                                                                                                                                                                                                                                                                                                                                                                                                                                                                                                                                                           |    |
|-----|-------------------------------------------------------------------------------------------------------------------------------------------------------------------------------------------------------------------------------------------------------------------------------------------------------------------------------------------------------------------------------------------------------------------------------------------------------------------------------------------------------------------------------------------------------------------------------------------------------------------------------------------------------------------------------------------|----|
| 1.1 | <b>Schematic of Forward UQ or error propagation.</b> Uncertain inputs, represented here as $\theta_i, \theta_j, \theta_k$ with their own distributions, are propagated through a model, from which a quantity of interest (QoI) is computed. Because the inputs are described by distributions, the QoI will necessarily have a distribution as well. . . . .                                                                                                                                                                                                                                                                                                                             | 3  |
| 1.2 | <b>Examples of Burnin and Autocorrelation for an estimated parameter.</b> The first 200,000 steps of the parameters MCMC trajectory (A) show an early convergence to the posterior, with burnin occurring within 50,000 steps. The autocorrelation of the chain (after burnin was removed) in (B) drops below the preset threshold of 0.05, indicating posterior samples are no longer strongly correlated, after approximately 200 lags (skipped samples in the chain). . . . .                                                                                                                                                                                                          | 8  |
| 1.3 | <b>Schematic of elements considered in KFHL model.</b> A) Diagram of clotting reactions, with blue arrows indicating chemical transport, magenta arrows activation processes, green segments binding and unbinding from surface. Boxed proteins indicate surface bound species while unboxed proteins are free floating in the plasma. Black lines show the actions of enzymes (catalysts of chemical reactions), with solid lines the forward direction and dashed the feedback loop. Red circles show inhibitory reactions. B) The KFHL assumes multiple compartments, with the reaction zone in the middle and C) the endothelial zone perpendicular to the flow. Image from [61]. . . | 14 |
| 1.4 | <b>Schematic of Chromogenic Substrate usage in Experiments.</b> Enzymes cleave the chromogenic substrates and gives rise to color within a sample, which is detectable by the absorption of light at the 405 nm wavelength. The absorbance ( $A$ ) in time is converted to concentration ( $C$ ) using Beer's Law, where $\epsilon$ is the molar absorptivity of the substrate and $\ell$ is the path length of the light in the sample. . . . .                                                                                                                                                                                                                                          | 16 |
| 2.1 | <b>Uncertainty Propagation.</b> In our mathematical framework we consider how uncertainties in model inputs (left), such as substrate hydrolysis ( $U_h$ ), pipetting error, and reported kinetic rates ( $K_M$ & $k_{cat}$ ) are propagated into uncertainties in model outputs (right). For simplicity, inputs are monte-carlo sampled from their distributions and the model solved, yielding an approximation of the output distribution. . . . .                                                                                                                                                                                                                                     | 31 |

|     |                                                                                                                                                                                                                                                                                                                                                                                                                                                                                                                                                                                                                                                                                                                                                                                                                                                                                                            |    |
|-----|------------------------------------------------------------------------------------------------------------------------------------------------------------------------------------------------------------------------------------------------------------------------------------------------------------------------------------------------------------------------------------------------------------------------------------------------------------------------------------------------------------------------------------------------------------------------------------------------------------------------------------------------------------------------------------------------------------------------------------------------------------------------------------------------------------------------------------------------------------------------------------------------------------|----|
| 2.2 | <b>Determination of output distribution.</b> Model output (blue histograms) and best fitting normal distribution (red line) at three different times: 30 seconds (A,D), 5 minutes (B,E), and 20 minutes (C,F) generated by sampling (N=100,000) the input parameters of the forward model given in equations (2.5) and (2.6) with the prior distributions from Table 2.1 (A-C) and with Uniform distributions (D-F). . . . .                                                                                                                                                                                                                                                                                                                                                                                                                                                                               | 32 |
| 2.3 | <b>Naive mathematical model based on the Null kinetic scheme compared with experimental data.</b> For each concentration of substrate, the initial rate of substrate cleavage was determined from the plot of product formation as a function of time (black points). Fitting the data to the Michaelis-Menten equation (blue) gave an estimated $K_M = 129 \mu\text{M}$ and $k_{\text{cat}} = 78\text{s}^{-1}$ . B) The absorbance data (grey) and concentration of F output from the mathematical model using the manufacturer supplied kinetic rates of $k^- = 106 \mu\text{M}$ and $k^{\text{cat}} = 140\text{s}^{-1}$ (red) and experimentally measured rates (blue) in units of absorbance (right axis) and concentration (left axis) for experiments with 5 nM of factor Xa using the Null kinetic scheme (2.1), with no uncertainty assumed in the initial conditions or model parameters. . . . . | 34 |
| 2.4 | <b>Prior and Posterior distributions for <math>\alpha</math>, <math>K_M</math>, <math>k_{\text{cat}}</math>, and hydrolysis.</b> Prior (grey) and Posterior (histograms) distributions for $K_M$ , $k_{\text{cat}}$ , and hydrolysis for both the Null (orange) and Alternative (blue) Model. The priors for the kinetic rates were chosen such that a 95% confidence interval about the mean would be within $\pm 10\%$ of the manufacturer reported values. The prior for $\alpha$ and $U_h$ was set as maximum entropy distributions, specifically uniform between 0 and 10, and uniform between 0 and 0.2, respectively. Posterior distributions were computed using a Metropolis-Hastings algorithm with approximately $5.0 \times 10^4$ samples (after burnin and thinning). Black dashed bars show the measured kinetic parameters from initial rate experiments. . . . .                           | 35 |
| 2.5 | <b>MCMC fitted models compared with data.</b> The Null (orange) and Alternative (blue) model results are shown with the experimental data from 2.3 (circles). The models were fit using an MCMC procedure and produce a distribution in time, which was estimated by sampling the input variables according to their posterior distribution. From this a 95% credibility interval (slight shaded regions) was constructed for each point in time. . . . .                                                                                                                                                                                                                                                                                                                                                                                                                                                  | 36 |
| 2.6 | <b>Estimated E:PF concentrations with model comparisons.</b> Initial rates of product formation from the antithrombin inhibition experiments gives an estimate of the concentration of E:PF in the system (black/grey), with and without previously cleaved substrate. The experiment was simulated using both the Null (orange) and Alternative (blue) models. Uncertainty in the experiment arises from differences in replicates, while the uncertainty in the model is due to pipetting error, hydrolysis, and uncertain kinetic rates, all estimated from the data using a likelihood approach. . . . .                                                                                                                                                                                                                                                                                               | 39 |

|     |                                                                                                                                                                                                                                                                                                                                                                                                                                                                                                                                                                                                                                                                                                                                                                 |    |
|-----|-----------------------------------------------------------------------------------------------------------------------------------------------------------------------------------------------------------------------------------------------------------------------------------------------------------------------------------------------------------------------------------------------------------------------------------------------------------------------------------------------------------------------------------------------------------------------------------------------------------------------------------------------------------------------------------------------------------------------------------------------------------------|----|
| 2.7 | <b>Concentrations of reactants in fixed-enzyme assay, generated by numerical simulation.</b> Numerically computed concentrations of enzyme (A), enzyme bound to CS and CS product (B), pNA (C). Results are produced with the Null Model in the absence (green) and presence (orange) of CS, and with the Alternative model (blue). Initial concentrations were 5 nM factor Xa and 400 $\mu$ M CS; kinetic rates were set to the means of the posterior distributions estimated in this study. . . . .                                                                                                                                                                                                                                                          | 41 |
| 2.8 | <b>Concentrations of reactants in enzyme generation assay, generated by numerical simulation.</b> Numerically computed concentrations of enzyme (A), enzyme bound to CS and CS product (B), pNA (C), and enzyme inactivated by antithrombin (D). Results are produced with the Null Model in the absence (green) and presence (orange) of CS, and with the Alternative model (blue). Initial concentrations were 0.2 nM TF:VIIa, 170 nM factor X, 3.2 $\mu$ M antithrombin, and 400 $\mu$ M CS; kinetic rates for TF:VIIa activation of FX were $K_M = 230$ nM, $k_{cat} = 4.6/s$ , and antithrombin inactivation was $1.96 \times 10^3/Ms$ [55], all other kinetic rates were set to the means of the posterior distributions estimated in this study. . . . . | 42 |
| 3.1 | <b>Schematic of (A) coagulation reactions included in our model.</b> Dashed magenta arrows show cellular or chemical activation processes. Blue arrows show chemical transport in the fluid or on a surface. Green segments with two arrowheads depict binding and unbinding from a surface. Rectangular boxes denote surface-bound species. Solid black lines with open arrows show enzyme action in a forward direction, while dashed black lines with open arrows show feedback action of enzymes. Red disks show chemical inhibitors. Schematic of (B) reaction zone and (C) endothelial zone. . . . .                                                                                                                                                      | 52 |
| 3.2 | <b>Schematic of Thrombin Metrics.</b> Three physiologically relevant metrics of Thrombin generation were calculated for sensitivity analysis: 1) lag time ( <i>Red</i> ), 2) maximum relative rate of thrombin generation, measured after 0.1nM of thrombin have been obtained ( <i>Green</i> ), and 3) final concentration, the total concentration of thrombin at 20 minutes ( <i>Blue</i> ). . . . .                                                                                                                                                                                                                                                                                                                                                         | 58 |
| 3.3 | <b>Monotonicity of Change in Thrombin Generation due to Variation in plasma levels.</b> Variation in the three physiologically relevant metrics of thrombin generation: 1) lag time; 2) maximum relative rate; and 3) final concentration that occur with variations in plasma levels. . . . .                                                                                                                                                                                                                                                                                                                                                                                                                                                                  | 59 |

- 3.4 **Sensitivity of total thrombin generation to plasma levels.** Variation in the **A,D)** lag time; **B,E)** maximum relative rate; **C,F)** final concentration; to zymogen and chemical inhibitor levels using the local (OAT) method (**A-C**) and global Sobol method (**D-F**). *Local:* Sensitivities  $LS_j^i$  that lie between 0.75 and 1 (blue), between 0.25 and 0.75 (magenta), less than 0.25 (cyan) determine the rank-ordered list of initial levels. The percent change of thrombin generation measures from baseline model output for each initial condition are represented by triangles. The direction of variation of the input parameter is indicated with an upwards or downwards facing triangle. *Global:* First and Total Order Sobol indices are plotted as bars with errors of 2 standard deviation about the mean, computed with 5,000 bootstrap samples of the original 110,000 function evaluations. The coefficient of variation is included to provide a scale for the fraction of variance. No total order index was statistically significantly larger than the first order index, indicating that the model output is not significantly effected by interactions between the parameters considered here. . . . . 64
- 3.5 **Variation in thrombin generation as a result of varying plasma levels.** **A)** *Left Axis:* Thrombin concentration time series showing the mean (solid black line) and boundaries that encompass 50% of the data (pink), 90% of the data (orange), and the maximum/minimum of the computed solutions (gray-dashed) generated by uniformly varying initial zymogen plasma levels from 50-150% of normal simultaneously (110,000 total function evaluations). *Right Axis:* Marginal histogram of final thrombin concentration at  $t = 1200$  seconds. **B)** Heatmap and marginal histograms relating three important thrombin generation metrics: lag time (*y-axis*), maximum relative rate (*x-axis*), and final concentration (*color-axis*). Results were obtained by post-processing samples used to compute the global sensitivity indices. Dashed black bar in (A) and (B) represents the baseline case of 275nM of thrombin at 20 minutes. . . . . 77
- 3.6 **Sensitivity of thrombin generation to KRCs.** Variation in the **A,D)** lag time; **B,E)** maximum relative rate; **C,F)** final concentration; to platelet characteristics using the local (OAT) method (**A-C**) and global Sobol method (**D-F**). *Local:* Sensitivities  $LS_j^i$  that lie between 0.75 and 1 (blue), between 0.25 and 0.75 (magenta), less than 0.25 (cyan) determine the rank-ordered list of kinetic rate constants. The percent change of thrombin generation measures from standard model output for each initial condition are represented by triangles. The direction of variation is indicated with an upwards or downwards facing triangle. *Global:* First and Total Order Sobol indices are plotted as bars with errors of 2 standard deviation about the mean, computed with 5,000 bootstrap samples of the original 540,000 function evaluations. The coefficient of variation is included to provide a scale for the fraction of variance. PCs with Total Order index statistically significantly larger than the First order index are indicated with a star. . . . . 78

- 3.7 **Variation in thrombin generation as a result of varying kinetic rate constants.** **A)** *Left Axis:* Thrombin concentration time series showing the mean (solid black line) and boundaries that encompass 50% of the data (pink), 90% of the data (orange), and the maximum/minimum of the computed solutions (gray-dashed) generated by uniformly varying kinetic rates sampled uniformly between 50-150% of their nominal value simultaneously (270,000 total function evaluations). *Right Axis:* Marginal histogram of final thrombin concentration at  $t = 1200$  seconds. **B)** Heatmap and marginal histograms relating three important thrombin generation metrics: lag time ( $y$ -axis), maximum relative rate ( $x$ -axis), and final concentration ( $color$ -axis). Results obtained by post-processing samples used to compute the global sensitivity indices. Dashed black bar in (A) and (B) represents the baseline case of 275nM of thrombin at 20 minutes. . . . . 79
- 3.8 **Sensitivity of thrombin generation to platelet characteristics.** Variation in the **A,D)** lag time; **B,E)** maximum relative rate; **C,F)** final concentration; to platelet characteristics using the local (OAT) method (**A-C**) and global Sobol method (**D-F**). *Local:* Sensitivities  $LS_j^i$  that lie between 0.75 and 1 (blue), between 0.25 and 0.75 (magenta), less than 0.25 (cyan) determine the rank-ordered list of platelet characteristics. The percent change of thrombin generation measures from standard model output for each initial condition are represented by triangles. The direction of variation is indicated with an upwards or downwards facing triangle. *Global:* First and Total Order Sobol indices are plotted as bars with errors of 2 standard deviation about the mean, computed with 5,000 bootstrap samples of the original 170,000 function evaluations. The coefficient of variation is included to provide a scale for the fraction of variance. PCs with Total Order index statistically significantly larger than the First order index are indicated with a star. . . . . 80
- 3.9 **Variation in thrombin generation as a result of varying platelet characteristics.** **A)** *Left Axis:* Thrombin concentration time series showing the mean (solid black line) and boundaries that encompass 50% of the data (pink), 90% of the data (orange), and the maximum/minimum of the computed solutions (gray-dashed) generated by varying platelet characteristics uniformly between 50-150% of their baseline values simultaneously (170,000 total function evaluations). *Right Axis:* Marginal histogram of final thrombin concentration at  $t = 1200$  seconds. **B)** Heatmap and marginal histograms relating three important thrombin generation metrics: lag time ( $y$ -axis), maximum relative rate ( $x$ -axis), and final concentration ( $color$ -axis). Results obtained by post-processing samples used to compute the global sensitivity indices. Dashed black bar in (A) and (B) represents the baseline case of 275nM of thrombin at 20 minutes. . . . . 81

|      |                                                                                                                                    |                                                                                                                                                                                                                                                                                                                                                                                                                                                                                                                                                                                                                                                                                                                                                                                                                                                                                                                                                                                                                                                                                                     |    |
|------|------------------------------------------------------------------------------------------------------------------------------------|-----------------------------------------------------------------------------------------------------------------------------------------------------------------------------------------------------------------------------------------------------------------------------------------------------------------------------------------------------------------------------------------------------------------------------------------------------------------------------------------------------------------------------------------------------------------------------------------------------------------------------------------------------------------------------------------------------------------------------------------------------------------------------------------------------------------------------------------------------------------------------------------------------------------------------------------------------------------------------------------------------------------------------------------------------------------------------------------------------|----|
| 3.10 | <b>Sensitivity of thrombin generation to a subset of all model parameters.</b>                                                     | Variation in the <b>A,D)</b> lag time; <b>B,E)</b> maximum relative rate; <b>C,F)</b> final concentration; to a subset of all model parameters using the local (OAT) method ( <b>A-C</b> ) and global Sobol method ( <b>D-F</b> ). <i>Local</i> : Sensitivities $LS_j^i$ that lie between 0.75 and 1 (blue), between 0.25 and 0.75 (magenta), less than 0.25 (cyan) determine the rank-ordered list of platelet characteristics. The percent change of thrombin generation measures from standard model output for each initial condition are represented by triangles. The direction of variation is indicated with an upwards or downwards facing triangle. <i>Global</i> : First and Total Order Sobol indices are plotted as bars with errors of 2 standard deviation about the mean, computed with 5,000 bootstrap samples of the original 740,000 function evaluations. The coefficient of variation is included to provide a scale for the fraction of variance. PCs with Total Order index statistically significantly larger than the First order index are indicated with a star. . . . . | 82 |
| 3.11 | <b>Variation in thrombin generation as a result of varying a subset of all model parameters.</b>                                   | <b>A)</b> <i>Left Axis</i> : Thrombin concentration time series showing the mean (solid black line) and boundaries that encompass 50% of the data (purple), 90% of the data (orange), and the maximum/minimum of the computed solutions (gray-dashed) generated by uniformly varying a subset of all parameters (found via the Morris method) sampled between 50-150% of their nominal value simultaneously (740,000 total function evaluations). <i>Right Axis</i> : Marginal histogram of final thrombin concentration at $t = 1200$ seconds. <b>B)</b> Heatmap and marginal histograms relating three important thrombin generation metrics: lag time ( <i>y-axis</i> ), maximum relative rate ( <i>x-axis</i> ), and final concentration ( <i>color-axis</i> ). Results obtained by post-processing samples used to compute the global sensitivity indices. Dashed black bar in (A) and (B) represents the baseline case of 275nM of thrombin at 20 minutes. . . . .                                                                                                                            | 83 |
| 3.12 | <b>Conditional input distributions for globally varied subset of all parameters, of thrombin lag time and final concentration.</b> | The subset of parameters were sampled uniformly between 50-150% of their baseline value and the lag time of total thrombin was computed. The input distributions were conditioned on a slow burst: the largest 1% of lag time (A) and a fast burst: the smallest 1% of lag time (B). Distributions were colored dark blue if the empirical skew was greater than 0.5 in magnitude and light blue otherwise. Distributions of lag times for slow bursts (C) and fast bursts (D); skew shown when the mean (dot) and median (square) are not aligned. . . . .                                                                                                                                                                                                                                                                                                                                                                                                                                                                                                                                         | 84 |
| 3.13 | <b>2D Projections of output coagulation metric envelopes for different classes of varying inputs.</b>                              | Three classes of model parameters (plasma levels, a subset of important kinetic rate constants, and platelet characteristics) are varied within normal ranges. The envelope of three important coagulation metrics (lag time, maximum relative rate, and final concentration) are recorded and projected into two dimensions, where <b>A</b> , <b>B</b> , and <b>C</b> are the different orthogonal directions. . . . .                                                                                                                                                                                                                                                                                                                                                                                                                                                                                                                                                                                                                                                                             | 85 |

|      |                                                                                                                                                                                                                                                                                                                                                                                                                                                                                                                                                                                                                                                                                                                                                                                                                                                                                                                                                                                                               |     |
|------|---------------------------------------------------------------------------------------------------------------------------------------------------------------------------------------------------------------------------------------------------------------------------------------------------------------------------------------------------------------------------------------------------------------------------------------------------------------------------------------------------------------------------------------------------------------------------------------------------------------------------------------------------------------------------------------------------------------------------------------------------------------------------------------------------------------------------------------------------------------------------------------------------------------------------------------------------------------------------------------------------------------|-----|
| 3.14 | <b>Variation in thrombin generation as a result of varying shear rate.</b><br><b>A)</b> Time series of the amount of thrombin showing the the maximum and minimum of the data (blue) generated by varying the shear rate from 1-1500 (1/s) as well as thrombin curves generated with shear rates 1, 10, 100, 500, and 1500 (1/s). Dependence of <b>B)</b> lag time*; <b>C)</b> maximum relative rate*; <b>D)</b> final amount on shear rate. . . . .                                                                                                                                                                                                                                                                                                                                                                                                                                                                                                                                                          | 86  |
| 3.15 | <b>Effects of shear rate on production and removal of thrombin:</b> Total production and removal of thrombin by flow, diffusion and chemical inhibition by antithrombin AT generated by varying shear rate from <b>A)</b> 1 - 1500 (1/s); <b>B)</b> 0.01 - 1 (1/s). At small and large shear rates (1-1500 (1/s)), the removal of thrombin is dominated by the effects of flow. Significantly smaller shear rates that approach static conditions result in diffusion and chemical inhibition dominated removal of thrombin. Static experiments support significant removal of thrombin by AT inhibition. . . . .                                                                                                                                                                                                                                                                                                                                                                                             | 87  |
| 4.1  | <b>Global sensitivity analysis for mathematical model of flow-mediated coagulation.</b> <b>A)</b> Critical TF distributions for normal and FVIII deficient plasma. Dashed black line at 5 fmol/cm <sup>2</sup> is the fixed TF for all further simulations. <b>B)</b> Thrombin concentration time series generated by uniformly and independently varying plasma protein levels $\pm 50\%$ from normal (110,000 total simulations); mean (solid black line), boundaries that encompass 50% (pink), and 90% of the data (orange), and the maximum/minimum of the computed solutions (gray-dashed); blue line drawn at 1nM. <b>C)</b> First (blue) and total (orange) order Sobol indices are plotted as mean $\pm$ standard deviation computed with 5,000 bootstrap samples of the original 110,000 simulations. <b>D)</b> Plasma zymogen and inhibitor levels distributions shown as box-and-whisker plots (mean in red, whiskers $3IQR$ ), conditioned on achieving more than 1nM of total thrombin. . . . . | 119 |
| 4.2  | <b>Effects of variations in plasma FII and FV levels on thrombin generation and the evolution of enzyme complexes in the mathematical model.</b> "N" denotes 100%, "L" denotes 50%, and "H" denotes 150% of the respective baseline plasma level; "NFII" = 1400 nM, "NFV" = 10 nM. <b>A)</b> Total thrombin; <b>B)</b> prothrombinase (FVa:FXa); <b>C)</b> platelet tenase (FVI-Ia:FIXa); <b>D)</b> FVIII:FXa complex on plt; <b>E)</b> FV:FXa complex on plt; <b>F)</b> FV:FIIa complex on plt; during a time course of 40 min. Description of labels found in Table S1. . . . .                                                                                                                                                                                                                                                                                                                                                                                                                             | 122 |

|     |                                                                                                                                                                                                                                                                                                                                                                                                                                                                                                                                                                                                                                                                                                                                                                                                                                                                                                                                                                                                                                                                                                                       |     |
|-----|-----------------------------------------------------------------------------------------------------------------------------------------------------------------------------------------------------------------------------------------------------------------------------------------------------------------------------------------------------------------------------------------------------------------------------------------------------------------------------------------------------------------------------------------------------------------------------------------------------------------------------------------------------------------------------------------------------------------------------------------------------------------------------------------------------------------------------------------------------------------------------------------------------------------------------------------------------------------------------------------------------------------------------------------------------------------------------------------------------------------------|-----|
| 4.3 | <p><b>Flow assays with whole blood from FVIII deficient individuals. A)</b> Representative images of DiOC6 labeled platelets and leukocytes and Alexa Fluor 555 labeled fibrin(ogen) on collagen-TF surfaces at <math>100\text{ s}^{-1}</math> after 25 min for vehicle control, <math>50\text{ }\mu\text{g}/\text{mL}</math> exogenous prothrombin, <math>100\text{ }\mu\text{g}/\text{mL}</math> anti-FV, and exogenous prothrombin and anti-FV. Scale bar = <math>50\text{ }\mu\text{m}</math>. Individual fluorescent channels are found in Fig. S6. <b>B)</b> Representative fibrin(ogen) and platelet/leukocyte accumulation dynamics in terms of normalized fluorescent intensity (FI). <b>C)</b> Fibrin(ogen) normalized maximum fluorescence intensity and rate of deposition (normalized velocity) for FVIII levels of <math>\bigcirc = 3.0\%</math>, <math>\square = 7.5\%</math>, <math>\diamond = 8.5\%</math>. See SI and Fig. S7 for calculation of metrics. P-values represented as *, **, and **** for <math>10^{-2}</math>, <math>10^{-4}</math>, and <math>10^{-7}</math>, respectively. . . .</p> | 124 |
| 4.4 | <p><b>Calibrated automated thrombography. A)</b> FII and FV levels were varied using immunodepleted plasmas and purified FII and FV in the presence of an anti-FVIII function blocking antibody. 'N', 'H', and 'L' corresponds to normal, high, and low levels of respective zymogen. <b>B)</b> FVIII deficient (<math>&lt;1\%</math>) plasma treated with vehicle control, <math>50\text{ }\mu\text{g}/\text{mL}</math> exogenous prothrombin, <math>100\text{ }\mu\text{g}/\text{mL}</math> anti-FV, and exogenous prothrombin and anti-FV. All assays conducted with <math>5\text{ pM}</math> TF and phospholipids. Tables S3 and S4 contain the measured prothrombin, FV, and FVIII levels corresponding to each curve. .</p>                                                                                                                                                                                                                                                                                                                                                                                     | 125 |
| 4.5 | <p><b>Schematic of (A) coagulation reactions included in our model.</b> Dashed magenta arrows show cellular or chemical activation processes. Blue arrows show chemical transport in the fluid or on a surface. Green segments with two arrowheads depict binding and unbinding from a surface. Rectangular boxes denote surface-bound species. Solid black lines with open arrows show enzyme action in a forward direction, while dashed black lines with open arrows show feedback action of enzymes. Red disks show chemical inhibitors. Schematic of (B) reaction zone and (C) endothelial zone. . . . .</p>                                                                                                                                                                                                                                                                                                                                                                                                                                                                                                     | 139 |
| 4.6 | <p><b>Kinetic rate constant experiments where the rates of association of plt-FV with plt-FXa and plt-FVIII with plt-FXa increase or decrease by 50%.</b> Thrombin generation in FVIII-deficient plasma <b>A)</b> with thrombin activation of FV; and <b>B)</b> without thrombin activation of FV. We denote thrombin activation of FV on the platelet as "thrombin feedback". .</p>                                                                                                                                                                                                                                                                                                                                                                                                                                                                                                                                                                                                                                                                                                                                  | 140 |
| 4.7 | <p><b>Effects of variations in plasma FII and FV levels on intravascular thrombin generation and coagulation enzymes and complexes when thrombin activation of FV and FVIII as well as APC binding to FVa and FVIIIa are turned off.</b> "N" denotes 100%, "L" denotes 50%, and "H" denotes 150% of their respective baseline plasma level. <b>A)</b> Total thrombin; <b>B)</b> prothrombinase (FVa:FXa); <b>C)</b> plt. tenase (FVIIa:FIXa); <b>D)</b> FVIII:FXa complex; <b>E)</b> FV:FXa complex; <b>F)</b> FV:FIIa complex; during a time course of 40 minutes. Concentrations are in units of nM. Description of labels found in Table 1. . . . .</p>                                                                                                                                                                                                                                                                                                                                                                                                                                                            | 141 |
| 4.8 | <p><b>Exploration of the race to platelet tenase production.</b> Evolution of <b>A)</b> concentration of total FIXa and FVIIIa on the platelet; <b>B)</b> rate of FIX activation on the subendothelium (SE); and <b>C)</b> rate of FIX activation on the platelet; in the HFII-LFV and NFII-NFV cases over 40 minutes. . . . .</p>                                                                                                                                                                                                                                                                                                                                                                                                                                                                                                                                                                                                                                                                                                                                                                                    | 142 |

|      |                                                                                                                                                                                                                                                                                                                                                                                                                                                                                                                                                |     |
|------|------------------------------------------------------------------------------------------------------------------------------------------------------------------------------------------------------------------------------------------------------------------------------------------------------------------------------------------------------------------------------------------------------------------------------------------------------------------------------------------------------------------------------------------------|-----|
| 4.9  | <b>FV activity in pooled normal plasma as a function of anti-FV antibody concentration as measured in a modified prothrombin time assay.</b>                                                                                                                                                                                                                                                                                                                                                                                                   | 143 |
| 4.10 | <b>Representative images of DiOC6 labeled platelets and leukocytes and Alexa-555 labeled fibrin(ogen) formed in whole blood flow assays. Scale bar = 50 <math>\mu\text{m}</math></b>                                                                                                                                                                                                                                                                                                                                                           | 144 |
| 4.11 | <b>Example of metrics fitted from fluorescence time series curves.</b> Maximum is determined using the max function in Numpy, and velocity is determined by fitting a line to the experimental data in the linear growth region of the fluorescence curve.                                                                                                                                                                                                                                                                                     | 145 |
| 4.12 | <b>DiOC6 normalized maximum fluorescence intensity and rate of deposition (normalized velocity) for FVIII levels of <math>\circ = 3.0\%</math>, <math>\square = 7.5\%</math>, <math>\diamond = 8.5\%</math>. No significant difference was found between groups.</b>                                                                                                                                                                                                                                                                           | 146 |
| 5.1  | <b>Standard model for FXa inactivation by AT is a poor match to data.</b> The fitted model from Chapter 2, with product inhibition incorporated, and literature values for the inactivation rate, do not qualitatively match the data. The model predicts nearly complete inactivation by 30 minutes, while the experimental data continues to show active enzyme throughout.                                                                                                                                                                  | 153 |
| 5.2  | <b>Preliminary MCMC fits to data for the Null and Alternative AT inactivation models.</b> The Null (orange) and Alternative (Blue) models were fit to the data (Circles) using an MCMC procedure. The posterior distributions were sampled 1,000 times and used to construct 95% credibility intervals for the concentration of product at a fixed time (shaded regions).                                                                                                                                                                      | 157 |
| 5.3  | <b>Preliminary study varying Plasma Levels, Platelet Characteristics, and TF simultaneously.</b> Plasma levels (PL) of zymogens were varied $\pm 50\%$ , platelet characteristics (PC) were varied at different percentage levels (x-axis), and TF varied between 1 and 30fmol/cm <sup>2</sup> (N=5,000 for each PC var % and fixed TF value). The minimum (red) and maximum (blue) TF levels that allowed 99.5% of samples to have a time to 1 nM of total thrombin between 3 and 10 minutes, <i>i.e.</i> , the metric for a normal response. | 158 |
| 5.4  | <b>Preliminary Sobol index results for the time to 1 nM of thrombin for hemophilic models.</b> The variance for the time to 1 nM of total thrombin was decomposed using Sobol indices where plasma protein levels and platelet characteristics were allowed to vary within a hypothetical normal range for normal ( <b>A</b> ), hemophilia A ( <b>B</b> ), hemophilia B ( <b>C</b> ), and hemophilia C ( <b>D</b> ) type blood.                                                                                                                | 159 |

# List of Tables

|     |                                                                                                                                                                                                                                                                                                                                                                                                                                                                                                                                                                                                                                                                                                                                       |     |
|-----|---------------------------------------------------------------------------------------------------------------------------------------------------------------------------------------------------------------------------------------------------------------------------------------------------------------------------------------------------------------------------------------------------------------------------------------------------------------------------------------------------------------------------------------------------------------------------------------------------------------------------------------------------------------------------------------------------------------------------------------|-----|
| 2.1 | <b>Model parameters and their distributions.</b> Prior and Posterior estimates of unknown parameters for both the Null and Alternative models. *Because there were several individual initial concentrations measured, we only report here the overall average pipetting error for all cases. . . . .                                                                                                                                                                                                                                                                                                                                                                                                                                 | 37  |
| 4.1 | <b>Description of variations in FII and FV plasma levels.</b> . . . . .                                                                                                                                                                                                                                                                                                                                                                                                                                                                                                                                                                                                                                                               | 147 |
| 4.2 | <b>Description of variations in FII and FV plasma levels and variations in association constants describing FV:FXa and FVIII:FXa complex formation.</b> . . . . .                                                                                                                                                                                                                                                                                                                                                                                                                                                                                                                                                                     | 147 |
| 4.3 | <b>Thrombin generation metrics for plasmas with normal prothrombin and FV levels (NFII-NFV), normal prothrombin and low FV (NFII-LFV), high prothrombin and normal FV (HFII-NFV), or high prothrombin and low FV (HFII-LFV) in the presence of a function blocking anti-FVIII antibody (12 nM).</b> Prothrombin and FV levels were altered using a combination of prothrombin and FV immunodepleted plasmas in combination with purified zymogens. Lag time, endogenous thrombin potential (ETP, analogous to area-under-curve), peak thrombin, and time to peak were measured by calibrated automated thrombogram (CAT) using 5 pM tissue factor and phospholipids. Data presented as mean $\pm$ standard deviation of n=3 . . . . . | 148 |
| 4.4 | <b>Thrombin generation metrics for commercial (George King) and patient derived FVIII deficient plasma (Samples 1, 2, and 3) in the presence of a vehicle control, FV partial inhibitor (anti-FV, 100 <math>\mu</math>g/mL), exogeneous prothrombin (+prothrombin, 50 <math>\mu</math>g/mL), or both the anti-FV antibody and exogenous prothrombin (+prothrombin/anti-FV).</b> Lag time, endogenous thrombin potential (ETP, analogous to area-under-curve), peak thrombin, and time to peak were measured by calibrated automated thrombogram (CAT) using 5 pM tissue factor and phospholipids. . . . .                                                                                                                             | 149 |
| 5.1 | <b>Model parameters and their distributions.</b> Prior and Posterior estimates of unknown parameters for both the One and Two-Step Inactivation models. *Because there were several individual initial concentrations measured, we only report here the overall average pipetting error for all cases. †Estimated previously in Chapter 2. . . . .                                                                                                                                                                                                                                                                                                                                                                                    | 156 |

# Chapter 1

## Introduction

From the mysteries at the heart of the cell to the formation of new species, biological systems with their complicated origins and evolving adaptation can sometimes leave us with more questions after studying them than we had before [1]. Mathematical models, which transform a physical system into the clear rule-based language of mathematics, are necessary to study such complex systems. This translation from the physical world to a mathematical model is never perfect, or as statistician George Box put it, “All models are wrong, but some are useful” [2], which means they can still give us deeper insight into the confusing physical world than we originally had. The creation of a model is rarely the final goal. Instead, one hopes to use the model to learn more about the original physical system and to predict what will occur in novel situations. One way to do this is by understanding how uncertainty in the model - both from its inputs and its form - drive uncertainty in the model predictions. Two classes of methods designed for this are Uncertainty Quantification (UQ) and Sensitivity Analysis (SA). These methods give insight into the importance of parameters in a system and can be used as a predictive tool to guide experimental design and generate new hypotheses.

The focus of this dissertation will be on applying these methods to one such complex system: hemostasis, which is the arrest of bleeding from an injured vessel and encompasses blood coagulation and blood clot formation. Over the last several decades, many models have been proposed to better understand the intricacies of the hemostatic system, with varying mathematical levels of accuracy and complexity [3]. These models are formulated using different mathematical tools, such as the Law of Mass Action [4], with some only focusing on subsets of the coagulation system, for example, the role of platelet deposition and surface mediated biochemical reactions to clot formation [5]. Importantly, even with the abundance of extant models, open questions about the clotting system exist, leading to a novel model being developed, an old model reinterpreted, or both. However, with so many coexistent models, some natural questions arise: *How accurate can these models be? What, if anything, does the uncertainty in a model mean? Which parameters of the model are most important to successful coagulation?* The quickly growing discipline of UQ gives us some tools to answer these questions. A merging of applied mathematics, statistics, and experimental design, UQ offers a useful structure to calibrate, fit, and validate mathematical models incorporating uncertainty. This dissertation will showcase applications of UQ methods to 1) provide evidence for a missing reaction in a common chemical assay, 2) perform a detailed sensitivity analysis of a coagulation model, and 3) identify a potential

therapeutic target for a bleeding disorder.

We will first present a review of the mathematical methods used in this dissertation and background information on the coagulation system itself. Chapter 2 provides evidence for product inhibition in certain chromogenic assays, which is confirmed and validated by experimental evidence. In Chapter 3, we present a detailed sensitivity analysis of a coagulation model, comparing the results of local and global methods. Chapter 4 describes a potentially novel method of rescuing normal bleeding with Hemophilia A, by the unintuitive lowering of certain clotting proteins. Chapter 5 describes future directions and extensions for this work.

## 1.1 Background on Uncertainty Quantification

The models considered in this thesis are deterministic, *i.e.*, where a fixed input returns a fixed output, as opposed to a truly random model, such as Brownian motion (for more information, see [6]). However, while the models are deterministic, they still display stochastic output, owing to the inherent uncertainty in the model's parameters. The methods described below offer a means to better understand how this parametric uncertainty maps to a model's predictions, an important aspect for the types of biological models we will be focusing on.

### Classification of Uncertainty

General uncertainty can be divided into two classes, *aleatoric* and *epistemic*, depending on its source [7, 8]. The line between these categories is frequently blurred, especially as complex systems are continued to be better understood, but it is still a useful distinction for modeling purposes.

*Aleatoric* Often called *statistical* uncertainty, aleatoric uncertainty arises from either a truly random process, such as quantum interactions, or from a system that is so complex that it is indistinguishable from random, *e.g.*, the roll of a die. If we had absolute information about the rolling die, such as the exact angle and force of impact, the strength and direction of wind currents, *etc.*, then we could theoretically predict the die roll with no uncertainty. Since such precise information is not available, we are forced to treat the die as a "known unknown". Because of this, aleatoric uncertainties may be best represented as a true random variable with an associated probability distribution. Many physical parameters are aleatoric in nature, such as the rate of two proteins interacting or the occurrence of a mutation in a gene. Importantly, such uncertainties *cannot* be mitigated with increased precision. Rather, multiple replicate experiments are required to determine an average measurement.

*Epistemic* Also called *systematic* uncertainties, epistemic errors stem from a lack of knowledge about the full system, such that if we were to obtain more information, we would be able to reduce or remove the uncertainty. One source of epistemic error is numerical inaccuracy in computations (*e.g.*, rounding error, truncation error, *etc.*). These errors are often biased due to floating point arithmetic and are not a function of the underlying system. One important type of epistemic uncertainty is *model discrepancy* where, due to simplification or lack of knowledge, the model of a system does not accurately simulate the underlying reality. Every model contains these systematic errors to some extent, so quantifying their impact is important to understanding the reliability of the model.

### 1.1.1 Forward UQ

A major goal of UQ is to propagate error from uncertain model parameters to computable model outputs (see Figure 1.1), allowing for the creation of a prediction interval for a quantity of interest (QoI). Uncertain model parameters are first reinterpreted as probabilistic random variables with defined probability distributions. Given a standard mathematical model,

$$\mathcal{Y} = f(\mathcal{X}, \vec{\theta}) \quad (1.1)$$

where  $f$  represents the model,  $\mathcal{Y}$  the model output (*i.e.*, the QoI),  $\mathcal{X}$  the independent variables of the model (*e.g.*, *space* or *time*), and  $\vec{\theta} = (\theta_1, \dots, \theta_N)$  the  $N$  uncertain model parameters. We interpret  $\vec{\theta}$  as a  $N$  dimensional random variable with associated probability space  $(\Omega, \mathcal{F}, P)$ , where  $\Omega$  is the overall sample space,  $\mathcal{F}$  is the set of measured states, and  $P$  is a function mapping states to probabilities, and then reinterpret our QoI as a random variable itself, with its own associated probability space. After the model simulations, the last step in error propagation is finding statistics or properties of this QoI distribution, *e.g.*, its mean, variance, skew, *etc.*

Two main approaches are used to compute these statistics: Monte-Carlo methods and Surrogate Models, each with unique trade offs between accuracy and computational cost.

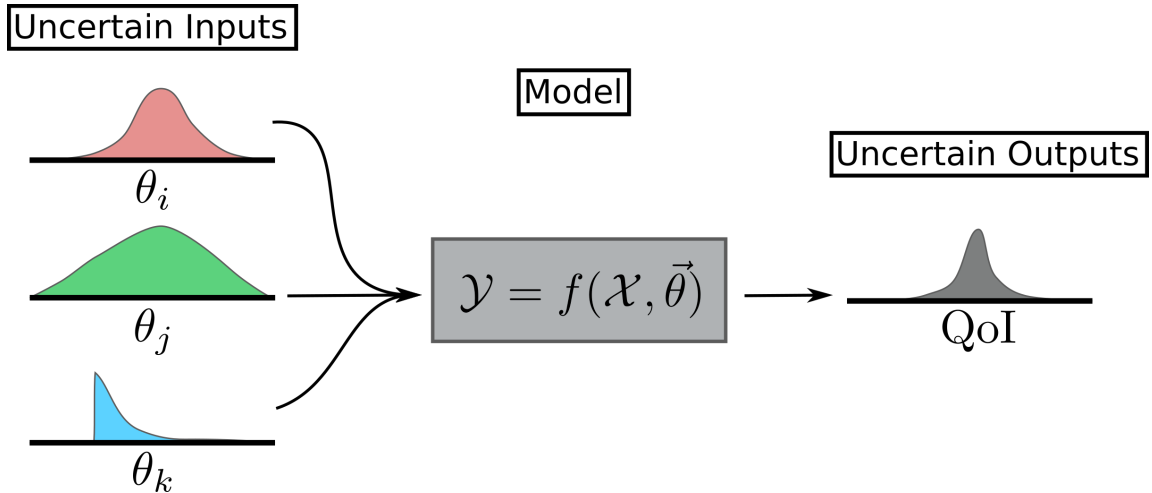


**Figure 1.1: Schematic of Forward UQ or error propagation.** Uncertain inputs, represented here as  $\theta_i, \theta_j, \theta_k$  with their own distributions, are propagated through a model, from which a quantity of interest (QoI) is computed. Because the inputs are described by distributions, the QoI will necessarily have a distribution as well.

#### Monte-Carlo Approach

One method of propagating uncertainty from parameters is to directly evaluate the model with parameters sampled from their specified distribution. This is only possible if the distributions of the parameters is known. First, a collection of  $M$  samples are drawn,  $\{\vec{\theta}_1, \dots, \vec{\theta}_M\}$ , according to their individual distribution,  $P(\vec{\theta})$ . These samples are then evaluated in the model,

$$\mathcal{Y}_i = f(\mathcal{X}, \vec{\theta}_i), \quad (1.2)$$

yielding an ensemble of model evaluations. Note, the evaluations here are deterministic according to their model  $f$ . These samples are then used to directly compute statistics of the QoI distribution in the classical fashion: the expected value,

$$\mathbb{E}[\mathcal{Y}] \approx \frac{1}{M} \sum_{i=1}^M \mathcal{Y}_i, \quad (1.3)$$

and the variance

$$\text{Var}[\mathcal{Y}] \approx \frac{1}{M(M-1)} \sum_{i=1}^M \sum_{j>i}^M (\mathcal{Y}_i - \mathcal{Y}_j)^2. \quad (1.4)$$

While intuitive and simple to implement, this approach suffers from slow convergence. The mean converges asymptotically like  $1/\sqrt{M}$  (due to the central limit theorem), which for computationally intensive models may be infeasible.

Several improvements to this method have been suggested, namely Quasi-Monte-Carlo (*e.g.*, Latin Hyper Cube) and sparse grid sampling methods [9, 10]. Both take advantage of low-discrepancy sequences to more efficiently sample the parameter distributions. For example, to draw  $N$  samples according to a Latin Hyper Cube sampling approach, the parameter space is first divided into  $N$  equal partitions, and then the  $N$  samples are drawn from the partitions uniformly. This prevents random samples from clustering together and instead forces points to more fully explore the entire domain.

## Surrogate Models

Many models of interest are computationally complex, such as PDE-based simulations of fluid flow, ignition, and hydrology. These models typically contain large numbers of parameters, incorporate complex physics, and have individual run times exceeding several hours. This makes sampling based approaches for UQ highly infeasible. One potential solution is to construct a *surrogate model*, variably referred to as a *meta-model* or *reduced order model* depending on the field. These models are approximations for the original simulation but with drastically lower model run times and yet are capable of reproducing the original model output within a specified tolerance.

Several such surrogate model candidates have been proposed, ranging from simple regression to more sophisticated Gaussian processes models (*i.e.*, kriging) [11]. All, however, rely on being able to efficiently reproduce the model output response. In general, there are two classes of surrogate models defined by how the approximations are implemented. Intrusive methods, such as classical Polynomial Chaos [12], change the fundamental governing equations of the model. Non-intrusive methods, such as regression or collocation based methods [13], use samples from the full forward model without altering the model itself.

### 1.1.2 Parameter Estimation

Another goal of UQ is the accurate estimation of model parameters that incorporate sources of uncertainty, such as experimental error, model discrepancy, or randomly varying parameters (aleatoric uncertainty). Many approaches to parameter estimation rely on optimization theory, making use of methods such as gradient descent, Newton's method, or pattern based searches such as Nelder-Mead [14–19]. These methods generally seek to

minimize a loss function that measures the misalignment of the model output with the available data,

$$L(\vec{\theta}) = \|\tilde{\mathcal{Y}} - D\|_2^2, \quad (1.5)$$

where  $\tilde{\mathcal{Y}}$  is the model output and  $D$  is the data. This loss function can in practice be difficult to work with as it may have rapidly changing gradients, saddle points, and sub-optimal local minima, which make the identification of the global extrema challenging to obtain. Furthermore, this approach generally only allows the identification of a single point estimate for  $\vec{\theta}$  with further analysis being required to determine confidence intervals or statistics about the parameter estimates.

### Maximum Likelihood Methods

With Maximal Likelihood Estimation (MLE) [18], instead of minimizing a loss function, one attempts to maximize the probability of observing the collected data given a parameter estimate, utilizing the so called ‘‘Likelihood’’ function,

$$\mathcal{L}(\vec{\theta}|x) = p_{\vec{\theta}}(x), \quad (1.6)$$

where  $p_{\vec{\theta}}$  is a probability density function indexed by the parameter  $\vec{\theta}$ . Note, while  $p_{\vec{\theta}}(x)$  necessarily integrates to 1, the Likelihood does not, since the independent variable is  $\vec{\theta}$  and not  $x$ . Finding  $\vec{\theta}$  that maximizes the Likelihood gives the parameter estimate that makes the data highly probable. The choice of  $p_{\vec{\theta}}(x)$  is determined by the user and the system being modeled.

### Bayesian

Instead of estimating a single best fitting parameter, the Bayesian framework interprets model parameters as distributions, with  $\vec{\theta}$  understood to be a random variable drawn from a distribution,  $\Theta(\omega)$ , and the data as individual realizations [14, 20–22]. Bayesian parameter estimation then results in a *posterior distribution* of  $\vec{\theta}$ , which incorporates information from the observed data, *e.g.*, the conditional distribution  $p(\vec{\theta}|D)$ . Computing this distribution in practice requires the eponymous Bayes rule

$$\pi(\theta|D) \propto \pi(D|\theta) \pi(\theta), \quad (1.7)$$

where  $D$  is the observed data,  $\pi(\theta|D)$  is the sought after posterior distribution of the model parameters,  $\pi(D|\theta)$  is the likelihood of the data, and  $\pi(\theta)$  is the prior distribution. This prior encodes the relative belief about the parameters before observing new data and is an important difference between Bayesian and non-Bayesian (*i.e.*, Frequentist, see [23–25]) methods. If nothing is known about the parameters beforehand, then an uninformative (or flat) prior is used. More likely, however, *some* information about the parameters is known, such as sign or relative magnitude, which can be encoded in a prior distribution.

There are pros and cons to the inclusion of priors in parameter estimates [25]. Some feel that prior distributions unnecessarily bias model estimates with the practitioners pre-conceived parameter opinions, yet they offer a major advantage when working with systems that have unidentifiable parameters. For example, in work described in Chapter 2, a kinetic reaction with unidentifiable parameters is still able to be fit to data because information

from the manufactured was able to be included as a prior. While these differences exist, it is important to note that with moderate assumptions and an uninformative prior - such as a uniform - it can be shown that the maximum *a posteriori* point from the Bayesian approach is recovered in the data limit (*i.e.*, the number of data points goes to infinity) when using MLE [20]. What we gain from the Bayesian approach is a full understanding of the parameter's distribution, from which statistical quantities, like credibility intervals, can be easily computed. Not without a cost, Bayesian methods require a larger computational budget as an exponentially increasing number of samples are needed to fully explore the high-dimensional posterior distribution.

*Markov Chain Monte Carlo* The direct evaluation of the posterior distribution is usually impossible. If the likelihood and prior satisfy certain conditions (*e.g.*, when the distributions are conjugate to one another), then the posterior can be determined analytically; however, such cases are rare in practice. In most practical applications, the posterior distribution has to be found via numerical calculation, with Markov chain Monte Carlo (MCMC) being the most common method used [26].

MCMC does not directly produce the posterior distribution, but instead gives a way to draw samples from it. These samples allow for statistics of the posterior distribution, such as its mean and variance, to be computed. A process to sample the distribution for  $\theta$ , *i.e.*, a sampler for  $\theta$ , is constructed by carefully defining an aperiodic and recurrent Markov process such that its long time stationary distribution is the desired posterior. This is accomplished by splitting the sampling process into two parts: 1) propose a new sample, and 2) decide to accept or reject it. Different MCMC methods utilize distinct strategies for the two steps, for example the standard Metropolis-Hastings algorithm [27] uses an arbitrary proposal distribution (*e.g.*, a uniform centered at the last sample) and carefully adjusts the acceptance probability so that the posterior distribution is obtained. So long as the Markov process is aperiodic with no absorbing states (*i.e.*, ergodic), then a *unique* equilibrium distribution is guaranteed to exist [26].

The major limitation of this approach is its computational expense. First, every step in the Markov Chain requires an evaluation of the likelihood, which can be computationally taxing if the model is complex and a large number of samples is required. Second, while convergence is guaranteed, the number of samples needed to achieve convergence is difficult to measure *a priori*. Because of this, several variants of MCMC have been developed that try and mitigate these challenges, among them are the Hamiltonian method [28, 29], which adds a momentum component to each parameter in order to accelerate convergence, and slice sampling [30], which automatically adjusts the proposal step size for each parameter. While MCMC methods have been used with thousands of unknowns [31], the applications described in Chapter 2 are sampling a posterior with approximately 10 dimensions. Furthermore, the likelihood model used in Chapter 2 is efficient to evaluate. With a modest dimension size and a fast likelihood model, advanced MCMC methods are not necessary.

One of the simplest and most effective additions to the standard Metropolis-Hastings algorithm is an adaptive learning of the parameter covariance (see Algorithm 1). In the standard algorithm, parameters are assumed to be independent of each other, a property that is likely inaccurate. This independence is encoded by the proposal distribution of the MCMC sampler, which generates new potential sample points. When the proposal distribution poorly matches the posterior (*e.g.*, has a large Kullback-Leibler divergence), newly generated samples will frequently be rejected, resulting in slow convergence to the poste-

rior. Instead of continuing with the independence assumption, the parameter covariance is numerically computed as successful samples are drawn. The efficiency of the sampler is then increased significantly by using this covariance, which essentially uses the previously computed samples as a template for generating new sample draws. To maintain ergodicity, the covariance updates must be stopped at some point (*e.g.*, a prescribed number of steps) after which actual posterior samples may be taken. For the applications discussed in Chapter 2, a normally distributed proposal is used and refined by the adaptive process described above.

---

**Algorithm 1** Adaptive Random Walk Metropolis-Hastings

---

**Require:** Initial parameters:  $\theta_0$ , Initial Likelihood:  $y_0 = \mathcal{L}(\theta_0|D)$ , Initial Covariance:  $V = I$

```

loop {Repeat until convergence is reached}
   $\hat{\theta} = \theta_{i-1} + z$ , where  $z \sim N_M(0, \epsilon V)$  {Construct new parameters}
   $\hat{y} = \mathcal{L}(\hat{\theta}|D)$  {Evaluate likelihood at new parameters}
   $A = \hat{y}\pi(\hat{\theta})/y_{i-1}\pi(\theta_{i-1})$  {Compute acceptance ratio}
   $r = \text{random}[0, 1]$  {Draw Uniform random between [0,1]}
  if  $r < A$ , then {Update parameters}
     $\theta_i = \hat{\theta}$ 
     $y_i = \hat{y}$ 
  else {Keep old parameters}
     $\theta_i = \theta_{i-1}$ 
     $y_i = y_{i-1}$ 
  end if
  if  $\text{mod}(i, T) = 0$  and  $i < B$ , then {Update covariance at preset intervals up until step  $B$ }
     $V = \text{COV}([\theta_0, \dots, \theta_i])$ 
  end if
end loop

```

---

One method to determine MCMC convergence is the Geweke diagnostic [32], which uses a standard difference between two sample means for the early and late sections of the Markov chain trajectory. It assumes that while the chain has yet to converge to the posterior distribution (a state known as “burn-in”), the chain mean will be different from the converged state (see Figure 1.2A). A threshold for acceptance (typically  $\alpha = 0.05$ ) is set and compared with the test. Other methods include comparing the sampled distributions directly, such as with a Kolmogorov-Smirnov test [33], to determine if convergence has taken place.

While the Markov-Chain provides samples of the posterior distribution, the samples are generally correlated. This means that the  $i$ th sample contains most of the information from the  $i-1$ st sample. To overcome this, the posterior chain is *thinned* [34] by only keeping 1 out of every  $M$ th sample, where  $M$  represents the number of lags, *i.e.*, the number of adjacent samples to skip (see Figure 1.2B), required to drop the autocorrelation of the chain below a preset threshold ( $\alpha = 0.05$ ). This thinning removes the strongly correlated posterior samples and drastically reduces the posterior sample size, simplifying any necessary post-processing.

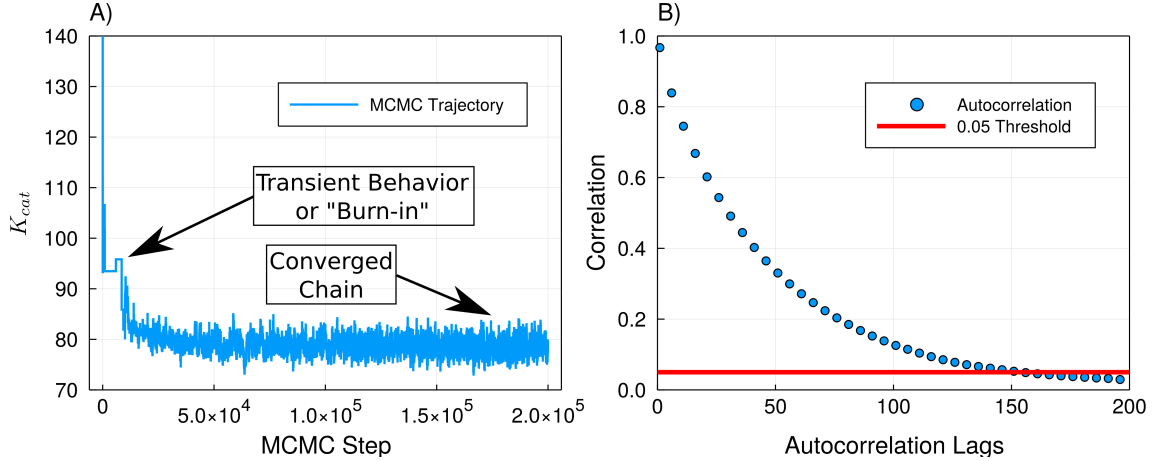


**Figure 1.2: Examples of Burnin and Autocorrelation for an estimated parameter.** The first 200,000 steps of the parameters MCMC trajectory (A) show an early convergence to the posterior, with burnin occurring within 50,000 steps. The autocorrelation of the chain (after burnin was removed) in (B) drops below the preset threshold of 0.05, indicating posterior samples are no longer strongly correlated, after approximately 200 lags (skipped samples in the chain).

### 1.1.3 Sensitivity Analysis

Sensitivity Analysis (SA) was developed to better understand the relationship between changes in inputs and their corresponding changes in output QoIs. There are several uses for general SA, including the reduction of the number of active parameters in a model and the identification of an important subset of parameters for further analysis [35].

SA can be separated into two general classes: local and global sensitivity analysis (LSA and GSA, respectively). LSA is used to examine how small, local perturbations to model parameters affect model outputs about some nominal point in parameter space [8]. GSA considers the impact of varying parameters *simultaneously* together over their full range of possible values [36]. Doing so comes at the added cost of computational complexity. Where LSA methods usually require  $O(N)$  function evaluations, GSA methods need significantly more. The increased information yielded from GSA over LSA has up until recently not been worth the added computational cost. For example, many of the most used GSA algorithms were first described in the late 1980s, but have only become popular in the last decade [37].

#### Local Sensitivity Analysis

LSA includes methods for quantifying the effect of parameters varying over a small range near a fixed point of the input space,  $\mathbf{x}^0 = [x_1^0, x_2^0, \dots, x_p^0]$ , with the mathematical definition for the sensitivity of parameter  $i$  written as

$$\phi_i = \frac{\partial \mathcal{Y}}{\partial x_i} \left( \frac{x_i}{\mathcal{Y}} \right), \quad (1.8)$$

where  $\mathcal{Y}$  is the measured QoI,  $x_i$  is the  $i$ th parameter, and the product of  $x_i/\mathcal{Y}$  normalizes the index [38]. These gradients can be computed analytically if the model contains gradient

information [39], or numerically using a derivative approximation, such as finite differences [40]. LSA is fast computationally, but inappropriate when the model input is uncertain or when the model is non-linear [36, 41].

## Global Sensitivity Analysis

Similar to the Bayesian framework for parameter estimation, GSA considers the underlying system output to be a random variable over a probability space of parameter inputs and quantifies the sensitivity of a model output by its variance. Determining analytical representations of system outputs with respect to the parameter space is only possible for simple systems, *e.g.*, linear systems, so most applications resort to Monte Carlo sampling to explore the parameter space. While computationally taxing, Monte Carlo sampling is easily implemented and applicable to all models, including those that contain non linearities between model parameters [36]. While other methods exist, such as the direct evaluation of global sensitivities via Polynomial Chaos expansions [42], this dissertation will only focus on their direct estimation.

*Sobol Indices* One method of GSA, first described by Sobol in 1990 [43], measures the portion of a model’s output variance attributable to an individual or set of parameters. Called Sobol sensitivity indices (SIs), this GSA method relies on the analysis of variance decomposition of a function to determine the fraction of variance for the QoI attributable to each individual parameter. A major benefit of SIs is that they require only function evaluations of the target model and no gradient information, making them applicable to complex or black-box models. Additionally, since the contribution to the output variance is the only quantity being determined, SIs are applicable to highly nonlinear models [44]. The method requires few strong assumptions, that parameters be independent and that the variance of the measured QoI be finite, or equivalently, that the forward model  $f(\mathbf{x})$  be square integrable,

$$\int_{\Omega} |f(\mathbf{x})|^2 p(\mathbf{x}) d\mathbf{x} < C, \quad (1.9)$$

where  $p$  is the probability density function associated with  $\mathbf{x}$ .

The SIs for a QoI, defined as a random variable,  $Q$ , with respect to a random parameter of inputs,  $\mathbf{x} = (x_1, x_2, \dots, x_P)$ , with the forward model  $f(\mathbf{x})$ , may be decomposed into

$$\text{Var}[Q(\mathbf{x})] = V = \sum_{j=1}^P V_j + \sum_{j=1}^P \sum_{k=j+1}^P V_{jk} + \dots + V_{1\dots P}. \quad (1.10)$$

Here the  $V_j$  are the contributions to the variance of  $Q$  from the individual random variables  $x_j$ ,  $V_{jk}$  are the second order terms, representing the contribution to the variance from the interaction between random variables  $x_j$  and  $x_k$ , which builds up to  $V_{1\dots P}$ , which represents the variance contribution from all  $P$  parameters interacting together.

To determine each parameter’s individual effects on  $Q$ , the so-called *First Order SIs* are formed by normalizing the first order variance terms by the total variance

$$S_j = \frac{V_j}{V}, \quad (1.11)$$

where  $\sum V_j = 1$  if and only if all interaction terms have zero contribution to the variance of the model output  $Q$ . To measure a parameter’s overall impact on the variance of  $Q$ , the

*Total Order SIs* capture the effect from both individual and interaction terms by summing all variance terms that contain the  $j$ -th parameter, typically written as

$$S_j^{Tot} = 1 - \frac{V_{-j}}{V}, \quad (1.12)$$

where  $V_{-j}$  is the set of all variance terms *not* containing the  $j$ -th parameter. Unlike the first order case, the total order SIs can sum to greater than one since interaction terms between parameters can be double counted.

*Computing Sobol SIs* While several methods for computing SIs exist, including the fashioning of specialized surrogate models (Polynomial Chaos expansions) [35], the most straightforward calculation is through Monte-Carlo estimators, which directly compute the indices. Several such estimators for partial variances are found in the literature [45–47], with varying accuracy and efficiency. One estimator for first order SIs comes from Sobol [48], defined as

$$V_j \approx \frac{1}{N} \sum_{k=1}^N Q(\mathbf{x}^{(k)}) Q(\mathbf{x}_j^{(k)}) - \mathbf{E}[Q], \quad (1.13)$$

where  $\mathbf{x}^{(k)}$  and  $\mathbf{x}_j^{(k)}$  are both samples of all model parameters, differing only in the  $j$ -th parameter. While this estimator is capable of producing negative estimates - a non-physical result as variance terms are always positive - it nevertheless produces estimates with low absolute error when compared to other methods [45].

Similarly, the total variance SIs are computed using an estimator from Jansen [49],

$$V_{-j} \approx \frac{1}{2N} \sum_{k=1}^N [Q(\mathbf{x}_j^{(k)}) - Q(\mathbf{x}_{-j}^{(k)})]^2, \quad (1.14)$$

where again  $\mathbf{x}^{(k)}$  and  $\mathbf{x}_{-j}^{(k)}$  are sample points of the model parameters, differing in all parameters *except* the  $j$ -th parameter, for which they share the same value. Due in part to the estimators non-negative nature, the calculation is extraordinarily efficient, producing estimates with low error, especially compared with the first order variance estimator in Equation (1.13).

Using the estimators given above, the total number of function evaluations required to compute both first and total order SIs is  $N(P + 2)$ , where  $N$  is the number of samples for each individual parameter and  $P$  is the number of parameters in the model. It is common practice to compute confidence intervals for the SI estimates, which can easily be generated using a bootstrap approach [50].

*Importance of Standardizing Model Outputs* Due to the normalization taking place in Equation (1.11) and (1.12), and to the following property of Variance

$$\text{Var}[\alpha x + \beta] = \alpha^2 \text{Var}[x], \quad (1.15)$$

the set of raw output for the QoI can be standardized, *e.g.*, by subtracting sample means and scaling by the sample standard deviations, without affecting the Sobol SIs. This standardizing, while never explicitly discussed in the literature, vastly improves the computational efficiency of the estimator in Equation (1.13), especially when the magnitude of the QoI

is large. This is due to the high variability inherent to the estimator’s product form between  $Q(\mathbf{x}^{(k)})$  and  $Q(\mathbf{x}_j^{(k)})$ . By preprocessing the raw QoI output, the variability in the estimator is markedly decreased, leading to an overall lower variance in the estimate of the SI.

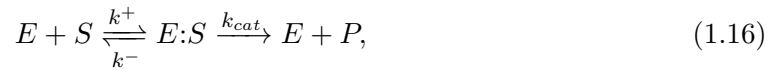
*Method of Morris* First described in 1991 by Morris, this one-at-a-time method gives a rough approximation of the total order SI (as in Equation (1.12)), but scales linearly with the number of inputs [51]. Each dimension of the  $p$ -dimensional input parameter space is discretized into  $p+1$  steps. Paths are constructed through this discretized space where each step changes a single parameter. At each step, the change in the QoI is measured. This change is then averaged over a large number of paths (less than 50), to give an indication of how an individual variable effects the model output.

Since this method does not have the necessary resolution to determine which parameters are important, its primary use is to filter out parameters that can be neglected in a model.

## 1.2 Applications

The methods described above allow for the calibration, validation, and analysis of mathematical models. This next section gives background information for the two application areas examined in this dissertation. Because the conversion of kinetic reactions to ordinary differential equations is central to both applications, we will first briefly give an overview on the use of the Law of Mass Action.

*From Kinetic Reactions to Differential Equations* Consider the standard kinetic reaction for the enzyme-substrate interaction:



where the enzyme,  $E$ , binds with the substrate,  $S$ , at rate  $k^+$ , unbinds at rate  $k^-$ , and forms the product,  $P$ , at rate  $k_{cat}$ . The Law of Mass Action [52] states that in a well mixed solution with constant temperature and pressure, the rate of a chemical reaction is directly proportional to the product of the concentrations of the individual reactants. Given this law and the reactions in Equation 1.16, we derive the follow system of differential equations

$$\frac{d}{dt}[E] = -k^+[E][S] + k^-[E:S] + k_{cat}[E:S], \quad (1.17)$$

$$\frac{d}{dt}[S] = -k^+[E][S] + k^-[E:S], \quad (1.18)$$

$$\frac{d}{dt}[E:S] = k^+[E][S] - k^-[E:S] - k_{cat}[E:S], \quad (1.19)$$

$$\frac{d}{dt}[P] = k_{cat}[E:S], \quad (1.20)$$

where  $[\cdot]$  represents concentration. Given appropriate initial conditions for the chemical species and values for the specified rates, this non-linear system of differential equations is numerically solved to obtain the concentration of chemical species at a desired time. While this system in itself will not be examined in detail, it is presented as a tool for understanding to the reader. The following listed applications, with their own research

questions and challenges, will make use of similar systems of differential equations derived using Mass Action kinetics.

### 1.2.1 Blood Coagulation

Blood coagulation has evolved over millions of years to maintain hemostasis and stop bleeding. It can be separated into four phases: initiation, amplification, propagation, and termination [53]. A schematic of the reactions involved in the blood coagulation system is shown in Figure 1.3A. Briefly, whenever the cell lining in human vasculature, the endothelium, is damaged, blood is exposed to the underlying proteins, including Tissue Factor (TF). A clotting protein in the blood, factor VIIa (FVIIa), binds with TF forming the FVIIa:TF complex. This enzyme complex activates other clotting proteins, namely FIX and FX. Platelets on the subendothelium (SE) are activated and become a localized surface for future clotting factors to be activated. The reduction of the dimension from free floating proteins in the blood to surface bound proteins on the platelet surface increases the catalytic efficiency of the clotting proteins. The activated form of FX (FXa) binds to the surface of platelets and activates its cofactor - FV (FVa). The activated platelets aggregate around the injury site and begin to form a leaky plug, slowing blood loss. The FVa:FXa complex, called prothrombinase, is then able to activate a small amount of FII (prothrombin) into FIIa (thrombin). Collectively, this cascade of reactions is responsible for the *initiation* of the clotting process [53].

With the appearance of a small amount of thrombin, too little to fully form a clot on its own, another pathway of reactions is accessible that results in the *amplification* of the coagulation signal. Thrombin, the final enzymatic product of coagulation, quickly catalyzes numerous clotting proteins (e.g. FV, FVIII, and FXI), activates additional platelets to create more surfaces for coagulation, and cleaves fibrinogen into fibrin, creating the polymer mesh which holds the platelet plug together. The newly activated FVIII (FVIIIa) binds with the previously activated FIX (FIXa) creating the FVIII:FIX (tenase) complex, greatly increasing the activation of more FX [54]. A strong positive feedback loop is thus established, leading to the *propagation* of greater amounts of thrombin and consequently greater amounts of fibrin, all leading to a stabilized clot.

Without some sort of *termination*, this process would continue well past the useful stage of clot formation and could become a dangerous vessel occlusion. Fortunately, the clotting system has several natural anticoagulants to limit the spread of the successfully formed clot, including antithrombin (AT), tissue factor pathway inhibitor (TFPI), and protein C (PC), among others. Collectively, these inhibitors are responsible for terminating the clotting signal, inactivating various clotting proteins, and returning the system to a functionally ready state [55]. While this summary provides enough background for this document, interested readers are encouraged to explore further [53, 56, 57].

### Static Vs Flow-Mediated Coagulation

Blood coagulation *in vivo* is always under flow within the human vasculature. As such, there are several important biophysical and mechanical forces at play in the clotting system. For example, red blood cells and fluid flow in the vessels cause platelets to be in a higher density along the walls of the vasculature - a process called margination - where they are able to more quickly react to injuries [58]. The target injury site is also continuously replenished

with new clotting proteins, so reactions must be inhibited by an anticoagulant process. This coagulation under flow is in contrast with *static* coagulation, which is standard in clinical clotting assays. In such assays, coagulation is studied without flow and with a finite supply of reactants. While results derived from static coagulation experiments can differ qualitatively from studies under flow [59], they have been instrumental in probing the underlying mechanisms of the clotting system [60].

## Mathematical Models of Coagulation

Hemostasis and fibrin formation constitute one of the best studied and most explored systems in all of medical biology [62]. Nearly every individual kinetic reaction in the coagulation system has been studied independently, with experimental estimates for most vital kinetic rates [63]. However, many of these estimates show extreme variability [64], with the same kinetic rate spanning a range of several orders of magnitude. The high intensity and frequency of experimental studies of coagulation has allowed the development of many mathematical models over the last several decades [65–70]. While some models are phenomenologically based, most use the biochemical reactions and mechanical relationships that have been well explored in the literature. These models are typically comprised of a system of ordinary differential equations derived from biochemical reactions that ultimately track the concentration of various clotting proteins over time. One popular model for static coagulation was created by Hockin et al. in 2002. Their model used 34 differential equations and 42 rate constants [71] to simulate a clotting response initiated by TF. While this model has been extensively investigated in literature, its lack of platelets and flow make it a poor choice for studying *in-vivo* coagulopathies, both of which are known to significantly effect thrombin production [5, 72].

A more applicable model for the study of human bleeding pathologies, since it includes both platelets and flow, was proposed in 2001 by Kuharsky and Fogelson [73] and was later expanded on by Hussain and Leiderman [74–77]. This updated model, the Kuharsky-Fogelson-Hussain-Leiderman (KFHL) model, simulates coagulation in a small, well-mixed region above an injury site. The model incorporates several key clotting features, including flow and platelet deposition. Coagulation proteins are assumed to either be free floating in the plasma, bound to the subendothelium, or bound to an activated platelet surface. These protein concentrations are tracked with a system of ordinary differential equations.

The KFHL model directly simulates flow, with new platelets and clotting proteins continuously being brought into the reaction zone, and removing activated platelets and proteins from the system. A diagram of the reactions and compartments considered in the model can be seen in Figure 1.3B. The KFHL model outputs a time-series for the concentration of each individual protein and the concentration of platelets in their different configurations for the entire requested simulation time. Chapter 3 contains more information on the model, with the full model equations in the supplement.

## Coagulopathies

Uncontrolled bleeding, typically resulting from acute trauma, is a leading cause of preventable death worldwide [78]. Additionally, more than 1 in every 5000 males - approximately half a million individuals worldwide - are born with some form of hemophilia, *i.e.*, a genetic bleeding disorder characterized by lower than normal levels of various clotting pro-



teins [79]. This document will focus on uncontrolled bleeding resulting from genetic bleeding disorders. What follows is a brief summary of some of the different types of hemophilia.

*Hemophilia A and B* The most well-known and common form of severe hemophilia, type A is identified by lower than normal amounts of clotting factor FVIII [80]. With symptoms indistinguishable from type A, hemophilia type B is caused by a corresponding deficiency in FIX and is only twenty percent as prevalent as type A. The severity of the disease, mild, moderate, or severe, is determined by the percentage of clotting factor present in the blood, as indicated by a blood assay [81]. When FVIII/FIX concentrations are severely deficient, with 1% or less than normal, patients suffer from spontaneous bleeding and experience significant bleeding after surgeries and accidents. If left untreated, severe hemophilia type A or B can be deadly, requiring constant and expensive treatment [82].

Interestingly, patients with hemophilia type A and B typically have no issues with “primary hemostasis”, the stage of clotting responsible for forming the initial platelet plug. It is in the propagation phase of clotting that symptoms occur. Due to the low concentration of FVIII/FIX, these individuals form very little tenase complex, so only the extrinsically activated FX is available to form prothrombinase. This leads to low levels of fibrin formation. While the platelet plug is successfully created, the fibrin needed to stabilize the clot is not available, leading to a “leaky” clot. Severe patients typically experience bleeding into joints and muscles, which can eventually lead to full immobility due to joint deformities if left untreated.

Treatment in the form of FVIII/FIX concentrates, which are administered intravenously at home, became widely available in the 1970s. This led to an improved quality of life for many patients. Since the 1990s, these concentrates have largely been replaced by recombinant therapies, which are not directly derived from humans or animals and are safer to use. While several new treatments are currently in development, the total cost of treatment is rising [83], with an average annual cost exceeding \$270,000 USD [84].

*No Bleeding Symptoms* While hemophilia type A and B patients typically experience increased bleeding risk in proportion to the degree of their protein deficiency (FVIII/FIX, respectively), it is not uncommon to see severe hemophilia type A patients with much milder symptoms [85]. The cause of this variability in bleeding phenotype is still largely unknown, though both genetic and environmental factors are suspected. Examining a potential cause for this variability is the subject of Chapter 4.

*Hemophilia C* Similar to types A and B, hemophilia type C is diagnosed as a deficiency in the specific clotting protein FXI. Since type C patients rarely have spontaneous bleeding events, it is regarded as a much milder form of hemophilia. Treatment, if any is needed at all, comes in the form of recombinant FXI, much like types A and B.

### 1.2.2 Static Clotting Assays: Chromogenic Substrates

First developed as early as 1961 [86], chromogenic peptide substrates have been a staple method for the continuous monitoring of blood clotting reactions since the 1970s [87]. These chromogenic substrates (CS) are manufactured with a high selectivity and affinity for specific enzymes which are required to study the individual reactions within the clotting system. CS contain a para-nitroaniline peptide that, when cleaved by an enzyme, gives rise to color formation (see Figure 1.4). This color change can in turn be measured with

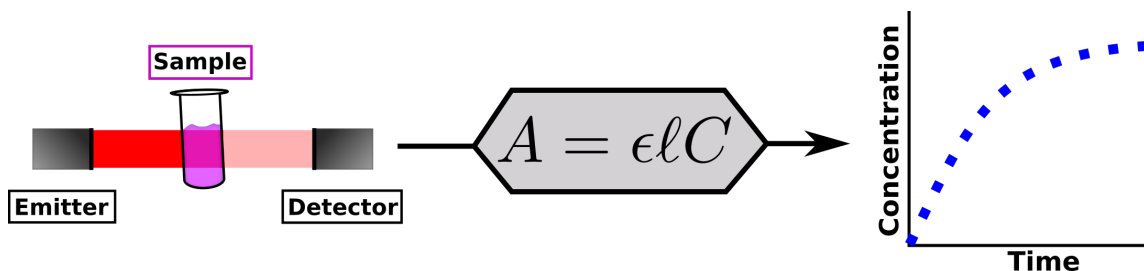


**Figure 1.4: Schematic of Chromogenic Substrate usage in Experiments.** Enzymes cleave the chromogenic substrates and gives rise to color within a sample, which is detectable by the absorption of light at the 405 nm wavelength. The absorbance ( $A$ ) in time is converted to concentration ( $C$ ) using Beer's Law, where  $\epsilon$  is the molar absorptivity of the substrate and  $\ell$  is the path length of the light in the sample.

a spectrophotometer, which records the attenuation of a particular wavelength of light in a medium over time. Because the physical dimensions of the experiment (*i.e.*, the size of the test tube) and the light absorptivity of para-nitroaniline are both constant, any change in the absorbance time-series must be due to changes in the chemical concentration. This idea is formalized in Beer's Law [88],

$$A = \epsilon \ell C, \tag{1.21}$$

where  $A$  is the absorbance,  $\epsilon$  is the molar absorptivity of the chemical compound,  $\ell$  is the path length of the experiment, and  $C$  is the chemical concentration.

Chemical reactions related to blood coagulation are complex phenomena, where a particular enzyme might have several natural targets. In such a system, the addition of an exogenous substrate may result in undesired competition between it and the true enzyme targets [89]. However, the effect is specific to the individual enzyme/substrate pair and may only have limited practical effect on the system [90]. More importantly, the *products* of the cleaved substrate may still interact with the enzyme, causing it to be inhibited in the reaction [91]. This last point, while noted in the literature, has not been rigorously examined. Chapter 2 explores a detailed analysis of the product inhibition resulting from the interaction between a single coagulation enzyme, FXa, and its enzyme specific CS.

## Bibliography

- [1] Yuri Lazebnik. Can a biologist fix a radio? Or, what i learned while studying apoptosis. Cancer cell, 2(3):179–182, 2002.
- [2] George EP Box. Robustness in the strategy of scientific model building. In Robustness in statistics, pages 201–236. Elsevier, 1979.
- [3] Pierre Chelle, Claire Morin, Aurélie Montmartin, Michèle Piot, Michel Cournil, and Brigitte Tardy-Poncet. Evaluation and calibration of in silico models of thrombin generation using experimental data from healthy and haemophilic subjects. Bulletin of mathematical biology, 80(8):1989–2025, 2018.
- [4] Matthew F Hockin, Kenneth C Jones, Stephen J Everse, and Kenneth G Mann. A model for the stoichiometric regulation of blood coagulation. The Journal of biological chemistry, 277(21):18322–33, may 2002.
- [5] Karin Leiderman and Aaron L Fogelson. Grow with the flow: a spatial–temporal model of platelet deposition and blood coagulation under flow. Mathematical medicine and biology: a journal of the IMA, 28(1):47–84, 2011.
- [6] Jim Pitman and Marc Yor. A guide to brownian motion and related stochastic processes. arXiv preprint arXiv:1802.09679, 2018.
- [7] Hermann G Matthies. Quantifying uncertainty: Modern computational representation of probability and applications. In Extreme man-made and natural hazards in dynamics of structures, pages 105–135. Springer, 2007.
- [8] Ralph C Smith. Uncertainty quantification: theory, implementation, and applications, volume 12. Siam, 2013.
- [9] Wei-Liem Loh et al. On latin hypercube sampling. The annals of statistics, 24(5):2058–2080, 1996.
- [10] Fenfen Xiong, Ying Xiong, Steven Greene, Wei Chen, and Shuxing Yang. A new sparse grid based method for uncertainty propagation. In ASME 2009 International Design Engineering Technical Conferences and Computers and Information in Engineering Conference, pages 1205–1215. American Society of Mechanical Engineers, 2009.
- [11] Jerome Sacks, William J Welch, Toby J Mitchell, and Henry P Wynn. Design and analysis of computer experiments. Statistical science, pages 409–423, 1989.
- [12] F Santonja and B Chen-Charpentier. Uncertainty quantification in simulations of epidemics using polynomial chaos. Computational and mathematical methods in medicine, 2012, 2012.
- [13] Dongbin Xiu. Efficient collocational approach for parametric uncertainty analysis. Commun. Comput. Phys, 2(2):293–309, 2007.
- [14] Albert Tarantola. Inverse problem theory and methods for model parameter estimation, volume 89. siam, 2005.

- [15] Johnathan M Bardsley. Computational Uncertainty Quantification for Inverse Problems, volume 19. SIAM, 2018.
- [16] Curtis R Vogel. Computational methods for inverse problems, volume 23. Siam, 2002.
- [17] Youcef Saad and Martin H Schultz. Gmres: A generalized minimal residual algorithm for solving nonsymmetric linear systems. SIAM Journal on scientific and statistical computing, 7(3):856–869, 1986.
- [18] James Vere Beck and Kenneth J Arnold. Parameter estimation in engineering and science. James Beck, 1977.
- [19] Jorge Nocedal and Stephen Wright. Numerical optimization. Springer Science & Business Media, 2006.
- [20] Jari Kaipio and Erkki Somersalo. Statistical and computational inverse problems, volume 160. Springer Science & Business Media, 2006.
- [21] Andrea Saltelli, Stefano Tarantola, Francesca Campolongo, and Marco Ratto. Sensitivity analysis in practice: a guide to assessing scientific models. Chichester, England, 2004.
- [22] Andrew M Stuart. Inverse problems: a Bayesian perspective. Acta numerica, 19:451–559, 2010.
- [23] Luis Tenorio. An introduction to data analysis and uncertainty quantification for inverse problems, volume 3. SIAM, 2017.
- [24] G Alastair Young, Richard L Smith, et al. Essentials of statistical inference, volume 16. Cambridge University Press, 2005.
- [25] M Jesús Bayarri and James O Berger. The interplay of Bayesian and frequentist analysis. Statistical Science, pages 58–80, 2004.
- [26] Walter R Gilks, Sylvia Richardson, and David Spiegelhalter. Markov chain Monte Carlo in practice. Chapman and Hall/CRC, 1995.
- [27] Siddhartha Chib and Edward Greenberg. Understanding the Metropolis-Hastings Algorithm. The American Statistician, 49(4):327–335, 1995.
- [28] Kenneth M Hanson. Markov chain monte carlo posterior sampling with the hamiltonian method. In Medical Imaging 2001: Image Processing, volume 4322, pages 456–468. International Society for Optics and Photonics, 2001.
- [29] Matthew D Hoffman and Andrew Gelman. The no-u-turn sampler: adaptively setting path lengths in hamiltonian monte carlo. Journal of Machine Learning Research, 15(1):1593–1623, 2014.
- [30] Maria Kalli, Jim E Griffin, and Stephen G Walker. Slice sampling mixture models. Statistics and computing, 21(1):93–105, 2011.

- [31] Gareth O Roberts and Jeffrey S Rosenthal. Examples of adaptive mcmc. Journal of Computational and Graphical Statistics, 18(2):349–367, 2009.
- [32] John Geweke et al. Evaluating the accuracy of sampling-based approaches to the calculation of posterior moments, volume 196. Federal Reserve Bank of Minneapolis, Research Department Minneapolis, MN, USA, 1991.
- [33] KERRIE L Mengersen, CHRISTIAN P Robert, and C Guihenneuc-Jouyaux. MCMC convergence diagnostics: a review. Bayesian statistics, 6:415–440, 1999.
- [34] William A Link and Mitchell J Eaton. On thinning of chains in mcmc. Methods in ecology and evolution, 3(1):112–115, 2012.
- [35] Bruno Sudret. Global sensitivity analysis using polynomial chaos expansions. Reliability engineering & system safety, 93(7):964–979, 2008.
- [36] Andrea Saltelli, Marco Ratto, Terry Andres, Francesca Campolongo, Jessica Cariboni, Debora Gatelli, Michaela Saisana, and Stefano Tarantola. Global sensitivity analysis: the primer. John Wiley & Sons, 2008.
- [37] Cosmin Safta, Richard L-Y Chen, Habib N Najm, Ali Pinar, and Jean-Paul Watson. Efficient uncertainty quantification in stochastic economic dispatch. IEEE Transactions on Power Systems, 32(4):2535–2546, 2017.
- [38] DM Hamby. A review of techniques for parameter sensitivity analysis of environmental models. Environmental monitoring and assessment, 32(2):135–154, 1994.
- [39] Dan G Cacuci, CF Weber, EM Oblow, and JH Marable. Sensitivity theory for general systems of nonlinear equations. Nuclear Science and Engineering, 75(1):88–110, 1980.
- [40] T Lenhart, K Eckhardt, N Fohrer, and H-G Frede. Comparison of two different approaches of sensitivity analysis. Physics and Chemistry of the Earth, Parts A/B/C, 27(9-10):645–654, 2002.
- [41] Yang Cao, Shengtai Li, Linda Petzold, and Radu Serban. Adjoint sensitivity analysis for differential-algebraic equations: The adjoint dae system and its numerical solution. SIAM journal on scientific computing, 24(3):1076–1089, 2003.
- [42] G. Deman, K. Konakli, B. Sudret, J. Kerrou, P. Perrochet, and H. Benabderrahmane. Using sparse polynomial chaos expansions for the global sensitivity analysis of groundwater lifetime expectancy in a multi-layered hydrogeological model. Reliability Engineering and System Safety, 147:156–169, 2016.
- [43] Il’ya Meerovich Sobol’. On sensitivity estimation for nonlinear mathematical models. Matematicheskoe modelirovanie, 2(1):112–118, 1990.
- [44] IM Sobol. Global sensitivity indices for nonlinear mathematical models and their monte carlo estimates. Math Comput Simulat, 55(1):271–280, 2001.

- [45] Andrea Saltelli, Paola Annoni, Ivano Azzini, Francesca Campolongo, Marco Ratto, and Stefano Tarantola. Variance based sensitivity analysis of model output. design and estimator for the total sensitivity index. Computer Physics Communications, 181(2):259–270, 2010.
- [46] Art B Owen. Better estimation of small sobol’sensitivity indices. ACM Transactions on Modeling and Computer Simulation (TOMACS), 23(2):11, 2013.
- [47] Graham Glen and Kristin Isaacs. Estimating sobol sensitivity indices using correlations. Environmental Modelling & Software, 37:157–166, 2012.
- [48] IM Sobol. Sensitivity estimates for nonlinear mathematical models. Mathematical Modelling and Computational Experiments, 1(4):407–414, 1993.
- [49] Michiel JW Jansen, Walter AH Rossing, and Richard A Daamen. Monte carlo estimation of uncertainty contributions from several independent multivariate sources. In Predictability and nonlinear modelling in natural sciences and economics, pages 334–343. Springer, 1994.
- [50] GEB Archer, Andrea Saltelli, and IM Sobol. Sensitivity measures, anova-like techniques and the use of bootstrap. Journal of Statistical Computation and Simulation, 58(2):99–120, 1997.
- [51] Max D Morris. Factorial sampling plans for preliminary computational experiments. Technometrics, 33(2):161–174, 1991.
- [52] Franklin C. McLean. Application of the law of chemical equilibrium (law of mass action) to biological problems. Physiological Reviews, 18(4):495—523, 1938.
- [53] Maureane Hoffman and Dougald M Monroe III. A cell-based model of hemostasis. Thrombosis and haemostasis, 85(06):958–965, 2001.
- [54] Cláudia Natália Ferreira, Marinez de Oliveira Sousa, Luci Maria Sant’Ana Dusse, and Maria das Graças Carvalho. A cell-based model of coagulation and its implications. Rev Bras Hematol Hemoter, 32(5):416–421, 2010.
- [55] Stephanie A Smith. The cell-based model of coagulation. Journal of veterinary emergency and critical care, 19(1):3–10, 2009.
- [56] HC Hemker and H Kessels. Feedback mechanisms in coagulation. Haemostasis, 21(4):189–196, 1991.
- [57] Aaron L Fogelson and Keith B Neeves. Fluid Mechanics of Blood Clot Formation. Annual review of fluid mechanics, 47:377–403, jan 2015.
- [58] GJ Tangelder, Harry C Teirlinck, DICK W Slaaf, and ROBERT S Reneman. Distribution of blood platelets flowing in arterioles. American Journal of Physiology-Heart and Circulatory Physiology, 248(3):H318–H323, 1985.

- [59] Satoru Ogawa, Fania Szlam, Tomoko Ohnishi, Ross J Molinaro, Kazuya Hosokawa, and Kenichi A Tanaka. A comparative study of prothrombin complex concentrates and freshfrozen plasma for warfarin reversal under static and flow conditions. Thrombosis and haemostasis, 106(12):1215–1223, 2011.
- [60] Marcus D Lancé. A general review of major global coagulation assays: thrombelastography, thrombin generation test and clot waveform analysis. Thrombosis journal, 13(1):1, 2015.
- [61] Kathryn G Link, Michael T Stobb, Jorge Di Paola, Keith B Neeves, Aaron L Fogelson, Suzanne S Sindi, and Karin Leiderman. A local and global sensitivity analysis of a mathematical model of coagulation and platelet deposition under flow. PloS one, 13(7):e0200917, 2018.
- [62] Scott L Diamond. Systems biology of coagulation. Journal of Thrombosis and Haemostasis, 11:224–232, 2013.
- [63] A Modepalli Susree and B Mohan Anand. Reaction mechanisms and kinetic constants used in mechanistic models of coagulation and fibrinolysis. Mathematical Modelling of Natural Phenomena, 11(6):71–90, 2016.
- [64] HC Hemker, S Kerdelo, and RMW Kremers. Is there value in kinetic modeling of thrombin generation? no (unless...). J Thromb Haemost, 10(8):1470–1477, 2012.
- [65] T Bodnár and A Sequeira. Numerical simulation of the coagulation dynamics of blood. Computational and Mathematical Methods in Medicine, 9(2):83–104, 2008.
- [66] Aaron L Fogelson and Robert D Guy. Platelet–wall interactions in continuum models of platelet thrombosis: formulation and numerical solution. Mathematical Medicine and Biology, 21(4):293–334, 2004.
- [67] Kenneth C Jones and Kenneth G Mann. A model for the tissue factor pathway to thrombin. ii. a mathematical simulation. Journal of Biological Chemistry, 269(37):23367–23373, 1994.
- [68] Zhiliang Xu, Nan Chen, Malgorzata M Kamocka, Elliot D Rosen, and Mark Alber. A multiscale model of thrombus development. Journal of the Royal Society Interface, 5(24):705–722, 2007.
- [69] Saulius Butenas, Cornelis vanÁcÁÁŽt Veer, and Kenneth G Mann. ÁcÁÁIInormalÁcÁÁÁ thrombin generation. Blood, 94(7):2169–2178, 1999.
- [70] S.D. Bungay, P.A. Gentry, and R.D. Gentry. A mathematical model of lipid-mediated thrombin generation. Math Med and Biol, 20(1):105–129, 2003.
- [71] Matthew F Hockin, Kenneth C Jones, Stephen J Everse, and Kenneth G Mann. A model for the stoichiometric regulation of blood coagulation. Journal of Biological Chemistry, 277(21):18322–18333, 2002.
- [72] Julia Riedl, Cihan Ay, and Ingrid Pabinger. Platelets and hemophilia: A review of the literature. Thrombosis research, 155:131–139, 2017.

- [73] Andrew L Kuharsky and Aaron L Fogelson. Surface-mediated control of blood coagulation: the role of binding site densities and platelet deposition. Biophysical journal, 80(3):1050–1074, 2001.
- [74] Aaron L Fogelson and Nessay Tania. Coagulation under flow: the influence of flow-mediated transport on the initiation and inhibition of coagulation. Pathophysiology of haemostasis and thrombosis, 34(2-3):91–108, 2005.
- [75] Aaron L Fogelson, Yasmeen H Hussain, and Karin Leiderman. Blood clot formation under flow: the importance of factor xi depends strongly on platelet count. Biophysical journal, 102(1):10–18, 2012.
- [76] Karin Leiderman, William C Chang, Mikhail Ovanesov, and Aaron L Fogelson. Synergy between tissue factor and exogenous factor xia in initiating coagulation. Arteriosclerosis, thrombosis, and vascular biology, pages ATVBAHA–116, 2016.
- [77] Priscilla Elizondo and Aaron L Fogelson. A mathematical model of venous thrombosis initiation. Biophysical journal, 111(12):2722–2734, 2016.
- [78] Donat R Spahn, Bertil Bouillon, Vladimir Cerny, Timothy J Coats, Jacques Duranteau, Enrique Fernández-Mondéjar, Daniela Filipescu, Beverley J Hunt, Radko Komadina, Giuseppe Nardi, et al. Management of bleeding and coagulopathy following major trauma: an updated european guideline. Critical care, 17(2):R76, 2013.
- [79] Massimo Franchini and Pier Mannuccio Mannucci. Past, present and future of hemophilia: a narrative review. Orphanet journal of rare diseases, 7(1):24, 2012.
- [80] Paula HB Bolton-Maggs and K John Pasi. Haemophilias a and b. The lancet, 361(9371):1801–1809, 2003.
- [81] Gilbert C II White, Frits Rosendaal, Louis M Aledort, Jeanne M Lusher, Chantal Rothschild, and Jørgen Ingerslev. Definitions in hemophilia. Thrombosis and haemostasis, 85(03):560–560, 2001.
- [82] H Pollmann, H Richter, H Ringkamp, and H Jürgens. When are children diagnosed as having severe haemophilia and when do they start to bleed? a 10-year single-centre pup study. European journal of pediatrics, 158(3):S166–S170, 1999.
- [83] Guy Young. New challenges in hemophilia: long-term outcomes and complications. ASH Education Program Book, 2012(1):362–368, 2012.
- [84] Jenny Gold. Miracle of hemophilia drugs comes at a steep price. National Public Radio, Mar 2018.
- [85] Massimo Franchini and Pier Mannuccio Mannucci. Modifiers of clinical phenotype in severe congenital hemophilia. Thrombosis research, 156:60–64, 2017.
- [86] Bernard F Erlanger, Nicholas Kokowsky, and William Cohen. The preparation and properties of two new chromogenic substrates of trypsin. Archives of biochemistry and biophysics, 95(2):271–278, 1961.

- [87] MJ Gallimore and P Friberger. Chromogenic peptide substrate assays and their clinical applications. Blood reviews, 5(2):117–127, 1991.
- [88] D. F. Swinehart. The Beer-Lambert Law. Journal of Chemical Education, 39(7):333, jul 1962.
- [89] S Butenas and KG Mann. Caution in the interpretation of continuous thrombin generation assays. Journal of Thrombosis and Haemostasis, 5(5):1084–1085, 2007.
- [90] HC Hemker and E De Smedt. Caution in the interpretation of continuous thrombin generation assays: a rebuttal. Journal of Thrombosis and Haemostasis, 5(5):1085–1086, 2007.
- [91] Hendrik Coenraad Hemker. Handbook of synthetic substrates. Springer Science & Business Media, 2012.

## Chapter 2

# Assessing the Significance of Product Inhibition In Chromogenic Assays (Journal Article)

This chapter originally published as “**Stobb, M.T.**, Monroe, D.M., Sindi, S.S., Leiderman, K. (2019). *Assessing the Significance of Product Inhibition In Chromogenic Assays*. Analytical Biochemistry.” Reprinted in accordance with the Creative Commons Attribution 4.0 International License (<http://creativecommons.org/licenses/by/4.0/>) with some changes for continuity. The co-authors listed in this publication directed and supervised research which formed the basis for the dissertation. Physical experiments were performed by DMM.

### 2.1 Abstract

Chromogenic substrates (CS) are synthetic substrates used to monitor the activity of a target enzyme. It has been reported that some CSs display competitive product inhibition with their target enzyme. Thus, in assays where enzyme activity is continuously monitored over long periods of time, the product inhibition may significantly interfere with the reactions being monitored. Despite this knowledge, it is rare for CSs to be directly incorporated into mathematical models that simulate these assays. This devalues the predictive power of the models. In this study, we examined the interactions between a single enzyme, coagulation factor Xa, and its chromogenic substrate. We developed, and experimentally validated, a mathematical model of a chromogenic assay for factor Xa that explicitly included product inhibition from the CS. We employed Bayesian inference, in the form of Markov-Chain Monte Carlo, to estimate the strength of the product inhibition and other sources of uncertainty such as pipetting error and kinetic rate constants. Our model, together with carefully calibrated biochemistry experiments, allowed for full characterization of the strength and impact of product inhibition in the assay. The effect of CS product inhibition in more complex reaction mixtures was further explored using mathematical models.

## 2.2 Introduction

Blood coagulation is a complex biochemical process in which dozens of plasma proteins take part in a series of enzymatic reactions. The reactions culminate in the generation of thrombin, an enzyme necessary for clot stabilization *in vivo*. One indicator of how well blood will clot is its ability to generate thrombin. Assays to measure thrombin generation are common to both clinical and research laboratories, used to monitor individuals clotting potential, study treatments for bleeding disorders, and test anticoagulant drugs [1–5]. These assays measure thrombin through a synthetic reporter whereby thrombin cleavage of either a chromogenic [6–8] or fluorogenic [9, 10] substrate is monitored. The coagulation network is inherently nonlinear with multiple positive and negative feedback loops, which can make its thrombin generation response challenging to predict. Blood samples from two individuals, that contain varying levels of plasma proteins, may give different results in thrombin generation assays in the presence of an anticoagulant drug, but similar results in its absence [11]. Since thrombin cleavage of a synthetic substrate is the sole output from these assays that have dozens of inputs, it is difficult to determine a mechanism underlying the observed differences using thrombin generation assays alone. Additional assays can be performed to measure activity of coagulation enzymes that aid in thrombin generation, e.g., coagulation factor Xa [12] or IXa [13]. Mathematical models can also be used, as an alternative to or in addition to experimental assays, to address such challenges in predicting coagulation responses. In particular, mathematical models are used to numerically simulate the desired enzyme and all other proteins or protein complexes within the assay, so that underlying biochemical mechanisms can be explored theoretically.

Multiple mathematical models exist to simulate coagulation reactions; our group has developed models of platelet surface-mediated coagulation under flow [14–19] to simulate microfluidic assays [20–22] and others have been developed to simulate static thrombin generation assays in the presence of phospholipid vesicles [23–27] and platelets [28]. Some existing models of static thrombin generation assays have been used to address questions with clinical relevance, e.g., to investigate normal variations of clotting factors in healthy individuals [11, 29], complications of trauma and coagulopathies [30, 31], and to assess the risk of disease [32].

The outputs from mathematical models, however, are only as trustworthy as the assumptions underlying the model. For example, models of coagulation and thrombin generation rely on numerous assumptions regarding biochemical reaction schemes, kinetic rate constants, and experimental noise in the assays that they are meant to simulate. To complicate things even further, thrombin generation simulated with different existing mathematical models may give contrasting results, even when using the same initial concentrations of plasma proteins [33]. For a model to be truly predictive and accurately simulate coagulation reactions and perturbations, it must be carefully validated with the experiments that it simulates and any additional sources of uncertainty should be identified and quantified.

In general, validating a model of enzyme reactions will consist of comparing a single model output (one enzyme concentration) to absorbance or fluorescence data from an experimental assay; the experimental readout is a measure of synthetic substrate cleavage by the enzyme. Since synthetic substrates both bind directly to their target enzyme and are known to exhibit product inhibition (product from the cleaved substrate rebinds to the enzyme) [34–36], their presence interferes with the reactions that they monitor. However,

synthetic substrates are not explicitly included in mathematical models, except in a few cases [12, 28]. In the current study, we carefully examine one synthetic substrate, a chromogenic substrate specific for coagulation factor Xa, to better understand and quantify its role both within a reaction mixture and within a mathematical model.

Chromogenic substrates (CS) are comprised of a peptide attached to a chemical group, p-nitroaniline (pNA), which is released after cleavage by a target enzyme and consequently gives rise to color [36]. Enzyme activity in the reaction mixture is then measured via photo-spectrometry. The progress curve (measured absorbance) is proportional to the proteolytic activity of the enzyme; the first derivative of the progress curve is related to the enzyme concentration. To obtain the desired enzyme concentration throughout the timecourse of the reaction, the data is manipulated; the raw absorbance is transformed into a concentration curve for the product (pNA) by a scaling that depends on the kinetics of the CS and certain assay conditions [37], a numerical derivative is applied to this curve and this results in an approximation to the enzyme concentration. However, this is only a good approximation while the intact CS concentration is much higher than the enzyme concentration.

Chromogenic substrates are used in different ways, but are common for measuring kinetic rate constants of single enzymatic reactions and also for continuously monitoring more complex reactions such as those involved in blood coagulation. When CSs are used to estimate kinetic rate constants, the data measured during the early part of the reactions is often the only data used; the rate of the reaction (velocity) is estimated from the slope of the progress curve, which is linear during the early stages of a single enzyme reaction. Kinetic rate constants are then determined by analyzing the saturation curve that relates the estimated velocities with various initial substrate concentrations [36, 38, 39].

Using data from the full progress curves, rather than using the initial rates alone, is known to yield more accurate estimates of kinetic rate constants. With this method, instead of differentiating the scaled absorbance data, one integrates a mathematical model that tracks the concentrations of the reactants and products, and explicitly incorporates CS [40, 41]. When CSs exhibit product inhibition, the reactions and kinetic rates describing the inhibition should be included in the mathematical model, even when modeling simple, steady state reactions [40, 42, 43]; since the full progress curves monitor the experiments for long periods of time, and CS product is continuously being cleaved during that time, then inhibition from the CS product may be increasingly significant in the assay. For continuous monitoring of complex reactions that include multiple enzymes and inhibitors, and run for long periods of time, such as coagulation reactions, the significance of CS interference has not been rigorously established.

The objective of this study was to carefully examine product inhibition of a CS specific for coagulation factor Xa, the enzyme that cleaves prothrombin into thrombin. We sought to i) determine if the CS truly exhibited product inhibition, ii) estimate the kinetic schemes and rates that described the product inhibition, and iii) better understand the impact of incorporating the product inhibition into mathematical models. We used a combination of mathematical modeling, statistical inference, and experimental biochemistry to characterize product inhibition of the CS. We used model selection to determine which of two potential mathematical models would best describe the reactions within a simple chromogenic assay; one model included production inhibition and one did not. We found that, while it was possible to numerically simulate accurate progress curves with both models, including product inhibition provided a statistically significant improvement to the fit. To validate

our hypothesis that product inhibition was exhibited by the CS, we developed a novel validation experiment using excess cleaved CS product; only the model with product inhibition was consistent with this experiment. We then used a mathematical model to simulate concentrations of reactants that cannot be measured experimentally. We found that, even in a simple reaction, a mathematical model that does not include production inhibition from CS overestimates the amount of free factor Xa. In a more complex reaction that allows for generation and inactivation of factor Xa, the same model underestimates the amount of factor Xa bound to CS and its product and additionally overestimates the amount of factor Xa inactivated by antithrombin.

## 2.3 Materials and Methods

### 2.3.1 Experimental Procedures

All solutions were prepared in buffer containing 20 *mM* 4-(2-Hydroxyethyl)piperazine-1-ethanesulfonic acid (pH 7.4), 150 *mM* sodium chloride, 0.2% polyethylene glycol. All reactions were run in Falcon 96 well U-bottom microtiter plates. Absorbances were measured at 405 nm in a Molecular Devices ThermoMax microplate reader. Factor Xa was purchased from Enzyme Research Labs (South Bend, IN) and repurified by pseudo-affinity chromatography [44]. Antithrombin was purified from plasma as described previously using polyethyleneglycol (PEG) precipitation of plasma followed by heparin Sepharose chromatography, and ion exchange chromatography was used to remove traces of heparin [45]. Antithrombin activity was determined by thrombin inhibition assay using the second order rate constant of  $4 \times 10^4 \text{ M}^{-1} \text{ sec}^{-1}$  [46]. Factor Xa substrate (methoxycarbonyl-D-cyclohexylalanyl-glycyl-arginine para-nitroanilide) was purchased from PentaPharm (Basel, Switzerland).

#### Standard chromogenic assay

For each concentration of factor Xa, a working solution was prepared at twice the final concentration. Fifty  $\mu\text{L}$  of this solution was added to the wells of a microtiter plate. Fifty  $\mu\text{L}$  of buffer was also added to separate wells of a microtiter plate. One working solution for each concentration of substrate was prepared at twice the final concentration. Fifty  $\mu\text{L}$  of substrate was added to 50  $\mu\text{L}$  of enzyme or buffer. Substrate was added with a multichannel pipetter so that each row of the microtiter plate was started at the same time. The microtiter plate was arranged so that each row represented a concentration of enzyme (or buffer control). Absorbance at 405 nm was measured as a function of time.

#### Antithrombin inhibition assay

Factor Xa (125 nM) was incubated either in buffer or with 1.25 mM substrate for 2 hours at room temperature. Preliminary studies had shown that 2 hours was sufficient to cleave all the substrate to product. Antithrombin was added to factor Xa to give: factor Xa - 100 nM; antithrombin - 3200 nM; product 1 mM or none. At timed intervals the reaction was diluted 1:10 into fresh substrate to give: factor Xa - 10 nM; antithrombin - 320 nM; product - 100  $\text{\AA}\text{tM}$  or none; substrate - 500  $\text{\AA}\text{tM}$ . Cleavage of substrate was monitored at

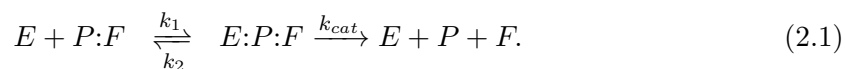
405 nm and the rate of substrate cleavage converted into a concentration of residual factor Xa.

### 2.3.2 Conversion of Absorbance to Concentration

Since the output from the mathematical models are in units of concentration, we converted the raw absorbance data to concentration for direct comparison. This conversion involves an initial subtraction of background absorbance and an application of Beer’s Law. The background absorbance from the microtiter plate is approximately 0.034 at 405 nm, estimated with linear regression applied to absorbance data collected in the absence of reactants (data not shown). This background absorbance was subtracted from all future experimental data. Beer’s Law was used to convert from absorbance to concentration [37], where the extinction coefficient for p-nitroaniline was  $9920 M^{-1}cm^{-1}$  [47] and the pathlength was calculated by measuring the absorbance of a known concentration of p-nitroaniline. We verified that the concentrations of substrate we used were in a range such that Beer’s law is still valid with the conditions and the microtiter plate reader. The absorbance readings remained linear below substrate concentrations of approximately 600  $\mu$ M (data not shown).

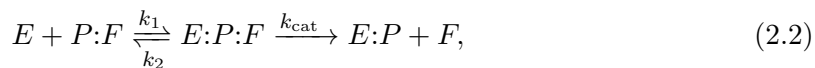
### 2.3.3 Kinetic Schemes

We assume potential kinetic schemes to describe the reactions between factor Xa and its chromogenic substrate. The first is the Null scheme, described as a single enzyme cleaving a single substrate into two products:



Here, the enzyme  $E$  represents the activated coagulation protein, factor Xa, the substrate  $P:F$  is the intact chromogenic substrate Pefachrome-FXa, and the products  $P$  and  $F$  are the peptide and the cleaved para-nitroanalide (pNA), respectively.

To allow for product inhibition, we modified the Null scheme to include a reversible reaction between the enzyme,  $E$ , and cleaved CS product,  $P$ , where the off rate of this reaction is assumed to be proportional to the off rate of the binding of intact CS to enzyme. This Alternative scheme is described as follows:



The parameter,  $\alpha$ , is the constant of proportionality that controls the ‘strength’ of the product inhibition. If  $\alpha \rightarrow 1$ , the  $P$  and  $P:F$  have equal binding affinity for the enzyme, and the Null model is recovered as  $\alpha \rightarrow \infty$ . In practice, however, we found that much smaller values of  $\alpha$  can numerically approximate the Null model.

### Naive Model

The Naive model considers the Null scheme (2.1) with the kinetic rates supplied by the CS manufacturer: ( $k_{cat} = 140s^{-1}$ ) and a Michaelis-Menten constant ( $K_M = 106\mu$ M) to

describe the CS kinetics. The Michaelis-Menten constant is also defined in terms of the other rates as  $K_M = (k_{cat} + k_2)/k_1$ . Assuming the reaction mixture has sufficiently high concentrations that are well combined, we apply the law of mass action [48] to derive a system of ordinary differential equations (ODEs) for all species' concentrations:

$$\begin{aligned}
\frac{d[E]}{dt} &= -k_1[E][P:F] + (k_2 + k_{cat})[E:P:F], \\
\frac{d[P:F]}{dt} &= -k_1[E][P:F] + k_2[E:P:F], \\
\frac{d[E:P:F]}{dt} &= k_1[E][P:F] - (k_2 + k_{cat})[E:P:F], \\
\frac{d[P]}{dt} &= k_{cat}[E:P:F] \\
\frac{d[F]}{dt} &= k_{cat}[E:P:F],
\end{aligned} \tag{2.4}$$

where  $[\cdot]$  represents concentration. Only enzyme and substrate have nonzero initial concentrations, denoted by  $E_0$  and  $P:F_0$ , and set to 5 nM and 400  $\mu$ M, respectively. The kinetic rates  $k_1$  and  $k_2$  are unspecified but are dependent on one another through  $K_M$  and  $k_{cat}$ . We varied the ratio  $k_1/k_2$  and observed no difference in model output (not shown) and thus, in all subsequent analysis,  $k_1$  is held fixed at  $10\mu\text{M}^{-1}\text{s}^{-1}$ , and  $k_2$  is computed via  $k_2 = k_1K_M - k_{cat}$ . Numerical solutions to the Naive model (2.4) and initial concentrations were calculated with numerical integrator, CVODE-BDF [49].

### The Null Model: Incorporating Uncertainty

Uncertainty was considered in pipetting to account for pipetting error, in initial concentration of CS and pNa to account for previous hydrolysis, and in kinetic rate constants. Error in pipetting occurs in every experiment (including replicates) and thus may be different for each experiment. However, because each experimental replicate employs the same stock solution, we assume the uncertain fraction of hydrolyzed CS is common to all experiments. Finally, since the experiments are performed simultaneously with identical enzyme preparation, the kinetic rates are assumed common to all experiments. Uncertainties were included in the model above by allowing  $K_M$  and  $k_{cat}$  to vary as distributions instead of point values, and by allowing the initial concentrations of the CS and enzyme to vary, also as distributions, to account for both pipetting error and hydrolysis, each of which have a distinct contribution. The ODE system from the Naive Model (2.4) with these uncertainties incorporated becomes our Null Model:

$$\begin{aligned}
\frac{d[E]}{dt} &= -k_1[E][P:F] + (\mathbf{k}_2 + \mathbf{k}_{cat})[E:P:F], \\
\frac{d[P:F]}{dt} &= -k_1[E][P:F] + \mathbf{k}_2[E:P:F], \\
\frac{d[E:P:F]}{dt} &= k_1[E][P:F] - (\mathbf{k}_2 + \mathbf{k}_{cat})[E:P:F], \\
\frac{d[P]}{dt} &= \mathbf{k}_{cat}[E:P:F] \\
\frac{d[F]}{dt} &= \mathbf{k}_{cat}[E:P:F],
\end{aligned} \tag{2.5}$$

with initial conditions

$$\begin{aligned}
[E]_0 &= \mathbf{U}_p(E_0), \\
[P:F]_0 &= (1 - \mathbf{U}_h)\mathbf{U}_p(P:F_0), \\
[E:P:F]_0 &= 0, \\
[P]_0 &= \mathbf{U}_h\mathbf{U}_p(P:F_0), \\
[F]_0 &= \mathbf{U}_h\mathbf{U}_p(P:F_0),
\end{aligned} \tag{2.6}$$

where bolded symbols represent distributions rather than single values. Specifically,  $\mathbf{k}_2 = k_1\mathbf{K}_M - k_{\text{cat}}$  and  $\mathbf{k}_{\text{cat}}$  are distributions on the kinetic parameters (in practice  $k_2$  is not directly varied, but rather  $K_M$  and  $k_{\text{cat}}$ ),  $\mathbf{U}_h$  is the distribution for the fraction of hydrolyzed CS, and  $\mathbf{U}_p(\cdot)$  are distributions for the initial enzyme and CS concentration due to pipetting error.

### The Alternative Model: Incorporating Product Inhibition

The Alternative Model consists of the ODEs that result from applying the law of mass action to the Alternative scheme (2.2), and incorporating uncertainty in the same way as with the Null Model. Thus the Alternative Model consists of the following equations:

$$\begin{aligned}
\frac{d[E]}{dt} &= -k_1[E][P:F] + \mathbf{k}_2[E:P:F] + \alpha\mathbf{k}_2[E:P], \\
\frac{d[P:F]}{dt} &= -k_1[E][P:F] + \mathbf{k}_2[E:P:F], \\
\frac{d[E:P:F]}{dt} &= k_1[E][P:F] - (\mathbf{k}_2 + \mathbf{k}_{\text{cat}})[E:P:F], \\
\frac{d[E:P]}{dt} &= \mathbf{k}_{\text{cat}}[E:P:F] + k_1[E][P] - \alpha\mathbf{k}_2[E:P], \\
\frac{d[P]}{dt} &= \mathbf{k}_{\text{cat}}[E:P:F] - k_1[E][P] + \alpha\mathbf{k}_2[E:P], \\
\frac{d[F]}{dt} &= \mathbf{k}_{\text{cat}}[E:P:F],
\end{aligned} \tag{2.7}$$

with initial conditions

$$\begin{aligned}
[E]_0 &= \mathbf{U}_p(E_0), \\
[P:F]_0 &= (1 - \mathbf{U}_h)\mathbf{U}_p(P:F_0), \\
[E:P:F]_0 &= 0, \\
[E:P]_0 &= 0, \\
[P]_0 &= \mathbf{U}_h\mathbf{U}_p(P:F_0), \\
[F]_0 &= \mathbf{U}_h\mathbf{U}_p(P:F_0),
\end{aligned} \tag{2.8}$$

where again bolded symbols represent distributions. The alternative Model has all the same parameter distributions with the addition of  $\alpha$ , which controls the strength of the product inhibition.

### 2.3.4 Uncertainty Propagation

The uncertain inputs, represented as distributions instead of single values, propagate through the models and result in output distributions (see Figure 2.1). These output distributions are estimated by Monte-Carlo sampling the input distributions and solving the model ODEs 10,000 times. Statistics (e.g., mean and standard deviation) are then calculated from the output distributions. For each time point, the model output distribution was determined to be approximately normal (not shown).

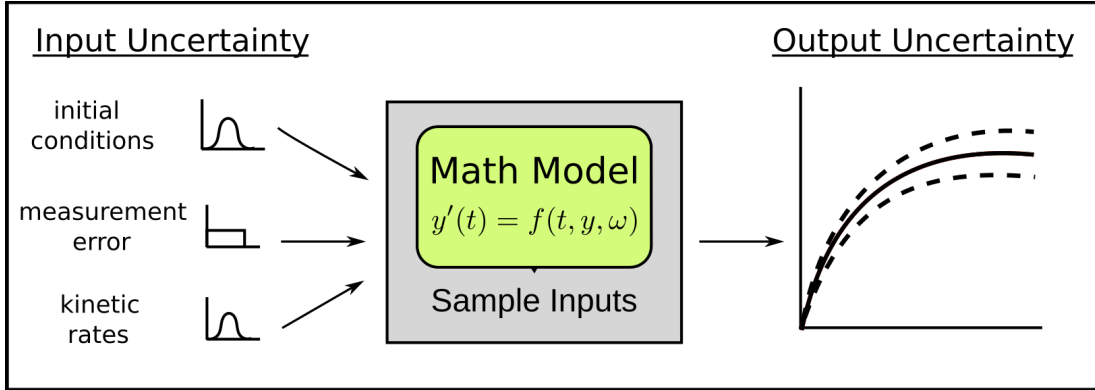


**Figure 2.1: Uncertainty Propagation.** In our mathematical framework we consider how uncertainties in model inputs (left), such as substrate hydrolysis ( $U_h$ ), pipetting error, and reported kinetic rates ( $K_M$  &  $k_{cat}$ ) are propagated into uncertainties in model outputs (right). For simplicity, inputs are monte-carlo sampled from their distributions and the model solved, yielding an approximation of the output distribution.

### 2.3.5 MCMC Estimation of Parameters

We employ a Bayesian framework [50] for estimating the uncertain parameters  $K_M$ ,  $k_{cat}$ ,  $U_h$ , and  $U_p$  (for enzyme and CS) for a total of  $3 + 2R$  learned parameters, where  $R$  is the number of experimental replicates. The Bayesian approach generates a distribution for each parameter rather than a single point estimate, which is propagated directly through the forward model. The posterior distribution for the parameters is given by Bayes' theorem

$$\pi(\theta|D_{i,j,k}) \propto \pi(D_{i,j,k}|\theta) \pi(\theta), \quad (2.9)$$

where  $D_{i,j,k}$  is the experimental data at time  $i$ , from initial enzyme concentration  $j$ , and initial CS concentration  $k$ ,  $\theta$  is the vector of parameters,  $\pi(D_{i,j,k}|\theta)$  is the likelihood of the data given the parameters, and  $\pi(\theta)$  is the prior distribution of the parameters (discussed below). An adaptive Metropolis-Hastings algorithm [50, 51] is used to numerically compute the posterior distributions given the aforementioned experimental uncertainties. We verified that for the given prior distributions, the model output distribution is approximately normally-distributed (see Figure 2.2), even when model inputs were sampled uniformly. This motivated the use for a Normal likelihood function:

$$\mathcal{L}(y_{i,j,k}(\theta)|D_{i,j,k}) = \prod_{i=1}^N \frac{1}{\sqrt{2\pi\sigma_i^2}} e^{-\frac{(y_{i,j,k}(\theta) - D_{i,j,k})^2}{2\sigma_i^2}}, \quad (2.10)$$

where  $y_{i,j,k}(\theta)$  is the ODE model solution at time  $i$  with initial enzyme concentration  $j$  and initial CS concentration  $k$  with parameters  $\theta$ , and  $\sigma_i^2$  is the variance at time  $i$  of the full forward model, solved using the assumed prior distributions of the parameters. These time dependent  $\sigma$  values control for the observed change in variance as time increases.

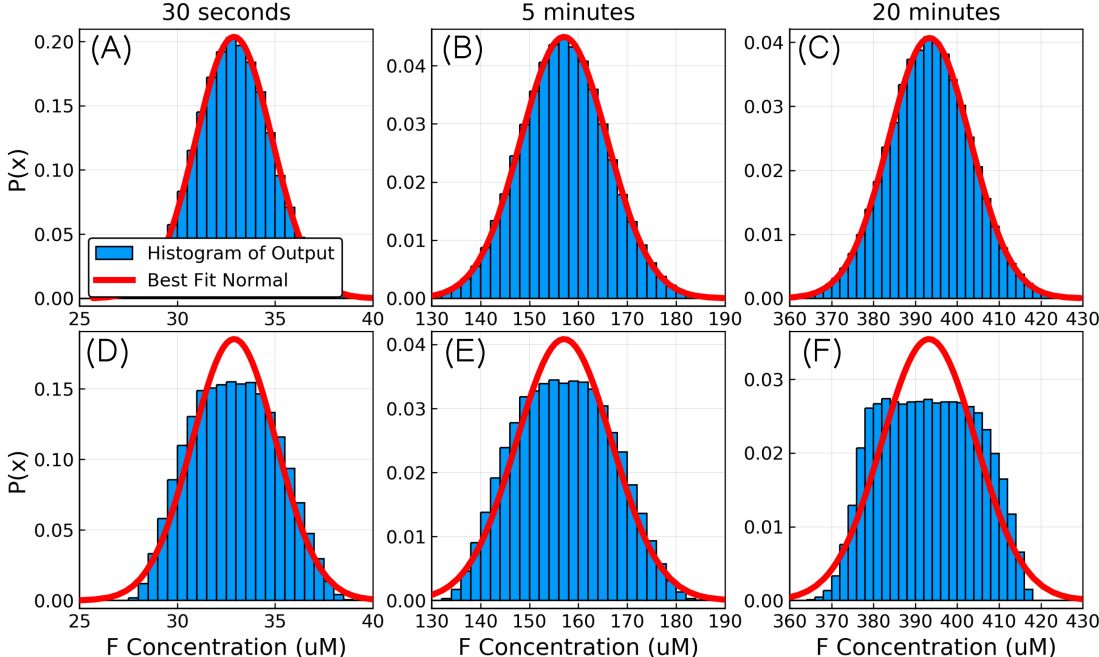


**Figure 2.2: Determination of output distribution.** Model output (blue histograms) and best fitting normal distribution (red line) at three different times: 30 seconds (A,D), 5 minutes (B,E), and 20 minutes (C,F) generated by sampling ( $N=100,000$ ) the input parameters of the forward model given in equations (2.5) and (2.6) with the prior distributions from Table 2.1 (A-C) and with Uniform distributions (D-F).

### Prior Distributions for Uncertain Parameters

We used manufacturer provided information and best practice experimental procedures to select prior distributions for the unknown, uncertain parameters (see Table 2.1). Because the manufacturer does not provide data used to derive their kinetic parameters,  $K_M$  and  $k_{cat}$ , we were unable to directly infer the uncertainty in their reported estimates. For simplicity, we set their prior distributions as normal distributions centered at the manufacturer reported value with a standard deviation set to allow a 95% confidence interval of the distribution to span a range of  $\pm 10\%$  of the parameter. Thus the prior distributions were set as  $K_M \sim N(106 \mu M, 5 \mu M)$  and  $k_{cat} \sim N(140 s^{-1}, 7.5 s^{-1})$ , noting that the posterior distributions were not highly sensitive to this choice of variance. Substrate hydrolysis ( $U_h$ ) is unknown but assumed to be small. Fitting the model with a standard least squares method yielded results for hydrolysis around 2.5% (not shown), so we used a non-informative prior distribution of uniform between 0-20%. The prior distribution for the pipetting errors of the initial concentration of enzyme and CS,  $Up(E_0)$  and  $Up(P:F_0)$ , were set as normal distributions centered at 0% with a standard deviation of 2.5%. We set

the prior distribution for  $\alpha$  as a non-informative uniform  $U(0,10)$ .

## Sampling the Posterior Distributions

The Geweke diagnostic [52], with default parameters, was used to determine that burn-in had successfully occurred after 500,000 steps. The parameter covariance was adapted for the first 100,000 steps and held fixed afterwards. Approximately 10 million steps were recorded and thinned, resulting in a total of approximately 50,000 sample points. Forward model evaluations employed parameter samples taken from the complete joint posterior distribution, unless otherwise noted. While individually the parameter’s posterior distributions were approximately normal, a strong correlation between some parameters ruled out sampling them independently for forward evaluations.

## Model Selection

We used both Akaike’s Information Criterion (AIC) and the Bayesian Information Criterion (BIC) to compare the Null and Alternative models listed above [53]. The equations for each are given by

$$\text{AIC} = 2k - 2\ln(\hat{\mathcal{L}}) \quad (2.11)$$

$$\text{BIC} = \ln(N)k - 2\ln(\hat{\mathcal{L}}), \quad (2.12)$$

where  $k$  is the number of fit parameters,  $\hat{\mathcal{L}}$  is the likelihood of the data at the best fit model values, and  $N$  is the sample size.

## 2.4 Results and Discussion

We performed a simple chromogenic assay in which fixed quantities of the enzyme, factor Xa (E), and its chromogenic substrate (CS) are allowed to react. We considered two kinetic schemes to describe the reactions within the assay: the Null and Alternative kinetic schemes; the difference being that the Alternative scheme included product inhibition from the CS. To determine the best mathematical description of the reactions, we used three mathematical model approaches: i) a Naive mathematical model based on the Null kinetic scheme, using kinetic rates reported by the CS manufacturer, ii) the Null model based on the Null kinetic scheme and statistically inferring kinetic rates and sources of experimental uncertainty, and iii) the Alternative model based on the Alternative kinetic scheme and statistically inferring kinetic rates and sources of experimental uncertainty. Support for one of the three models was experimentally validated with a multistage, continuous-monitoring experiment. Finally, using our validated Alternative model, we theoretically explored various concentrations of reactant species in the assays that go unmonitored in the experiment, e.g., true free enzyme concentration.

### 2.4.1 Naive Model Does Not Quantitatively Agree with CS Assay

We tested if a mathematical model, based on the Null kinetic scheme Equation (2.1), employing either the kinetic rate constants reported by the CS manufacturer or rate constants

determined by analyzing the initial rate of substrate cleavage at various substrate concentrations (Figure 2.3), would provide quantitative agreement with experiments in which a fixed amount of factor Xa and its CS react over time. For the experiment, cleavage of 400  $\mu\text{M}$  CS by 5 nM of factor Xa was continuously monitored. Figure 2.3 shows the measured absorbance (at 405 nm), converted to concentration using Beer’s law (see section on Conversion of Absorbance to Concentration), compared to the analogous species, F, that is produced with the mathematical model. The kinetic rates reported by the manufacturer, using different buffer conditions than these studies, for parameters are  $K_M = 106 \mu\text{M}$  and  $k_{\text{cat}} = 140\text{s}^{-1}$ . The parameters determined by the initial rate studies are  $K_M = 129 \mu\text{M}$  and  $k_{\text{cat}} = 79\text{s}^{-1}$ . As shown in Figure 2.3, the concentration of F produced with the

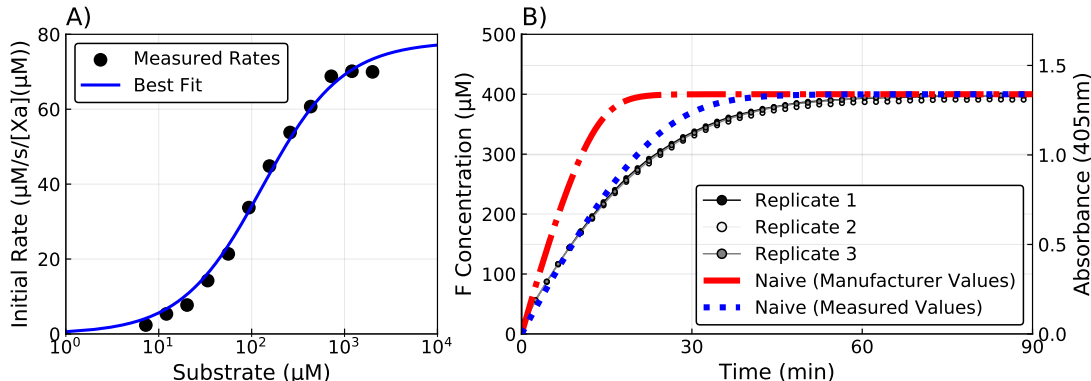


**Figure 2.3: Naive mathematical model based on the Null kinetic scheme compared with experimental data.** For each concentration of substrate, the initial rate of substrate cleavage was determined from the plot of product formation as a function of time (black points). Fitting the data to the Michaelis-Menten equation (blue) gave an estimated  $K_M = 129 \mu\text{M}$  and  $k_{\text{cat}} = 78\text{s}^{-1}$ . B) The absorbance data (grey) and concentration of F output from the mathematical model using the manufacturer supplied kinetic rates of  $k^- = 106 \mu\text{M}$  and  $k^{\text{cat}} = 140\text{s}^{-1}$  (red) and experimentally measured rates (blue) in units of absorbance (right axis) and concentration (left axis) for experiments with 5 nM of factor Xa using the Null kinetic scheme (2.1), with no uncertainty assumed in the initial conditions or model parameters.

mathematical model (red and blue) does not quantitatively agree with the experimental absorbance data (grays), with an average relative error of 18.5% and 6.6%, respectively. The mathematical model predicts a faster rate of cleavage than that observed experimentally, significantly more so for the model using the manufacturer rates. The lack of quantitative agreement in such a simple system suggests that either the scheme on which the mathematical model depends is incomplete, the kinetic rate constants are uncertain, or there are sources of experimental uncertainty that must be accounted for.

#### 2.4.2 Null Model: Introducing Uncertainty

We developed a mathematical and statistical framework that considers uncertainty in the kinetic rate constants and experimental conditions. In this framework, the mathematical model was based on the Null kinetic scheme so that the lack of quantitative agreement

between experimental and mathematical model outputs is assumed to come only from inaccurate kinetic rates or experimental conditions. We assumed that potential sources of experimental noise were due to pipetting error and substrate hydrolysis that occurred prior to the experiment. We incorporated these sources of noise into the mathematical model by considering them as uncertain parameter distributions, rather than point values. We then employed a Bayesian approach to infer the parameter distributions from the experiments: each uncertain parameter was assumed to have an uninformed prior distribution and, upon propagation of these distributions through the mathematical model and using the likelihood of the experimental data, we learned posterior distributions (schematic of this process in Figure 2.1); see section on MCMC Estimation of Parameters for details on the parameter inference procedure. The prior distributions (grey) and the histograms of the corresponding posterior distributions (orange) for the Michealis-Menten constant,  $K_M$ , the catalytic rate,  $k_{cat}$ , and the percent substrate hydrolysis,  $U_h$  are shown in Figure 2.4B-D, respectively, with means and standard deviations listed in Table 2.1.

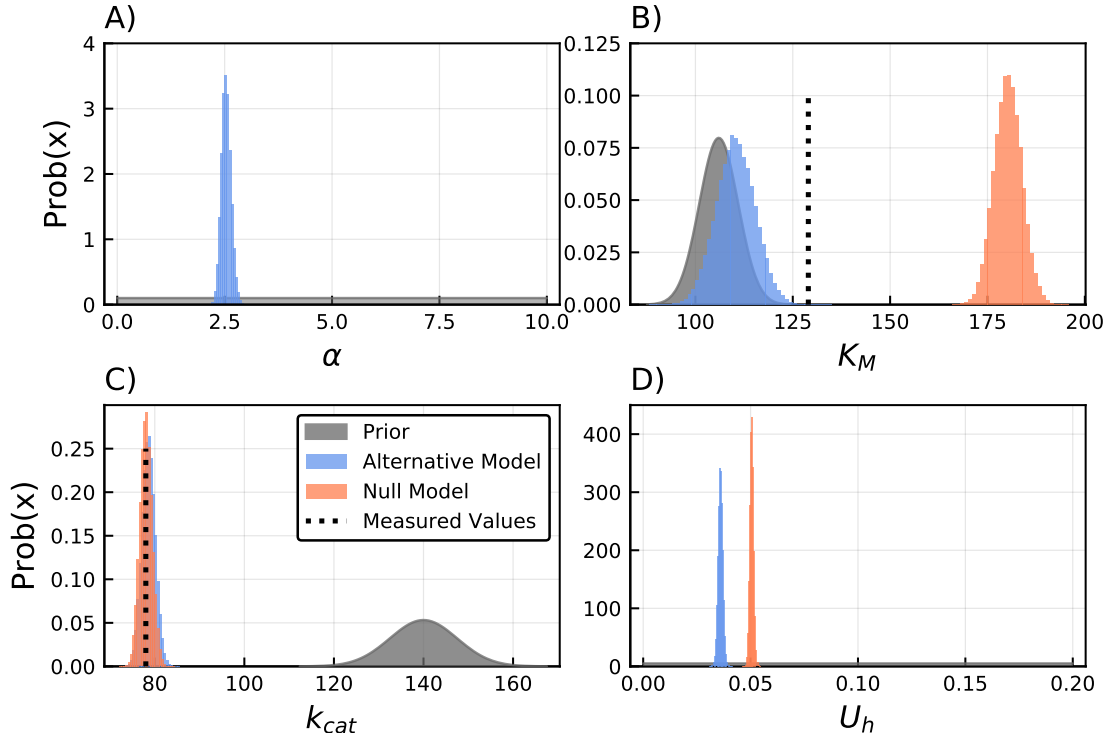


**Figure 2.4: Prior and Posterior distributions for  $\alpha$ ,  $K_M$ ,  $k_{cat}$ , and hydrolysis.** Prior (grey) and Posterior (histograms) distributions for  $K_M$ ,  $k_{cat}$ , and hydrolysis for both the Null (orange) and Alternative (blue) Model. The priors for the kinetic rates were chosen such that a 95% confidence interval about the mean would be within  $\pm 10\%$  of the manufacturer reported values. The prior for  $\alpha$  and  $U_h$  was set as maximum entropy distributions, specifically uniform between 0 and 10, and uniform between 0 and 0.2, respectively. Posterior distributions were computed using a Metropolis-Hastings algorithm with approximately  $5.0 \times 10^4$  samples (after burnin and thinning). Black dashed bars show the measured kinetic parameters from initial rate experiments.

The parameter distribution learning procedure supported a non-zero value for initial hy-

drolysis ( $5.1 \% \pm 0.1 \%$ ), showing hydrolysis was non-negligible. The mean of the posterior distribution for  $K_M$  was approximately 75% higher than that reported by the manufacturer, and the  $k_{cat}$  was estimated to be approximately 50% lower. While it is possible the observed difference in  $k_{cat}$  could indicate a loss in enzyme activity over time, the basis for the observed difference in  $K_M$  is less clear.

Figure 2.5 shows the experimental data (gray) and the distribution of the concentration of F from Null model (orange). The Null model F distribution appears to be only a single curve because the posterior parameter distributions were very tight around their means; in the figure we plot the mean along with a 95% credibility interval, represented by the shaded region. There is a significant improvement in quantitative agreement between the data and the Null Model over that of the Naive Model (compare Fig 2.5 (red) to Fig 2.3), with an average error of 4.4% (down from 24.4%). However, because the estimated kinetic rates were so different from the reported kinetic rates, the validity of the Null Model still rests on the possibility that the values reported by the manufacturer are incorrect. Alternatively, the reported values could be correct, but the kinetic scheme could be incomplete, leaving the possibility of an alternative scheme.

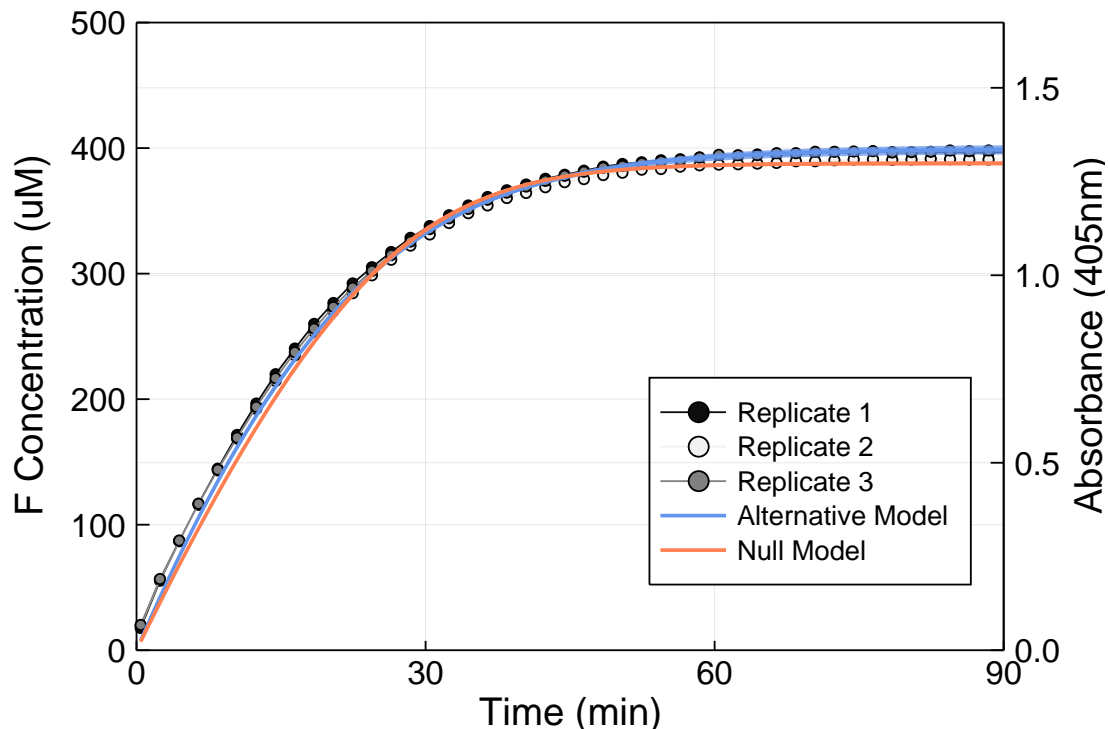


**Figure 2.5: MCMC fitted models compared with data.** The Null (orange) and Alternative (blue) model results are shown with the experimental data from 2.3 (circles). The models were fit using an MCMC procedure and produce a distribution in time, which was estimated by sampling the input variables according to their posterior distribution. From this a 95% credibility interval (slight shaded regions) was constructed for each point in time.

**Table 2.1: Model parameters and their distributions.** Prior and Posterior estimates of unknown parameters for both the Null and Alternative models. \*Because there were several individual initial concentrations measured, we only report here the overall average pipetting error for all cases.

| Parameter     | Prior                                | Null<br>(mean±std)  | Alternative<br>(mean±std) |
|---------------|--------------------------------------|---------------------|---------------------------|
| $K_M$         | $N(106.0\mu M, 5.0\mu M)$            | $180.3\pm 3.6\mu M$ | $110.4\pm 5.0\mu M$       |
| $k_{cat}$     | $N(140.0s^{-1}, 7.5s^{-1})$          | $78.1\pm 1.4s^{-1}$ | $78.7\pm 1.5s^{-1}$       |
| $k_1$         | Fixed at $10\mu M^{-1}s^{-1}$        | N/A                 | N/A                       |
| $k_2$         | Fixed at $(K_M \cdot k_1) - k_{cat}$ | N/A                 | N/A                       |
| $U_h$         | $N(0\%, 20\%)$                       | $5.1\%\pm 0.1\%$    | $3.6\%\pm 0.1\%$          |
| $\alpha$      | $U(0.0, 10.0)$                       | N/A                 | $2.5\pm 0.1$              |
| $Up(P:F_0)^*$ | $N(0\%, 2.5\%)$                      | $-3.0\%\pm 0.8\%$   | $-0.7\%\pm 0.9\%$         |
| $Up(E_0)^*$   | $N(0.0\%, 2.5\%)$                    | $-2.1\%\pm 1.6\%$   | $-2.1\%\pm 1.6\%$         |

### 2.4.3 Alternative Model: Including Product Inhibition

Because the posterior estimate for  $K_M$  deviated so far from manufacturer reported values, we considered the Alternative kinetic scheme Equation (2.2) that includes product inhibition of the enzyme. We assumed the binding rate of enzyme to the cleaved CS product and to the intact CS was equivalent; the off-rate of the enzyme from the cleaved CS product was then multiplied by non-dimensional parameter,  $\alpha$ , such that  $\alpha = 1$  gives equivalent dissociation constants for the product and intact CS, i.e., strong product inhibition, and increasing  $\alpha$  weakens the product inhibition. Dynamics of the Null model are recovered as  $\alpha \rightarrow \infty$ .

We considered uncertainty in pipetting error, substrate hydrolysis, and kinetic rates and learned new posterior distributions for each, assuming the same prior distributions as in the previous section. Because no prior estimates were available for  $\alpha$ , we considered a non-informative (uniform) prior distribution between 0 and 10. We used the same framework for parameter estimation for the Alternative model as we did for the Null Model. The output distribution for the concentration of F, generated with the Alternative Model, is shown in Fig 2.5 (blue), along with the mean of the output and a 95% credibility interval. While both models fit the experimental data extremely well, the Alternative Model (blue) had a decreased average relative error of 2.8%, down from 4.4% average relative error for the Null model.

The prior and posterior distributions for  $\alpha$  and the kinetic parameters are shown in Figure 2.4 (blue), with means and standard deviations listed in Table 2.1. The uninformed prior for  $\alpha$  was converted to a very tight posterior distribution ( $2.5\pm 0.1$ ), indicating strong statistical support for the presence of product inhibition. Moreover, inclusion of product inhibition led to significantly better agreement between the prior and posterior distributions of  $K_M$ , which suggests that the manufacturer reported value is consistent with our experiments under the assumptions of the Alternative Model.

While the Alternative Model has a lower relative error rate than the Null Model (orange

and blue in Fig 2.5), it also contains an additional parameter. To determine if the improvement in model fit was statistically significant, or merely due to the additional complexity in the Alternative Model, we performed a model selection test. The goal of such tests is to choose among different models by calculating a quantity that penalizes the likelihood of the data by the complexity of the model. We calculated the Akaike’s Information Criterion (AIC) and the Bayesian Information Criterion (BIC) for both the Null and Alternative Model, evaluated at the mean of their posterior distributions. Both metrics penalize the likelihood of the data with the complexity of the model, resulting in the Alternative model and its one extra parameter ( $\alpha$ ) having a greater penalty. For either criteria, the difference between the tested models gives evidence for statistical support, not the absolute numerical value, where the model with the lower value is preferred. Observing a difference greater than 10 indicates very strong statistical preference for the model with the lower value [54]. The differences between the models were computed as  $AIC_{Null} - AIC_{Alt} = 764.35$  and  $BIC_{Null} - BIC_{Alt} = 757.15$ . Thus, by either metric, we find statistical support for neglecting the Null model in favor of the Alternative model even with the added parameter  $\alpha$  and considering agreement/disagreement with manufacturer reported values of  $k_{cat}$ .

#### 2.4.4 Alternative Model with Production Inhibition is Experimentally Validated

We developed a two stage experiment to directly test our prediction of product inhibition from cleaved CS product. First, factor Xa was incubated with antithrombin, and with either 1 mM cleaved CS product (See section on Experimental Procedures) or no CS at all. Second, subsamples from each mixture were taken at timed intervals, diluted into intact CS, and monitored continuously, to measure the residual factor Xa that was not inactivated by antithrombin. The experiment was designed so that the subsamples from both initial mixtures, i.e., the one with CS product and the one with no CS, would result in the same amount of CS cleavage in the second stage, if there was no product inhibition. Thus, the initial velocities of each reaction in stage two would be identical, as they are proportional to factor Xa bound to CS. This is not what was observed. Figure 2.6 shows estimates of factor Xa bound to CS at timed intervals, where the initial rates from each timed subsample was converted to concentration of factor Xa bound to CS by dividing by  $k_{cat}$ . We have also plotted the analogous output distributions (E:PF) from the Alternative model (blue) and the Null model (orange) for each of the experimental conditions. The data in Figure 2.6 shows i) the resulting E:PF from the Null model is in poor agreement with the experimental data, and ii) the resulting E:PF from the Alternative model is in excellent agreement with the experiment, seen with the credibility intervals around the mean, and iii) disparate concentrations of factor Xa bound to CS between the two experimental conditions, which strongly supports the notion of experimentally-validated product inhibition.

#### 2.4.5 Further Impact of Product Inhibition: A Theoretical Investigation

In the previous sections we demonstrated that product inhibition is present in reactions with factor Xa and its CS. We also showed that, in an experiment with a fixed level of factor Xa and its CS, both the Null model and Alternative model provided strong quantitative agreement with both the absorbance data and one another, albeit with dissimilar kinetic rates. We want to know how other species within the reaction mixture were impacted by the

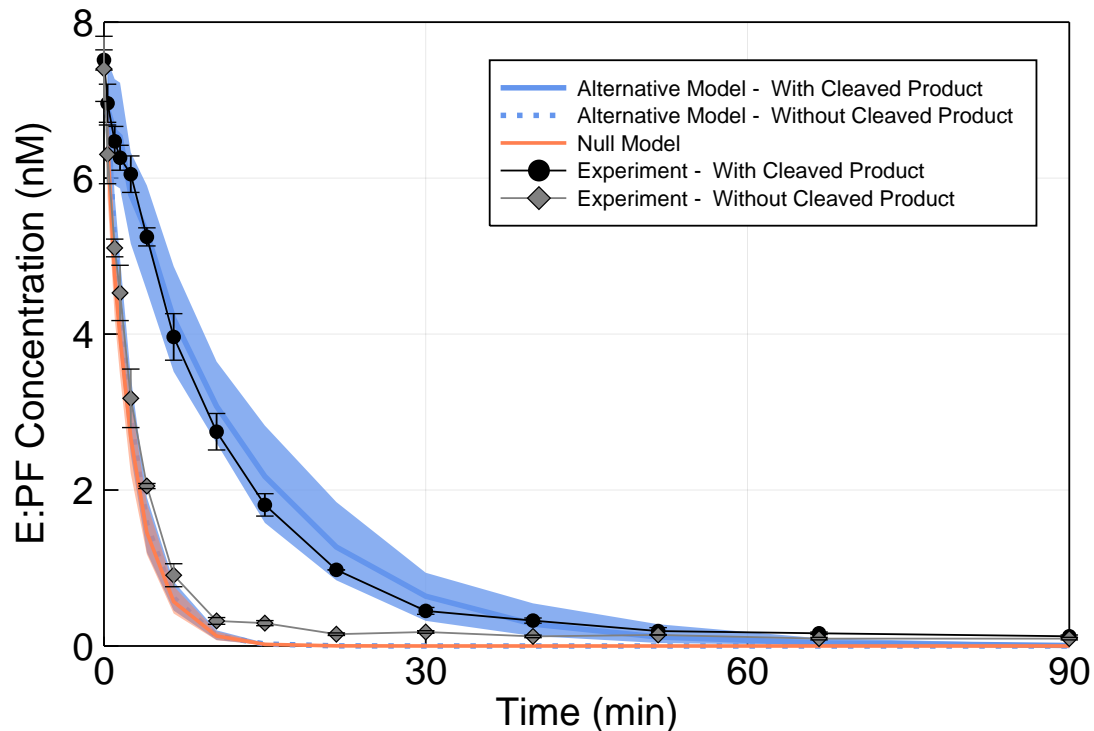


**Figure 2.6: Estimated E:PF concentrations with model comparisons.** Initial rates of product formation from the antithrombin inhibition experiments gives an estimate of the concentration of E:PF in the system (black/grey), with and without previously cleaved substrate. The experiment was simulated using both the Null (orange) and Alternative (blue) models. Uncertainty in the experiment arises from differences in replicates, while the uncertainty in the model is due to pipetting error, hydrolysis, and uncertain kinetic rates, all estimated from the data using a likelihood approach.

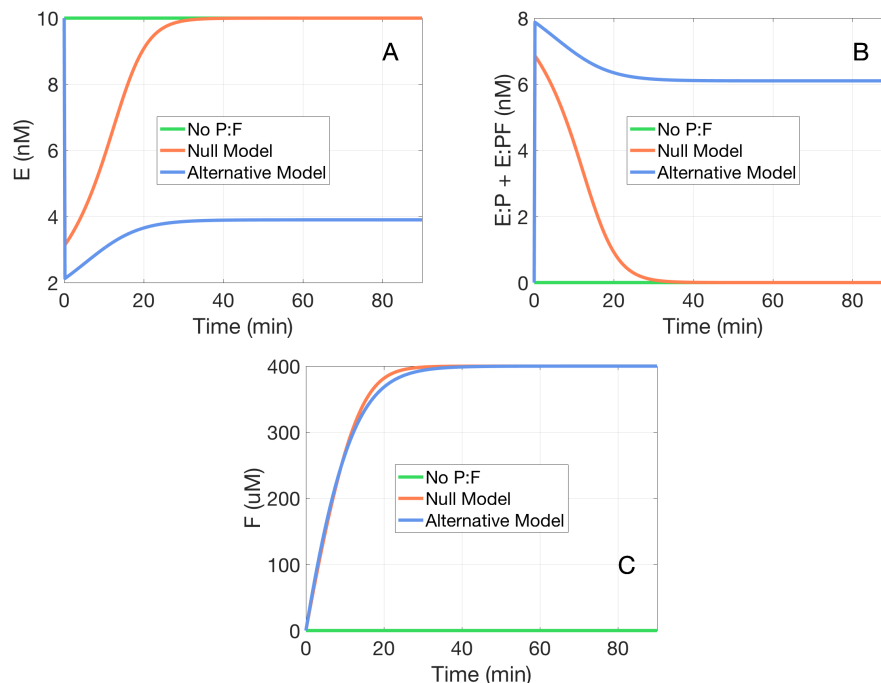
model choice and, when simulating more complex reactions, how much this choice matters. To investigate this, we used the Null model and Alternative model, with parameters fixed to the means from the estimated posterior distributions, and looked at intermediate species from our simple chromogenic assay reaction described above. We then used both models to simulate a reaction in which factor Xa is generated by the enzyme complex TF:VIIa and inactivated by antithrombin.

Figure 2.7 shows simulations of the experiment with fixed levels of Xa and CS. Panel A shows free factor Xa that is not bound to CS (E – free enzyme, available to bind other species) panel B shows the factor Xa that is bound to CS or CS product (E:P and E:PF – enzyme not available to bind anything else), and panel C shows the concentration of F, which we directly compare to absorbance, as shown previously. In each panel, we show the concentrations of each species generated with the Null model in the absence of CS (green), with the Null model in the presence of CS (orange), and with the Alternative model in the presence of CS (blue). The concentrations of F are roughly the same for the two models (panel C), but the resulting free enzyme, E, is drastically different (panel A). The Null model suggests that most of E is bound to P:F initially (E drops from 10 nM to 3 nM) but that it is all free again after about 40 minutes when all the CS has been cleaved; the Alternative model suggests that product inhibition shifts the equilibrium such that only about 38% of the enzyme is free (panel A) and the rest is bound to P or P:F (panel B). Simulations of this simple reaction with the two models show that the model choice leads to significantly different interpretations of the underlying reactions within the assay.

Next we considered a reaction in which factor Xa (E) was generated by TF:VIIa and also inactivated by antithrombin. We were motivated by an experiment originally conducted by Lu et al. [55] in which 170 nM factor X and 4.5  $\mu$ M antithrombin were added to a reaction mixture with 0.2 nM TF:VIIa. Factor Xa concentrations were measured by subsampling, rather than continuous monitoring, which removes the possibility of production inhibition. Thus, we have performed simulations without CS for comparison to this experiment. (Note that this should be considered as the 'true' reaction, with no interference from synthetic substrates.) The green curves in Figure 2.8 show the concentrations corresponding to the kinetic scheme and rates reported in their study, in the absence of CS, and with the antithrombin concentration adjusted to the physiologic level of 3.2  $\mu$ M. Factor Xa concentration peaks around five minutes and is completely inactivated by about 30 minutes. Comparing the results for the Null and Alternative models to these 'true' results is more interesting. With the Null and Alternative models, we used the same kinetic rates for the activation of X by TF:VIIa as in the no CS case, but used the means of our estimated distributions for all other kinetic rates.

Figure 2.8 shows the concentrations of free enzyme, E, bound enzyme (E:P + E:PF), pNA (F), and enzyme inactivated by antithrombin (E:AT), in panels A-D, respectively. Interestingly, the concentrations of F are indistinguishable between the Null versus the Alternative model (see panel C). This means that both models would be considered 'validated' against experimental data if validation included the single comparison of F to absorbance data. However, investigation of other reactant concentrations tells a different story.

The presence of CS is clearly shown to interfere with the reactions, as seen by the differing levels of free enzyme between the three simulations (compare orange and blue curve to the green curve in panel A). However, results from the Null model and Alternative model lead to different interpretations of the underlying reactions. The Null model overestimated



**Figure 2.7: Concentrations of reactants in fixed-enzyme assay, generated by numerical simulation.** Numerically computed concentrations of enzyme (A), enzyme bound to CS and CS product (B), pNA (C). Results are produced with the Null Model in the absence (green) and presence (orange) of CS, and with the Alternative model (blue). Initial concentrations were 5 nM factor Xa and 400  $\mu\text{M}$  CS; kinetic rates were set to the means of the posterior distributions estimated in this study.

the true peak of E by 17.5% (peak of 47 nM compared to 40 nM with no CS) due to less E being inactivated by antithrombin during the first 8 minutes of the reaction (panel D) because it was bound to P:F (panel B). The Alternative model underestimated the true peak of E by 30% (peak of 28 nM compared to 40 nM with no CS), and the peak was also delayed by about 2 minutes (panel A). This is because in the Alternative model, the CS product competes with antithrombin for free enzyme; thus, a considerable amount of E is protected from inactivation because it is bound to CS (compare blue to orange curve in panel B) and as a result, there is less free E.

## 2.5 Conclusion

In this study, we used a combined experimental, mathematical, and statistical approach to examine the effects of product inhibition in reactions containing a CS and its target enzyme, coagulation factor Xa. We developed two mathematical models based on distinct kinetic schemes, one with product inhibition and one without. Next we used a Bayesian approach to estimate parameter distributions for each model, based on the likelihood of experimental data. We found that both models with their estimated parameter distributions could provide simulations consistent with the experimental data, although we found statis-

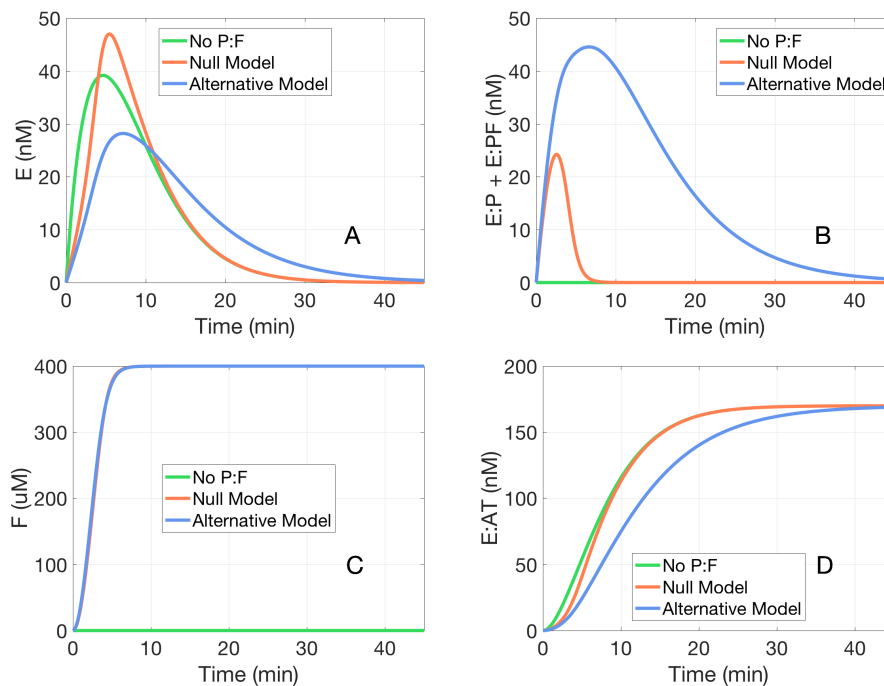


**Figure 2.8: Concentrations of reactants in enzyme generation assay, generated by numerical simulation.** Numerically computed concentrations of enzyme (A), enzyme bound to CS and CS product (B), pNA (C), and enzyme inactivated by antithrombin (D). Results are produced with the Null Model in the absence (green) and presence (orange) of CS, and with the Alternative model (blue). Initial concentrations were 0.2 nM TF:VIIa, 170 nM factor X, 3.2  $\mu$ M antithrombin, and 400  $\mu$ M CS; kinetic rates for TF:VIIa activation of FX were  $K_M = 230$  nM,  $k_{cat} = 4.6/s$ , and antithrombin inactivation was  $1.96 \times 10^3/Ms$  [55], all other kinetic rates were set to the means of the posterior distributions estimated in this study.

tically significant support for product inhibition. We designed a novel experiment which provided validation of our product inhibition model. Finally, to better inform the choice of mathematical model when simulating simple and complex reaction mixtures, we reported all concentrations that were output from the two models, including those that cannot be measured experimentally. Outputs from the two models that represented a measurable quantity (analogous to absorbance data) were indistinguishable; however, other quantities showed significantly different behavior between the two models. Both models indeed showed that the synthetic substrate strongly interferes with the reactions. We found that, when simulating a reaction where an enzyme is generated and inactivated, a mathematical model that does not account for product inhibition will seriously overestimate the amount of free enzyme in the system and underestimate the amount of inactivation. If the enzyme plays multiple, important roles when included in a more complex reaction, such as the roles of factor Xa in thrombin generation, our study suggests that the enzyme’s synthetic substrate, its kinetic schemes and corresponding rates must be carefully examined before comparing output from corresponding mathematical models and absorbance data from experiments. In particular, we found that when studying the characteristics of CSs, the following procedures

were useful for independently assessing the experimental uncertainty: i) using experimental replicates rather than technical replicates, ii) running experiments with buffer only, iii) running experiments with CS only and iv) running control experiments to complete substrate conversion.

## Bibliography

- [1] H Coenraad Hemker, Raed Al Dieri, and Suzette Béguin. Thrombin generation assays: accruing clinical relevance. Cur Opin Hematol, 11(3):170–175, 2004.
- [2] JJ Van Veen, A Gatt, and M Makris. Thrombin generation testing in routine clinical practice: are we there yet? Br J Haematol, 142(6):889–903, 2008.
- [3] Hugo ten Cate. Thrombin generation in clinical conditions. Thromb Res, 129(3):367–370, 2012.
- [4] Gines Escolar, Victor Fernandez-Gallego, Eduardo Arellano-Rodrigo, Jaume Roquer, Joan Carles Reverter, Victoria Veronica Sanz, Patricia Molina, Irene Lopez-Vilchez, Maribel Diaz-Ricart, and Ana Maria Galan. Reversal of apixaban induced alterations in hemostasis by different coagulation factor concentrates: significance of studies in vitro with circulating human blood. PLoS One, 8(11):e78696, 2013.
- [5] Iqbal H Jaffer, Alan R Stafford, James C Fredenburgh, Richard P Whitlock, Noel C Chan, and Jeffrey I Weitz. Dabigatran is less effective than warfarin at attenuating mechanical heart valve-induced thrombin generation. Journal of the American Heart Association, 4(8):e002322, 2015.
- [6] H Coenraad Hemker and Suzette Béguin. Thrombin generation in plasma: its assessment via the endogenous thrombin potential. Thromb Haemost, 73(01):134–138, 1995.
- [7] G. A. Allen, A.S. Wolberg, J.A. Oliver, H.R. Hoffman, M.and Roberts, and D.M. Monroe. Impact of procoagulant concentration on rate, peak and total thrombin generation in a model system. J Thromb Haem, 2(3):402–413, 2004.
- [8] Harold R Roberts, Maureane Hoffman, and Dougald M Monroe. A cell-based model of thrombin generation. In Seminars in thrombosis and hemostasis, volume 32, pages 032–038, 2006.
- [9] HC Hemker, P Giesen, R AlDieri, V Regnault, E De Smed, R Wagenvoord, T Lecompte, and S Beguin. The calibrated automated thrombogram (cat): a universal routine test for hyper-and hypocoagulability. Pathophysiol Haemost Thromb, 32(5-6):249–253, 2002.
- [10] H Coenraad Hemker, Peter Giesen, Raed Al Dieri, Vronique Regnault, Eric De Smedt, Rob Wagenvoord, Thomas Lecompte, and Suzette Béguin. Calibrated automated thrombin generation measurement in clotting plasma. Pathophysiol Haemos Thromb, 33(1):4–15, 2003.
- [11] Christopher M Danforth, Thomas Orfeo, Stephen J Everse, Kenneth G Mann, and Kathleen E Brummel-Ziedins. Defining the boundaries of normal thrombin generation: investigations into hemostasis. PloS One, 7(2):e30385, 2012.
- [12] Jen-Yea Chang, Pichika Chantrathammachart, Dougald M Monroe, and Nigel S Key. Studies on the mechanism of action of the aptamer bax499, an inhibitor of tissue factor pathway inhibitor. Thromb Res, 130(3):e151–e157, 2012.

- [13] Bruce Sullenger, Rebecca Woodruff, and Dougald M Monroe. Potent anticoagulant aptamer directed against factor ixa blocks macromolecular substrate interaction. Journal of Biological Chemistry, 287(16):12779–12786, 2012.
- [14] Andrew L Kuharsky and Aaron L Fogelson. Surface-mediated control of blood coagulation: the role of binding site densities and platelet deposition. Biophysical journal, 80(3):1050–1074, 2001.
- [15] Aaron L Fogelson and Nessay Tania. Coagulation under flow: the influence of flow-mediated transport on the initiation and inhibition of coagulation. Pathophysiology of haemostasis and thrombosis, 34(2-3):91–108, 2005.
- [16] Aaron L Fogelson, Yasmeen H Hussain, and Karin Leiderman. Blood clot formation under flow: the importance of factor xi depends strongly on platelet count. Biophysical journal, 102(1):10–18, 2012.
- [17] K. Leiderman and A.L. Fogelson. Grow with the flow: a spatial-temporal model of platelet deposition and blood coagulation under flow. Math Med Biol, 28:47–84, 2011.
- [18] K. Leiderman and A.L. Fogelson. The influence of hindered transport on the development of platelet thrombi under flow. Bull of Math Biol, 75(8):1255–1283, 2013.
- [19] Leiderman, K., W Chang, M Ovanesov, and A.L. Fogelson. Synergy between tissue factor and factor XIa in initiating coagulation. Arterioscl Thromb Vasc Biol, 36:2334–2345, 2016.
- [20] U. Okorie, W.S. Denney, M.S. Chatterjee, K.B. Neeves, and S.L. Diamond. Determination of surface tissue factor thresholds that trigger coagulation at venous and arterial shear rates: Amplification of 100 fM circulating tissue factor by flow. Blood, 111:3507–13, 2008.
- [21] A.A. Onasoga-Jarvis, Leiderman, K., A.L. Fogelson, M. Wang, M.J. Manco-Johnson, J.A. Di Paola, and K.B. Neeves. The effect of factor viii deficiencies and replacement and bypass therapies on thrombus formation under venous flow conditions in microfluidic and computational models. PLoS One, 8(11):e78732, 2013.
- [22] RM Schoeman, K Rana, N Danes, M Lehmann, JA Di Paola, AL Fogelson, K Leiderman, and KB Neeves. A microfluidic model of hemostasis sensitive to platelet function and coagulation. Cell Mol. Bioeng., 10(1):3–15, 2017.
- [23] M. E. Nesheim, R. P. Tracy, and K. G. Mann. ‘Clotspeed’, a mathematical simulation of the functional properties of prothrombinase. J Biol Chem, 259:1447–1453, 1984.
- [24] M.F. Hockin, K.C. Jones, S.J. Everse, and K. G. Mann. A model for the stoichiometric regulation of blood coagulation. J Biol Chem, 277:18322–18333, 2002.
- [25] KC Jones and K. G. Mann. A model for the Tissue Factor pathway to thrombin. II. A mathematical simulation. J Biol Chem, 269:23367–73, 1994.
- [26] Saulius Butenas, Cornelis van’t Veer, and Kenneth G. Mann. “normal” thrombin generation. Blood, 94(7):2169–2178, 1999.

- [27] S.D. Bungay, P.A. Gentry, and R.D. Gentry. A mathematical model of lipid-mediated thrombin generation. Math Med and Biol, 20(1):105–129, 2003.
- [28] M.S. Chatterjee, W.S. Denney, H. Jing, and S.L. Diamond. Systems biology of coagulation initiation: Kinetics of thrombin generation in resting and activated human blood. PLoS Comput Biol, 6, 2010.
- [29] K Brummel-Ziedins, CY Vossen, FR Rosendaal, K Umezaki, and KG Mann. The plasma hemostatic proteome: thrombin generation in healthy individuals. J Thromb Haemost, 3(7):1472–1481, 2005.
- [30] Alexander Y Mitrophanov, Frits R Rosendaal, and Jaques Reifman. Computational analysis of intersubject variability and thrombin generation in dilutional coagulopathy. Transfusion, 52(11):2475–2486, 2012.
- [31] Alexander Y Mitrophanov, Frits R Rosendaal, and Jaques Reifman. Computational analysis of the effects of reduced temperature on thrombin generation: the contributions of hypothermia to coagulopathy. Anesth Analg, 117(3):565–574, 2013.
- [32] K Brummel-Ziedins. Models for thrombin generation and risk of disease. J Thromb Haemost, 11:212–223, 2013.
- [33] HC Hemker, S Kerdelo, and RMW Kremers. Is there value in kinetic modeling of thrombin generation? no (unless...). J Thromb Haemost, 10(8):1470–1477, 2012.
- [34] S Butenas and KG Mann. Caution in the interpretation of continuous thrombin generation assays. J Thromb Haemost, 5(5):1084–1085, 2007.
- [35] HC Hemker and E De Smedt. Caution in the interpretation of continuous thrombin generation assays: a rebuttal. J Thromb Haemost, 5(5):1085–1086, 2007.
- [36] Hendrik Coenraad Hemker. Handbook of synthetic substrates. Springer Science & Business Media, 2012.
- [37] D. F. Swinehart. The Beer-Lambert Law. Journal of Chemical Education, 39(7):333, jul 1962.
- [38] Victor Henri. Lois générales de l’action des diastases. Librairie Scientifique A. Hermann, 1903.
- [39] Kenneth A Johnson and Roger S Goody. The original michaelis constant: translation of the 1913 michaelis–menten paper. Biochemistry, 50(39):8264–8269, 2011.
- [40] Ronald G. Duggleby. Quantitative analysis of the time courses of enzyme-catalyzed reactions. Methods, 24(2):168–174, June 2001.
- [41] Basil Perdicakis, Heather J Montgomery, J Guy Guillemette, and Eric Jervis. Validation and characterization of uninhibited enzyme kinetics performed in multiwell plates. Analytical Biochemistry, 332(1):122–136, 2004.

- [42] Anna Tanka-Salamon, Kiril Tenekedjiev, Raymund Machovich, and Krasimir Kolev. Suppressed catalytic efficiency of plasmin in the presence of long-chain fatty acids: Identification of kinetic parameters from continuous enzymatic assay with monte carlo simulation. FEBS J, 275(6):1274–1282, 2008.
- [43] Joris Messens, José C Martins, Elke Brosens, Karolien Van Belle, Doris M Jacobs, Rudolph Willem, and Lode Wyns. Kinetics and active site dynamics of staphylococcus aureus arsenate reductase. J Biol Inorg Chem, 7(1-2):146–156, 2002.
- [44] SC Betty Yan, Pam Razzano, Y Bernice Chao, Jenna D Walls, David T Berg, Don B McClure, and Brain W Grinnell. Characterization and novel purification of recombinant human protein c from three mammalian cell lines. Nature Biotechnology, 8(7):655, 1990.
- [45] Michael J Griffith, CM Noyes, and FC Church. Reactive site peptide structural similarity between heparin cofactor ii and antithrombin iii. J Biol Chem, 260(4):2218–2225, 1985.
- [46] JC Rau, LM Beaulieu, JA Huntington, and Frank C Church. Serpins in thrombosis, hemostasis and fibrinolysis. J Thromb Haemost, 5(s1):102–115, 2007.
- [47] Richard Lottenberg and Craig M Jackson. Solution composition dependent variation in extinction coefficients for p-nitroaniline. Biochim Biophys Acta, 742(3):558–564, 1983.
- [48] Franklin C. McLean. Application of the law of chemical equilibrium (law of mass action) to biological problems. Physiological Reviews, 18(4):495—523, 1938.
- [49] Alan C Hindmarsh, Peter N Brown, Keith E Grant, Steven L Lee, Radu Serban, Dan E Shumaker, and Carol S Woodward. Sundials: Suite of nonlinear and differential/algebraic equation solvers. ACM Transactions on Mathematical Software (TOMS), 31(3):363–396, 2005.
- [50] Ralph C. Smith. Uncertainty Quantification: Theory, Implementation, and Applications. Society for Industrial and Applied Mathematics, Philadelphia, PA, USA, 2013.
- [51] Siddhartha Chib and Edward Greenberg. Understanding the Metropolis-Hastings Algorithm. The American Statistician, 49(4):327–335, 1995.
- [52] John Geweke et al. Evaluating the accuracy of sampling-based approaches to the calculation of posterior moments, volume 196. Federal Reserve Bank of Minneapolis, Research Department Minneapolis, MN, USA, 1991.
- [53] Benjamin M Bolker. Ecological models and data in R. Princeton University Press, 2008.
- [54] Robert E. Kass and Adrian E. Raftery. Bayes factors. J Am Stat Assoc, 90(430):773–795, 1995.
- [55] G. Lu, G.J. Broze, and S. Krishnaswamy. Formation of factors IXa and Xa by the extrinsic pathway: Differential regulation by tissue factor pathway inhibitor and antithrombin III. Journal of Biological Chemistry, 279:17241–17249, 2004.

## Chapter 3

# A local and global sensitivity analysis of a mathematical model of coagulation and platelet deposition under flow (Journal Article)

This chapter originally published as “Link, K. G., **Stobb, M. T.**, Di Paola, J., Neeves, K. B., Fogelson, A. L., Sindi, S. S., & Leiderman, K. (2018). *A local and global sensitivity analysis of a mathematical model of coagulation and platelet deposition under flow*. PloS one, 13(7), e0200917.” Reprinted in accordance with the Creative Commons Attribution 4.0 International License (<http://creativecommons.org/licenses/by/4.0/>) with some changes for continuity. KGL conducted the local analysis, all other co-authors listed in this publication directed and supervised research.

### 3.1 Abstract

The hemostatic response involves blood coagulation and platelet aggregation to stop blood loss from an injured blood vessel. The complexity of these processes make it difficult to intuit the overall hemostatic response without quantitative methods. Mathematical models aim to address this challenge but are often accompanied by numerous parameters choices and thus need to be analyzed for sensitivity to such choices. Here we use local and global sensitivity analyses to study a model of coagulation and platelet deposition under flow. To relate with clinical assays, we measured the sensitivity of three specific thrombin metrics: lag time, maximum relative rate of generation, and final concentration after 20 minutes. In addition, we varied parameters of three different classes: plasma protein levels, kinetic rate constants, and platelet characteristics. In terms of an overall ranking of the model’s sensitivities, we found that the local and global methods provided similar information. Our local analysis, in agreement with previous findings, shows that varying parameters within 50-150% of baseline values, in a one-at-a-time (OAT) fashion, always leads to significant thrombin generation in 20 minutes. Our global analysis gave a different and novel result

highlighting groups of parameters, still varying within the normal 50-150%, that produced little or no thrombin in 20 minutes. Variations in either plasma levels or platelet characteristics, using either OAT or simultaneous variations, always led to strong thrombin production and overall, relatively low output variance. Simultaneous variation in kinetics rate constants or in a subset of all three parameter classes led to the highest overall output variance, incorporating instances with little to no thrombin production. The global analysis revealed multiple parameter interactions in the lag time and final concentration leading to relatively high variance; high variance was also observed in the thrombin generation rate, but parameters attributed to that variance acted independently and additively.

## 3.2 Introduction

When vascular injury causes blood to flow out of a vessel, the body's response is hemostasis. Often the hemostatic response is thought of as being comprised of two stages, primary hemostasis and secondary hemostasis, though these processes begin simultaneously and are intricately intertwined. Primary hemostasis involves formation of a platelet plug which prevents the loss of blood cells and slows the outflow of plasma from the vessel. The plug forms by platelet adhesion to collagen and von Willebrand factor on the injured vessel wall and by aggregation of platelets to the wall-adherent platelets and to one another. Secondary hemostasis involves formation of a fibrin mesh in and around the platelet plug that mechanically stabilizes the plug. Blood coagulation is a key process in secondary hemostasis; it involves a network of enzyme reactions that produce the enzyme thrombin. Thrombin removes small peptide chains from the plasma protein fibrinogen thereby producing fibrin monomers. These monomers polymerize to form the fibrin mesh.

It is important to localize the hemostatic processes, in particular the production and action of thrombin, to the site of injury. Doing so is a challenge because hemostasis occurs in the presence of continued blood flow. A major part of accomplishing localization relies on the fact that the critical coagulation enzymes are enzyme complexes that form on surfaces of cells that are themselves part of or attached to the injured vessel. These include subendothelial cells and aggregated platelets. An important aspect of coagulation is that coagulation reactions are regulated by the properties of these cellular surfaces in that the formation of the enzyme complexes on them is influenced by the limited availability of binding sites and by competition among coagulation proteins to bind to these sites [1]. Additional localization mechanisms involve inhibitors in the plasma or on the endothelial cells which line intact vessels which clear active enzymes that are carried downstream of the injury by flow.

The diversity and complexity of the processes comprising hemostasis make it extremely difficult to intuit the system's response without quantitative methods and a growing number of mathematical models have been developed to try to address this challenge. Such models can be powerful tools because they allow one to track the concentrations of every protein, enzyme complex, and cell during simulations of hemostasis. This makes them potentially very helpful in interpreting experimental data, elucidating biochemical and biophysical mechanisms, and in guiding experimental design. Recently developed models differ from one another in that they focus on different aspects of the hemostatic process and attempt to simulate events under different conditions. For example, many models of coagulation were developed as companion tools for static in vitro coagulation experiments using synthetic

plasma with lipid vesicles providing the reaction surfaces in place of platelet surfaces [2–5] or using whole blood [6, 7]. Most models regard all species as well-mixed and only track the variation in concentrations in time. Others account for spatial and temporal variations, treating transport from one location to another to simulate the reaction-diffusion waves observed in some in vitro studies of coagulation in plasma [8, 9], to simulate in vitro flow assays with whole blood [10, 11], or to simulate small vascular injuries under flow [11–19].

Mathematical models of static situations simulate a “closed system” in which coagulation reactions occur in buffer (or plasma) in the presence of phospholipid surfaces (either lipid vesicles or platelets), and there is no resupply of proteins. Although the biochemical species vary from model to model because of differing assumptions on the underlying kinetic schemes, these models typically consist of a system of ordinary differential equations used to track concentrations of coagulation proteins in time starting with prescribed initial concentrations (initial conditions). The expressions that model enzymatic reactions are formed using the classical two-step reactions of enzyme kinetics in which there are association rates ( $k^+$ ) for binding of the substrate and enzyme, rates for the dissociation of the enzyme-substrate complex ( $k^-$ ), and catalytic turn over rates ( $k^{cat}$ ) for the rate that the complex turns over enzymes. Most of these models assume that there is a vast excess of cell (phospholipid) surface [2–5, 7] and do not track the binding sites. The first model to track limited numbers of cell binding sites [12] is the original version of the model considered in this paper. That model was further developed in [14, 16, 20, 21] and inspired similar models [4, 6]. These models account for reversible binding of proteins to these sites with rates  $k^{on}$  and rates  $k^{off}$  for binding and unbinding, respectively.

Experimentally-measured values of the Michaelis-Menten constant,  $K_M = (k^- + k^{cat})/k^+$ , and catalytic rate  $k^{cat}$  can be found in the literature for most of the coagulation reactions. However, these rate constants are often measured in isolation, i.e., considering only one reaction and the reactants involved in that reaction and are measured under varying experimental conditions, e.g., temperature, chromogenic vs. fluorogenic substrate, etc., so there is uncertainty in the parameter values. Further, it is questionable whether it is valid to use Michaelis-Menten reaction kinetics to model enzyme reactions for which either the enzyme or substrate, or both, are involved in other reactions. Hence, mass action descriptions of complex formation, dissociation, and product formation may be preferable. To parameterize such reactions, using the experimentally measured  $K_M$  and  $k^{cat}$  values, it is typical to choose a value for one of  $k^{on}$  or  $k^{off}$  and use the measured  $k^{cat}$  and  $K_M$  values to determine the other [12]. Similarly, for surface binding, published dissociation constants are ratios  $K_d = k^{off} / k^{on}$  of the parameters  $k^{on}$  and  $k^{off}$  needed for the mathematical model, and again it is typical to choose  $k^{off}$  and use the measured  $K_d$  to determine  $k^{on}$ . Because of the uncertainties in experimental measurements (of  $K_M$ ,  $k^{cat}$ ,  $K_d$ ) and choices of kinetic schemes and rates, there is considerable variation in the inputs to mathematical models. How these uncertainties affect the models’ outputs is a major focus of this paper that we address through a systematic local and global sensitivity analysis. As we will describe in greater detail, we seek to understand how uncertainties in system inputs are propagated to uncertainties in particular model outputs taken to represent clinically relevant clotting behavior.

Mathematical models of microfluidic assays or small vessel injuries under flow simulate “open systems” in which there is a continual supply of coagulation reactants and removal of reactants and products at rates that depend on the flow rate. The supply and removal of

coagulation proteins slow some reactions (e.g., by lowering the concentration of an enzyme) and speed other reactions (e.g., by maintaining a near-constant level of the substrates). Moreover, platelets provide their procoagulant surfaces to further enzyme production, but also inhibit coagulation activity on the subendothelium when they pave it over during adhesion and aggregation [12, 16, 22]. The contributions of these platelet-mediated processes should depend on the platelet count, the rate of adhesion of platelets to the subendothelium, and the numbers of binding sites on each platelet for the various coagulation proteins.

It is for precisely these nonintuitive situations that mathematical models are needed to predict system responses. Of the models mentioned above, the ones developed by our group are the most comprehensive in terms of coagulation reactions in plasma and also, perhaps even more importantly, the reactions taking place on the subendothelium and the surface of activated platelets [12, 14, 16, 20]. The sensitivity of mathematical models to biophysical attributes, i.e., flow (shear) rate, platelet adhesion rates, activation rates, as well as numbers of specific binding site numbers on activated platelet surfaces has never been thoroughly studied. So, in addition to analyzing the model’s sensitivity to kinetic and binding rates, investigating its sensitivity to biophysical parameters is a major goal of the current work.

In what follows, we describe the main features of the mathematical model that we analyze in this paper and then give an overview of sensitivity analysis methods and how they have been applied to other models of coagulation.

### 3.2.1 Mathematical model of coagulation under flow

We analyze the model of Fogelson et al. [16] that simulates the clotting response due to a small injury in a blood vessel wall. Here we give an overview of the model but more details can be found in our previous works [12, 14, 16, 20]. The full list of reactions, rate constants, and model equations can be found in S1 Appendix.

In the model, the clotting response is simulated within a small reaction zone located just above a small patch of exposed subendothelium (SE). Tissue factor (TF) and collagen embedded in the SE come into contact with clotting factors and platelets in the flowing plasma (see Fig 3.1B) to initiate the response. The initial height of the reaction zone is determined by the flow’s shear rate (the derivative of the tangential velocity component in a direction normal to the vessel wall) and platelet and protein diffusivities. Clotting factor concentrations in the reaction zone change due to their involvement in the coagulation reactions depicted in Fig 3.1C and also by transport in and out of the zone. Similarly, platelet concentrations change as platelets adhere to the injured wall, become activated, and as platelets are transported in and out of the zone. As platelets build up in the reaction zone the height and volume of the reaction zone increase with the volume of plasma and platelets in it changing accordingly. The concentration of each species in the reaction zone plasma is tracked with an ordinary differential equation; this choice relies on the assumption that each species is uniformly distributed (well-mixed). An additional well-mixed endothelial zone is located adjacent to the reaction zone, in the direction perpendicular to the flow (Fig 3.1C) with height equal to that of the reaction zone and width dependent on the flow shear rate and protein diffusion coefficients [14]. Thrombin produced in the reaction zone can diffuse from the reaction zone into the endothelial zone, bind to thrombomodulin (TM), and produce activated protein C (APC), which may then diffuse back into the reaction zone.

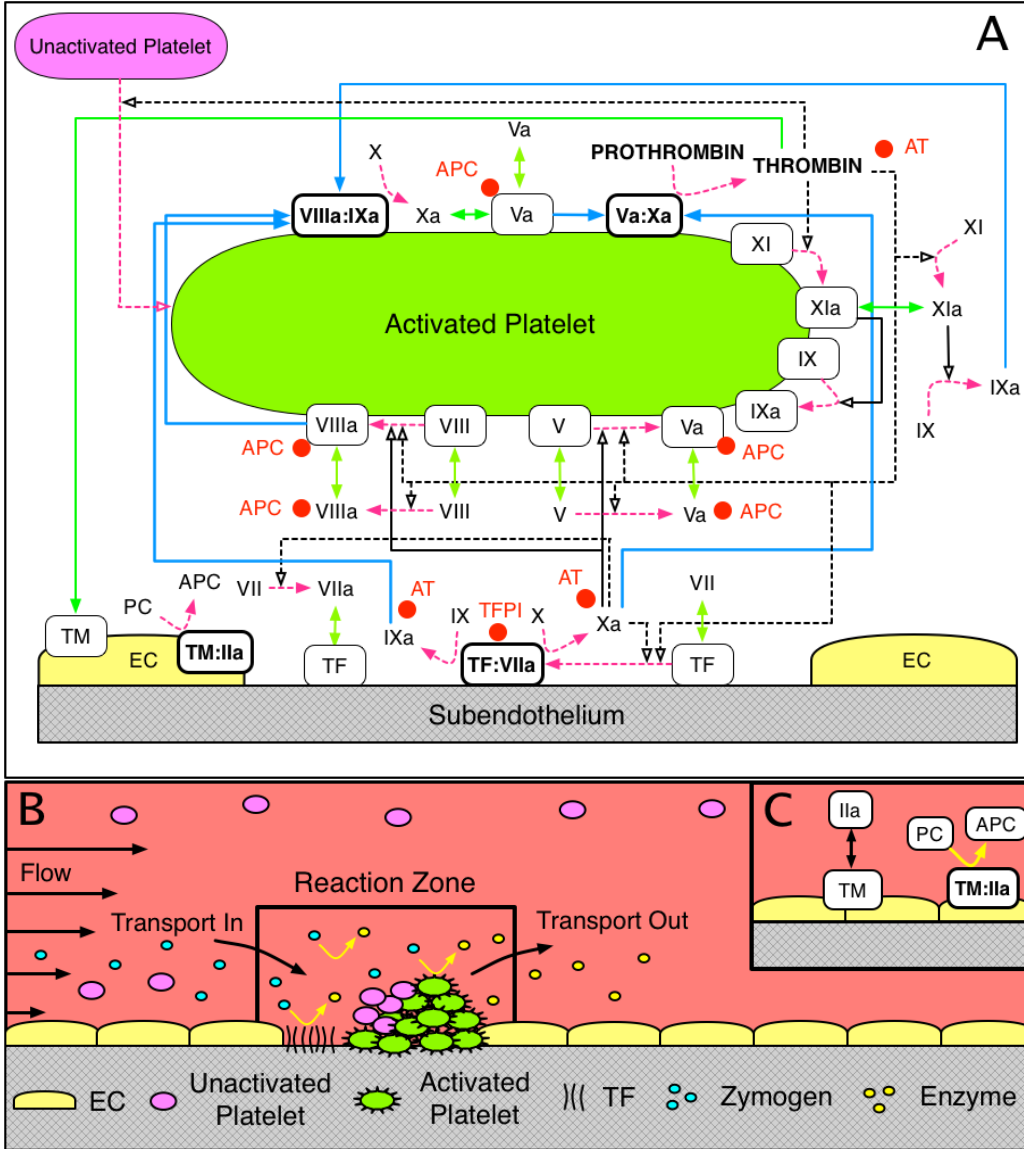


**Figure 3.1: Schematic of (A) coagulation reactions included in our model.** Dashed magenta arrows show cellular or chemical activation processes. Blue arrows show chemical transport in the fluid or on a surface. Green segments with two arrowheads depict binding and unbinding from a surface. Rectangular boxes denote surface-bound species. Solid black lines with open arrows show enzyme action in a forward direction, while dashed black lines with open arrows show feedback action of enzymes. Red disks show chemical inhibitors. Schematic of (B) reaction zone and (C) endothelial zone.

Platelets are assumed to be either mobile and unactivated, or stationary, activated and bound either to collagen in the SE or to other activated platelets. Platelets become activated at prescribed rates upon contact with the SE, exposure to thrombin, or contact with other activated platelets. The last of these types of activation is used as a surrogate for activation by platelet-released ADP which we do not explicitly track in this model. Protein species are

assumed to be either freely moving in the fluid, bound to the SE, or bound to an activated platelet surface (APS). To move from the SE to an APS, or vice versa, a protein is subject to flow and thus might be transported out of the reaction zone.

Fig 3.1A shows the schematic of the coagulation reactions we consider in the model. The reactions involve many coagulation factors and cofactors: inactive enzyme precursors (zymogens), active enzymes, as well as inactive and active cofactors. Although cofactors have an active form, they do not function as enzymes, i.e., they do not activate other proteins; rather, they make the enzymes to which they bind vastly more effective than the enzymes would be alone. Next, we describe the coagulation reactions using the typical Roman numeral notation to represent the factors involved in them. For example, we refer to factor X as either ‘factor X’ or ‘fX’. Since most of the proteins have an inactive and active form, we differentiate these forms with the letter ‘a’ attached to the Roman numeral, e.g., fXa represents the active form of factor X.

In Fig 3.1A, the zymogens are factors VII, IX, X, and II (prothrombin) and have corresponding active enzyme factors VIIa, IXa, Xa, and IIa (thrombin), respectively. The inactive/active cofactor pairs are V/Va, and VIII/VIIIa. Also seen in Fig 3.1A is that many of the coagulation reactions occur only on a cellular surface, either SE or APS. We point out that there are three important surface-bound enzyme-cofactor complexes: TF:VIIa on the SE (“extrinsic tenase”) and VIIIa:IXa (“intrinsic tenase” which below we refer to simply as tenase) and Va:Xa (“prothrombinase”) on APS. Their substrates (i.e., the proteins that the enzyme complexes activate) must also be bound to the cellular surface to become activated [1].

As described above, our model incorporates specific binding sites on an APS to which each zymogen/enzyme pair compete; this is in contrast to a competing view of a surface on which all zymogen/enzyme pairs compete for one large number of shared binding sites [23]. Our assumptions are based on numerous studies in [24–29] that underscore specific binding of factors V/Va, VIII/VIIIa, IX/IXa, X/Xa, XI/XIa, respectively. Additional support for the existence of two populations of FIXa receptors comes from a series of studies,[30, 31], in which the authors characterized the numbers and binding parameters of the receptors. Other assumptions about protein interactions follow, and further discussion of them including citations to the literature can be found in [12, 14, 16]:

- Factors VII and VIIa can bind to TF in the SE. Factor Xa can activate fVII in plasma and when it is bound to TF. Factor Xa can bind the TF:VII complex directly from plasma without having to first bind the SE.
- Factors IX and X are activated by the TF:VIIa complex on the SE; they bind TF:VIIa directly from plasma. Factor X is also activated by the VIIIa:IXa (‘tenase’) complex on an APS.
- Cofactors V and VIII are activated by thrombin in plasma and by thrombin and fXa on an APS.
- Factor IX is activated by fXIa in plasma and on an APS. Factor XI is activated by thrombin in plasma and on an APS.
- The chemical inhibitors/inactivators that we include in the model are antithrombin (AT), activated protein C (APC), and tissue factor pathway inhibitor (TFPI). Since

the concentration of AT is high in plasma, we assume it acts in a first-order manner to inactivate fluid-phase fIXa, fXa, fXIa, and thrombin. APC can bind to fluid-phase and platelet-bound fVa and fVIIIa to permanently inactivate them with second-order kinetics, but cannot bind to fVIIIa within a tenase complex or to fVa within a prothrombinase complex. APC is produced in the endothelial zone by a complex of thrombomodulin and thrombin. TFPI present in the plasma must first bind to fXa and then the complex TFPI:Xa must bind to the TF:VIIa complex to inhibit it.

- The activity of the TF:VIIa complex decreases as platelet deposition on the injured tissue increases, i.e., we assume that a platelet physically blocks the activity of the TF:VIIa complexes on the patch of SE to which the platelet has adhered.

Each simulation with the mathematical model requires setting numerous input values. We specify the initial plasma concentrations of platelet and protein species, the rate constants for all reactions, the numbers of specific binding sites for coagulation factors on each APS, the dimensions of the injury, the flow velocity near the injured wall, the diffusion coefficients for all fluid-phase species, and the density of exposed TF. The outputs of the model are the concentration of every protein species in the reaction zone at each instant of time from initiation of the injury until the completion of the simulation, and the concentrations of platelets attached either directly to the SE or to other platelets. A complete listing of the model’s differential equations and of the base parameter values used in the simulations can be found in S1 Appendix.

### 3.2.2 Uncertainty and sensitivity analyses

Sensitivity analysis (SA) refers to a broad set of mathematical approaches designed to quantify how variation in model outputs may be attributed to model inputs (e.g., initial conditions and rate constants) [32–34]. These approaches allow researchers to assess how much trust to put in results obtained from a particular mathematical model. In addition, because the relevant output behavior of high-dimensional systems, such as biochemical reaction networks, is often dominated by relatively few parameters, SA provides a way to isolate these parameters so that they can be targeted by further studies.

One of the most straightforward ways to perform a SA is to vary each model input parameter one at a time (OAT) while other input parameters remain constant. Such methods typically assign importance to inputs by their impact on the approximate derivatives of outputs with respect to a change in the input [33–35]. These methods are inherently “local” in that they do not study the impact of varying parameters together. Local approaches can be informative if there is little uncertainty in model inputs or if there is little interaction between inputs (i.e., inputs act linearly or additively) [36]. However, it is unclear if this is the case in coagulation due to multiple positive and negative feedback mechanisms. Thus, in this study we employ both local and global methods to gain additional information about model sensitivity.

Global sensitivity analysis (GSA) methods consider the changes in model outputs as input parameters are allowed to vary simultaneously over specified ranges [32, 33, 35]. Typically, global methods require more computational work than local methods, but have the ability to uncover relationships between multiple parameters and they cope well with nonlinear and non-additive responses. GSA methods are often probabilistic in nature;

they consider the uncertainty in model inputs and outputs as probability distributions. In these approaches the variance in model output is decomposed to attribute fractions of the variance to individual model inputs and also groups of model inputs. Many variance-based sensitivity methods consider Sobol indices [33] to express the decomposed variance as being due to variations in a single model input in isolation (first-order Sobol index), variations due to interactions involving two input parameters together (second-order Sobol index), and so on to variations due to all possible interactions, (total order Sobol index) [33]. As we describe in greater detail below, we utilize Sobol indices in our analysis and compute them through Monte-Carlo sampling. Before developing the details of our SA approach, we first describe prior SA studies of mathematical models of coagulation.

We are aware of four major SA studies of coagulation models, all of which simulate static coagulation. Danforth and colleagues [37, 38] studied sensitivity to kinetic rate constants and initial clotting factor concentrations in a model that simulates synthetic plasma in the presence of lipid vesicles (not platelets) [3, 5] with the lipids present at excess concentrations. They used an OAT, local SA that included varying individual kinetic rate constants in their first study [37]. There they examined the changes in a number of output protein species concentrations in time as kinetic rate constants were varied between 10 - 1000% of their reported literature value. Overall, they identified 5 of 44 kinetic rate constants that explained 50% of the variation in all model species' outputs and 25% of the variation in thrombin output. They report many of the highest sensitivities of thrombin levels to rate constants for chemical inhibition/inactivation, i.e., by AT and TFPI, and to the reactions involving TF and VIIa. In addition, they examined how uncertainty in the output varies at a set of fixed time points, chosen to represent key moments in the process of thrombin generation. For example, they examined the time of a thrombin "burst", described as the time that the thrombin concentration rises rapidly to physiologically relevant levels (they assume this level to be 2 nM). However, the timing of these events in their model changed significantly due to variations in the kinetic rate constants themselves, and thus it is not clear how one should interpret the sensitivities they computed at fixed time values. In a subsequent study, Danforth and colleagues studied sensitivity in the same model to variations in the initial plasma concentrations; there they analyzed sensitivity of three thrombin metrics (analogous to the ones used in the current study) to individual variations and pairwise variations of parameters within a "normal" range [38]. They reported that individual variations in two factors (TFPI and prothrombin) accounted for about 50% of the observed sensitivity of the model output. In regards to their three thrombin metrics, they reported that the pairwise changes in factor levels resulted in higher output variation than with individual variations. They found that the pairs, AT with TFPI, and AT with prothrombin, had the largest effect on the time to 2 nM thrombin and the maximum thrombin concentration. They concluded that the inhibitors TFPI and AT were the most potent inducers of overall variation. In a closed, static system, it is clear that these inhibitors play an important role in regulating thrombin generation because not only are they the sole inhibitors in the system, but because all enzymes susceptible to inhibition in a closed system will be fully inhibited (or inactivated) in a finite amount of time. Our mathematical model with platelets and flow is less sensitive to such inhibitors since the flow and platelet coverage of the SE are often the dominant inhibitors of different parts of the process [12, 14, 16]; more discussion of these model differences will be described below.

Anand and colleagues used the SA method of Danforth to analyze sensitivity of a model

of fibrin generation to kinetic rate constants [39, 40]. They reported that the fibrin concentration was most sensitive to the rate constants responsible for inactivation of FVIIIa (both intrinsic and by APC). Although their model incorporated diffusion near an injury patch in a static fluid, their sensitivity measure was reported for the average concentration throughout the spatial domain. The same group used this SA method in two follow up studies of a static model of thrombin generation that included platelets; they investigated the sensitivity of the model to rate constants [41] and to initial concentrations [42]. Thrombin generation was reported to be most sensitive to the rate constant responsible for activation of FX by tenase; however this reaction was assumed to obey Michaelis-Menton kinetics and it is unclear how this assumption affected the SA. In terms of the varied initial concentrations, they reported that thrombin generation was most sensitive to initial levels of FVIII and FVIIIa, but it is not clear why FVIIIa levels were varied in the study.

Chatterjee, Diamond, and colleagues [7] built on the models in [3, 5] and developed a different static model that accounted for platelets and platelet activation. They used this model to investigate the behavior of blood treated by corn trypsin inhibitor (CTI inhibits the intrinsic pathway via XIa). They did not consider protein binding to and unbinding from platelet surfaces, but instead assumed that reaction rates increased as a function of number of activated platelets. A brief summary of a SA was included in S1 Appendix. Similar to the approach taken by Danforth et al. [37], they conducted a local SA of 105 kinetic parameters. However, rather than a variance-based sensitivity, they considered the derivatives of system outputs at a large set of points in parameter space in an OAT fashion. Following the approach of Bentele et al. [43], their sensitivities were weighted by how closely the resulting thrombin response matched the thrombin response with the mean parameter values using a Boltzmann distribution. They then observed the most sensitive parameters were those involved with direct TF and fVIIa interactions.

Finally, Luan and colleagues [6] studied the sensitivity of a model very similar to the one used in this work, but without flow. Their model included binding/unbinding of proteins to/from specific surface binding sites, but their analysis considered only the sensitivity of kinetic rate constants (including binding rates) and not binding site numbers or other aspects of platelet function. Their goal was to identify fragile mechanisms, small perturbations to which the system output exhibited high sensitivity, and robust ones where the system maintained its performance in the face of perturbation and uncertainty. They argued that the most sensitive (or fragile) mechanisms represented ideal therapeutic targets. They conducted a local sensitivity analysis of 148 kinetic parameters, computing what they called overall state sensitivity coefficients (OSSCs) following the approach taken in [44]. Four of the top five mechanisms they identified as fragile involved factors X and Xa or the activation of platelets by thrombin. They found the mechanisms involving factors IX and IXa were moderately robust by their definitions.

In this study, we use both local and global sensitivity analysis methods to better understand what information can be gleaned from each, in the context of coagulation and platelet deposition under flow. As we explain in greater detail below, our local methods consider the direction and magnitude of change for three metrics of thrombin production. Our global sensitivity analysis methods consider the fraction of variance in these thrombin metrics that is attributable to each parameter according to computed Sobol indices.

We have divided our sensitivity analysis into four parts according to the class of parameters under study: A) sensitivity to plasma levels of zymogens and inhibitors, B) sensitivity

to kinetic rate constants including those for surface binding/unbinding, C) sensitivity to biophysical and platelet attributes and, D) sensitivity to all classes of parameters considered together. In parts A and C we found the local and global analyses produced consistent results in terms of ranking the overall sensitivity of the thrombin metrics to the parameters in those classes. This suggests that the dominant impacts of input uncertainty in these restricted classes may be understood through consideration of each parameter in isolation. However, in parts B and D, we observed a number of instances where varying parameters together resulted in much greater variance in model output than varying them in isolation. While the variance attributable to higher-order effects was not a majority of the total system variance in these cases, the higher-order effects were particularly pronounced for two of our three output metrics when all parameters were varied together (part D). Overall, our results provide compelling evidence that to fully characterize the behavior of coagulation, the joint impact of multiple parameters should be considered. Beyond measuring the amount of variance in the output, as we illustrate in our analysis, global methods also proved useful for identifying groupings of parameters associated with extreme model output behavior, which is notable since the parameters varied within normal physiological ranges.

### 3.3 Materials and methods

Here we describe the methods used to analyze the sensitivity of our model’s output. We focus on the model’s production of thrombin and quantify this in terms of three metrics, similar to those used in the in vitro experiments from our previous study [45]:

1. **Lag time:** A measure of how fast the system is turned on. Specifically, we quantify the amount of time it takes for thrombin to reach 1 nM, denoted by  $t_{1nM}$ . This concentration of thrombin is known to have significant effects on platelet activation and coagulation [46].
2. **Maximum relative rate:** A measure of how fast thrombin is produced once the system is turned on. Specifically, it is defined by

$$\max_{t > t_{1nM}} \left\{ \frac{d[\text{thrombin}]}{dt} / [\text{thrombin}] \right\},$$

where  $t_{1nM}$  is the time it takes for thrombin concentration to reach 1.0 nM.

3. **Final concentration:** The total thrombin concentration after 20 minutes.

Fig 3.2 illustrates how these metrics relate to a curve of thrombin concentration vs. time. In all comparisons that follow, we assess the variation and sensitivity of thrombin generation according to these three metrics.

Next, we detail the mathematical and statistical methods used in our local and global sensitivity analyses. We examined the sensitivity of the model’s output to three types of parameter variations: (i) the plasma levels of seven zymogens and two inhibitors, (ii) the values of 96 kinetic rate constants, and (iii) the platelet number density (“platelet count”), the numbers per activated platelet of nine types of platelet surface binding sites, and the rates of six platelet responses. We also studied the effect of the flow’s shear rate on model outputs. We conducted local and global sensitivity studies in parallel for the plasma

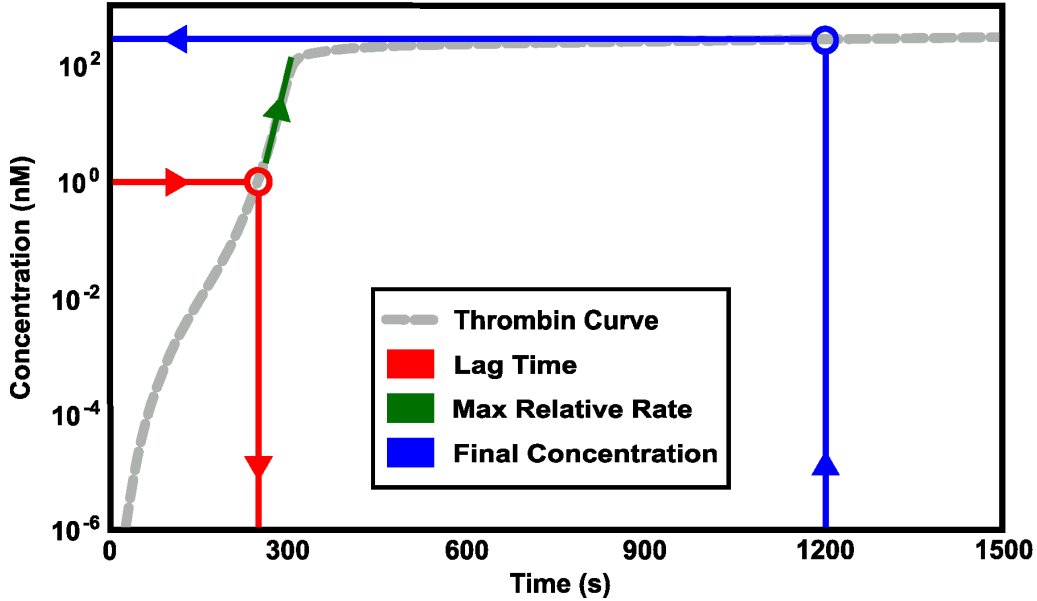


**Figure 3.2: Schematic of Thrombin Metrics.** Three physiologically relevant metrics of Thrombin generation were calculated for sensitivity analysis: 1) lag time (*Red*), 2) maximum relative rate of thrombin generation, measured after 0.1nM of thrombin have been obtained (*Green*), and 3) final concentration, the total concentration of thrombin at 20 minutes (*Blue*).

levels and platelet characteristics. For the 96-dimensional parameter space of kinetic rate constants, a full global analysis would have been too computationally costly. For these parameters, we used the Morris Method [47] as a screening method to determine a subset that seemed likely to have a strong influence on the thrombin concentration, either through direct effects by themselves or through interactions with other parameters. This subset was then analyzed with our global methods. A similar process was carried out on the union of the three classes of parameters to generate a subset that was then used for global analysis.

### 3.3.1 Local Sensitivity Analysis

The local approach we use is a variant of the one-at-a-time (OAT) method used by Saltelli et al. [34, 48]. Our initial approach to local sensitivity was to pursue a derivative based method to quantify the sensitivity of each metric with respect to changes in the parameter. We used a centered difference to approximate the derivative with respect to each parameter OAT at a range of parameter values (50%, 75%, 100%, 125%, and 150% of the baseline values.) However, we observed some unexpected behavior with respect to the system’s metrics which caused us to develop an alternative approach to local sensitivity.

Despite the nonlinearity of the model equations, and the multiple positive and negative feedback loops in the coagulation system, we found that each of the metrics we were interested in behaved monotonically with respect to varying each plasma level and kinetic rate constant OAT from 50% to 150% of the standard values. For example, in Fig 3.3 we show how each of our three metrics varies with plasma levels and note that, as each level ranges from 50% to 150% of its standard value, the metric is either monotonically increasing or

decreasing. The monotonicity property was also seen for nearly all instances of OAT variation in platelet characteristics (see S1 and S2 Figs). The only exception was non-monotonic variation in the lag time with the platelet count  $PL^{UP}$  and adhesion rate  $k_{adh}$ . Because of this surprising behavior of system outputs, we quantified parameters by the absolute difference they produced in each metric when considering their extremal values (i.e., 50% and 150%). For each metric, we ranked the parameters by considering their relative absolute difference.

More specifically, let  $\mathbf{x} = (x_1, x_2, \dots, x_P)$  be the standard model parameter values and  $m_i(\mathbf{x}_{j,y\%})$  represent the value of the  $i$ -th metric when parameter  $j$  is chosen to be  $y\%$  of its standard value and all other parameters are chosen to be their standard value. We define the local sensitivity of the  $i$ -th metric to the  $j$ -th parameter as:

$$LS_j^i = \frac{|m_i(\mathbf{x}_{j,150\%}) - m_i(\mathbf{x}_{j,50\%})|}{\max_k (|m_i(\mathbf{x}_{k,150\%}) - m_i(\mathbf{x}_{k,50\%})|)}. \quad (3.1)$$

Each  $LS_j^i$  is a number between 0 and 1 and we use these values to rank input sensitivities. In our local sensitivity results (e.g., top of Fig 3.4), we color results in blue when  $LS_j^i \in (0.75, 1]$ , magenta when  $LS_j^i \in (0.25, 0.75]$  and cyan otherwise. In addition, because the response of the system outputs is monotonic throughout the entire range, we show separately the change in each metric for the 50% increase and decrease for each parameter indicating with a up/down triangle if the metric increases or decreases.

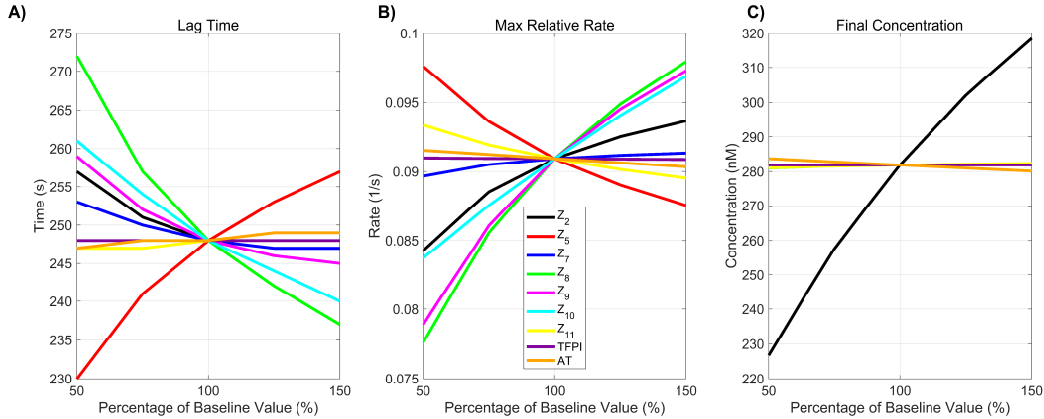


**Figure 3.3: Monotonicity of Change in Thrombin Generation due to Variation in plasma levels.** Variation in the three physiologically relevant metrics of thrombin generation: 1) lag time; 2) maximum relative rate; and 3) final concentration that occur with variations in plasma levels.

### 3.3.2 Morris Method

Because a full global analysis of all model parameters or of the 96 kinetic rate constant subset was computationally expensive, we sought to select subsets of parameters that seemed likely to have strong effects. To determine which model parameters may be considered to have effects which are negligible, linear or involved in interactions with each other, we

implemented the method of Morris [47]. Here, we briefly detail this method and discuss our basis for selecting which parameters were used in our global sensitivity results.

The Morris method involves individually randomized OAT experiments and the calculation of two sensitivity measures  $\mu^*$ , the Morris mean, and  $\sigma$ , the standard deviation. The lower and upper bounds of the interval of sampling were set to 50% and 150% of the standard parameter values. The Morris design requires a random selection of a "base" sample point  $\mathbf{x}^*$ , which is a vector of length equal to the number  $P$  of parameters. Using five Morris levels ( $p = 5$ ), each parameter value is increased or decreased by 25% of its standard value ( $\Delta = 1/(p - 1) = 1/4$ ). A sequence of  $P + 1$  sample points  $\mathbf{x}^*, \mathbf{x}^{(1)}, \mathbf{x}^{(2)}, \dots, \mathbf{x}^{(P)}$ , called a trajectory, is generated with the property that two consecutive points differ only one parameter's value. For this analysis, we generated 1000 random trajectories and selected  $r = 25$  samples in a way to maximize their "spread" in the input space. The spread is based on the sum of the geometric distances between coupled points of any two fixed trajectories. More details regarding sample selection are found in [49].

An elementary effect for each parameter on each metric was calculated from the sample trajectories. For example, suppose that in the  $k^{\text{th}}$  trajectory a step in the  $j^{\text{th}}$  model parameter occurs between sample points  $\mathbf{x}_k^{(\ell_j)}$  and  $\mathbf{x}_k^{(\ell_j+1)}$ . For a given choice of parameters,  $\mathbf{x}$ , let  $m_i(\mathbf{x})$  be the value of the  $i^{\text{th}}$  metric of thrombin generation. The elementary effect for model parameter  $j$  and trajectory  $k$  associated with the thrombin generation metric  $i$  is:

$$d_{j,k}^i = \frac{1}{\Delta} \left| m_i(\mathbf{x}_k^{(\ell_j)}) - m_i(\mathbf{x}_k^{(\ell_j+1)}) \right|. \quad (3.2)$$

The Morris mean and standard deviation for the  $j^{\text{th}}$  parameter and the  $i^{\text{th}}$  thrombin generation metric are defined as the empirical mean and variance over all trajectories:

$$\mu_{i,j}^* = \frac{1}{r} \sum_{k=1}^r d_{j,k}^i \quad \text{and} \quad \sigma_{i,j} = \sqrt{\frac{1}{(r-1)} \sum_{k=1}^r (d_{j,k}^i - \mu_{i,j}^*)^2},$$

where  $r$  is the number of trajectories. Thus the method produces a coordinate pair,  $(\mu_{i,j}^*, \sigma_{i,j})$ , for each thrombin generation metric and each parameter. Typically, the coordinate pairs  $\{(\mu_{i,j}^*, \sigma_{i,j})\}$  are grouped into three sets according to those that have a negligible effect on the metric (both  $\mu_{i,j}^*, \sigma_{i,j}$  small), a linear effect on the metric ( $\mu_{i,j}^* > \sigma_{i,j}$  with  $\sigma$  small) and those likely to have interaction effects ( $\mu_{i,j}^* < \sigma_{i,j}$  with both  $\mu_{i,j}^*, \sigma_{i,j}$  large).

When determining which parameters to select for global analysis, we took a different approach. First, we performed the procedure detailed above, with parameter space filling trajectory selection, three times to generate path sets  $P_1, P_2$ , and  $P_3$ . Because results selected by this method are path-dependent, these multiple path sets allowed to mitigate the risk of missing important parameters. Next, we normalized all  $\mu_{i,j}^*$  and  $\sigma_{i,j}$  by dividing each by the largest values observed for that metric:

$$\mu_{i,\max}^* = \max_j \{\mu_{i,j}^*\} \quad \text{and} \quad \sigma_{i,\max} = \max_j \{\sigma_{i,j}\}.$$

This normalization restricts all coordinate pairs to the unit square. Inputs with an  $\ell_2$ -norm less than 0.5 are deemed to have negligible effects on thrombin generation, whereas parameters with an  $\ell_2$ -norm greater than or equal to 0.5 were viewed as potentially able to induce significant change in thrombin generation (individually or via interactions). We

selected all parameters whose normalized coordinate pair was at a distance  $\geq 0.5$  from the origin for the lag time, maximum relative rate, or final concentration for any of the path sets ( $P_1$ ,  $P_2$ , and  $P_3$ ).

### 3.3.3 Global Sensitivity Analysis

Global sensitivity analysis considers the impact of varying parameters *simultaneously* and uniformly over their full range of possible values, here values between 50% and 150% of baseline. As such, we consider the underlying system output to be a random variable over a probability space of parameter inputs, and quantify the sensitivity of a model output by its variance. We estimate the effects of parameter variations by using Monte Carlo sampling to explore our parameter space. While computationally taxing, Monte Carlo sampling is easily implemented and applicable to all models, including those that contain non-linear interactions among model parameters [33].

We quantify the variance of model outputs by Sobol sensitivity indices (SIs) [48, 50]. Assuming that parameters are independent, the variance of the  $i$ -th model metric,  $m_i$ , with respect to random parameter inputs  $\mathbf{x} = (x_1, x_2, \dots, x_P)$ , may be decomposed as:

$$\text{Var}[m_i(\mathbf{x})] = V^i = \sum_{j=1}^P V_j^i + \sum_{j=1}^P \sum_{k=j+1}^P V_{jk}^i + \dots + V_{1\dots P}^i. \quad (3.3)$$

The total variance is a sum of first order effects of the  $j$ -th parameter on metric  $i$ ,  $V_j^i$ , as well as higher order effects from interactions of parameters. (For example,  $V_{jk}^i$  is the contribution to the variance of metric  $i$  from  $j$ -th and  $k$ -th parameters.) The first order SIs are formed by normalizing the first order variance terms by the total variance

$$GS_j^i = \frac{V_j^i}{V^i}, \quad (3.4)$$

where  $\sum GS_j^i = 1$  if and only if all interaction terms have zero contribution to the variance of the model metric  $m_i$ . The total order SI,  $GS_j^{i,Tot}$ , captures the effect on  $V^i$  of parameter  $j$ , including those from interaction terms, by summing all variance terms where the  $j$ -th parameter appears, typically written as

$$GS_j^{i,Tot} = \frac{V^i - V_{-j}^i}{V^i}, \quad (3.5)$$

where  $V_{-j}^i$  is the sum over the set of all variance terms *not* containing the  $j$ -th parameter. Unlike the first order SIs, the total order SIs can sum to greater than one as all of the interaction terms between parameters appear in each parameter's total SI.

Several estimators for the partial variances are found in the literature [48], with varying accuracy and efficiency. We have elected to use the first order variance estimator [50], defined as

$$V_j^i \approx \frac{1}{N} \sum_{k=1}^N m_i(\mathbf{x}^{(k)}) m_i(\mathbf{x}_j^{(k)}) - \mathbf{E}[m_i], \quad (3.6)$$

where  $\mathbf{x}^{(k)}$  and  $\mathbf{x}_j^{(k)}$  are each a sample of all model parameters and differ only in the  $j$ -th parameter's value. While true variances are never negative, this estimator may produce

negative estimates, but it generally produces estimates with a low absolute error compared to other methods [48].

Similarly, the total variance due to the  $j$ -th parameter, (i.e. the sum of all variance terms containing the  $j$ -th parameter) is estimated using the following estimator (from [51]), with

$$V^i - V_{-j}^i \approx \frac{1}{2N} \sum_{k=1}^N \left[ m_i(\mathbf{x}^{(k)}) - m_i(\mathbf{x}_{-j}^{(k)}) \right]^2, \quad (3.7)$$

where again  $\mathbf{x}^{(k)}$  and  $\mathbf{x}_{-j}^{(k)}$  are sample points in the parameter space of the model parameters, however these differ in all parameter values *except* that of the  $j$ -th parameter, for which they share the same value. Due to this estimator's non-negative nature, it is extraordinarily efficient, producing estimates with extremely low error, especially compared with the first order variance estimator in 3.6. So while the true first order variance is less than or equal to the total variance, the noise in the computed estimates can lead to violations of this relationship.

The total number of function evaluations required are  $N(P + 2)$ , where  $N$  is the number of samples for each individual parameter and  $P$  is the number of parameters. Unless otherwise stated, we used  $N = 10,000$ . Confidence intervals for the SI estimates were generated using a bootstrap approach [52]. Unless otherwise specified, confidence intervals were computed based on 5,000 resamples.

### 3.3.4 Robustness to Shear Rate

The shear rate we use in the sensitivity analyses of this paper is fixed at  $100 \text{ s}^{-1}$ . Previous work [12, 14, 16, 45] includes the investigation of coagulation and platelet deposition dynamics in an environment with this shear rate and other shear rates and shows that large variations in shear rate affects thrombin generation. This raises the question of the robustness of the sensitivity analyses to small perturbations in shear rate. Due to computational limitations, we did not test robustness of the global Sobol method to shear rate. We did, however, explore the effects of small perturbations in shear rate on the Morris method screening. The method of Morris with the same path set was conducted three times using three shear rates, 90, 100, 110 (1/s). Results from this experiment represent the effects of a 10% change in shear rate (see S3 Fig) and give the associated  $\ell_2$ -norm of the Morris sensitivity measures  $\mu^*$ ,  $\sigma$  for lag time\*, maximum relative rate\*, and final amount. Parameters with the normalized  $\ell_2$ -norm of the Morris mean  $\mu^*$  and standard deviation  $\sigma$  greater than 0.5 for any of the path subsets were chosen for comparison across shear rates. The Morris sensitivity norms for all three thrombin generation metrics are essentially the same across all three shear rates. These results highlight that the method of Morris is not sensitive to small perturbations in shear rate. We proceed with confidence in our analyses at a fixed shear rate of  $100 \text{ s}^{-1}$ .

## 3.4 Results

### 3.4.1 Varying Plasma Levels

Plasma levels of procoagulant and anticoagulant species (e.g., zymogens and chemical inhibitors) naturally vary between 50% and 150% of their baseline physiological value [53]. In this section we explore how thrombin generation is affected by variations within this normal range of zymogen and chemical inhibitor levels. We use a local SA approach in which thrombin generation is simulated using three samples from each zymogen and chemical inhibitor level, 50%, 100%, and 150% of normal. We report only these three cases due to the monotonicity in the model responses to changes in plasma levels (see Methods section). A global SA was also used in which each zymogen and chemical inhibitor were simultaneously sampled from a uniform distribution between 50% and 150% of normal, resulting in a total of 110,000 distinct evaluations of the model. Fig 3.4 A-C show results from the local SA and display the percent changes in each thrombin metric and identify the directionality of the sensitivity for each measure of generation, with upward/downward facing triangles indicating a 50% increase/decrease in the input from baseline. The color of the triangle indicates overall sensitivity,  $LS_j^i$ , where highest to lowest sensitivity is represented by the ordering blue, magenta, and cyan. Fig 3.4 D-F display results from the global SA and show the first and total order Sobol indices computed for each initial condition and metric. The height of the bars indicate the fraction of variance that is attributable to the model output from each parameter individually (first order) and from the parameter itself and its interactions with other parameters (total order).

The local SA results in Fig 3.4 A-C reveal the most influential zymogen concentrations when perturbed one at a time for each thrombin metric. We found that variations in fVIII ( $Z_8$ ) and fV ( $Z_5$ ) levels have the greatest effect on the lag time. An increase/decrease of fVIII and fV levels by 50% leads to approximately a 10% change in lag time from baseline. This is equivalent to an increase/decrease of 25 seconds. Both chemical inhibitor levels, TFPI and AT, have little effect on the lag time (Fig 3.4 A). Variations in fVIII and fIX ( $Z_9$ ) levels, which influence the rate of formation of the tenase complex on platelets, have the largest effect on the maximum relative rate of thrombin generation (Fig 3.4 B). Increasing fVIII or fIX levels by 50% leads to less than a 10% increase in this rate. A stronger effect is seen when both zymogens are (individually) decreased by 50%. The maximum relative rate decreases by 14% and 13%, when fVIII and fIX levels are decreased. Lastly, prothrombin ( $Z_2$ ) levels most dramatically affect the final concentration (see Fig 3.4 C). A 50% decrease in prothrombin level results in a 20% decrease in thrombin levels (55 nM), making it the largest OAT effect on thrombin generation produced by varying plasma levels.

The global SA results are in agreement with the findings of the local analysis in that the ranking of the most influential parameters are nearly identical for the two methods on all three metrics ( $p < 0.001$  from a rank permutation test [54]). Varying all zymogen and chemical inhibitor levels between 50% and 150% of normal simultaneously resulted in a coefficient of variation in the lag time of 0.06 (Fig 3.4 D), indicating that the lag time is robust to changes in plasma levels within the normal range. As in the local SA, fVIII and fV play the largest role in changes to the lag time, accounting for 26% and 42% of the output variance, respectively. The maximum relative rate of thrombin generation (Fig 3.4 E) had the greatest coefficient of variation across all three metrics at 0.11. The global SA shows that fVIII, fIX, and fX are the main contributors to the model variance, at 36%, 30%, and

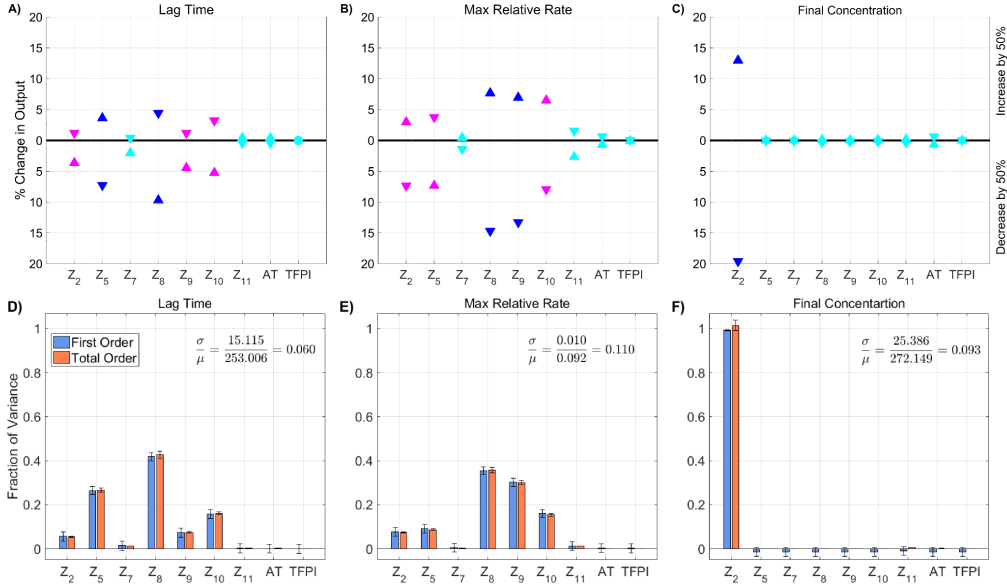


**Figure 3.4: Sensitivity of total thrombin generation to plasma levels.** Variation in the **A,D)** lag time; **B,E)** maximum relative rate; **C,F)** final concentration; to zymogen and chemical inhibitor levels using the local (OAT) method (**A-C**) and global Sobol method (**D-F**). *Local*: Sensitivities  $LS_j^i$  that lie between 0.75 and 1 (blue), between 0.25 and 0.75 (magenta), less than 0.25 (cyan) determine the rank-ordered list of initial levels. The percent change of thrombin generation measures from baseline model output for each initial condition are represented by triangles. The direction of variation of the input parameter is indicated with an upwards or downwards facing triangle. *Global*: First and Total Order Sobol indices are plotted as bars with errors of 2 standard deviation about the mean, computed with 5,000 bootstrap samples of the original 110,000 function evaluations. The coefficient of variation is included to provide a scale for the fraction of variance. No total order index was statistically significantly larger than the first order index, indicating that the model output is not significantly effected by interactions between the parameters considered here.

16% respectively, as in the case of the local SA. The variation in the final concentration (Fig 3.4 F) is entirely explained by variation in the plasma prothrombin levels. For all three metrics, the output variance is dominated by the first-order effects of parameters. No total-order Sobol index statistically exceeds the first-order index ( $p < 0.05$ ). This implies that the model is additive in this regime and is not strongly impacted by interactions between parameters.

The samples used in the global SA not only allow us to probe the sensitivity of the model parameters, but also to interrogate the resulting distribution of thrombin generation metrics. Fig 3.5 shows the resulting output from the 110,000 samples of the coagulation model used to compute the Sobol indices above in which plasma levels varied independently between 50% and 150%. Fig 3.5 A shows a quantile plot in time of the thrombin curves generated from the samples, with the max/min corresponding to the empirical support (note, the lines on the graph do *not* refer to actual thrombin curves but instead to computed quantiles).

The individual distributions of the three thrombin generation metrics resulting from the sampling are shown as histograms (final concentration in A, with lag time (*y-axis*) and the maximum relative rate (*x-axis*) in B), along with their joint distribution, shown as a colored 2D histogram in B. The dependent relationship between the three metrics is clearly seen, as lag time decreases almost linearly with the maximum relative rate, while the average final concentration increases nearly linearly in the same range. While moderate variations in each metric can be seen, the mean and median of the full collection is within 3% of a baseline reference thrombin curve for all metrics, implying that though variations do exist, the typical response is always consistent with that of the baseline case.

### 3.4.2 Varying Kinetic Rate Constants

In this section we explore how variations in the values of kinetic rate constants (KRCs) affect thrombin generation. First, we use our local SA approach and vary the KRC values to 50% and 150% of their baseline values. In addition to a local SA method, we performed a screening using the method of Morris as a precursor to a global SA. The screening selected parameters that either had large individual effects upon the model output or a high likelihood of interacting with other parameters. With this screening, we determined a subset of 25 parameters (out of 96) to include in our global SA.

#### Local Sensitivity Analysis

We performed a local SA by varying each of the 96 KRCs individually and report the 25 most sensitive parameters in S4 Fig. The greatest effect on lag time (an increase of 27% or 1 min) occurred with a 50% decrease in the rate of activation of fX by TF:VIIa  $k_{z_{10}^m:e_7}^{cat}$ . The greatest effects on the maximum relative rate of thrombin generation occurred for variations in nine KRCs; a 50% change in any one of these altered this rate by about 20%. The nine KRCs are the rate  $k_8^{off}$  of fVIII/fVIIIa unbinding from its platelet surface binding sites, the rates of activation of prothrombin by prothrombinase  $k_{z_2^m:PRO}^{cat}$ , of fX by tenase  $k_{z_{10}^m:TEN}^{cat}$ , and of fIX by TF:VIIa  $k_{z_9:e_7}^{cat}$ , the Michaelis-Menten constant for activation of TF:VII by fXa  $K_{z_7^m:e_{10}}^M$ , the rates of fIX/fIXa binding to and unbinding from receptors on platelet surfaces,  $k_9^{on}$  and  $k_9^{off}$ , and of thrombin binding to the platelet surface  $k_2^{*,on}$ . The most dramatic effects on the final thrombin concentration occurred with 50% decreases in the rate of prothrombin binding to platelets  $k_2^{on}$  and the rate of activation of prothrombin to thrombin  $k_{z_2^m:PRO}^{cat}$ . These changes caused an 18% and 15% reduction in the final thrombin concentration, respectively. The largest effect on any of the metrics was that which occurred with a 50% reduction in the rate of activation of fX by TF:VIIa.

The local SA reveals that overall the ten most sensitive KRCs, when perturbed one at a time to 50% or 150% of their baseline values, are  $k_{z_9:e_7}^{cat}$ ,  $k_{z_{10}^m:e_7}^{cat}$ , and  $K_{z_7^m:e_{10}}^M$ , which are involved in activation of fIX and fX by TF:VIIa on the subendothelium;  $k_9^{on}$ ,  $k_9^{off}$ , and  $k_8^{off}$  which influence the rate of formation of tenase on the platelet surfaces;  $k_{z_{10}^m:TEN}^{cat}$ , which is the rate of activation of fX by tenase;  $k_2^{on}$  and  $k_{z_2^m:PRO}^{cat}$  which directly affect thrombin production by prothrombinase; and  $k_2^{*,on}$  which affects the ability of thrombin to feedback and activate the cofactors fVIIIa and fVa of tenase and prothrombinase, respectively. This analysis identifies parameters that are potential candidates for the global SA, but selection of this subset is not informed by interaction effects. This motivates our use of the method of

Morris to do additional screening. We note that the maximum percent change in output for any of these KRCs, varied one at a time, is less than 30% and that many of them induced changes of less than 10%.

## Method of Morris

The method of Morris procedure was applied to 96 kinetic rate constants with three path sets  $P_1$ ,  $P_2$ , and  $P_3$ . S5 Fig highlights the KRCs screened as candidates for the global Sobol method. Selection of parameters was based on the criteria that the normalized  $\ell_2$ -norm of the Morris mean  $\mu^*$  and standard deviation  $\sigma$  be  $\geq 0.5$  for any of the path subsets and any of the thrombin generation metrics. The selected subset of 25 KRCs includes activation rates of zymogens by enzymes, binding/unbinding rates on a platelet surface and formation/dissociation rates of complexes. Kinetic rates with  $\ell_2$ -norms  $\geq 0.5$  in all three thrombin generation metrics include binding rates of fVIII/fVIIIa, fIX/fIXa, and thrombin to their respective binding sites on an activated platelet surface ( $k_8^{on}$ ,  $k_9^{on}$ ,  $k_2^{on,*}$ ), activation rates of fX by tenase and prothrombin by prothrombinase ( $k_{z_{10}^m}^{cat:TEN}$ ,  $k_{z_2^m}^{cat:PRO}$ ), and the formation rate of tenase ( $k_{e_8^m:e_9^m}^+$ ).

The activation rates of fIX and fX by TF:VIIa, the unbinding rates of fV/fVa, fVIII/fVIIIa, fIX/fIXa, and fX/fXa from a platelet surface, the activation rates of fV by thrombin and fXa, and the formation rate of prothrombinase on a platelet surface have significant Morris sensitivity norms associated with lag time. All parameters selected except the binding rate of prothrombin and the unbinding rates of thrombin, fV/fVa, and fX/fXa on the platelet surface have significant Morris  $\ell_2$ -norms associated with the maximum relative rate of thrombin generation. Lastly, the binding rate of prothrombin, the unbinding rate of thrombin and the formation rate of prothrombinase all have significant  $\ell_2$ -norms associated with the final concentration of thrombin. The final list of 25 kinetic rate constants all correspond to the formation of tenase and prothrombinase on a platelet surface and the activation of thrombin.

## Global Sensitivity Analysis

Fig 3.6 shows the global SA for the 25 KRCs obtained by the Morris screening. The KRCs were uniformly sampled, simultaneously, from 50% to 150% of their baseline values. Note, only parameters with a non-trivial total order index are displayed ( $p < 0.05$ ). While not shown here, the local SA results for the omitted parameters agree well with the global SA results in that they were all approximately zero. The coefficients of variation for all metrics range between 0.12 for the final concentration and 0.37 for the maximum relative rate and are significantly greater than those observed when varying plasma zymogen and inhibition levels, indicating that the model output is more strongly dependent on the values of the KRCs, at least when they are varied simultaneously and uniformly. The global Sobol indices agree with the local SA results, yielding the same relative ranking of parameter importance for the tested variables in all metrics ( $p < 0.05$  from a rank permutation test [54]). The global results show that several parameters have non-trivial interaction effects (i.e., total order effect is statistically larger than the first order effect with  $p < 0.05$ ), which we have indicated with an asterisk. For lag time, both  $k_{z_{10}^m}^{cat:e_9^m}$  and  $k_8^{off}$  have statistically significant interaction effects ( $p < 0.05$ ), which account for approximately 3% and 2% of the total output variance, respectively. While the final concentration output is dominated

by the two first order effects of  $k_2^{\text{on}}$ , the binding rate of fII to the platelet surface, and  $k_{z_2^{\text{m}}:PRO}^{\text{cat}}$ , the activation of fII by prothrombinase, numerous significant interaction effects also are present, most of which have no significant first order effect at all (i.e., the first order term’s confidence intervals contain zero). These interaction effects are potentially important, accounting for up to 10% of the variance in the final concentration.

Interestingly, the ability to simultaneously vary parameters results in radically different output from the model than seen when they are varied in a OAT fashion. This is most easily seen in the output distribution for thrombin (Fig 3.7 A), where the support spans a significantly larger range than seen in the local SA of plasma levels. While the local SA found a maximum change of less than 30% across all metrics, the global SA produced variations exceeding 50% for all three thrombin generation metrics, even though parameters were varied over the same individual range. The observed output for the three metrics fell between 98-1200s for the lag time (39-482% of baseline),  $0.011\text{-}0.267\text{s}^{-1}$  for the maximum relative rate (11-281% of baseline) and  $0.02\text{-}355.69\text{nM}$  for the final concentration (0-129% of baseline).

### 3.4.3 Varying Platelet Characteristics

In this section we show how thrombin generation is modified due to variations in the platelet characteristics (PCs) in our model, specifically the rate of platelet adhesion to the subendothelium, rates of platelet activation by different agonists, platelet count (upstream platelet concentration), and the number and type of receptors/binding sites on activated platelet surfaces. We analyze local sensitivity by varying each platelet characteristic in a OAT fashion, from 50 to 150% of their baseline values. Fig 3.8A-C show the most influential platelet characteristics for each thrombin metric; the triangle colors and directionality are as previously described. Fig 3.8D-F show the first and total order Sobol indices computed for each platelet characteristic and metric, with the height of the bars indicating the fraction of variance that is attributable to the model output from each parameter individually (first order) and to the parameter including its interactions with other parameters (total order).

In Fig 3.8A-C, we see that varying the number  $N_{10}$  of binding sites for fX/fXa on each activated platelet gives the greatest effect on the lag time; decreasing  $N_{10}$  by 50% leads to a 24% longer lag time. Variations in six platelet characteristics (binding site number per activated platelet for fIIa, fIXa, fVIII/fVIIIa and fII as well as platelet count and the platelet rate of adhesion) have the most effect on the maximum relative rate of thrombin generation (Fig 3.8B). A 50% reduction in platelet count or the rate of platelet adhesion increased the maximum relative rate by about 20%, while a 50% increase in these parameters decreased the maximum relative rate by about 10% (see Fig 3.8B). This reflects the role of platelet coverage of the injury in physically inhibiting TF:VIIa activity.

Lastly, the binding site numbers for fII and fIIa most dramatically affect the final thrombin concentration (Fig 3.8C). An increase of 50% in the value of  $N_2^*$  or  $N_2$  leads to an increase of 28% or 22% in thrombin, respectively (Fig 3.8C). A 50% decrease in the two binding site numbers results in a 28% and 25% decrease in thrombin levels, respectively. Increasing or decreasing the binding site number for thrombin have the largest effects on the final concentration.

The global SA is in agreement with the findings from the local SA, with regard to the relative ranking of important parameters ( $p < 10^{-6}$ ) from a rank permutation test [54]).

As seen when KRCs were varied, changes in the platelet characteristics had a much larger impact on the model variance in all three metrics than when plasma levels of zymogens and inhibition were varied, with coefficients of variations between 0.15 and 0.24. The lag time (Fig 3.8D) was most strongly influenced by variations in  $N_{10}$ , with 37% of the variance explained by it alone. Two parameters,  $PL^{up}$ , the upstream platelet concentration, and  $k_{adh}^+$ , the rate of platelet adhesion to the subendothelium, have statistically significant interaction effects ( $p < 0.05$ ), as indicated by their increased total order indices (marked with a star). We note that the first order index for these two parameters are close to zero (less than 0.03), indicating that variations in the two parameters individually contribute little to the model output. Instead, only the interaction terms appear to be significant. This behavior is not directly observed in the local analysis, but it may be hinted at in the non-monotonic nature of the local SA endpoints for these two parameters (S2A Fig, solid black and dashed purple curves). For the maximum relative rate metric, several parameters have a non-zero Sobol index (Fig 3.8E), yet none explains more than 21% of the model output variance. Again,  $PL^{up}$  and  $k_{adh}^+$  have statistically significant interaction effects but with non-trivial first order effects at 12% and 10%, respectively. For the final concentration of thrombin, almost 90% of the output variation can be explained by the first order effects of three parameters:  $PL^{up}$ ,  $N_2$ , and  $N_2^*$  with 17%, 29%, and 41% of the variance, respectively. It is interesting to note that while these parameters strongly influence the final thrombin concentration, they appear to do so in a nearly independent fashion, as no parameters appear to have significant interactions within this metric.

As with the KRC global results, the observed distribution of the thrombin curves (Fig 3.9A) and the resulting distribution of the coagulation metrics (Fig 3.9B), have a far larger variance than in the plasma level case. This is especially true for the final concentration of thrombin, where extremely high output is made possible by the combination of high platelet count and large numbers of fII/fIIa platelet binding sites (results not shown here).

### 3.4.4 Varying All Model Parameters

In the previous sections, we examined both the local and global sensitivity resulting from variations in three classes of parameters: initial plasma levels, kinetic rate constants, and platelet characteristics. In this section, the three classes are combined and a sensitivity analysis on a subset of the parameters is performed. To identify a subset of parameters that have either a large individual effect on the thrombin output or interact strongly with other parameters, we again use the method of Morris to screen and select parameters. For this screening, the associated  $\ell_2$ -norm of the Morris sensitivity measures  $\mu^*$ ,  $\sigma$  for lag time, maximum relative rate, and final concentration are shown in S6 Fig Parameters with the normalized  $\ell_2$ -norm of the Morris mean  $\mu^*$  and standard deviation  $\sigma$  greater than 0.5, for any of the paths, were chosen as candidates for the parameter subset.

The result of the screen is a subset of 33 parameters: four from plasma levels ( $Z_2, Z_9, Z_{10}, Z_{11}$ ), six from platelet characteristics ( $PL^{up}, N_2, N_5, N_9, N_9^*$ , and  $N_{11}^*$ ), with the remaining 23 from kinetic rate constants. There are six kinetic rate constants in the new subset that were not identified in the original Morris screen for KRCs only:  $k_{z_5^m:e_{10}^m}^{cat}$ ,  $k_{z_8^m:e_2^m}^{cat}$ ,  $K_{PC:TM:e_2}^M$ ,  $k_{z_7:e_9}^-$ , and  $k_{11}^{in}$ . Six of the KRCs were also excluded from the new subset that were previously identified in the KRC-only Morris screen:  $k_{10}^{off}$ ,  $k_5^{off}$ ,  $k_2^{off,*}$ ,  $K_{z_8^m:e_{10}^m}^M$ ,  $K_{z_8^m:e_2^m}^M$ , and  $k_{e_5^m:e_{10}^m}^+$ .

We note that some of the parameters show significant sensitivity, according to the Morris method, for all three of the thrombin generation metrics: the activation rates of fX by TF:VIIa and tenase ( $k_{z_{10}^m:e_7}^{cat}$ ,  $k_{z_{10}^m:TEN}^{cat}$ ), the activation rate of prothrombin by prothrombinase ( $k_{z_2^m:PRO}^{cat}$ ), the binding rates of thrombin and fVIII/fVIII to a platelet surface ( $k_2^{on,*}$ ,  $k_8^{on}$ ), the unbinding rate of fIX/fIXa from a platelet surface ( $k_9^{off}$ ), the inactivation rate of fXIa ( $k_{11}^{in}$ ), and binding site numbers for fII, fIX/fIXa, and fXIa ( $N_2$ ,  $N_9$ ,  $N_{11}^*$ ).

Next, a global SA was performed on the identified subset of parameters, in which the parameters again varied simultaneously between 50-150% of their baseline values. The results of the global SA were compared to those from the local SA, for each of the parameters in the subset, as shown in Fig 3.10. The local and global sensitivity analyses for the lag time and final concentration metrics agree in terms of ranking the parameter importance ( $p < 0.001$  from a rank permutation test [54]), but for the maximum relative rate metric, the local and global methods were in less agreement ( $p < 0.1$ ). The global Sobol information was able to identify interactions that influence the output variance for the lag time and the final concentration metrics (Fig 3.10D,F) but not for the maximum relative rate metric (Fig 3.10E).

In regard to the sensitivity of the lag time (see Fig 3.10D), the single parameter  $k_{z_{10}^m:e_7}^{cat}$  had the largest individual effect, accounting for approximately 15% of the total model variance, with the remaining parameters individually contributing less than 10%. A sum of the non-zero first-order terms for the lag time reveals that approximately 87% of the variance in lag time can be described by the individual effects of the sampled parameters, with the remaining 13% being attributable to interactions between parameters. The large importance of first-order effects helps to explain why the local and global parameter rankings match so well, since first-order effects (the only effects that are measurable by local methods) dominate the system in this regime.

The variance in the final thrombin concentrations at 20 minutes (see Fig 3.10F) was dominated by the number of binding sites for prothrombin,  $N_2$ , which accounted for more than 30% of the total model variance. Also playing a significant role was the plasma level of prothrombin,  $z_2$ , the rate of prothrombin binding to platelet binding sites  $k_2^{on}$ , the rate of prothrombin activation by prothrombinase,  $K_{z_2^m:PRO}^{cat}$ , and the platelet count  $PL^{up}$ . The sum of the first-order terms was approximately 84%, which means that about 16% of the output variance was due to parameter interactions.

While no significant interactions were detected for the maximum relative rate (Fig 3.10E), most of the parameters made small individual contributions to the output variance. A few of the parameters, namely  $k_2^{on}$ ,  $K_{PC:TM:e_2}^M$ ,  $k_{11}^{in}$ ,  $N_9$ ,  $N_{11}$ , and  $z_{11}$  had nearly zero effect as measured by first and total order Sobol indices. Of the parameters that did have an effect, we note that even though they each only contributed a small amount (less than 10% of the variance), there was still a high value for the coefficient of variation (about 40%). In other words, our global analysis revealed that there was high variation in the output, relative to the mean, due to a large number of individual, additive effects; this result would not have been captured with local SA alone.

The coefficient of variation was, in fact, high for all three thrombin metrics, relative to those from the previous studies in which we varied each parameter class individually. This means that simultaneously varying all three types of parameters leads to higher variation in the model output. This result can also be visualized by looking at the variation in thrombin

time series output in Fig 3.11A. There we see very wide boundaries that encompass 90% of the data for the thrombin time series plots (orange region) and also a large total area within the grey dashed lines that represents the max/min boundary of all the data. In addition, the data revealed that almost 1% of the model evaluations in this case failed to generate 1nM of thrombin by 20 minutes (blue dots in heatmap in Fig 3.11B).

We found that for the lag time and the final concentration, a fraction of the variance originates from higher-order interactions among parameters whereas for the maximum relative rate, there were no interactions but a large number of individual additive effects. Because it is difficult to determine exactly which parameters are directly interacting and determine if they are interacting synergistically or antagonistically, we next further examine extreme behavior in the thrombin output to check for patterns or groupings in the parameter variations that lead to the extreme behavior.

### Conditional Input Distributions for Fast/Slow Thrombin Production

To determine if there is a clear way to identify groupings of interacting parameters, we examined two extreme situations, one in which thrombin generation occurs quickly (fast bursts) and one in which thrombin forms very slowly (low producers). To do this we further filtered the simulations used for the global SA in Fig 3.11D-F. In particular, we characterized those simulations that led to fast bursts or were low producers, defined by the smallest and largest 1% of the recorded lag times. In other words, we conditioned the input parameters on leading to fast or slow bursts, and then computed the resulting conditional distributions of parameters.

Interesting patterns emerge in the resulting conditional parameter distributions, as shown in Fig 3.12. We see that specific combinations of parameters, when varied in concert, can achieve extreme responses in the thrombin production. For example, when we condition on low production of thrombin, (Fig 3.12A,C), we observe very low values for  $k_{z_{10}:e_7^m}^{\text{cat}}$ ,  $k_2^{*,\text{on}}$ ,  $K_{z_5^m:e_{10}^m}^{\text{M}}$ ,  $k_{z_5^m:e_{10}^m}^{\text{cat}}$ ,  $k_{z_{10}^m:TEN}^{\text{cat}}$ ,  $k_{z_2^m:PRO}^{\text{cat}}$ ,  $k_{e_8^m:e_9^m}^+$ , and  $N_2$  and a few others to a lesser degree. In addition, we see higher values of  $K_{z_{10}:e_7^m}^{\text{M}}$ ,  $k_8^{\text{off}}$ ,  $PL^{\text{up}}$ , and  $N_5$ . These parameter values slow the production of thrombin by decreasing the activation of fX by TF:VIIa, the rate that thrombin binds to platelet binding sites, the Michaelis-Menten constant for fV and fXa on the platelet surface and the catalytic rate for the same reaction, the catalytic rate for activation of fX by tenase, the catalytic rate for prothrombin conversion to thrombin by prothrombinase, the formation of tenase complexes, and the number of binding sites for prothrombin on the platelet surfaces. These parameter values slow the production of thrombin by increasing the Michaelis-Menten constant for fX and TF:VIIa on the platelet surface, the rate that fVIII/fVIIIa unbind from the platelet surface, the platelet count in the plasma, and the number of platelet binding sites for fV/fVa.

When we condition on fast thrombin production, (Fig 3.12B,D), we observe very low values for  $K_{z_7:e_{10}^m}^{\text{M}}$ ,  $K_{z_{10}:e_7^m}^{\text{M}}$ ,  $k_8^{\text{off}}$ , and  $N_5$ , with higher values for  $k_{z_7^m:e_{10}^m}^{\text{cat}}$ ,  $k_{z_{10}:e_7^m}^{\text{cat}}$ ,  $k_{z_{10}^m:TEN}^{\text{cat}}$ ,  $k_{z_2^m:PRO}^{\text{cat}}$ ,  $k_{e_8^m:e_9^m}^+$ , and  $Z_{10}$ . The skew of the distributions for the fast bursters are generally opposite from the skew of the same parameters for the low producers. In particular, reactions that increase/decrease the activation of fX by TF:VIIa intuitively affect the fast/slow production, including higher fX levels in the plasma. Similarly, the reactions that increase/decrease the activation of fX and prothrombin by tenase and prothrombinase intuitively affect the fast/slow production. Not so intuitively, perhaps, are the distributions

for the binding rates for fVIII/fVIIIa to the platelet, the platelet count in the plasma, and binding site numbers for prothrombin and fV/fVa. But using our intuition with this model, we speculate that allowing fVIII/fVIIIa to stay bound to the platelets longer with fewer binding sites for fV/fVa can induce faster thrombin production in the following way: the more fVIIIa is available on the platelet surface, the more tenase could potentially form and thus the more fXa could be produced on the platelet surface; from here the fXa produced by the tenase feeds back and activates more bound fVIII, especially since there is less fV bound to the platelet that would compete with the fVIII for fXa. This is similar to the results in our previous study showing that fXa produced by tenase has an impact on the timing of the thrombin burst by feeding back to enhance more tenase formation [20]. Interestingly, the slow bursters are characterized by high numbers of binding sites for fV/fVa but also a highly skewed distribution for platelet count; here the platelets are inhibiting the system by covering the activity at the SE, similar to the interplay between fXI and platelet count reported in our previous study [16].

### Thrombin metric dependence on parameter class

Further inspection of Figs 3.5B, 3.7B, 3.9B, and 3.11B leads to two important observations. First, we see that the mean of each thrombin metric is very close to the value produced when the input parameters are at their baseline level. Second, we see that these means are similar independent of parameter class variation. However, we have also demonstrated a wide range of coefficients of variation across the previous sections, with the highest values resulting from simultaneous variation of all three classes of parameters. Even though the thrombin metric means are similar, the spread in the thrombin metric output is shown to vary greatly across parameter class.

The thrombin metric outputs are the result of hundreds of thousands of samples through parameter space and can be represented as a three-dimensional cloud of points, where each dimension is a different thrombin metric: lag time, max relative rate, and final concentration. Note that we have compiled four of these point clouds, one for each of the parameter classes. To visualize the spread in the outputs, for each parameter class, we constructed a hull around the point clouds and projected them onto all possible two-dimensional planes to see how they compare. In Fig 3.13, we show these projections, with the result for each parameter class overlaid on top of one another, where plasma levels are in black, platelet characteristics are in blue, kinetic rate constants are in green, and the subset of all classes is red. It is clear from Fig 3.13 that the spread in the thrombin metric outputs is largest when all classes of parameters are varied simultaneously. In addition, we found that there are strong negative correlations among certain thrombin metrics. To quantify this, we computed the Pearson correlation coefficient between pairs of thrombin metrics. The correlation coefficients between the lag time and maximum relative rate showed strong negative correlation: -0.93, -0.68, -0.81, and -0.73, corresponding to variations in the plasma levels, kinetic rate constants, platelet characteristics, and subset of all classes. Interestingly, the Pearson correlation coefficients between lag time and final concentration were between -0.23 and -0.41, showing weak negative correlation, while the coefficients between maximum relative rate and final concentration ranged between 0.25 and 0.37, showing weak positive correlation.

### 3.4.5 Varying Flow

While higher blood flow velocities bring platelets and coagulation proteins to the site of injury at a faster rate, they also carry away enzymes produced at that site at a faster rate. Therefore, flow can both facilitate and inhibit thrombin generation and, thus, thrombus formation. This makes it difficult to intuit the exact response that the system will have to changes in flow. In this section, we show how thrombin generation in our model is modified due to variations in shear rate over the range of those found physiologically. To address overall variation in thrombin generation, samples using shear rates within the range of 1-1500 (1/s) were generated.

Fig 3.14A shows variations in thrombin generation with respect to time for several shear rates spanning the physiological range. Fig 3.14B-D highlight the effect of shear rate on the three thrombin generation metrics. In our model, variations in shear rate lead to variations in the volume of the reaction zone in which the model's reactions occur because of changes in the average boundary layer thickness. Therefore, rather than concentrations, we look at the amount (fmols) of thrombin in the reaction zone to assess the effect of shear rate on the system. To coordinate the three metrics of thrombin generation with those used in the previous analyses, we redefined the first metric to be the time to  $2(10^{-7})$  fmol (lag time\*). This quantity was determined using the average volume of the reaction zone for shear rate 100 (1/s) to calculate the number of moles of thrombin that are in the reaction zone when the thrombin concentration is 1 nM. The maximum relative rate\* is calculated using the corresponding amounts of thrombin. The third metric is the amount of thrombin in the reaction zone at 20 minutes (final amount).

Lag time\* varies from a little more than 200 seconds for shear rate 10/s to a little less than 400 seconds for shear rate 1500/s (Fig 3.14B). It is interesting that lag time\* has a minimum for a shear rate about 10/s. The maximum relative rate\* metric rises to a maximum at shear rate about 10/s and then falls by more than 50% as the shear rate increases to 1500/s (Fig 3.14C). The final amount of thrombin in the reaction zone decreases monotonically by about 10-fold as the shear rate increases from 1/s to 1500/s (Fig 3.14D). The decrease is fastest as the shear rate increases from 10/s to 150/s.

In Fig 3.15, we show the effect of shear rate on total thrombin production and on thrombin's removal by flow, by lateral diffusion in a direction perpendicular to the flow direction, and by chemical inhibition by AT. For shear rates between 1/s and 1500/s, the removal of thrombin is dominated by the effects of flow. Indeed, the removal of thrombin by AT is approximately one hundred-fold smaller than that by flow. For very low shear rates (0.01/s to 0.4/s), the amount of thrombin removed by lateral diffusion or by chemical inhibition by AT is each larger than the amount removed by flow. This is consistent with static experiments which show significant removal of thrombin by AT inhibition [55, 56].

We also examined whether small variations in shear rate elicited large changes in model output that could effect the sensitivity analyses of this paper. To do this, we conducted the Method of Morris analysis on all model parameters at shear rates 90, 100, and 110 (1/s). Results of this analysis are shown in S3 Fig. From those plots it is clear that small changes in shear rate from the value 100/s used in most of our analyses do not effect the sensitivity of thrombin generation to variations in the model's parameters, and do not effect the results of the Morris method based selection of parameters for the global SA.

## 3.5 Discussion

In this study, we performed local and global sensitivity analyses of a mathematical model of coagulation and platelet deposition under flow. For the local analysis, input parameters were varied one at a time (OAT), whereas for the global methods, input parameters were varied simultaneously. We quantified the sensitivity of three thrombin metrics: lag time, maximum relative rate of generation, and final concentration after 20 minutes, to variations in three parameter classes: plasma levels, platelet characteristics, and kinetic rate constants. In addition, we examined sensitivity of the metrics to a subset of the union of all three parameter classes. For the cases of kinetic rate constants and all three parameter classes varied simultaneously, due to the large number of parameters under consideration, we performed subset selection using the method of Morris as a screening tool. Because our mathematical model considers flow and thus, the effect of flow on platelet adhesion and coagulation, we also examined the sensitivity of the thrombin metrics to changes in shear rate and the removal by flow, diffusion, and chemical inhibition/inactivation.

### 3.5.1 Plasma levels

The local and global sensitivity analysis of the thrombin metrics due to variations in initial plasma levels were in good agreement with one another. No OAT variation in plasma levels led to more than a 20% change in any thrombin metric output; variations in prothrombin ( $Z_2$ ) produced the largest change in output, specifically in the final concentration. The results of global analysis reveals that there are no significant interactions between the plasma levels and thus suggests that the model is additive in this regime. The coefficient of variation for the maximum relative rate was 11% but was less than 1% for lag time and final concentration, indicating relatively small overall sensitivity of the model to normal variations in plasma levels. We also observed that all variations in plasma levels, using local or global methods, led to strong and steady thrombin generation.

To our knowledge, Danforth and colleagues [38] were the first and only other group to perform a sensitivity analysis on thrombin metrics, not simply overall thrombin sensitivity, and thus our results would compare more naturally with theirs than with other SA approaches on coagulation models. One limitation of their methodology, however, is the small number of parameters that they vary simultaneously (pairwise only), whereas our global methods vary all plasma levels simultaneously. Another difference is that their model simulated a closed system, which can provide a partial explanation for their observation that variations in initial levels of AT and TFPI had the most significant effects on the system. We also only compare to their data in which the plasma levels were varied within a normal range, but in their study and ours, there is always substantial thrombin generation by 20 minutes.

### 3.5.2 Platelet characteristics

The local and global sensitivity analysis of the thrombin metrics due to variations in platelet characteristics were also in good agreement with each other. No OAT variation in platelet characteristics led to more than a 28% change in any thrombin metric output, and there was strong thrombin production in all cases. The prothrombin- and thrombin-specific binding site numbers,  $N_2, N_2^*$ , produced the largest % change in the final concentration

while the platelet count and adhesion rate,  $PL^{up}$ ,  $k_{adh}^+$ , produced the largest % change in the maximum relative rate. The global analysis highlights that  $PL^{up}$ ,  $k_{adh}^+$  have statistically significant interaction effects. Interestingly, the non-monotonic behavior of the lag time when  $PL^{up}$  and  $k_{adh}^+$  vary from 50% to 150% of the baseline values (S2 Fig) suggests such interaction effects. Both parameters are involved with platelet adhesion and determine how quickly the injury zone is paved over by platelets. Given that many reactions occur on platelet surfaces, it is intuitive that the thrombin metrics would be affected by the platelet count and rate of subendothelial coverage. The global analysis further suggests that the model is additive for most parameters in this regime. The coefficients of variation were 15%, 24%, and 24% for the lag time, maximum relative rate, and final concentration, respectively.

### 3.5.3 Kinetic rate constants

The local sensitivity of thrombin metrics to kinetic rate constants (KRCs) showed that the maximum percent change in thrombin metric output due to OAT variation of any KRC is less than 30%. This means that in all of these simulations, there was always strong and steady thrombin generation. The global SA, however, showed something considerably different; when varying the KRCs simultaneously, there were situations (<1% of the total samples) where thrombin never reached 1 nM within 20 minutes. Interestingly, this resulted from variation in the KRCs from 50-150% of their baseline value. This is different from the results shown in the 2009 study by Danforth and colleagues [37]. In this early study by this group, overall thrombin sensitivity due to OAT variations of KRCs ranging from 10-1000% of baseline values was quantified, but not sensitivity of specific thrombin metrics. However, they showed that variations in the rate of TFPI inhibition (shown later to be one of their more sensitive parameters) still resulted in substantial thrombin generation by 20 minutes (see Fig 2A in [37]).

The global SA further revealed parameter interactions on a subset of KRCs selected by the method of Morris screen. Specifically, relating to the variance in lag time, the catalytic rate of activation of fX by TF:VIIa was found to interact with the rate that fVIII/fVIIIa unbind from the platelet surface, albeit these interactions only accounted for a small fraction of the variance. The coefficient of variation for the lag time was about 30%. The maximum relative rate metric had a larger coefficient of variation (37%) but there were no significant parameter interactions observed; all of the parameters accounted for small, additive, fractions of the variance. As for the variance in final concentration, the rate that prothrombin binds to the platelet surface accounted for about 50% of the variance but was not found to interact with other parameters, while the catalytic rate of activation of prothrombin by prothrombinase (accounting for about 30% of the variance) was shown to interact with other parameters that each accounted for only small fractions of the variance. It was not possible to discern which of these parameters were specifically interacting with the others. The coefficient of variation for the final concentration was low, about 12%.

### 3.5.4 Varying all parameter classes

To our knowledge, this is the first sensitivity analysis of a model of coagulation in which multiple parameter classes were varied simultaneously. A variation in the subset of all parameter classes led to the largest change in output of thrombin metrics, compared to variations in each parameter class alone. Interestingly, carrying out this variation in a OAT

fashion leads to a maximum change in output of only about 25%, and again shows that every simulation in this case would lead to strong and steady thrombin generation. The global analysis further revealed potential interactions amongst parameters in regard to the lag time and final concentration while the maximum relative rate had the highest coefficient of variation but due to parameters that acted additively.

Again, the catalytic rate of activation of fX by TF:VIIa significantly affected the lag time, along with the rate that fVIII/fVIIIa unbinds from the platelet surface and the catalytic rate of activation of fV by fXa on the platelet surface. In addition to these KRCs, potential interactions were found between these and other parameters within the platelet characteristics class. The coefficient of variation for the lag time was about 36%. The final concentration metric was affected by multiple parameters from all classes, but involved platelet count and parameters associated with prothrombin: the plasma level for prothrombin, the binding rate for prothrombin to the surface of platelets, the number of platelet binding sites for prothrombin, and the catalytic rate of activation of prothrombin by prothrombinase on the platelet surface. The coefficient of variation for the final concentration was 23%. To better understand how the interactions affected extreme thrombin behavior, we conditioned the input distributions for globally varied parameters for fast/slow thrombin bursts. With this conditioning, we were able to clearly identify groups of parameters that resulted in fast/slow bursting behavior.

### 3.5.5 Flow

We found that as the shear rate is increased from  $1 \text{ s}^{-1}$  to  $1500 \text{ s}^{-1}$ , there is non-monotonic behavior in the lag time and the maximum relative rate, while the final thrombin amount decreases monotonically in this regime. A potential explanation for these results, as shown in Fig 3.14A-D and Fig 3.15, is the following. At large shear rates the height of the average chemical boundary layer and the platelet layers is smaller, producing a thinner reaction zone. Although higher shear rates imply that more platelets are brought into the reaction zone by the flow, the flow simultaneously washes more platelets away, which results in fewer platelets in the reaction zone overall (and thus, fewer platelet surfaces on which reactions may occur), although this also depends on adhesion and activation rates, proving that the effect of flow on each individual process is complex. We found, however, that there was both fewer active platelet surfaces and an increase in the removal of thrombin by flow that together, resulted in longer lag times, slower maximum relative rates of generation, and smaller final amounts.

### 3.5.6 Limitations of our methodology

While our results from global SA showed considerable interactions between kinetic parameters, we emphasize that these results depend on the specific distributions and ranges that were chosen for each parameter. Because the uniform distribution is a maximum entropy distribution, it is possible that we have either over or underrepresented interaction strengths. Beyond the shape of the distribution, the range of viable kinetic rate constant values would similarly impact these findings. More accurate information on reasonable ranges of these values could greatly improve the ability of global SA methods to determine meaningful parameter interactions. In addition, we have assumed that parameters are independently distributed. However, if these values are in fact correlated among individu-

als (perhaps through a common genetic or biochemical mutation) an independent sampling method may again over or underrepresent interaction strengths depending on the functional consequences of the correlation. Finally, although the Morris method is a common screening tool for large sets of parameters, we note it is possible that in our global SA method we have missed interactions due to this screening method.

We note that the effects of flow and diffusion are given simplified treatment in this model. Despite these assumptions, results from this model have led to multiple experimentally-validated hypotheses regarding the TF-dependent threshold behavior of thrombin [57] and the synergistic behavior between TF and exogenous FXIa [20]. Extensions to this model include detailed fluid dynamics together with a continuum model of platelet aggregation [17, 18]. Performing sensitivity analysis of those model extensions will be the focus of future work.

### 3.5.7 Local versus global analysis: what have we learned?

One important question that has resulted from this study is how to determine if and when it is more appropriate to use a local versus a global SA on models of complex biological systems. In terms of identifying and ranking our model's most sensitive parameters, we found that the results of the local and global SA are in excellent agreement with one another, in all cases. However, we found that there were cases where if we wanted to explain the details of the variance in model outputs, the impact on the variance from parameters was not independent. This suggests that if a parameter ranking is the primary interest, a local SA may be sufficient, but if precise quantitative attribution of model output variance is necessary, global SA should be employed.

Beyond the information on parameter interactions, our global SA determined parameters whose variation significantly contributes to the variance of model output by themselves. In addition, the global SA provided the opportunity to examine subsets of input parameter space which were linked with strongly extremal output behavior, such as having a lag time in excess of 20 minutes despite still being in normal parameter ranges. Global SA results determined groupings of parameters that are more/less likely to lead to fast/slow thrombin bursting behavior. Finally, we note that all of our analyses were based on analyzing normal parameter ranges, it is possible that dependencies between parameters will be even stronger, and thus the global SA is more appropriate when considering disease states. Results of the local SA, method of Morris, and the global SA motivated the construction of a tailored sensitivity analysis approach for the model system described above. However, this methodology could potentially be employed to help identify biochemical and biophysical parameters that determine bleeding phenotype in some bleeding disorders, which is the focus of our future work.

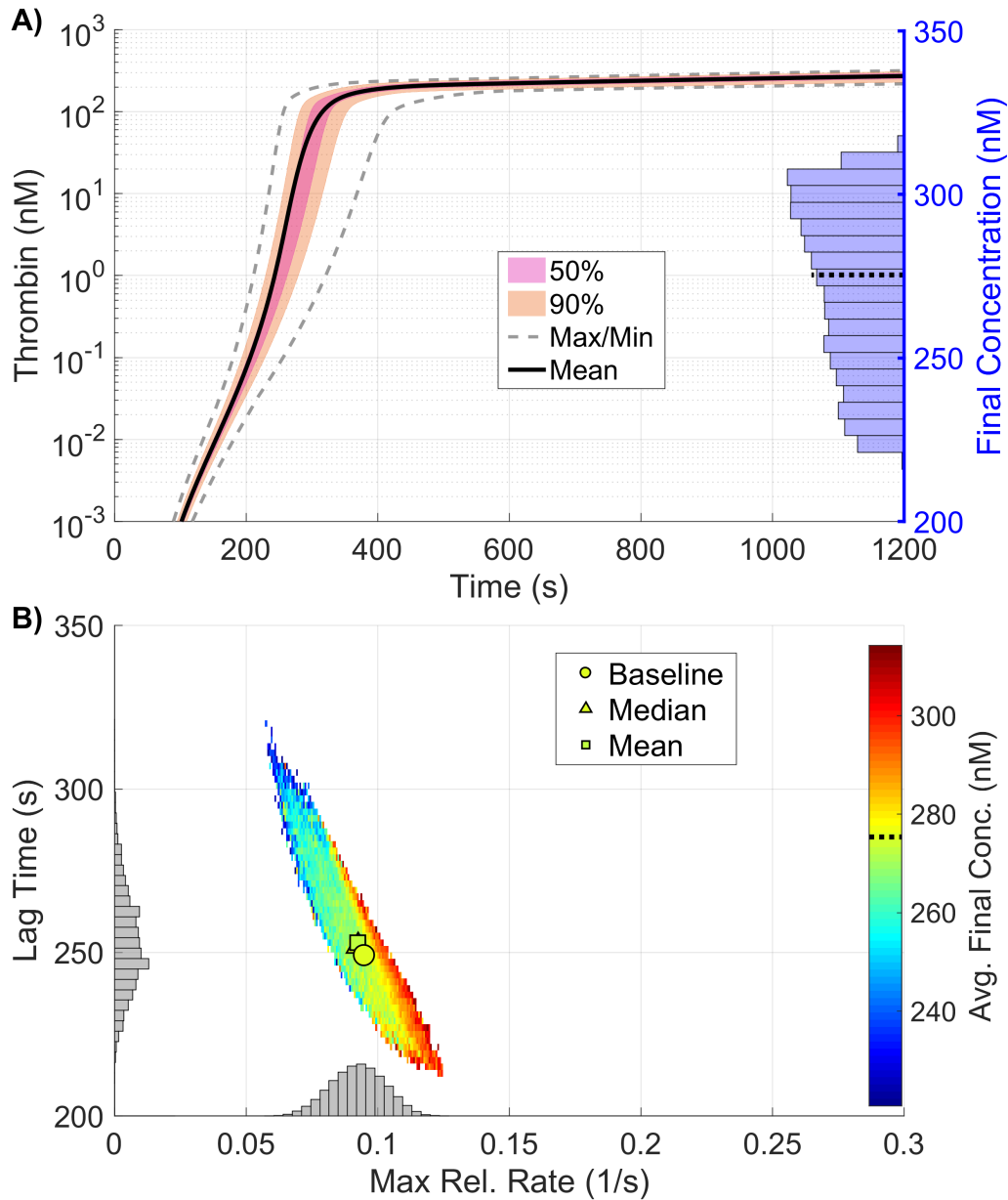


**Figure 3.5: Variation in thrombin generation as a result of varying plasma levels.** **A)** *Left Axis:* Thrombin concentration time series showing the mean (solid black line) and boundaries that encompass 50% of the data (pink), 90% of the data (orange), and the maximum/minimum of the computed solutions (gray-dashed) generated by uniformly varying initial zymogen plasma levels from 50-150% of normal simultaneously (110,000 total function evaluations). *Right Axis:* Marginal histogram of final thrombin concentration at  $t = 1200$  seconds. **B)** Heatmap and marginal histograms relating three important thrombin generation metrics: lag time (*y-axis*), maximum relative rate (*x-axis*), and final concentration (*color-axis*). Results were obtained by post-processing samples used to compute the global sensitivity indices. Dashed black bar in (A) and (B) represents the baseline case of 275nM of thrombin at 20 minutes.

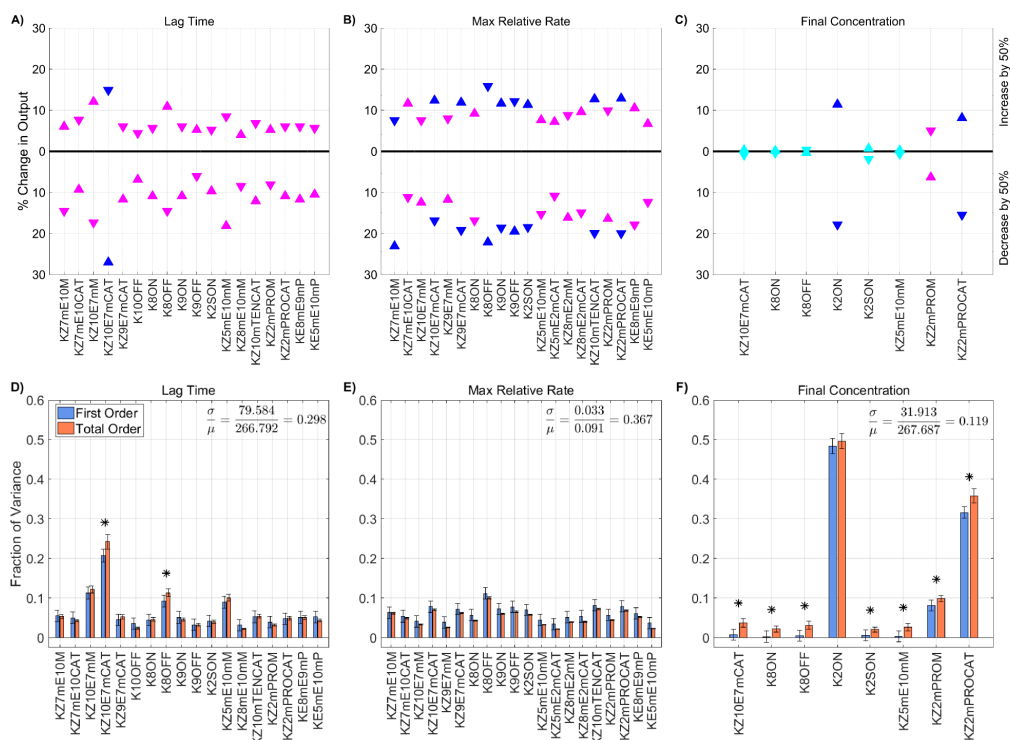


**Figure 3.6: Sensitivity of thrombin generation to KRCs.** Variation in the **(A,D)** lag time; **(B,E)** maximum relative rate; **(C,F)** final concentration; to platelet characteristics using the local (OAT) method (**A-C**) and global Sobol method (**D-F**). *Local*: Sensitivities  $LS_j^i$  that lie between 0.75 and 1 (blue), between 0.25 and 0.75 (magenta), less than 0.25 (cyan) determine the rank-ordered list of kinetic rate constants. The percent change of thrombin generation measures from standard model output for each initial condition are represented by triangles. The direction of variation is indicated with an upwards or downwards facing triangle. *Global*: First and Total Order Sobol indices are plotted as bars with errors of 2 standard deviation about the mean, computed with 5,000 bootstrap samples of the original 540,000 function evaluations. The coefficient of variation is included to provide a scale for the fraction of variance. PCs with Total Order index statistically significantly larger than the First order index are indicated with a star.

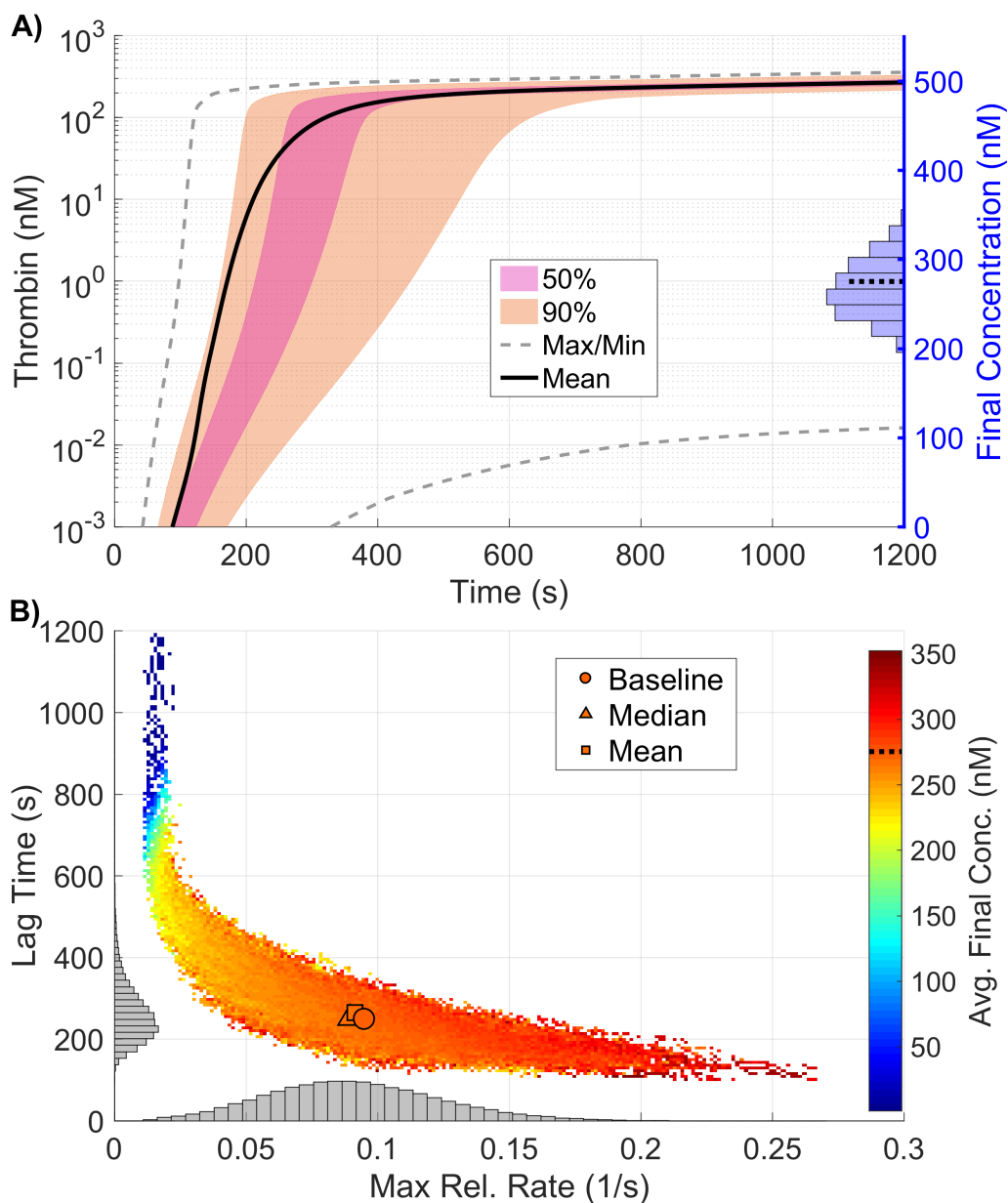


**Figure 3.7: Variation in thrombin generation as a result of varying kinetic rate constants.** **A)** *Left Axis:* Thrombin concentration time series showing the mean (solid black line) and boundaries that encompass 50% of the data (pink), 90% of the data (orange), and the maximum/minimum of the computed solutions (gray-dashed) generated by uniformly varying kinetic rates sampled uniformly between 50-150% of their nominal value simultaneously (270,000 total function evaluations). *Right Axis:* Marginal histogram of final thrombin concentration at  $t = 1200$  seconds. **B)** Heatmap and marginal histograms relating three important thrombin generation metrics: lag time ( $y$ -axis), maximum relative rate ( $x$ -axis), and final concentration ( $color$ -axis). Results obtained by post-processing samples used to compute the global sensitivity indices. Dashed black bar in (A) and (B) represents the baseline case of 275nM of thrombin at 20 minutes.

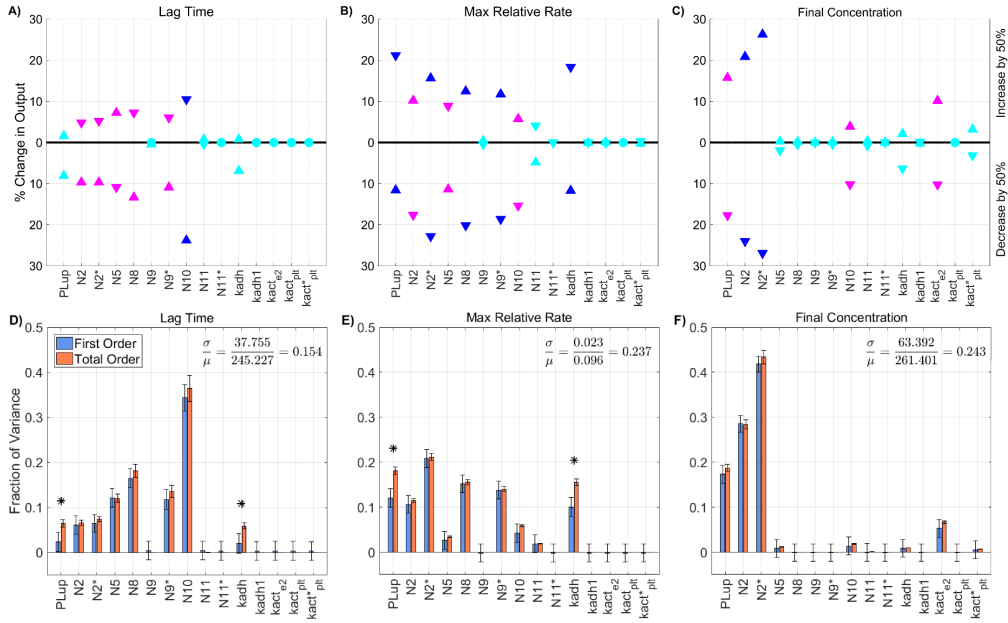


**Figure 3.8: Sensitivity of thrombin generation to platelet characteristics.** Variation in the **A,D)** lag time; **B,E)** maximum relative rate; **C,F)** final concentration; to platelet characteristics using the local (OAT) method (**A-C**) and global Sobol method (**D-F**). *Local*: Sensitivities  $LS_j^i$  that lie between 0.75 and 1 (blue), between 0.25 and 0.75 (magenta), less than 0.25 (cyan) determine the rank-ordered list of platelet characteristics. The percent change of thrombin generation measures from standard model output for each initial condition are represented by triangles. The direction of variation is indicated with an upwards or downwards facing triangle. *Global*: First and Total Order Sobol indices are plotted as bars with errors of 2 standard deviation about the mean, computed with 5,000 bootstrap samples of the original 170,000 function evaluations. The coefficient of variation is included to provide a scale for the fraction of variance. PCs with Total Order index statistically significantly larger than the First order index are indicated with a star.

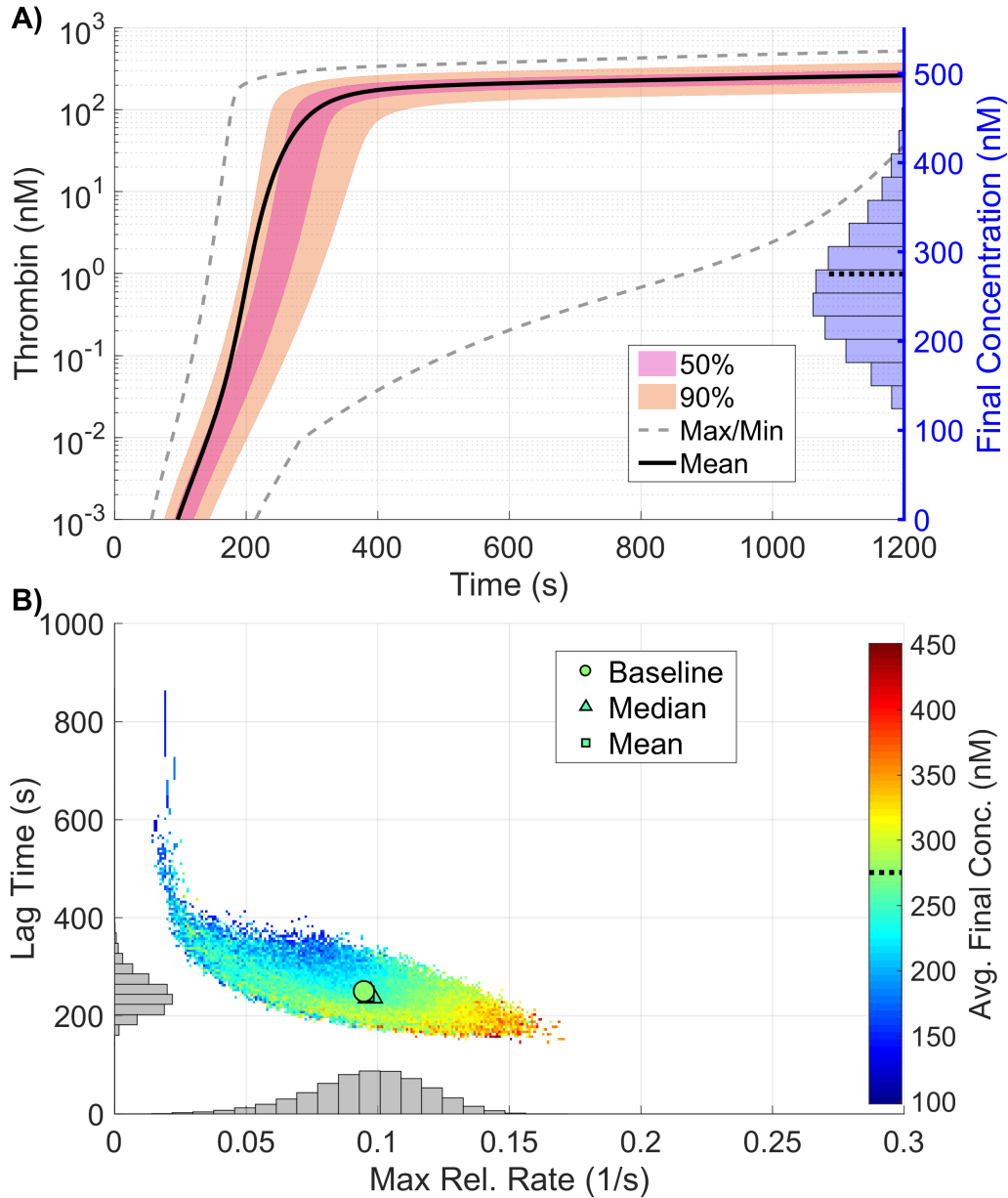


**Figure 3.9: Variation in thrombin generation as a result of varying platelet characteristics.** **A)** *Left Axis:* Thrombin concentration time series showing the mean (solid black line) and boundaries that encompass 50% of the data (pink), 90% of the data (orange), and the maximum/minimum of the computed solutions (gray-dashed) generated by varying platelet characteristics uniformly between 50-150% of their baseline values simultaneously (170,000 total function evaluations). *Right Axis:* Marginal histogram of final thrombin concentration at  $t = 1200$  seconds. **B)** Heatmap and marginal histograms relating three important thrombin generation metrics: lag time ( $y$ -axis), maximum relative rate ( $x$ -axis), and final concentration ( $color$ -axis). Results obtained by post-processing samples used to compute the global sensitivity indices. Dashed black bar in (A) and (B) represents the baseline case of 275nM of thrombin at 20 minutes.

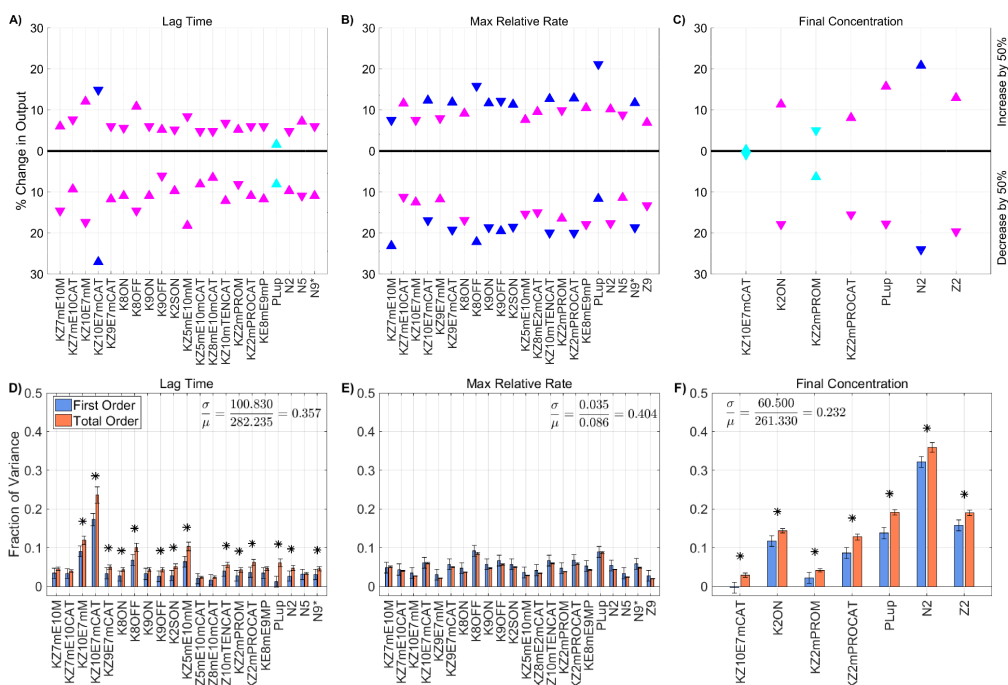


**Figure 3.10: Sensitivity of thrombin generation to a subset of all model parameters.** Variation in the **A,D)** lag time; **B,E)** maximum relative rate; **C,F)** final concentration; to a subset of all model parameters using the local (OAT) method (**A-C**) and global Sobol method (**D-F**). *Local*: Sensitivities  $LS_j^i$  that lie between 0.75 and 1 (blue), between 0.25 and 0.75 (magenta), less than 0.25 (cyan) determine the rank-ordered list of platelet characteristics. The percent change of thrombin generation measures from standard model output for each initial condition are represented by triangles. The direction of variation is indicated with an upwards or downwards facing triangle. *Global*: First and Total Order Sobol indices are plotted as bars with errors of 2 standard deviation about the mean, computed with 5,000 bootstrap samples of the original 740,000 function evaluations. The coefficient of variation is included to provide a scale for the fraction of variance. PCs with Total Order index statistically significantly larger than the First order index are indicated with a star.

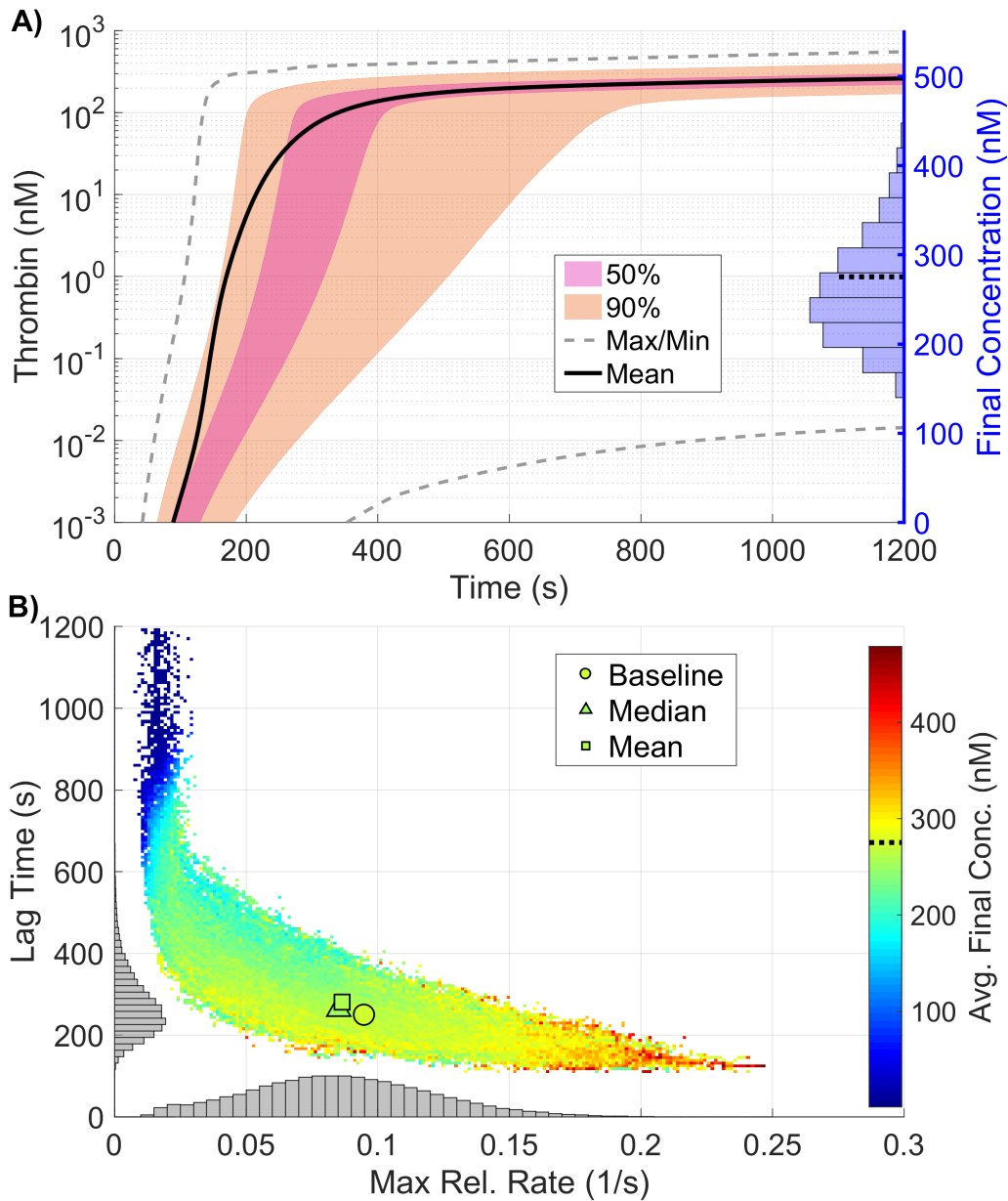


**Figure 3.11: Variation in thrombin generation as a result of varying a subset of all model parameters.** **A)** *Left Axis:* Thrombin concentration time series showing the mean (solid black line) and boundaries that encompass 50% of the data (purple), 90% of the data (orange), and the maximum/minimum of the computed solutions (gray-dashed) generated by uniformly varying a subset of all parameters (found via the Morris method) sampled between 50-150% of their nominal value simultaneously (740,000 total function evaluations). *Right Axis:* Marginal histogram of final thrombin concentration at  $t = 1200$  seconds. **B)** Heatmap and marginal histograms relating three important thrombin generation metrics: lag time ( $y$ -axis), maximum relative rate ( $x$ -axis), and final concentration ( $color$ -axis). Results obtained by post-processing samples used to compute the global sensitivity indices. Dashed black bar in (A) and (B) represents the baseline case of 275nM of thrombin at 20 minutes.

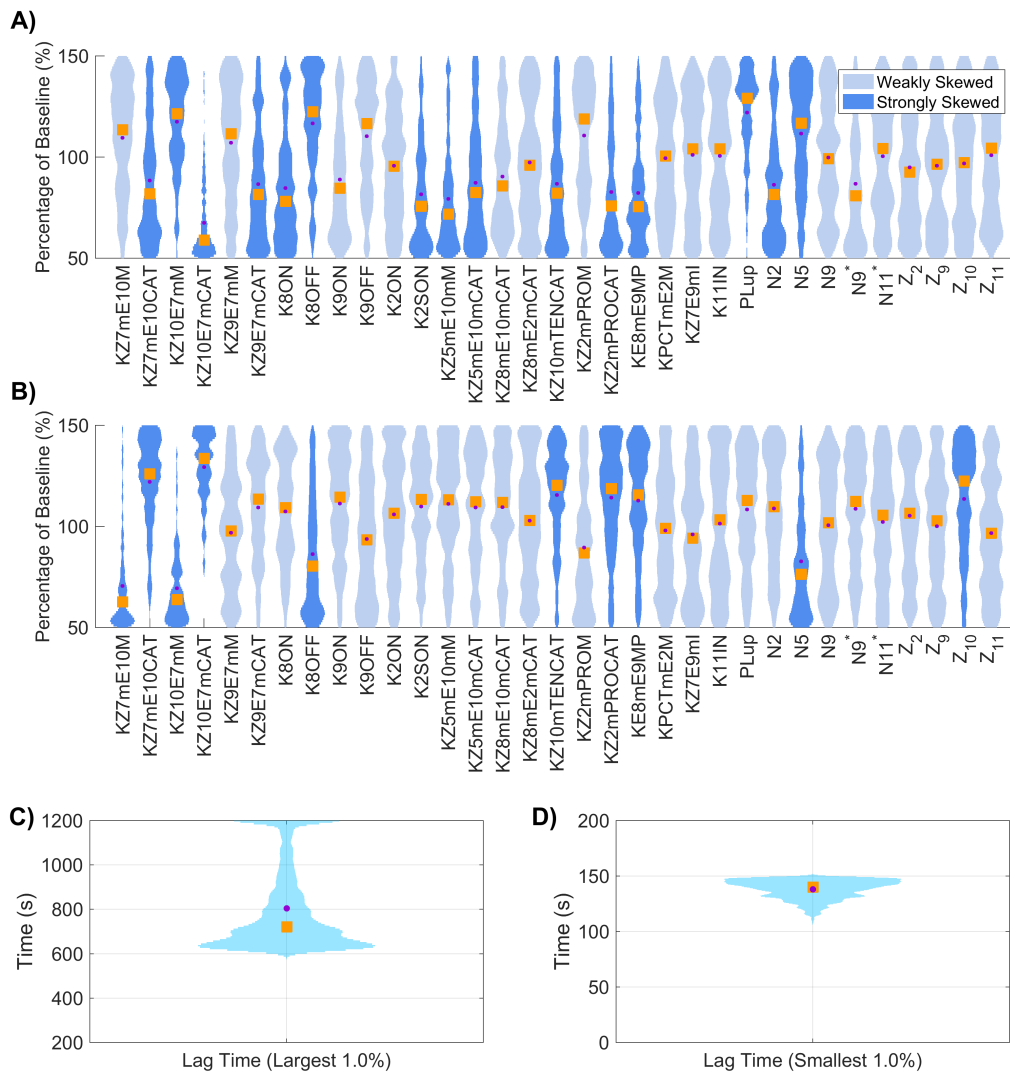


**Figure 3.12: Conditional input distributions for globally varied subset of all parameters, of thrombin lag time and final concentration.** The subset of parameters were sampled uniformly between 50-150% of their baseline value and the lag time of total thrombin was computed. The input distributions were conditioned on a slow burst: the largest 1% of lag time (A) and a fast burst: the smallest 1% of lag time (B). Distributions were colored dark blue if the empirical skew was greater than 0.5 in magnitude and light blue otherwise. Distributions of lag times for slow bursts (C) and fast bursts (D); skew shown when the mean (dot) and median (square) are not aligned.

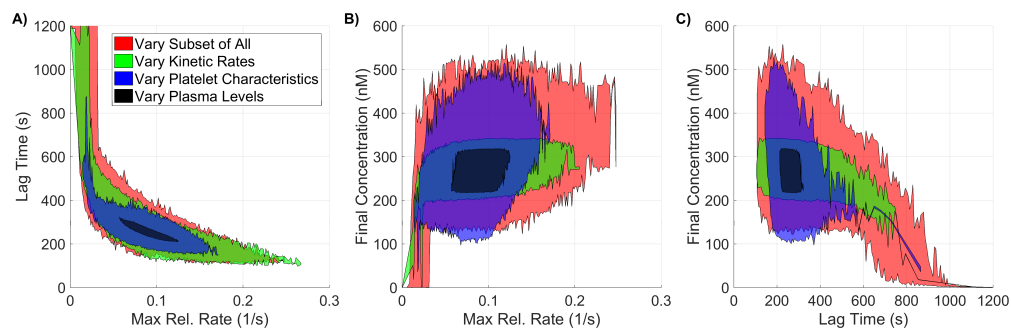


**Figure 3.13: 2D Projections of output coagulation metric envelopes for different classes of varying inputs.** Three classes of model parameters (plasma levels, a subset of important kinetic rate constants, and platelet characteristics) are varied within normal ranges. The envelope of three important coagulation metrics (lag time, maximum relative rate, and final concentration) are recorded and projected into two dimensions, where **A**, **B**, and **C** are the different orthogonal directions.

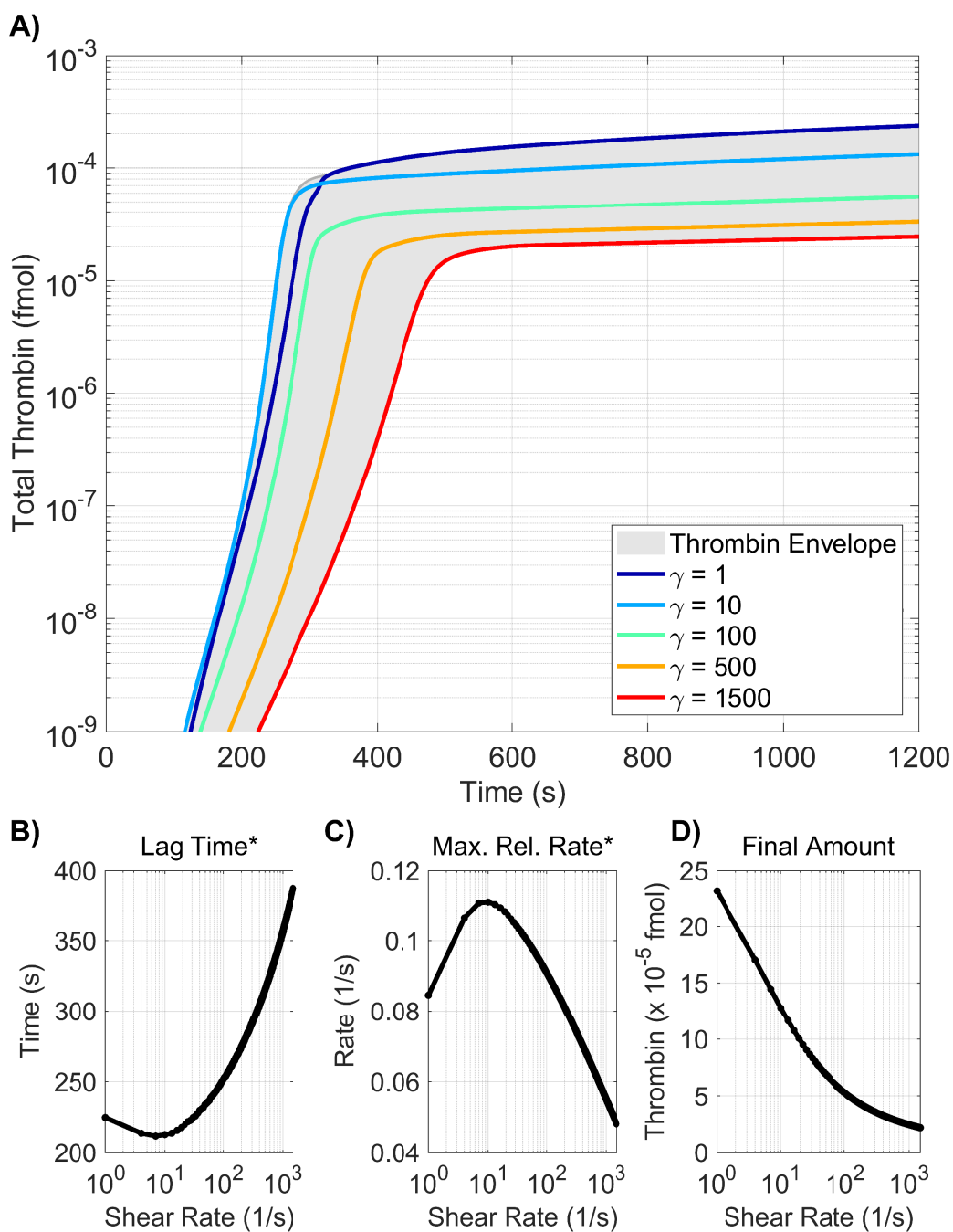


**Figure 3.14: Variation in thrombin generation as a result of varying shear rate.** **A)** Time series of the amount of thrombin showing the the maximum and minimum of the data (blue) generated by varying the shear rate from 1-1500 (1/s) as well as thrombin curves generated with shear rates 1, 10, 100, 500, and 1500 (1/s). Dependence of **B)** lag time\*; **C)** maximum relative rate\*; **D)** final amount on shear rate.

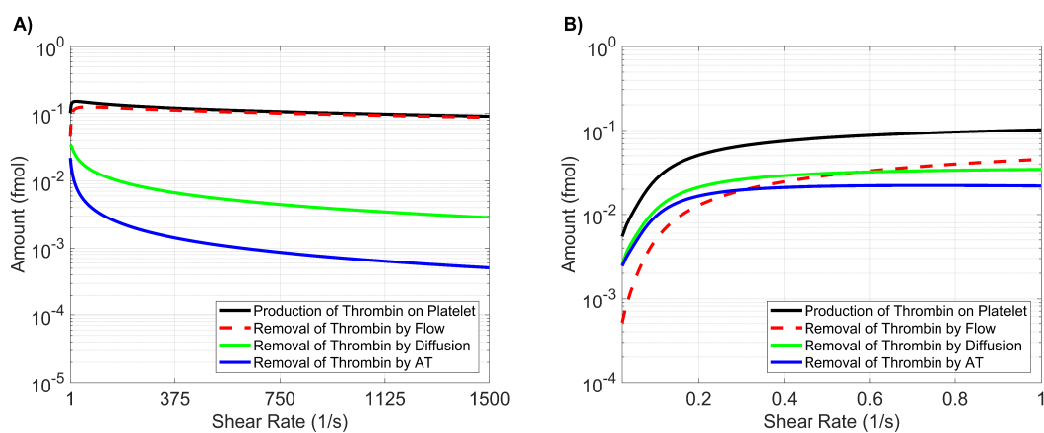


**Figure 3.15: Effects of shear rate on production and removal of thrombin:** Total production and removal of thrombin by flow, diffusion and chemical inhibition by antithrombin AT generated by varying shear rate from **A)** 1 - 1500 (1/s); **B)** 0.01 - 1 (1/s). At small and large shear rates (1-1500 (1/s)), the removal of thrombin is dominated by the effects of flow. Significantly smaller shear rates that approach static conditions result in diffusion and chemical inhibition dominated removal of thrombin. Static experiments support significant removal of thrombin by AT inhibition.

## Bibliography

- [1] Hoffman M, Monroe DM. A Cell-based Model of Hemostasis. *Thromb Haemost.* 2001;85:958–65.
- [2] Butenas S, van't Veer C, Mann KG. “Normal” thrombin generation. *Blood.* 1999;94(7):2169–2178.
- [3] Hockin MF, Jones KC, Everse SJ, Mann KG. A model for the stoichiometric regulation of blood coagulation. *J Biol Chem.* 2002;277:18322–18333.
- [4] Bungay SD, Gentry PA, Gentry RD. A mathematical model of lipid-mediated thrombin generation. *Math Med and Biol.* 2003;20(1):105–129.
- [5] Butenas S, Orfeo T, Gissel MT, Brummel KE, Mann KG. The Significance of Circulating Factor IXa in Blood. *J Biol Chem.* 2004;279(22):22875–22882.
- [6] Luan D, Zai M, Varner JD. Computationally derived points of fragility of a human cascade are consistent with current therapeutic strategies. *PLoS Comp Bio.* 2007;3(7):e142.
- [7] Chatterjee MS, Denney WS, Jing H, Diamond SL. Systems Biology of Coagulation Initiation: Kinetics of Thrombin Generation in Resting and Activated Human Blood. *PLoS Comput Biol.* 2010;6.
- [8] Zarnitsina VI, Ataulakhanov FI, Lobanov AI, Morozova OL. Dynamics of spatially nonuniform patterning in the model of blood coagulation. *Chaos.* 2001;11:57–70.
- [9] Ataulakhanov FI, Krasotkina YV, Sarbash VI, Volkova RI, Sinauridse EI, Kondratovich AY. Spatio-temporal dynamics of blood coagulation and pattern formation: an experimental study. *Int J Bifurc Chaos.* 2002;12(09):1969–1983.
- [10] Flamm MH, Colace TV, Chatterjee MS, Jing H, Zhou S, Jaeger DL, et al. Multiscale prediction of patient-specific platelet function under flow. *Blood.* 2012;120(1):190–198.
- [11] Govindarajan V, Rakesh V, Reifman J, Mitrophanov AY. Computational study of thrombus formation and clotting factor effects under venous flow conditions. *Biophys J.* 2016;110(8):1869–1885.
- [12] Kuharsky AL, Fogelson AL. Surface-mediated Control of Blood Coagulation: The Role of Binding Site Densities and Platelet Deposition. *Biophys J.* 2001;80:1050–1074.
- [13] Anand M, Rajagopal K, Rajagopal KR. A model incorporating some of the mechanical and biochemical factors underlying clot formation and dissolution in flowing blood. *J Theoret Med.* 2003;5:183–218.
- [14] Fogelson AL, Tania N. Coagulation under flow: The influence of flow-mediated transport on the initiation and inhibition of coagulation. *Pathophysiol Haemost Thromb.* 2005;34:91–108.

- [15] Xu Z, Lioi J, Mu J, Kamocka MM, Liu X, Chen DZ, et al. A multiscale model of venous thrombus formation with surface-mediated control of blood coagulation cascade. *Biophys J*. 2010;98(9):1723–1732.
- [16] Fogelson AL, Hussain YH, Leiderman K. Blood clot formation under flow: The importance of factor XI depends strongly on platelet count. *Biophys J*. 2012;102:10–18.
- [17] Leiderman K, Fogelson AL. Grow with the flow: a spatial-temporal model of platelet deposition and blood coagulation under flow. *Math Med Biol*. 2011;28:47–84.
- [18] Leiderman K, Fogelson AL. The influence of hindered transport on the development of platelet thrombi under flow. *Bull of Math Biol*. 2013;75(8):1255–1283.
- [19] Govindarajan V, Zhu S, Li R, Lu Y, Diamond SL, Reifman J, et al. Impact of Tissue Factor Localization on Blood Clot Structure and Resistance under Venous Shear. *Biophys J*. 2018;114(4):978–991.
- [20] Leiderman K, Chang W, Ovanesov M, Fogelson AL. Synergy Between Tissue Factor and Factor XIa in Initiating Coagulation. *Arterioscl Thromb Vasc Biol*. 2016;36:2334–2345.
- [21] Elizondo P, Fogelson AL. A model of venous thrombosis initiation. *Biophys J*. 2016;111:2722–2734.
- [22] Monroe DM, Hoffman M. What does it take to make a perfect clot? *Arterioscler Thromb Vasc Biol*. 2006;26.
- [23] Pantelev M, Ananyeva N, Greco N, Ataullakhanov F, Saenko E. Two subpopulations of thrombin-activated platelets differ in their binding of the components of the intrinsic factor X-activating complex. *Journal of Thrombosis and Haemostasis*. 2005;3(11):2545–2553.
- [24] Walsh PN. Platelet-Coagulant Protein Interactions. In: Colman RW, Hirsh J, Marder VJ, Salzman EW, editors. *Hemostasis and Thrombosis: Basic Principles and Clinical Practice*. 3rd ed. Philadelphia, PA: J.B. Lippincott Company; 1994. p. 629–651.
- [25] Nesheim ME, Pittman DD, Wang JH, Slonosky D, Giles AR, Kaufman RJ. The binding of S-labeled recombinant Factor VIII to activated and unactivated human platelets. *J Biol Chem*. 1988;263:16467.
- [26] Ahmad M, Syed S, Rawala-Sheikh R, Walsh P. Comparative interactions of factor IX and factor IXa with human platelets. *Journal of Biological Chemistry*. 1989;264(6):3244–3251.
- [27] Mann KG, Krishnaswamy S, Lawson JH. Surface-dependent Hemostasis. *Semin Hematol*. 1992;29:213–26.
- [28] Baglia FA, Jameson BA, Walsh PN. Identification and Characterization of a Binding Site for Platelets in the Apple 3 domain of coagulation Factor XI. *J Biol Chem*. 1995;270:6734–40.

- [29] Miller TN, Sinha D, Baird TR, Walsh PN. A Catalytic Domain Exosite (Cys<sup>527</sup>-Cys<sup>542</sup>) in Factor XIa mediates binding to a site on activated platelets. *Biochemistry*. 2007;46:14450–60.
- [30] London FS, Marcinkiewicz M, Walsh PN. A subpopulation of platelets responds to thrombin-or SFLLRN-stimulation with binding sites for factor IXa. *Journal of Biological Chemistry*. 2004;.
- [31] Wilkinson FH, Ahmad M, Syed S, Walsh PN. The factor IXa second epidermal growth factor (EGF2) domain mediates platelet binding and assembly of the factor X activating complex. *Journal of Biological Chemistry*. 2001;.
- [32] Marino S, Hogue IB, Ray CJ, Kirschner DE. A methodology for performing global uncertainty and sensitivity analysis in systems biology. *J Theor Biol*. 2008;254(1):178–196.
- [33] Saltelli A, Ratto M, Andres T, Campolongo F, Cariboni J, Gatelli D, et al. *Global sensitivity analysis: the primer*. John Wiley & Sons; 2008.
- [34] Saltelli A, Tarantola S, Campolongo F, Ratto M. *Sensitivity analysis in practice: a guide to assessing scientific models*. John Wiley & Sons; 2004.
- [35] Iooss B, Lemaitre P. A review on global sensitivity analysis methods. In: *Uncertainty Management in Simulation-Optimization of Complex Systems*. Springer; 2015. p. 101–122.
- [36] Saltelli A, Annoni P. How to avoid a perfunctory sensitivity analysis. *Environmental Modelling & Software*. 2010;25(12):1508–1517.
- [37] Danforth CM, Orfeo T, Mann KG, Brummel-Ziedins KE, Everse SJ. The impact of uncertainty in a blood coagulation model. *Mathematical medicine and biology: a journal of the IMA*. 2009;26(4):323–336.
- [38] Danforth CM, Orfeo T, Everse SJ, Mann KG, Brummel-Ziedins KE. Defining the boundaries of normal thrombin generation: investigations into hemostasis. *PloS one*. 2012;7(2):e30385.
- [39] Anand M, Rajagopal K, Rajagopal KR. A model for the formation, growth, and lysis of clots in quiescent plasma. A comparison between the effects of antithrombin III deficiency and protein C deficiency. *J Theor Biol*. 2008;253(4):725–738.
- [40] Naidu P, Anand M. Importance of VIIIa inactivation in a mathematical model for the formation, growth, and lysis of clots. *Mathematical Modelling of Natural Phenomena*. 2014;9(6):17–33.
- [41] Susree M, Anand M. A mathematical model for in vitro coagulation of blood: role of platelet count and inhibition. *Sādhanā*. 2017;42(3):291–305.
- [42] Susree M, Anand M. Importance of Initial Concentration of Factor VIII in a Mechanistic Model of In Vitro Coagulation. *Acta biotheoretica*. 2018; p. 1–12.

- [43] Bentele M, Lavrik I, Ulrich M, Stösser S, Heermann D, Kalthoff H, et al. Mathematical modeling reveals threshold mechanism in CD95-induced apoptosis. *J Cell Biol.* 2004;166(6):839–851.
- [44] Stelling J, Gilles ED, Doyle FJ. Robustness properties of circadian clock architectures. *Proceedings of the National Academy of Sciences of the United States of America.* 2004;101(36):13210–13215.
- [45] Leiderman K, Chang WC, Ovanesov M, Fogelson AL. Synergy between tissue factor and exogenous factor XIa in initiating coagulation. *Arteriosclerosis, thrombosis, and vascular biology.* 2016; p. ATVBAHA–116.
- [46] Kahn ML, Hakanishi-Matsui M, Shapiro MJ, Ishihara H, Coughlin SR. Protease-activated receptors 1 and 4 mediate activation of human platelets by thrombin. *Journal of Clinical Investigation.* 1999;103:879–887.
- [47] Morris MD. Factorial sampling plans for preliminary computational experiments. *Technometrics.* 1991;33:161–174.
- [48] Saltelli A, Annoni P, Azzini I, Campolongo F, Ratto M, Tarantola S. Variance based sensitivity analysis of model output. Design and estimator for the total sensitivity index. *Computer Physics Communications.* 2010;181(2):259–270.
- [49] Campolongo F, Cariboni J, Saltelli A. An effective screening design for sensitivity analysis of large models. *Environmental modelling & software.* 2007;22(10):1509–1518.
- [50] Sobol I. Sensitivity estimates for nonlinear mathematical models. *Mathematical Modelling and Computational Experiments.* 1993;1(4):407–414.
- [51] Jansen MJ, Rossing WA, Daamen RA. Monte Carlo estimation of uncertainty contributions from several independent multivariate sources. In: *Predictability and nonlinear modelling in natural sciences and economics.* Springer; 1994. p. 334–343.
- [52] Archer G, Saltelli A, Sobol I. Sensitivity measures, ANOVA-like techniques and the use of bootstrap. *Journal of Statistical Computation and Simulation.* 1997;58(2):99–120.
- [53] Andrew M, Vegh P, Johnston M, Bowker J, Ofosu F, Mitchell L. Maturation of the hemostatic system during childhood. *Blood.* 1992;80(8):1998–2005.
- [54] Edgington E, Onghena P. *Randomization Tests, Fourth Edition.* Statistics: A Series of Textbooks and Monographs. Taylor & Francis; 2007.
- [55] van't Veer C, Mann KG. Regulation of Tissue Factor initiated thrombin generation by the stoichiometric inhibitors Tissue Factor Pathway Inhibitor, Antithrombin-III, and Heparin Cofactor-II. *J Biol Chem.* 1997;272:4367–4377.
- [56] Lu G, Broze GJ, Krishnaswamy S. Formation of factors IXa and Xa by the Extrinsic Pathway: Differential regulation by tissue factor pathway inhibitor and antithrombin III. *Journal of Biological Chemistry.* 2004;279:17241–17249.

- [57] Okorie U, Denney WS, Chatterjee MS, Neeves KB, Diamond SL. Determination of surface tissue factor thresholds that trigger coagulation at venous and arterial shear rates: Amplification of 100 fM circulating tissue factor by flow. *Blood*. 2008;111:3507–13.

### 3.6 Supplement

S1-S4 Tables list input parameters that describe the physical processes and coagulation reactions we consider listed in S5-S12 Tables.  $Z_i$  and  $E_i$  refer to zymogen  $i$  and enzyme  $i$  in solution. A superscript 'm' indicates a membrane-bound versions of these proteins (e.g.,  $E_7^m$  refers to the TF:VIIIa complex and  $E_5^m$  refers to Factor Va bound to the platelet surface). Concentrations are denoted in a similar way but with lower-case  $z$  and  $e$ . A complex of  $Z_i$  and  $E_j$  is denoted  $Z_i : E_j$  and its concentration is denoted  $[Z_i : E_j]$ . Special symbols are used for the platelet-bound 'tenase' VIIIa:IXa and 'prothrombinase' Va:Xa complexes,  $TEN = \text{VIIIa:IXa}$  and  $PRO = \text{Va:Xa}$ , and  $[TEN]$  and  $[PRO]$  denote their respective concentrations. The special symbol  $TFPIa$  is used for the fluid-phase complex TFPI:Xa, and  $[TFPIa]$  denotes its concentration. The inhibitors are denoted  $APC$  and  $TFPI$  and their concentrations are denoted  $[APC]$  and  $[TFPI]$ .

The concentrations of unactivated, subendothelial bound, and activated but not subendothelial bound platelets are denoted  $PL$ ,  $PL_s^a$ , and  $PL_a^v$ , respectively. Platelet binding sites for coagulation proteins are denoted  $P_i$  or  $P_i^*$ . The former refers to binding sites for the zymogen  $i$  or for zymogen and enzyme  $i$ . The latter refers to binding sites only for enzyme  $i$ . The number of  $P_i$  or  $P_i^*$  binding sites is denoted  $N_i$  or  $N_i^*$ . The concentration  $p_i$  or  $p_i^*$  of each of these binding sites is needed in the model equations. It is obtained by multiplying the corresponding  $N_i$  or  $N_i^*$ , respectively, by the concentration of activated platelets  $PL_s^a + PL_a^v$ .

Further discussion of model assumptions and parameter estimation can be found in [1, 2].

$$\begin{aligned}
[TF]^{\text{avail}} &= [TF] - z_7^m - e_7^m - [Z_7^m : E_{10}] - [Z_7^m : E_2] - [Z_{10} : E_7^m] \\
&\quad - [Z_9 : E_7^m] - [TPFI : E_{10} : E_7^m] - [Z_7^m : E_9] \\
p_{PLAS}^{\text{avail}} &= p_{PLAS} - [PL_a^s] \\
p_5^{\text{avail}} &= p_5 - z_5^m - e_5^m - [Z_5^m : E_{10}^m] - [Z_5^m : E_2^m] \\
&\quad - [APC : E_5^m] - [PRO] - [Z_2^m : PRO] \\
p_8^{\text{avail}} &= p_8 - z_8^m - e_8^m - [TEN] - [Z_8^m : E_{10}^m] - [Z_8^m : E_2^m] \\
&\quad - [Z_{10}^m : TEN] - [APC : E_8^m] - [TEN^*] - [Z_{10}^m : TEN^*] \\
p_9^{\text{avail}} &= p_9 - z_9^m - e_9^m - [TEN] - [Z_{10}^m : TEN] \\
&\quad - [Z_9^m : E_{11}^{h,m}] - [Z_9^m : E_{11}^{m*}] \\
p_9^{*,\text{avail}} &= p_9^* - e_9^{m*} - [TEN^*] - [Z_{10}^m : TEN^*] \\
p_{10}^{\text{avail}} &= p_{10} - z_{10}^m - e_{10}^m - [Z_5^m : E_{10}^m] - [Z_8^m : E_{10}^m] \\
&\quad - [PRO] - [Z_2^m : PRO] - [Z_{10}^m : TEN] - [Z_{10}^m : TEN^*] \\
p_2^{\text{avail}} &= p_2 - z_2^m - [Z_2^m : PRO] \\
p_2^{*,\text{avail}} &= p_2^* - e_2^m - [Z_5^m : E_2^m] - [Z_8^m : E_2^m] - [Z_{11}^m : E_2^m] - [E_{11}^{h,m*} : E_2^m] \\
p_{11}^{\text{avail}} &= p_{11} - z_{11}^m - e_{11}^{h,m} - [Z_9^m : E_{11}^{h,m}] - [Z_{11}^m : E_2^m] \\
p_{11}^{*,\text{avail}} &= p_{11}^* - e_{11}^{h,m*} - e_{11}^{m*} - [Z_9^m : E_{11}^{m*}] - [E_{11}^{h,m*} : E_2^m] \\
[TM]^{\text{avail}} &= ([TM] - [TM : E_2^{ec}] - [TM : E_2^{ec} : APC])
\end{aligned}$$

$$\begin{aligned}
\frac{d}{dt} z_7 &= k_{\text{flow}}(z_7^{\text{up}} - z_7) - k_7^{\text{on}} z_7 [TF]^{\text{avail}} + k_7^{\text{off}} z_7^m - k_{z_7:e_2}^+ z_7 e_2 \\
&\quad + k_{z_7:e_2}^- [Z_7 : E_2] - k_{z_7:e_{10}}^+ z_7 e_{10} + k_{z_7:e_{10}}^- [Z_7 : E_{10}] \\
\frac{d}{dt} e_7 &= k_{\text{flow}}(e_7^{\text{up}} - e_7) - k_7^{\text{on}} e_7 [TF]^{\text{avail}} + k_7^{\text{off}} e_7^m \\
&\quad + k_{z_7:e_2}^{\text{cat}} [Z_7 : E_2] + k_{z_7:e_{10}}^{\text{cat}} [Z_7 : E_{10}] \\
\frac{d}{dt} z_7^m &= k_7^{\text{on}} z_7 [TF]^{\text{avail}} - k_7^{\text{off}} z_7^m - k_{z_7^m:e_{10}}^+ z_7^m e_{10} + k_{z_7^m:e_{10}}^- [Z_7^m : E_{10}] \\
&\quad - k_{z_7^m:e_2}^+ z_7^m e_2 + k_{z_7^m:e_2}^- [Z_7^m : E_2] - z_7^m \frac{d}{dt} [PL_a^s] \frac{1}{p_{PLAS}^{\text{avail}}} \\
\frac{d}{dt} e_7^m &= k_7^{\text{on}} e_7 [TF]^{\text{avail}} - k_7^{\text{off}} e_7^m \\
&\quad - k_{TFPI:e_{10}:E_7^m}^+ e_7^m [TFPI : E_{10}] + k_{TFPI:e_{10}:E_7^m}^- [TFPI : E_{10} : E_7^m] \\
&\quad + k_{z_7^m:e_{10}}^{\text{cat}} [Z_7^m : E_{10}] + k_{z_7^m:e_2}^{\text{cat}} [Z_7^m : E_2] \\
&\quad + (k_{z_{10}:e_7^m}^{\text{cat}} + k_{z_{10}:e_7^m}^-) [Z_{10} : E_7^m] - k_{z_{10}:e_7^m}^+ z_{10} e_7^m \\
&\quad + (k_{z_9:e_7^m}^{\text{cat}} + k_{z_9:e_7^m}^-) [Z_9 : E_7^m] - k_{z_9:e_7^m}^+ z_9 e_7^m - e_7^m \frac{d}{dt} [PL_a^s] \frac{1}{p_{PLAS}^{\text{avail}}} \\
\frac{d}{dt} z_{10} &= k_{\text{flow}}(z_{10}^{\text{up}} - z_{10}) - k_{10}^{\text{on}} z_{10} p_{10}^{\text{avail}} + k_{10}^{\text{off}} z_{10}^m - k_{z_{10}:e_7^m}^+ z_{10} e_7^m \\
&\quad + k_{z_{10}:e_7^m}^- [Z_{10} : E_7^m] \\
\frac{d}{dt} e_{10} &= k_{\text{flow}}(e_{10}^{\text{up}} - e_{10}) - k_{\text{diff}}(e_{10} - e_{10}^{ec}) - k_{10}^{\text{on}} e_{10} p_{10}^{\text{avail}} + k_{10}^{\text{off}} e_{10}^m \\
&\quad + k_{z_{10}:e_7^m}^{\text{cat}} [Z_{10} : E_7^m] + (k_{z_7:e_{10}}^{\text{cat}} + k_{z_7:e_{10}}^-) [Z_7 : E_{10}] - k_{z_7:e_{10}}^+ z_7 e_{10} \\
&\quad + (k_{z_7^m:e_{10}}^{\text{cat}} + k_{z_7^m:e_{10}}^-) [Z_7^m : E_{10}] - k_{z_7^m:e_{10}}^+ z_7^m e_{10} \\
&\quad - k_{TFPI:e_{10}}^+ e_{10} [TFPI] + k_{TFPI:e_{10}}^- [TFPI : E_{10}] - k_{AT:e_{10}}^{\text{in}} e_{10} \\
\frac{d}{dt} z_{10}^m &= k_{10}^{\text{on}} z_{10} p_{10}^{\text{avail}} - k_{10}^{\text{off}} z_{10}^m - k_{z_{10}^m:ten}^+ z_{10}^m [TEN] + k_{z_{10}^m:ten}^- [Z_{10}^m : TEN] \\
&\quad - k_{z_{10}^m:ten}^+ z_{10}^m [TEN^*] + k_{z_{10}^m:ten}^- [Z_{10}^m : TEN^*] \\
\frac{d}{dt} e_{10}^m &= k_{10}^{\text{on}} e_{10} p_{10}^{\text{avail}} - k_{10}^{\text{off}} e_{10}^m + k_{z_{10}^m:ten}^{\text{cat}} [Z_{10}^m : TEN] \\
&\quad + (k_{z_5^m:e_{10}}^{\text{cat}} + k_{z_5^m:e_{10}}^-) [Z_5^m : E_{10}] - k_{z_5^m:e_{10}}^+ z_5^m e_{10}^m \\
&\quad + (k_{z_8^m:e_{10}}^{\text{cat}} + k_{z_8^m:e_{10}}^-) [Z_8^m : E_{10}] - k_{z_8^m:e_{10}}^+ z_8^m e_{10}^m \\
&\quad + k_{e_5^m:e_{10}}^- [PRO] - k_{e_5^m:e_{10}}^+ e_{10}^m e_5^m + k_{z_{10}^m:ten}^{\text{cat}} [Z_{10}^m : TEN^*]
\end{aligned}$$

$$\begin{aligned}\frac{d}{dt} z_5 &= k_{\text{flow}}(z_5^{\text{up}} - z_5) - k_5^{\text{on}} z_5 p_5^{\text{avail}} + k_5^{\text{off}} z_5^m - k_{z_5:e_2}^+ z_5 e_2 + k_{z_5:e_2}^- [Z_5 : E_2] \\ &\quad + n_5 \left( k_{\text{adh}}^+ p_{PLAS}^{\text{avail}} + k_{\text{plt}}^{\text{act}} \left( [PL_a^v] + [PL_a^s] \right) + k_{e_2}^{\text{act}} \frac{e_2}{(e_2 + 0.001)} \right) [PL]\end{aligned}$$

$$\begin{aligned}\frac{d}{dt} e_5 &= k_{\text{flow}}(e_5^{\text{up}} - e_5) - k_5^{\text{on}} e_5 p_5^{\text{avail}} + k_5^{\text{off}} e_5^m \\ &\quad + k_{z_5:e_2}^{\text{cat}} [Z_5 : E_2] + k_{e_5:APC}^- [APC : E_5] - k_{e_5:APC}^+ [APC] e_5\end{aligned}$$

$$\begin{aligned}\frac{d}{dt} z_5^m &= k_5^{\text{on}} z_5 p_5^{\text{avail}} - k_5^{\text{off}} z_5^m - k_{z_5^m:e_{10}^m}^+ z_5^m e_{10}^m + k_{z_5^m:e_{10}^m}^- [Z_5^m : E_{10}^m] \\ &\quad - k_{z_5^m:e_2^m}^+ z_5^m e_2^m + k_{z_5^m:e_2^m}^- [Z_5^m : E_2^m]\end{aligned}$$

$$\begin{aligned}\frac{d}{dt} e_5^m &= k_5^{\text{on}} e_5 p_5^{\text{avail}} - k_5^{\text{off}} e_5^m + k_{z_5^m:e_{10}^m}^{\text{cat}} [Z_5^m : E_{10}^m] + k_{z_5^m:e_2^m}^{\text{cat}} [Z_5^m : E_2^m] \\ &\quad + k_{e_5^m:APC}^- [APC : E_5^m] - k_{e_5^m:APC}^+ [APC] e_5^m \\ &\quad - k_{e_5^m:e_{10}^m}^+ e_5^m e_{10}^m + k_{e_5^m:e_{10}^m}^- [PRO]\end{aligned}$$

$$\frac{d}{dt} z_8 = k_{\text{flow}}(z_8^{\text{up}} - z_8) - k_8^{\text{on}} z_8 p_8^{\text{avail}} + k_8^{\text{off}} z_8^m - k_{z_8:e_2}^+ z_8 e_2 + k_{z_8:e_2}^- [Z_8 : E_2]$$

$$\begin{aligned}\frac{d}{dt} e_8 &= k_{\text{flow}}(e_8^{\text{up}} - e_8) - k_8^{\text{on}} e_8 p_8^{\text{avail}} + k_8^{\text{off}} e_8^m + k_{z_8:e_2}^{\text{cat}} [Z_8 : E_2] - 0.005 e_8 \\ &\quad + k_{e_8:APC}^- [APC : E_8] - k_{e_8:APC}^+ [APC] e_8\end{aligned}$$

$$\begin{aligned}\frac{d}{dt} z_8^m &= k_8^{\text{on}} z_8 p_8^{\text{avail}} - k_8^{\text{off}} z_8^m - k_{z_8^m:e_{10}^m}^+ z_8^m e_{10}^m + k_{z_8^m:e_{10}^m}^- [Z_8^m : E_{10}^m] \\ &\quad - k_{z_8^m:e_2^m}^+ z_8^m e_2^m + k_{z_8^m:e_2^m}^- [Z_8^m : E_2^m]\end{aligned}$$

$$\begin{aligned}\frac{d}{dt} e_8^m &= k_8^{\text{on}} e_8 p_8^{\text{avail}} - k_8^{\text{off}} e_8^m + k_{z_8^m:e_{10}^m}^{\text{cat}} [Z_8^m : E_{10}^m] + k_{z_8^m:e_2^m}^{\text{cat}} [Z_8^m : E_2^m] \\ &\quad - k_{e_8^m:APC}^+ [APC] e_8^m + k_{e_8^m:APC}^- [APC : E_8^m] - 0.005 e_8^m \\ &\quad - k_{e_8^m:e_9^m}^+ e_8^m e_9^m + k_{e_8^m:e_9^m}^- [TEN] - k_{e_8^m:e_9^m}^+ e_8^m e_9^{m*} + k_{e_8^m:e_9^m}^- [TEN^*]\end{aligned}$$

$$\begin{aligned}\frac{d}{dt} z_9 &= k_{\text{flow}}(z_9^{\text{up}} - z_9) - k_9^{\text{on}} p_9^{\text{avail}} z_9 + k_9^{\text{off}} z_9^m - k_{z_9:e_7^m}^+ z_9 e_7^m + k_{z_9:e_7^m}^- [Z_9 : E_7^m] \\ &\quad - k_{z_9:e_{11}^h}^+ z_9 e_{11}^h + k_{z_9:e_{11}^h}^- [Z_9 : E_{11}^h] - k_{z_9:e_{11}}^+ z_9 e_{11} + k_{z_9:e_{11}}^- [Z_9 : E_{11}]\end{aligned}$$

$$\begin{aligned}\frac{d}{dt} e_9 &= k_{\text{flow}}(e_9^{\text{up}} - e_9) - k_{\text{diff}}(e_9 - e_9^{\text{ec}}) - k_9^{\text{on}} p_9^{\text{avail}} e_9 + k_9^{\text{off}} e_9^m + k_{z_9:e_7^m}^{\text{cat}} [Z_9 : E_7^m] \\ &\quad - k_{AT:e_9}^{\text{in}} e_9 + (k_{z_7:e_9}^{\text{cat}} + k_{z_7:e_9}^-) [Z_7 : E_9] - k_{z_7:e_9}^+ z_7 e_9 \\ &\quad + (k_{z_7^m:e_9}^{\text{cat}} + k_{z_7^m:e_9}^-) [Z_7^m : E_9] - k_{z_7^m:e_9}^+ z_7^m e_9 \\ &\quad - k_9^{\text{on}} p_9^{*,\text{avail}} e_9 + k_9^{\text{off}} e_9^{m*} + k_{z_9:e_{11}^h}^{\text{cat}} [Z_9 : E_{11}^h] + k_{z_9:e_{11}}^{\text{cat}} [Z_9 : E_{11}]\end{aligned}$$

$$\begin{aligned}\frac{d}{dt} z_9^m &= k_9^{\text{on}} p_9^{\text{avail}} z_9 - k_9^{\text{off}} z_9^m - k_{z_9^m:e_{11}^{h,m}}^+ z_9^m e_{11}^{h,m} + k_{z_9^m:e_{11}^{h,m}}^- [Z_9^m : E_{11}^{h,m}] \\ &\quad - k_{z_9^m:e_{11}^{m*}}^+ z_9^m e_{11}^{m*} + k_{z_9^m:e_{11}^{m*}}^- [Z_9^m : E_{11}^{m*}]\end{aligned}$$

$$\begin{aligned}\frac{d}{dt} e_9^m &= k_9^{\text{on}} p_9^{\text{avail}} e_9 - k_9^{\text{off}} e_9^m + k_{e_8^m:e_9^m}^- [TEN] - k_{e_8^m:e_9^m}^+ e_8^m e_9^m \\ &\quad + k_{z_9^m:e_{11}^{h,m}}^{\text{cat}} [Z_9^m : E_{11}^{h,m}] + k_{z_9^m:e_{11}^{m*}}^{\text{cat}} [Z_9^m : E_{11}^{m*}]\end{aligned}$$

$$\frac{d}{dt} z_2 = k_{\text{flow}}(z_2^{\text{up}} - z_2) - k_2^{\text{on}} p_2^{\text{avail}} z_2 + k_2^{\text{off}} z_2^m$$

$$\begin{aligned}\frac{d}{dt} e_2 &= k_{\text{flow}}(e_2^{\text{up}} - e_2) - k_{\text{diff}}(e_2 - e_2^{\text{ec}}) + k_{z_2m:PRO}^{\text{cat}} [Z_2^m : PRO] \\ &\quad - k_{2*}^{\text{on}} p_2^{*,\text{avail}} e_2 + k_{2*}^{\text{off}} e_2^m - k_{AT:e_2}^{\text{in}} e_2 \\ &\quad + (k_{z_5:e_2}^{\text{cat}} + k_{z_5:e_2}^-) [Z_5 : E_2] - k_{z_5:e_2}^+ z_5 e_2 \\ &\quad + (k_{z_8:e_2}^{\text{cat}} + k_{z_8:e_2}^-) [Z_8 : E_2] - k_{z_8:e_2}^+ z_8 e_2 \\ &\quad + (k_{z_7:e_2}^{\text{cat}} + k_{z_7:e_2}^-) [Z_7 : E_2] - k_{z_7:e_2}^+ z_7 e_2 \\ &\quad + (k_{z_7^m:e_2}^{\text{cat}} + k_{z_7^m:e_2}^-) [Z_7^m : E_2] - k_{z_7^m:e_2}^+ z_7^m e_2 \\ &\quad - k_{z_{11}:e_2}^+ z_{11} e_2 + (k_{z_{11}:e_2}^- + k_{z_{11}:e_2}^{\text{cat}}) [Z_{11} : E_2] \\ &\quad - k_{e_{11}:e_2}^+ e_{11}^h e_2 + (k_{e_{11}:e_2}^- + k_{e_{11}:e_2}^{\text{cat}}) [E_{11}^h : E_2]\end{aligned}$$

$$\frac{d}{dt} z_2^m = k_2^{\text{on}} p_2^{\text{avail}} z_2 - k_2^{\text{off}} z_2^m - k_{z_2^m:PRO}^+ z_2^m PRO + k_{z_2^m:PRO}^- [Z_2^m : PRO]$$

$$\begin{aligned}\frac{d}{dt} e_2^m &= k_{2*}^{\text{on}} p_2^{\text{avail}} e_2 - k_{2*}^{\text{off}} e_2^m + (k_{z_5^m:e_2^m}^{\text{cat}} + k_{z_5^m:e_2^m}^-) [Z_5^m : E_2^m] - k_{z_5^m:e_2^m}^+ z_5^m e_2^m \\ &\quad + (k_{z_8^m:e_2^m}^{\text{cat}} + k_{z_8^m:e_2^m}^-) [Z_8^m : E_2^m] - k_{z_8^m:e_2^m}^+ z_8^m e_2^m \\ &\quad - k_{z_{11}^m:e_2^m}^+ z_{11}^m e_2^m + (k_{z_{11}^m:e_2^m}^- + k_{z_{11}^m:e_2^m}^{\text{cat}}) [Z_{11}^m : E_2^m] \\ &\quad - k_{e_{11}^h:e_2^m}^+ e_{11}^{h,m*} e_2^m + (k_{e_{11}^h:e_2^m}^- + k_{e_{11}^h:e_2^m}^{\text{cat}}) [E_{11}^{h,m*} : E_2^m]\end{aligned}$$

$$\begin{aligned}\frac{d}{dt} [TEN] &= -k_{e_8^m:e_9^m}^- [TEN] + k_{e_8^m:e_9^m}^+ e_8^m e_9^m \\ &\quad + (k_{z_{10}^m:TEN}^{\text{cat}} + k_{z_{10}^m:TEN}^-) [Z_{10}^m : TEN] - k_{z_{10}^m:TEN}^+ z_{10}^m [TEN]\end{aligned}$$

$$\begin{aligned}\frac{d}{dt} [PRO] &= -k_{e_5^m:e_{10}^m}^- [PRO] + k_{e_5^m:e_{10}^m}^+ e_{10}^m e_5^m \\ &\quad + (k_{z_2^m:PRO}^{\text{cat}} + k_{z_2^m:PRO}^-) [Z_2^m : PRO] - k_{z_2^m:PRO}^+ z_2^m [PRO]\end{aligned}$$

$$\frac{d}{dt} [PL_a^s] = k_{\text{adh}}^+ p_{PLAS}^{\text{avail}} [PL] - k_{\text{adh}}^- [PL_a^s] + k_{\text{adh}}^+ [PL_a^v] p_{PLAS}^{\text{avail}}$$

$$\begin{aligned}\frac{d}{dt} [PL] &= k_{\text{flow}}^p ([PL]^{\text{up}} - [PL]) - \left( k_{\text{adh}}^+ p_{PLAS}^{\text{avail}} + k_{\text{plt}}^{\text{act}} ([PL_a^v] + [PL_a^s]) \right. \\ &\quad \left. + k_{e_2}^{\text{act}} \frac{e_2}{e_2 + 0.001} \right) [PL]\end{aligned}$$

$$\begin{aligned}\frac{d}{dt} [PL_a^v] &= k_{\text{adh}}^- [PL_a^s] - k_{\text{adh}}^+ [PL_a^v] p_{PLAS}^{\text{avail}} \\ &\quad + \left( k_{\text{plt}}^{\text{act}} ([PL_a^v] + [PL_a^s]) + k_{e_2}^{\text{act}} \frac{e_2}{e_2 + 0.001} \right) [PL]\end{aligned}$$

$$\begin{aligned}\frac{d}{dt} [TFPI] &= k_{\text{flow}} ([TFPI]^{\text{up}} - [TFPI]) - k_{TFPI:e_{10}}^+ e_{10} [TFPI] \\ &\quad + k_{TFPI:e_{10}}^- [TFPI : Xa]\end{aligned}$$

$$\begin{aligned}\frac{d}{dt} [TFPI : E_{10}] &= -k_{\text{flow}} [TFPI : E_{10}] + k_{TFPI:e_{10}}^+ e_{10} [TFPI] \\ &\quad - k_{TFPI:e_{10}}^- [TFPI : E_{10}] + k_{TFPI:e_{10}:e_7^m}^- [TFPI : E_{10} : E_7^m] \\ &\quad - k_{TFPI:e_{10}:e_7^m}^+ e_7^m [TFPI : E_{10}]\end{aligned}$$

$$\begin{aligned}\frac{d}{dt} [TFPI : E_{10} : E_7^m] &= -k_{TFPI:e_{10}:e_7^m}^- [TFPI : E_{10} : E_7^m] \\ &\quad + k_{TFPI:e_{10}:e_7^m}^+ e_7^m [TFPI : E_{10}] \\ &\quad - [TFPI : E_{10} : E_7^m] \frac{d}{dt} [PL_a^s] \frac{1}{p_{PLAS}^{\text{avail}}}\end{aligned}$$

$$\begin{aligned}
\frac{d}{dt} [APC] &= k_{\text{flow}} \left( [APC]^{\text{up}} - [APC] \right) - k_{\text{diff}} \left( [APC] - [APC^{\text{ec}}] \right) \\
&\quad + (k_{e_5^m:APC}^{\text{cat}} + k_{e_5^m:APC}^-) [APC : E_5^m] - k_{e_5^m:APC}^+ e_5^m [APC] \\
&\quad + (k_{e_8^m:APC}^{\text{cat}} + k_{e_8^m:APC}^-) [APC : E_8^m] - k_{e_8^m:APC}^+ e_8^m [APC] \\
&\quad + (k_{e_5:APC}^{\text{cat}} + k_{e_5:APC}^-) [APC : E_5] - k_{e_5:APC}^+ e_5 [APC] \\
&\quad + (k_{e_8:APC}^{\text{cat}} + k_{e_8:APC}^-) [APC : E_8] - k_{e_8:APC}^+ e_8 [APC]
\end{aligned}$$

$$\frac{d}{dt} [APC : E_8^m] = k_{e_8^m:APC}^+ e_8^m [APC] - (k_{e_8^m:APC}^{\text{cat}} + k_{e_8^m:APC}^-) [APC : E_8^m]$$

$$\frac{d}{dt} [APC : E_5^m] = k_{e_5^m:APC}^+ e_5^m [APC] - (k_{e_5^m:APC}^{\text{cat}} + k_{e_5^m:APC}^-) [APC : E_5^m]$$

$$\frac{d}{dt} [APC : E_5] = k_{e_5:APC}^+ e_5 [APC] - (k_{e_5:APC}^{\text{cat}} + k_{e_5:APC}^-) [APC : E_5]$$

$$\frac{d}{dt} [APC : E_8] = k_{e_8:APC}^+ e_8 [APC] - (k_{e_8:APC}^{\text{cat}} + k_{e_8:APC}^-) [APC : E_8]$$

$$\begin{aligned}
\frac{d}{dt} [Z_7 : E_2] &= k_{\text{flow}} \left( [Z_7 : E_2]^{\text{up}} - [Z_7 : E_2] \right) + k_{z_7:e_2}^+ z_7 e_2 \\
&\quad - (k_{z_7:e_2}^{\text{cat}} + k_{z_7:e_2}^-) [Z_7 : E_2]
\end{aligned}$$

$$\begin{aligned}
\frac{d}{dt} [Z_7 : E_{10}] &= k_{\text{flow}} \left( [Z_7 : E_{10}]^{\text{up}} - [Z_7 : E_{10}] \right) + k_{z_7:e_{10}}^+ z_7 e_{10} \\
&\quad - (k_{z_7:e_{10}}^{\text{cat}} + k_{z_7:e_{10}}^-) [Z_7 : E_{10}]
\end{aligned}$$

$$\begin{aligned}
\frac{d}{dt} [Z_7^m : E_{10}] &= k_{z_7^m:e_{10}}^+ z_7^m e_{10} - (k_{z_7^m:e_{10}}^{\text{cat}} + k_{z_7^m:e_{10}}^-) [Z_7^m : E_{10}] \\
&\quad - [Z_7^m : E_{10}] \frac{d}{dt} [PL_a^s] \frac{1}{p_{PLAS}^{\text{avail}}}
\end{aligned}$$

$$\begin{aligned}
\frac{d}{dt} [Z_7^m : E_2] &= k_{z_7^m:e_2}^+ z_7^m e_2 - (k_{z_7^m:e_2}^{\text{cat}} + k_{z_7^m:e_2}^-) [Z_7^m : E_2] \\
&\quad - [Z_7^m : E_2] \frac{d}{dt} [PL_a^s] \frac{1}{p_{PLAS}^{\text{avail}}}
\end{aligned}$$

$$\begin{aligned}
\frac{d}{dt} [Z_{10} : E_7^m] &= k_{z_{10}:e_7^m}^+ z_{10} e_7^m - (k_{z_{10}:e_7^m}^{\text{cat}} + k_{z_{10}:e_7^m}^-) [Z_{10} : E_7^m] \\
&\quad - [Z_{10} : E_7^m] \frac{d}{dt} [PL_a^s] \frac{1}{p_{PLAS}^{\text{avail}}}
\end{aligned}$$

$$\begin{aligned}
\frac{d}{dt} [Z_{10}^m : TEN] &= k_{z_{10}^m : TEN}^+ z_{10}^m [TEN] - (k_{z_{10}^m : TEN}^{\text{cat}} + k_{z_{10} : TEN}^-) [Z_{10}^m : TEN] \\
\frac{d}{dt} [Z_5 : E_2] &= k_{\text{flow}} \left( [Z_5 : E_2]^{\text{up}} - [Z_5 : E_2] \right) + k_{z_5 : e_2}^+ z_5 e_2 \\
&\quad - (k_{z_5 : e_2}^{\text{cat}} + k_{z_5 : e_2}^-) [Z_5 : E_2] \\
\frac{d}{dt} [Z_5^m : E_{10}^m] &= k_{z_5^m : e_{10}^m}^+ z_5^m e_{10}^m - (k_{z_5^m : e_{10}^m}^{\text{cat}} + k_{z_5^m : e_{10}^m}^-) [Z_5^m : E_{10}^m] \\
\frac{d}{dt} [Z_5^m : E_2^m] &= k_{z_5^m : e_2^m}^+ z_5^m e_2^m - (k_{z_5^m : e_2^m}^{\text{cat}} + k_{z_5^m : e_2^m}^-) [Z_5^m : E_2^m] \\
\frac{d}{dt} [Z_8^m : E_{10}^m] &= k_{z_8^m : e_{10}^m}^+ z_8^m e_{10}^m - (k_{z_8^m : e_{10}^m}^{\text{cat}} + k_{z_8^m : e_{10}^m}^-) [Z_8^m : E_{10}^m] \\
\frac{d}{dt} [Z_8^m : E_2^m] &= k_{z_8^m : e_2^m}^+ z_8^m e_2^m - (k_{z_8^m : e_2^m}^{\text{cat}} + k_{z_8^m : e_2^m}^-) [Z_8^m : E_2^m] \\
\frac{d}{dt} [Z_8 : E_2] &= k_{\text{flow}} \left( [Z_8 : E_2]^{\text{up}} - [Z_8 : E_2] \right) + k_{z_8 : e_2}^+ z_8 e_2 \\
&\quad - (k_{z_8 : e_2}^{\text{cat}} + k_{z_8 : e_2}^-) [Z_8 : E_2] \\
\frac{d}{dt} [Z_9 : E_7^m] &= k_{z_9 : e_7^m}^+ z_9 e_7^m - (k_{z_9 : e_7^m}^{\text{cat}} + k_{z_9 : e_7^m}^-) [Z_9 : E_7^m] \\
&\quad - [Z_9 : E_7^m] \frac{d}{dt} [PL_a^s] \frac{1}{p_{PLAS}^{\text{avail}}} \\
\frac{d}{dt} [Z_2^m : PRO] &= k_{z_2^m : PRO}^+ z_2^m [PRO] - (k_{z_2^m : PRO}^{\text{cat}} + k_{z_2^m : PRO}^-) [Z_2^m : PRO] \\
\frac{d}{dt} [TF] &= -[TF] \frac{d}{dt} [PL_a^s] \frac{1}{p_{PLAS}^{\text{avail}}} \\
\frac{d}{dt} e_9^{m*} &= k_9^{\text{on}} p_9^{*,\text{avail}} e_9 - k_9^{\text{off}} e_9^{m*} + k_{e_8^m : e_9^m}^- [TEN^*] - k_{e_8^m : e_9^m}^+ e_8^m e_9^{m*} \\
\frac{d}{dt} [TEN^*] &= -k_{e_8^m : e_9^m}^- [TEN^*] + k_{e_8^m : e_9^m}^+ e_8^m e_9^{m*} \\
&\quad + (k_{z_{10}^m : TEN}^{\text{cat}} + k_{z_{10} : TEN}^-) [Z_{10}^m : TEN^*] - k_{z_{10}^m : TEN}^+ z_{10}^m [TEN^*] \\
\frac{d}{dt} [Z_{10}^m : TEN^*] &= k_{z_{10}^m : TEN}^+ z_{10}^m [TEN^*] - (k_{z_{10}^m : TEN}^{\text{cat}} + k_{z_{10} : TEN}^-) [Z_{10}^m : TEN^*]
\end{aligned}$$

$$\begin{aligned}
\frac{d}{dt} e_2^{ec} &= k_{\text{flow}}(e_2^{\text{up}} - e_2^{ec}) + k_{\text{diff}}(e_2 - e_2^{ec}) - k_{AT:e_2}^{\text{in}} e_2^{ec} \\
&\quad - k_{TM}^{\text{on}} e_2^{ec} [TM]^{\text{avail}} + k_{TM}^{\text{off}} [TM : E_2^{ec}] \\
\frac{d}{dt} [APC^{ec}] &= k_{\text{flow}}([APC]^{\text{up}} - [APC^{ec}]) + k_{\text{diff}}([APC] - [APC^{ec}]) \\
&\quad + k_{PC:TM:e_2^{ec}}^{\text{cat}} [TM : E_2^{ec} : APC] \\
\frac{d}{dt} [TM : E_2^{ec}] &= k_{TM}^{\text{on}} e_2^{ec} [TM]^{\text{avail}} - k_{TM}^{\text{off}} [TM : E_2^{ec}] - k_{PC:TM:e_2^{ec}}^+ [TM : E_2^{ec}] \\
&\quad + (k_{PC:TM:e_2^{ec}}^- + k_{PC:TM:e_2^{ec}}^{\text{cat}}) [TM : E_2^{ec} : APC] \\
\frac{d}{dt} [TM : E_2^{ec} : APC] &= k_{PC:TM:e_2^{ec}}^+ [TM : E_2^{ec}] \\
&\quad - (k_{PC:TM:e_2^{ec}}^- + k_{PC:TM:e_2^{ec}}^{\text{cat}}) [TM : E_2^{ec} : APC] \\
\frac{d}{dt} e_9^{ec} &= k_{\text{flow}}(e_9^{\text{up}} - e_9^{ec}) + k_{\text{diff}}(e_9 - e_9^{ec}) - k_{AT:e_9}^{\text{in}} e_9^{ec} \\
\frac{d}{dt} e_{10}^{ec} &= k_{\text{flow}}(e_{10}^{\text{up}} - e_{10}^{ec}) + k_{\text{diff}}(e_{10} - e_{10}^{ec}) - k_{AT:e_{10}}^{\text{in}} e_{10}^{ec} \\
\frac{d}{dt} z_{11} &= k_{\text{flow}}(z_{11}^{\text{up}} - z_{11}) - k_{z_{11}}^{\text{on}} z_{11} p_{11}^{\text{avail}} + k_{z_{11}}^{\text{off}} z_{11}^m - k_{z_{11}:e_2}^+ z_{11} e_2 \\
&\quad + k_{z_{11}:e_2}^- [Z_{11} : E_2] \\
\frac{d}{dt} e_{11}^h &= k_{\text{flow}}(e_{11}^{h,\text{up}} - e_{11}^h) - k_{e_{11}^h}^{\text{on}*} e_{11}^h p_{11}^{*,\text{avail}} + k_{e_{11}^h}^{\text{off}*} e_{11}^{h,m*} \\
&\quad - k_{e_{11}^h}^{\text{on}} e_{11}^h p_{11}^{\text{avail}} + k_{e_{11}^h}^{\text{off}} e_{11}^{h,m} - k_{z_9:e_{11}^h}^+ z_9 e_{11}^h \\
&\quad + (k_{z_9:e_{11}^h}^- + k_{z_9:e_{11}^h}^{\text{cat}}) [Z_9 : E_{11}^h] + k_{z_{11}:e_2}^{\text{cat}} [Z_{11} : E_2] \\
&\quad - k_{e_{11}^h:e_2}^+ e_{11}^h e_2 + k_{e_{11}^h:e_2}^- [E_{11}^h : E_2] - k_{AT:e_{11}^h}^{\text{in}} e_{11}^h \\
\frac{d}{dt} e_{11} &= k_{\text{flow}}(e_{11}^{\text{up}} - e_{11}) - k_{e_{11}}^{\text{on}*} e_{11} p_{11}^{*,\text{avail}} + k_{e_{11}}^{\text{off}*} e_{11}^{m*} \\
&\quad - k_{z_9:e_{11}}^+ z_9 e_{11} + (k_{z_9:e_{11}}^- + k_{z_9:e_{11}}^{\text{cat}}) [Z_9 : E_{11}] \\
&\quad + k_{e_{11}^h:e_2}^{\text{cat}} [E_{11}^h : E_2] - k_{AT:e_{11}}^{\text{in}} e_{11}
\end{aligned}$$

$$\begin{aligned}
\frac{d}{dt} z_{11}^m &= k_{z_{11}}^{\text{on}} z_{11} p_{11}^{\text{avail}} - k_{z_{11}}^{\text{off}} z_{11}^m - k_{z_{11}:e_2}^+ z_{11}^m e_2^m + k_{z_{11}:e_2}^- [Z_{11}^m : E_2^m] \\
\frac{d}{dt} e_{11}^{h,m} &= k_{e_{11}}^{\text{on}} e_{11}^h p_{11}^{\text{avail}} - k_{e_{11}}^{\text{off}} e_{11}^{h,m} + k_{z_9:e_{11}}^{\text{cat}} [Z_9^m : E_2^m] \\
&\quad - k_{z_9:e_{11}}^+ z_9^m e_{11}^{h,m} + (k_{z_9:e_{11}}^- + k_{z_9:e_{11}}^{\text{cat}}) [Z_9^m : E_{11}^{h,m}] \\
\frac{d}{dt} e_{11}^{h,m*} &= k_{e_{11}}^{\text{on}*} e_{11}^h p_{11}^{*,\text{avail}} - k_{e_{11}}^{\text{off}*} e_{11}^{h,m*} \\
&\quad - k_{e_{11}:e_2}^+ e_{11}^{h,m*} e_2^m + k_{e_{11}:e_2}^- [E_{11}^{h,m*} : E_2^m] \\
\frac{d}{dt} e_{11}^{m*} &= k_{e_{11}}^{\text{on}*} e_{11} p_{11}^{*,\text{avail}} - k_{e_{11}}^{\text{off}*} e_{11}^{m*} + k_{e_{11}:e_2}^{\text{cat}} [E_{11}^{h,m*} : E_2^m] \\
&\quad - k_{z_9:e_{11}}^+ z_9^m e_{11}^{m*} + (k_{z_9:e_{11}}^- + k_{z_9:e_{11}}^{\text{cat}}) [Z_9^m : E_{11}^{m*}] \\
\frac{d}{dt} [Z_9 : E_{11}^h] &= k_{\text{flow}} \left( [Z_9 : E_{11}^h]^{\text{up}} - [Z_9 : E_{11}^h] \right) + k_{z_9:e_{11}}^+ z_9 e_{11}^h \\
&\quad - (k_{z_9:e_{11}}^- + k_{z_9:e_{11}}^{\text{cat}}) [Z_9 : E_{11}^h] \\
\frac{d}{dt} [Z_9 : E_{11}] &= k_{\text{flow}} \left( [Z_9 : E_{11}]^{\text{up}} - [Z_9 : E_{11}] \right) + k_{z_9:e_{11}}^+ z_9 e_{11} \\
&\quad - (k_{z_9:e_{11}}^- + k_{z_9:e_{11}}^{\text{cat}}) [Z_9 : E_{11}] \\
\frac{d}{dt} [Z_9^m : E_{11}^{h,m}] &= k_{z_9:e_{11}}^+ z_9^m e_{11}^{h,m} - (k_{z_9:e_{11}}^- + k_{z_9:e_{11}}^{\text{cat}}) [Z_9^m : E_{11}^{h,m}] \\
\frac{d}{dt} [Z_9^m : E_{11}^{m*}] &= k_{z_9:e_{11}}^+ z_9^m e_{11}^{m*} - (k_{z_9:e_{11}}^- + k_{z_9:e_{11}}^{\text{cat}}) [Z_9^m : E_{11}^{m*}] \\
\frac{d}{dt} [Z_{11} : E_2] &= k_{\text{flow}} \left( [Z_{11} : E_2]^{\text{up}} - [Z_{11} : E_2] \right) \\
&\quad + k_{z_{11}:e_2}^+ z_{11} e_2 - (k_{z_{11}:e_2}^- + k_{z_{11}:e_2}^{\text{cat}}) [Z_{11} : E_2] \\
\frac{d}{dt} [E_{11}^h : E_2] &= k_{\text{flow}} \left( [E_{11}^h : E_2]^{\text{up}} - [E_{11}^h : E_2] \right) \\
&\quad + k_{e_{11}:e_2}^+ e_{11}^h e_2 - (k_{e_{11}:e_2}^- + k_{e_{11}:e_2}^{\text{cat}}) [E_{11}^h : E_2] \\
\frac{d}{dt} [Z_{11}^m : E_2^m] &= k_{z_{11}:e_2}^+ z_{11}^m e_2^m - (k_{z_{11}:e_2}^- + k_{z_{11}:e_2}^{\text{cat}}) [Z_{11}^m : E_2^m] \\
\frac{d}{dt} [E_{11}^{h,m*} : E_2^m] &= k_{e_{11}:e_2}^+ e_{11}^{h,m*} e_2^m - (k_{e_{11}:e_2}^- + k_{e_{11}:e_2}^{\text{cat}}) [E_{11}^{h,m*} : E_2^m]
\end{aligned}$$

**S1 Table. INITIAL PLASMA LEVELS.** Descriptions, notation and labels for each parameter associated with initial plasma levels are listed. The value of each parameter is found in the corresponding table listed above.

| Description | Notation                                                                   | Label           | Table |
|-------------|----------------------------------------------------------------------------|-----------------|-------|
| Prothrombin | $z_2$                                                                      | Z <sub>2</sub>  | S5    |
| Factor V    | $z_5$                                                                      | Z <sub>5</sub>  | S5    |
| Factor VII  | $z_7$                                                                      | Z <sub>7</sub>  | S5    |
| Factor VIII | $z_8$                                                                      | Z <sub>8</sub>  | S5    |
| Factor IX   | $z_9$                                                                      | Z <sub>9</sub>  | S5    |
| Factor X    | $z_{10}$                                                                   | Z <sub>10</sub> | S5    |
| Factor XI   | $z_{11}$                                                                   | Z <sub>11</sub> | S5    |
| TFPI        | [TFPI]                                                                     | TFPI            | S5    |
| AT          | $k_{AT:e_2}^{in}, k_{AT:e_9}^{in}, k_{AT:e_{10}}^{in}, k_{AT:e_{11}}^{in}$ | AT              | S11   |

**S2 Table. PLATELET CHARACTERISTICS.** Descriptions, notation and labels for each parameter associated with platelet characteristics are listed. The value of each parameter is found in the corresponding table listed above.

| Description                                         | Notation          | Label                | Table |
|-----------------------------------------------------|-------------------|----------------------|-------|
| Platelet count                                      | $PL^{up}$         | PLup                 | S5    |
| Binding site number for II                          | $N_2$             | N2                   | S5    |
| Binding site number for IIa                         | $N_2^*$           | N2*                  | S5    |
| Binding site number for V/Va                        | $N_5$             | N5                   | S5    |
| Binding site number for VIII/VIIIa                  | $N_8$             | N8                   | S5    |
| Binding site number for IX                          | $N_9$             | N9                   | S5    |
| Binding site number for IXa                         | $N_9^*$           | N9*                  | S5    |
| Binding site number for X/Xa                        | $N_{10}$          | N10                  | S5    |
| Binding site number for XI                          | $N_{11}$          | N11                  | S5    |
| Binding site number for XIa                         | $N_{11}^*$        | N11*                 | S5    |
| Rate of unactivated platelets adhering to SE        | $k_{adh}^+$       | kadh                 | S12   |
| Rate of activated platelets adhering to SE          | $k_{adh}^{+,*}$   | kadh1                | S12   |
| Rate of platelet activation by platelet in solution | $k_{plt}^{act}$   | kact <sub>plt</sub>  | S12   |
| Rate of platelet activation on SE                   | $k_{plt}^{act,*}$ | kact* <sub>plt</sub> | S12   |
| Rate of platelet activation by thrombin             | $k_{e_2}^{act}$   | kact <sub>e2</sub>   | S7    |

**S3 Table. KINETIC RATE CONSTANTS.** Descriptions, notation and labels for each parameter associated with kinetic rate constants are listed. The value of each parameter is found in the corresponding table listed above.

| Description                                      | Notation                       | Label           | Table |
|--------------------------------------------------|--------------------------------|-----------------|-------|
| Rates of activation of TF:VII by fX              | $K_M$                          | KZ7mE10M        | S7    |
|                                                  | $k_{z7:e_{10}}^{cat}$          | KZ7mE10CAT      | S7    |
|                                                  | $k_{z7:e_{10}}^-$              | KZ7mE10MI       | S7    |
| Rates of activation of fX by TF:VIIa             | $K_M$                          | KZ10E7mM        | S7    |
|                                                  | $k_{z10:e_7}^{cat}$            | KZ10E7mCAT      | S7    |
|                                                  | $k_{z10:e_7}^-$                | KZ10E7mMI       | S7    |
| Rates of activation of fIX by TF:VIIa            | $K_M$                          | KZ9E7mM         | S7    |
|                                                  | $k_{z9:e_7}^{cat}$             | KZ9E7mCAT       | S7    |
|                                                  | $k_{z9:e_7}^-$                 | KZ9E7mMI        | S7    |
| Rates of binding of fVII/fVIIa to TF             | $k_7^{on}$                     | K7ON            | S7    |
|                                                  | $k_7^{off}$                    | K7OFF           | S8    |
| Rates of activation of TF:VII by fXa             | $K_M$                          | KZ7E10M         | S8    |
|                                                  | $k_{z7:e_{10}}^{cat}$          | KZ7E10CAT       | S8    |
|                                                  | $k_{z7:e_{10}}^-$              | KZ7E10MI        | S8    |
| Rates of activation of TF:VII by fIIa            | $K_M$                          | KZ7E2M          | S8    |
|                                                  | $k_{z7:e_2}^{cat}$             | KZ7E2CAT        | S8    |
|                                                  | $k_{z7:e_2}^-$                 | KZ7E2MI         | S8    |
| Rates of activation of TF:VII by fIXa            | $K_M$                          | KZ7E9M          | S8    |
|                                                  | $k_{z7:e_9}^{cat}$             | KZ7E9CAT        | S8    |
|                                                  | $k_{z7:e_9}^-$                 | KZ7E9MI         | S8    |
| Rates of activation of fV by fIIa                | $K_M$                          | KZ5E2M          | S8    |
|                                                  | $k_{z5:e_2}^{cat}$             | KZ5E2CAT        | S8    |
|                                                  | $k_{z5:e_2}^-$                 | KZ5E2MI         | S8    |
| Rates of activation of fVIII by fIIa             | $K_M$                          | KZ8E2M          | S8    |
|                                                  | $k_{z8:e_2}^{cat}$             | KZ8E2CAT        | S8    |
|                                                  | $k_{z8:e_2}^-$                 | KZ8E2MI         | S8    |
| Rates of activation of fIX by fXIa-fXIa          | $k_{z9:e_{11}}^+$              | KZ9E11P         | S8    |
|                                                  | $k_{z9:e_{11}}^{cat}$          | KZ9E11CAT       | S8    |
|                                                  | $k_{z9:e_{11}}^-$              | KZ9E11MI        | S8    |
| Rates of activation of fIX by fXIa-fXI           | $k_{z9:e_{11}}^+$              | KZ9E11P         | S8    |
|                                                  | $k_{z9:e_{11}}^{cat}$          | KZ9E11CAT       | S8    |
|                                                  | $k_{z9:e_{11}}^-$              | KZ9E11MI        | S8    |
| Rates of activation of fXI by fIIa               | $k_{z11:e_2}^+$                | KZ11E2P         | S8    |
|                                                  | $k_{z11:e_2}^{cat}$            | KZ11E2CAT       | S8    |
|                                                  | $k_{z11:e_2}^-$                | KZ11E2MI        | S9    |
| Rates of binding of fX/fXa to plt. surface       | $k_{10}^{on}$                  | K10ON           | S9    |
|                                                  | $k_{10}^{off}$                 | K10OFF          | S9    |
| Rates of binding of fV/fVa to plt. surface       | $k_5^{on}$                     | K5ON            | S9    |
|                                                  | $k_5^{off}$                    | K5OFF           | S9    |
| Rates of binding of fVIII/fVIIIa to plt. surface | $k_8^{on}$                     | K8ON            | S9    |
|                                                  | $k_8^{off}$                    | K8OFF           | S9    |
| Rates of binding of fIX/fIXa to plt. surface     | $k_9^{on}$                     | K9ON            | S9    |
|                                                  | $k_9^{off}$                    | K9OFF           | S9    |
| Rates of binding of fII/fIIa to plt. surface     | $k_2^{on}, k_2^{on,*}$         | K2ON, K2SON     | S9    |
|                                                  | $k_2^{off}, k_2^{off,*}$       | K2OFF, K2SOFF   | S9    |
| Rates of binding of fXI/fXIa to plt. surface     | $k_{11}^{on}, k_{11}^{on,*}$   | K11ON, K11SON   | S9    |
|                                                  | $k_{11}^{off}, k_{11}^{off,*}$ | K11OFF, K11SOFF | S10   |

**S4 Table. KINETIC RATE CONSTANTS.** Descriptions, notation and labels for each parameter associated with kinetic rate constants are listed. The value of each parameter is found in the corresponding table listed above.

| Description                                              | Notation                 | Label        | Table |
|----------------------------------------------------------|--------------------------|--------------|-------|
| Rates of activation of fV by fXa on plt. surface         | $K_M$                    | KZ5mE10mM    | S10   |
|                                                          | $k_{z_5:e_{10}}^{cat}$   | KZ5mE10mCAT  | S10   |
|                                                          | $k_{z_5:e_{10}}^-$       | KZ5mE10mMI   | S10   |
| Rates of activation of fV by fIIa on plt. surface        | $K_M$                    | KZ5mE2mM     | S10   |
|                                                          | $k_{z_5:e_2}^{cat}$      | KZ5mE2mCAT   | S10   |
|                                                          | $k_{z_5:e_2}^-$          | KZ5mE2mMI    | S10   |
| Rates of activation of fVIII by fXa on plt. surface      | $K_M$                    | KZ8ME10MM    | S10   |
|                                                          | $k_{z_8:e_{10}}^{cat}$   | KZ8ME10MCAT  | S10   |
|                                                          | $k_{z_8:e_{10}}^-$       | KZ8ME10MMI   | S10   |
| Rates of activation of fVIII by fIIa on plt. surface     | $K_M$                    | KZ8ME2MM     | S10   |
|                                                          | $k_{z_8:e_2}^{cat}$      | KZ8mE2mCAT   | S10   |
|                                                          | $k_{z_8:e_2}^-$          | KZ8mE2mMI    | S10   |
| Rates of activation of fX by TEN on plt. surface         | $K_M$                    | KZ10mTENM    | S10   |
|                                                          | $k_{z_{10}^m:TEN}^{cat}$ | KZ10mTENCAT  | S10   |
| Rates of activation of fII by PRO on plt. surface        | $K_M$                    | KZ2mPROM     | S10   |
|                                                          | $k_{z_2^m:PRO}^{cat}$    | KZ2mPROCAT   | S10   |
| Rates of activation of fXI by fIIa on plt. surfaces      | $k_{z_{11}^m:e_2}^+$     | KZ11mE2mP    | S10   |
|                                                          | $k_{z_{11}^m:e_2}^{cat}$ | KZ11mE2mCAT  | S10   |
|                                                          | $k_{z_{11}^m:e_2}^-$     | KZ11mE2mMI   | S10   |
| Rates of activation of fIX by fXIa-fXIIa on plt. surface | $K_M$                    | KZ9mE11mP    | S10   |
|                                                          | $k_{z_9^m:e_{11}}^{cat}$ | KZ9mE11mCAT  | S10   |
|                                                          | $k_{z_9^m:e_{11}}^-$     | KZ9mE11mMI   | S10   |
| Rates of formation of TEN on plt. surface                | $k_{e_8^+e_9^m}^+$       | KE8mE9mP     | S10   |
|                                                          | $k_{e_8^+e_9^m}^-$       | KE8mE9mMI    | S10   |
| Rates of formation of PRO on plt. surface                | $k_{e_5^+e_{10}^m}^+$    | KE5mE10mP    | S10   |
|                                                          | $k_{e_5^+e_{10}^m}^-$    | KE5mE10mMI   | S10   |
|                                                          | $k_{e_5^m:e_{10}}^-$     | KE5mE10mMI   | S10   |
| Rates of inhibition of fXa by TFPI                       | $k_{tfpia:e_{10}}^+$     | KTFPI_E10_P  | S11   |
|                                                          | $k_{tfpia:e_{10}}^-$     | KTFPI_E10_M  | S11   |
| Rates of inhibition of TF:VIIa by TFPIa                  | $k_{tfpia:e_7^m}^+$      | KTFPIa_E7m_P | S11   |
|                                                          | $k_{tfpia:e_7^m}^-$      | KTFPIa_E7m_M | S11   |
| Rates of inhibition of fVa by APC on plt. surface        | $K_M$                    | KE5mAPCM     | S11   |
|                                                          | $k_{e_5^m:APC}^{cat}$    | KE5mAPCCAT   | S11   |
|                                                          | $k_{e_5^m:APC}^-$        | KE5mAPCMI    | S11   |
| Rates of inhibition of fVIIIa by APC on plt. surface     | $K_M$                    | KE8mAPCM     | S11   |
|                                                          | $k_{e_8^m:APC}^{cat}$    | KE8mAPCCAT   | S11   |
|                                                          | $k_{e_8^m:APC}^-$        | KE8mAPCMI    | S11   |
| Rates of inhibition of fIIa by TM on plt. surface        | $k_{TM}^{on}$            | KTMP         | S11   |
|                                                          | $k_{TM}^{off}$           | KTMM         | S12   |

**Kinetic and Physical Parameter Values:**

**S5 Table. DIFFUSION COEFFICIENTS FOR PLATELETS AND FLUID-PHASE CHEMICAL SPECIES** (a) From [3]. (b) From [4].

|           |                                            |   |
|-----------|--------------------------------------------|---|
| Platelets | $2.5 \times 10^{-7} \text{ cm}^2/\text{s}$ | a |
| Proteins  | $5 \times 10^{-7} \text{ cm}^2/\text{s}$   | b |

**S6 Table. NORMAL CONCENTRATIONS AND SURFACE BINDING SITE NUMBERS** (a) From [5]. (b) From [6]. (c) [7] suggests that normal plasma concentration of fVIIa is about 1% of the normal fVII concentration. (d) From [8]. (e) (f) From [9]. (g) Estimated as described in the text of the Supplementary Information. (h) From [10]. (i) From [11]. (j) From [12]. (k) From [13]. (l) From [14, 15]. (m) Number of fV molecules released per activated platelet [16]. (n) Maximum concentration of platelets in a  $2 \mu\text{m}$  high reaction zone assuming that 20 platelets can cover a  $10\mu\text{m}$ -by- $10\mu\text{m}$  injured surface [17].

|                |                         |   |
|----------------|-------------------------|---|
| Prothrombin    | $1.4 \mu\text{M}$       | a |
| Factor V       | $0.01 \mu\text{M}$      | b |
| Factor VII     | $0.01 \mu\text{M}$      | a |
| Factor VIIa    | $0.1 \text{ nM}$        | c |
| Factor VIII    | $1.0 \text{ nM}$        | a |
| Factor IX      | $0.09 \mu\text{M}$      | a |
| Factor X       | $0.17 \mu\text{M}$      | a |
| Factor XI      | $30.0 \text{ nM}$       | a |
| TFPI           | $2.5 \text{ nM}$        | d |
| Protein C      | $65 \text{ nM}$         | e |
| Platelet count | $2.5(10)^5/\mu\text{l}$ | f |
| $N_2$          | $1000/\text{plt}$       | g |
| $N_2^*$        | $1000/\text{plt}$       | g |
| $N_5$          | $3000/\text{plt}$       | h |
| $N_8$          | $450/\text{plt}$        | i |
| $N_9$          | $250/\text{plt}$        | j |
| $N_9^*$        | $250/\text{plt}$        | j |
| $N_{10}$       | $2700/\text{plt}$       | k |
| $N_{11}$       | $1500/\text{plt}$       | l |
| $N_{11}^*$     | $250/\text{plt}$        | l |
| $n_5$          | $3000/\text{plt}$       | m |
| $p_{PLAS}$     | $0.167 \text{ nM}$      | n |

**S7 Table. REACTIONS ON SUBENDOTHELIUM** (a)  $k_{z_7^m:e_{10}}^{\text{cat}} = 5.0 \text{ sec}^{-1}$  and  $K_M = 1.2 \cdot 10^{-6} \text{ M}$  [18]. (b)  $k_{z_7^m:e_2}^{\text{cat}} = 6.1 \cdot 10^{-2} \text{ sec}^{-1}$  and  $K_M = 2.7 \cdot 10^{-6} \text{ M}$  [18]. (c)  $k_{z_{10}:e_7^m}^{\text{cat}} = 1.15 \text{ sec}^{-1}$  and  $K_M = 4.5 \cdot 10^{-7} \text{ M}$  [5]. (d)  $k_{z_9:e_7^m}^{\text{cat}} = 1.15 \text{ sec}^{-1}$  and  $K_M = 2.4 \cdot 10^{-7} \text{ M}$  [19]. (e)  $K_d = 1.0 \cdot 10^{-10} \text{ M}$  [20].

|                            |                 |                  |          |                                       |                                        |                                                  |   |
|----------------------------|-----------------|------------------|----------|---------------------------------------|----------------------------------------|--------------------------------------------------|---|
| Activation<br>(of -, by -) |                 |                  |          |                                       |                                        |                                                  |   |
| (TF:VII,fXa)               | $E_{10}, Z_7^m$ | $Z_7^m : E_{10}$ | $E_7^m$  | $k_{z_7^m:e_{10}}^+ = 5.0 \cdot 10^6$ | $k_{z_7^m:e_{10}}^- = 1.0$             | $k_{z_7^m:e_{10}}^{\text{cat}} = 5.0$            | a |
| (TF:VII, fIIa)             | $E_2, Z_7^m$    | $Z_7^m : E_2$    | $E_7^m$  | $k_{z_7^m:e_2}^+ = 3.92 \cdot 10^5$   | $k_{z_7^m:e_2}^- = 1.0$                | $k_{z_7^m:e_2}^{\text{cat}} = 6.1 \cdot 10^{-2}$ | b |
| (fX, TF:VIIa)              | $E_7^m, Z_{10}$ | $Z_{10} : E_7^m$ | $E_{10}$ | $k_{z_{10}:e_7^m}^+ = 5.0 \cdot 10^6$ | $k_{z_{10}:e_7^m}^- = 1.0$             | $k_{z_{10}:e_7^m}^{\text{cat}} = 1.15$           | c |
| (fIX, TF:VIIa)             | $E_7^m, Z_9$    | $Z_9 : E_7^m$    | $E_9$    | $k_{z_9:e_7^m}^+ = 9.4 \cdot 10^6$    | $k_{z_9:e_7^m}^- = 1.0$                | $k_{z_9:e_7^m}^{\text{cat}} = 1.15$              | d |
| Binding<br>(of -, with -)  |                 |                  |          |                                       |                                        |                                                  |   |
| (fVII, TF)                 | $Z_7, TF$       |                  | $Z_7^m$  | $k_7^{\text{on}} = 5.0 \cdot 10^7$    | $k_7^{\text{off}} = 5.0 \cdot 10^{-3}$ |                                                  | e |
| (fVIIa, TF)                | $E_7, TF$       |                  | $E_7^m$  | $k_7^{\text{on}} = 5.0 \cdot 10^7$    | $k_7^{\text{off}} = 5.0 \cdot 10^{-3}$ |                                                  | e |

**S8 Table. REACTIONS IN THE PLASMA** (a)  $k_{z_7:e_{10}}^{\text{cat}} = 5.0 \text{ sec}^{-1}$  and  $K_M = 1.2 \cdot 10^{-6} \text{ M}$  [18]. (b)  $k_{z_7:e_2}^{\text{cat}} = 6.1 \cdot 10^{-2} \text{ sec}^{-1}$  and  $K_M = 2.7 \cdot 10^{-6} \text{ M}$  [18] (c)  $k_{z_5:e_2}^{\text{cat}} = 0.23 \text{ sec}^{-1}$  and  $K_M = 7.17 \cdot 10^{-8} \text{ M}$  [21]. (d)  $k_{z_8:e_2}^{\text{cat}} = 0.9 \text{ sec}^{-1}$  [22] and  $K_M = 2 \cdot 10^{-7} \text{ M}$  [23]. (e)  $k_{z_{11}:e_2}^{\text{cat}} = 1.3 \cdot 10^{-4}$ ,  $K_M = 50\text{nM}$  [24]. Rate constants apply also for thrombin-activation of XIa-XI. (f)  $k_{z_9:e_{11}^h}^{\text{cat}} = 0.21$ ,  $K_M = 0.2\mu\text{M}$  [25, 26]. Rate constants apply also for activation of IX by XIa-XIa.

| Reaction                   | Reactants       | Complex          | Product    | $\text{M}^{-1}\text{sec}^{-1}$          | $\text{sec}^{-1}$          | $\text{sec}^{-1}$                                 | Note |
|----------------------------|-----------------|------------------|------------|-----------------------------------------|----------------------------|---------------------------------------------------|------|
| Activation<br>(of -, by -) |                 |                  |            |                                         |                            |                                                   |      |
| (fVII, fXa)                | $Z_7, E_{10}$   | $Z_7 : E_{10}$   | $E_7$      | $k_{z_7:e_{10}}^+ = 5 \cdot 10^6$       | $k_{z_7:e_{10}}^- = 1.0$   | $k_{z_7:e_{10}}^{\text{cat}} = 5.0$               | a    |
| (fVII, fIIa)               | $Z_7, E_2$      | $Z_7 : E_2$      | $E_7$      | $k_{z_7:e_2}^+ = 3.92 \cdot 10^5$       | $k_{z_7:e_2}^- = 1.0$      | $k_{z_7:e_2}^{\text{cat}} = 6.1 \cdot 10^{-2}$    | b    |
| (fV, fIIa)                 | $Z_5, E_2$      | $Z_5 : E_2$      | $E_5$      | $k_{z_5:e_2}^+ = 1.73 \cdot 10^7$       | $k_{z_5:e_2}^- = 1.0$      | $k_{z_5:e_2}^{\text{cat}} = 0.23$                 | c    |
| (fVIII, fIIa)              | $Z_8, E_2$      | $Z_8 : E_2$      | $E_8$      | $k_{z_8:e_2}^+ = 2.64 \cdot 10^7$       | $k_{z_8:e_2}^- = 1.0$      | $k_{z_8:e_2}^{\text{cat}} = 0.9$                  | d    |
| (fXI-fXI, fIIa)            | $Z_{11}, E_2$   | $Z_{11} : E_2$   | $E_{11}^h$ | $k_{z_{11}:e_2}^+ = 2.0 \cdot 10^7$     | $k_{z_{11}:e_2}^- = 1.0$   | $k_{z_{11}:e_2}^{\text{cat}} = 1.3 \cdot 10^{-4}$ | e    |
| (fIX, fXIa)                | $Z_9, E_{11}^h$ | $Z_9 : E_{11}^h$ | $E_9$      | $k_{z_9:e_{11}^h}^+ = 0.6 \cdot (10)^7$ | $k_{z_9:e_{11}^h}^- = 1.0$ | $k_{z_9:e_{11}^h}^{\text{cat}} = 0.21$            | f    |

**S9 Table. BINDING TO PLATELET SURFACES** (a) For fIX binding to platelets,  $K_d = 2.5 \cdot 10^{-9}$  M [12], and for fX binding to platelets,  $K_d$  has approximately the same value [10]. For fX binding to PCPS vesicles, the on-rate is about  $10^7$  M<sup>-1</sup>sec<sup>-1</sup> and the off-rate is about 1.0 sec<sup>-1</sup> [27] giving a dissociation constant of about  $10^{-7}$  M. To estimate on- and off-rates for the higher-affinity binding of fX to platelets, we keep the on-rate the same as for vesicles and adjust the off-rate to give the correct dissociation constant. The rates for fIX binding with platelets are taken to be the same as for fX binding. (b) We assume binding constants for fIXa binding to the specific fIXa binding sites are the same as for shared sites. (c) fV binds with high-affinity to phospholipids (PCPS) [27] and we use the same rate constants reported there to describe fV binding to platelets. (d) The  $K_d$  for fVIII binding with platelets is taken from [11]. We set the off-rate  $k_8^{\text{off}}$  for fVIII binding to platelets equal to that for fV binding to platelets, and calculate the on-rate  $k_8^{\text{on}}$ . (e) For prothrombin interactions with platelets,  $K_d$  is reported to be  $5.9 \cdot 10^{-7}$  M [28]. We choose  $k_2^{\text{off}}$  and set  $k_2^{\text{on}} = k_2^{\text{off}}/K_d$ . (f) Estimated as described in the text of the Supplementary Information. (g)  $K_d = 10$  nM [29]. (h)  $K_d = 1.7$  nM [15].

| Reaction     | Reactants          | Products    | M <sup>-1</sup> sec <sup>-1</sup>         | sec <sup>-1</sup>                         | Note |
|--------------|--------------------|-------------|-------------------------------------------|-------------------------------------------|------|
| Factor IX    | $Z_9, P_9$         | $Z_9^m$     | $k_9^{\text{on}} = 1.0 \cdot 10^7$        | $k_9^{\text{off}} = 2.5 \cdot 10^{-2}$    | a    |
| Factor IXa   | $E_9, P_9$         | $E_9^m$     | $k_9^{\text{on}} = 1.0 \cdot 10^7$        | $k_9^{\text{off}} = 2.5 \cdot 10^{-2}$    | a    |
| Factor IXa   | $E_9, P_9^*$       | $E_9^{m,*}$ | $k_9^{\text{on}} = 1.0 \cdot 10^7$        | $k_9^{\text{off}} = 2.5 \cdot 10^{-2}$    | b    |
| Factor X     | $Z_{10}, P_{10}$   | $Z_{10}^m$  | $k_{10}^{\text{on}} = 1.0 \cdot 10^7$     | $k_{10}^{\text{off}} = 2.5 \cdot 10^{-2}$ | a    |
| Factor Xa    | $E_{10}, P_{10}$   | $E_{10}^m$  | $k_{10}^{\text{on}} = 1.0 \cdot 10^7$     | $k_{10}^{\text{off}} = 2.5 \cdot 10^{-2}$ | a    |
| Factor V     | $Z_5, P_5$         | $Z_5^m$     | $k_5^{\text{on}} = 5.7 \cdot 10^7$        | $k_5^{\text{off}} = 0.17$                 | c    |
| Factor Va    | $E_5, P_5$         | $E_5^m$     | $k_5^{\text{on}} = 5.7 \cdot 10^7$        | $k_5^{\text{off}} = 0.17$                 | c    |
| Factor VIII  | $Z_8, P_8$         | $Z_8^m$     | $k_8^{\text{on}} = 5.0 \cdot 10^7$        | $k_8^{\text{off}} = 0.17$                 | d    |
| Factor VIIIa | $E_8, P_8$         | $E_8^m$     | $k_8^{\text{on}} = 5.0 \cdot 10^7$        | $k_8^{\text{off}} = 0.17$                 | d    |
| Factor II    | $Z_2, P_2$         | $Z_2^m$     | $k_2^{\text{on}} = 1.0 \cdot 10^7$        | $k_2^{\text{off}} = 5.9$                  | e    |
| Factor IIa   | $E_2, P_2$         | $E_2^m$     | $k_2^{*,\text{on}} = 1.0 \cdot 10^7$      | $k_2^{*,\text{off}} = 0.2$                | f    |
| Factor XI    | $Z_{11}, P_{11}$   | $Z_{11}^m$  | $k_{z_{11}}^{\text{on}} = 1.0 \cdot 10^7$ | $k_{z_{11}}^{\text{off}} = 0.1$           | g    |
| Factor XIa   | $E_{11}, P_{11}^*$ | $E_{11}^m$  | $k_{e_{11}}^{\text{on}} = 1.0 \cdot 10^7$ | $k_{e_{11}}^{\text{off}} = 0.017$         | h    |

**S10 Table. REACTIONS ON PLATELET SURFACES** (a)  $k_{z_5^m:e_{10}^m}^{\text{cat}} = 0.046 \text{ sec}^{-1}$  and  $K_M = 10.4 \cdot 10^{-9} \text{ M}$  [30]. (b) The rate constants for thrombin activation of fV on platelets are assumed to be the same as in plasma. (c)  $k_{z_8^m:e_{10}^m}^{\text{cat}} = 0.023 \text{ sec}^{-1}$  and  $K_M = 2.0 \cdot 10^{-8} \text{ M}$  [23]. (d) The rate constants for thrombin activation of fVIII on platelets are assumed to be the same as in plasma. (e) The formation of the tenase and prothrombinase complexes is assumed to be very fast with  $K_d = 1.0 \cdot 10^{-10} \text{ M}$  [31]. (f)  $k_{z_{10}^m:ten}^{\text{cat}} = 20 \text{ sec}^{-1}$  and  $K_M = 1.6 \cdot 10^{-7} \text{ M}$  [32]. (g)  $k_{z_2^m:pro}^{\text{cat}} = 30 \text{ sec}^{-1}$  and  $K_M = 3.0 \cdot 10^{-7} \text{ M}$  [33]. (h)  $k_{z_{11}^m:e_2^m}^{\text{cat}} = 1.3 \cdot 10^{-4}$ ,  $K_M = 50 \text{ nM}$  [24]. Rate constants apply also for thrombin-activation of Plt-XIa-XI. (i)  $k_{z_9^m:e_{11}^{h,m}}^{\text{cat}} = 0.21$ ,  $K_M = 0.2 \mu\text{M}$  [25, 26]. Rate constants apply also for activation of platelet-bound IX by Plt-XIa-XIa.

| Reaction                   | Reactants             | Complex                | Product        | $\text{M}^{-1}\text{sec}^{-1}$              | $\text{sec}^{-1}$                | $\text{sec}^{-1}$                                     | Note |
|----------------------------|-----------------------|------------------------|----------------|---------------------------------------------|----------------------------------|-------------------------------------------------------|------|
| Activation<br>(of -, by -) |                       |                        |                |                                             |                                  |                                                       |      |
| (V, Xa)                    | $Z_5^m, E_{10}^m$     | $Z_5^m : E_{10}^m$     | $E_5^m$        | $k_{z_5^m:e_{10}^m}^+ = 1.0 \cdot 10^8$     | $k_{z_5^m:e_{10}^m}^- = 1.0$     | $k_{z_5^m:e_{10}^m}^{\text{cat}} = 4.6 \cdot 10^{-2}$ | a    |
| (V, IIa)                   | $Z_5^m, E_2^m$        | $Z_5^m : E_2^m$        | $E_5^m$        | $k_{z_5^m:e_2^m}^+ = 1.73 \cdot 10^7$       | $k_{z_5^m:e_2^m}^- = 1.0$        | $k_{z_5^m:e_2^m}^{\text{cat}} = 0.23$                 | b    |
| (VIII, Xa)                 | $Z_8^m, E_{10}^m$     | $Z_8^m : E_{10}^m$     | $E_8^m$        | $k_{z_8^m:e_{10}^m}^+ = 5.1 \cdot 10^7$     | $k_{z_8^m:e_{10}^m}^- = 1.0$     | $k_{z_8^m:e_{10}^m}^{\text{cat}} = 2.3 \cdot 10^{-2}$ | c    |
| (VIII, IIa)                | $Z_8^m, E_2^m$        | $Z_8^m : E_2^m$        | $E_8^m$        | $k_{z_8^m:e_2^m}^+ = 2.64 \cdot 10^7$       | $k_{z_8^m:e_2^m}^- = 1.0$        | $k_{z_8^m:e_2^m}^{\text{cat}} = 0.9$                  | d    |
| (X, VIIIa:IXa)             | $Z_{10}^m, TEN$       | $Z_{10}^m : TEN$       | $E_{10}^m$     | $k_{z_{10}^m:ten}^+ = 1.31 \cdot 10^8$      | $k_{z_{10}^m:ten}^- = 1.0$       | $k_{z_{10}^m:ten}^{\text{cat}} = 20.0$                | f    |
| (X, VIIIa:IXa*)            | $Z_{10}^m, TEN^*$     | $Z_{10}^m : TEN^*$     | $E_{10}^m$     | $k_{z_{10}^m:ten}^+ = 1.31 \cdot 10^8$      | $k_{z_{10}^m:ten}^- = 1.0$       | $k_{z_{10}^m:ten}^{\text{cat}} = 20.0$                | f    |
| (II, Va:Xa)                | $Z_2^m, PRO$          | $Z_2^m : PRO$          | $E_2^m$        | $k_{z_2^m:pro}^+ = 1.03 \cdot 10^8$         | $k_{z_2^m:pro}^- = 1.0$          | $k_{z_2^m:pro}^{\text{cat}} = 30.0$                   | g    |
| (XI-XI, IIa)               | $Z_{11}^m, E_2^m$     | $Z_{11}^m : E_2^m$     | $E_{11}^{h,m}$ | $k_{z_{11}^m:e_2^m}^+ = 2.0 \cdot 10^7$     | $k_{z_{11}^m:e_2^m}^- = 1.0$     | $k_{z_{11}^m:e_2^m}^{\text{cat}} = 1.3 \cdot 10^{-4}$ | h    |
| (IX, XIa)                  | $Z_9^m, E_{11}^{h,m}$ | $Z_9^m : E_{11}^{h,m}$ | $E_9$          | $k_{z_9^m:e_{11}^{h,m}}^+ = 0.6 \cdot 10^7$ | $k_{z_9^m:e_{11}^{h,m}}^- = 1.0$ | $k_{z_9^m:e_{11}^{h,m}}^{\text{cat}} = 0.21$          | i    |
| Binding<br>(of -, with -)  |                       |                        |                |                                             |                                  |                                                       |      |
| (VIIIa, IXa)               | $E_8^m, E_9^m$        |                        | $TEN$          | $k_{ten}^+ = 1.0 \cdot 10^8$                | $k_{ten}^- = 0.01$               |                                                       | e    |
| (VIIIa, IXa*)              | $E_8^m, E_9^{m,*}$    |                        | $TEN^*$        | $k_{ten}^+ = 1.0 \cdot 10^8$                | $k_{ten}^- = 0.01$               |                                                       | e    |
| (Va, Xa)                   | $E_5^m, E_{10}^m$     |                        | $PRO$          | $k_{pro}^+ = 1.0 \cdot 10^8$                | $k_{pro}^- = 0.01$               |                                                       | e    |

**S11 Table. INHIBITION REACTIONS** (a) We estimate these parameters based on the half-lives of Factors IXa, Xa, IIa in plasma [34] and assume that the rate of fXIa inactivation is the same as that of fXa and thrombin. (b) For inhibition of fVa by APC,  $k_{e_5^m:APC}^{\text{cat}} = 0.5 \text{ sec}^{-1}$  and  $K_M = 12.5 \cdot 10^{-9}$  [35]. We assume the same reaction rates for the inhibition of fVIIIa by APC. (c) From [36]. (d)  $K_d = 0.5 \text{ nM}$  and  $[PC] = 65 \text{ nM}$  [37]. (e)  $k_{PC:TM:e_2^c} = 0.167 \text{ sec}^{-1}$ ,  $K_M = 0.7 \cdot 10^{-6} \text{ M}$  [38].

| Reaction                     | Reactants      | Product         | $\text{M}^{-1}\text{sec}^{-1}$        | $\text{sec}^{-1}$                         | $\text{sec}^{-1}$                     | Note |
|------------------------------|----------------|-----------------|---------------------------------------|-------------------------------------------|---------------------------------------|------|
| Inactivation<br>(of -, by -) |                |                 |                                       |                                           |                                       |      |
| (IXa, AT-III)                | $E_9$          | none            |                                       | $k_{AT:e_9}^{\text{in}} = 0.1$            |                                       | a    |
| (Xa, AT-III)                 | $E_{10}$       | none            |                                       | $k_{AT:e_{10}}^{\text{in}} = 0.1$         |                                       | a    |
| (IIa, AT-III)                | $E_2$          | none            |                                       | $k_{AT:e_2}^{\text{in}} = 0.2$            |                                       | a    |
| (XIa, AT-III)                | $E_{11}$       | none            |                                       | $k_{AT:e_{11}}^{\text{in}} = 0.2$         |                                       | a    |
| (APC, Va)                    | $APC, E_5^m$   | none            | $k_{e_5^m:APC}^+ = 1.2 \cdot 10^8$    | $k_{e_5^m:APC}^- = 1.0$                   | $k_{e_5^m:APC}^{\text{cat}} = 0.5$    | b    |
| (APC, VIIIa)                 | $APC, E_8^m$   | none            | $k_{e_8^m:APC}^+ = 1.2 \cdot 10^8$    | $k_{e_8^m:APC}^- = 1.0$                   | $k_{e_8^m:APC}^{\text{cat}} = 0.5$    | b    |
| Binding<br>(of -, with -)    |                |                 |                                       |                                           |                                       |      |
| (TFPI, Xa)                   | $TFPI, E_{10}$ | $TFPIa$         | $k_{tfpia:e_{10}}^+ = 1.6 \cdot 10^7$ | $k_{tfpia:e_{10}}^- = 3.3 \cdot 10^{-4}$  |                                       | c    |
| (TFPIa, TF:VIIa)             | $TFPIa, E_7^m$ | $TFPIa : E_7^m$ | $k_{tfpia:e_7^m}^+ = 1.0 \cdot 10^7$  | $k_{tfpia:e_7^m}^- = 1.1 \cdot 10^{-3}$   |                                       | c    |
| (TM, Thrombin)               | $TM, E_2^c$    | $TM : E_2^c$    | $k_{TM}^{\text{on}} = 1.0 \cdot 10^8$ | $k_{TM}^{\text{off}} = 5.0 \cdot 10^{-2}$ |                                       | d    |
| Activation<br>(of -, by -)   |                |                 |                                       |                                           |                                       |      |
| (PC, TM: $E_2^c$ )           | $TM : E_2^c$   | $APC$           | $k_{PC:TM:e_2^c}^+ = 1.7 \cdot 10^6$  | $k_{PC:TM:e_2^c}^- = 1.0$                 | $k_{PC:TM:e_2^c}^{\text{cat}} = 0.16$ | e    |

**S12 Table. PLATELET TRANSITIONS** (a) Estimated from data in [39, 40] as described in [1]. (b) Estimated from data in [41] as described in [1]. SE=subendothelium.

| Reactants                                   | Reactants    | Products         | $M^{-1}sec^{-1}$               | $sec^{-1}$            | Note |
|---------------------------------------------|--------------|------------------|--------------------------------|-----------------------|------|
| Unactivated platelet adhering to SE         | $PL, SE$     | $PL_a^s$         | $k_{adh}^+ = 2 \cdot 10^{10}$  | $k_{adh}^- = 0$       | a    |
| Activated platelet adhering to SE           | $PL_a^v, SE$ | $PL_a^v$         | $k_{adh}^+ = 2 \cdot 10^{10}$  | $k_{adh}^- = 0$       | a    |
| Platelet activation by platelet in solution | $PL, PL_a^v$ | $2PL_a^v$        | $k_{plt}^{act} = 3 \cdot 10^8$ |                       | b    |
| Platelet activation on SE                   | $PL, PL_a^s$ | $PL_a^v, PL_a^s$ | $k_{plt}^{act} = 3 \cdot 10^8$ |                       | b    |
| Platelet activation by thrombin             | $PL, E_2$    | $PL_a^v$         |                                | $k_{e2}^{act} = 0.50$ | b    |

## Bibliography

- [1] Kuharsky AL, Fogelson AL. Surface-mediated Control of Blood Coagulation: The Role of Binding Site Densities and Platelet Deposition. *Biophys J*. 2001;80:1050–1074.
- [2] Fogelson AL, Tania N. Coagulation under flow: The influence of flow-mediated transport on the initiation and inhibition of coagulation. *Pathophysiol Haemost Thromb*. 2005;34:91–108.
- [3] Turitto VT, Leonard EF. Platelet adhesion to a spinning surface. *Trans Amer Soc Artif Int Organs*. 1972;18:348–54.
- [4] Young M, Carroad P, Bell R. Estimation of diffusion coefficients of proteins. *Biotech and Bioeng*. 1980;22(5):947–955.
- [5] Mann KG, Nesheim ME, Church WR, Haley P, Krishnaswamy S. Surface-dependent Reactions of the Vitamin K-dependent enzyme complexes. *Blood*. 1990;76:1–16.
- [6] Mann KG, Bovill EG, Krishnaswamy S. Surface-dependent reactions in the propagation phase of blood coagulation. *Ann N Y Acad Sci*. 1991;614:63–75.
- [7] Morrissey JH. Tissue Factor Modulation of Factor VIIa Activity: Use in Measuring Trace Levels of Factor VIIa in Plasma,. *Thromb Haemost*. 1995;74:185–188.
- [8] Novotny WF, Brown SG, Miletich JP, Rader DJ, Broze GJ. Plasma antigen levels of the lipoprotein-associated coagulation inhibitor in patient samples. *Blood*. 1991;78:387–93.
- [9] Weiss HJ. Platelet Physiology and Abnormalities of Platelet Function (Part 1). *New Engl J Med*. 1975;293:531–541.
- [10] Walsh PN. Platelet-Coagulant Protein Interactions. In: Colman RW, Hirsh J, Marder VJ, Salzman EW, editors. *Hemostasis and Thrombosis: Basic Principles and Clinical Practice*. 3rd ed. Philadelphia, PA: J.B. Lippincott Company; 1994. p. 629–651.
- [11] Nesheim ME, Pittman DD, Wang JH, Slonosky D, Giles AR, Kaufman RJ. The binding of S-labeled recombinant Factor VIII to activated and unactivated human platelets. *J Biol Chem*. 1988;263:16467.
- [12] Ahmad SS, Rawala-Sheikh R, Walsh PN. Comparative interactions of Factor IX and Factor IXa with human platelets. *Journal of Biological Chemistry*. 1989;264:3244–3251.
- [13] Mann KG, Krishnaswamy S, Lawson JH. Surface-dependent Hemostasis. *Semin Hematol*. 1992;29:213–26.
- [14] Baglia FA, Jameson BA, Walsh PN. Identification and Characterization of a Binding Site for Platelets in the Apple 3 domain of coagulation Factor XI. *J Biol Chem*. 1995;270:6734–40.
- [15] Miller TN, Sinha D, Baird TR, Walsh PN. A Catalytic Domain Exosite (Cys<sup>527</sup>-Cys<sup>542</sup>) in Factor XIa mediates binding to a site on activated platelets. *Biochemistry*. 2007;46:14450–60.

- [16] Tracy PB, Eide LL, Bowie EJ, Mann KG. Radioimmunoassay of factor V in human plasma and platelets. *Blood*. 1982;60:59–63.
- [17] Hubbell JA, McIntire LV. Platelet Active Concentration Profiles Near Growing Thrombi. A Mathematical Consideration. *Biophys J*. 1986;50:937–945.
- [18] Butenas S, Mann KG. Kinetics of Human Factor VII activation. *Biochemistry*. 1996;35:1904–1910.
- [19] Limentani SA, Furie BC, Furie B. The Biochemistry of Factor IX. In: Colman R, Hirsh J, Marder V, Salzman E, editors. *Hemostasis and Thrombosis: Basic Principles and Clinical Practice*. 3rd ed. Philadelphia, PA: J.B. Lippincott Company; 1994. p. 94–108.
- [20] Nemerson Y. The Tissue Factor Pathway of Blood Coagulation. *Semin Hematol*. 1992;29:170–176.
- [21] Monkovic DD, Tracy PB. Functional Characterization of Human Platelet-released Factor V and its Activation by Factor Xa and Thrombin. *J Biol Chem*. 1990;265:17132–40.
- [22] Hill-Eubanks DC, Lollar P. von Willibrand factor is a cofactor for thrombin-catalyzed cleavage of the Factor VIII light chain. *J Biol Chem*. 1990;265:17854–8.
- [23] Lollar P, Knutson GJ, Fass DN. Activation of Porcine Factor VIII:C by Thrombin and Factor Xa. *Biochemistry*. 1985;24:8056–8064.
- [24] Gailani D, Broze Jr GJ. Factor XI activation in a revised model of blood coagulation. *Science*. 1991;253:909–12.
- [25] Gailani D, Ho D, Sun MF, Cheng Q, Walsh PN. Model for a Factor IX activation complex on blood platelets: dimeric conformation of Factor XIa is essential. *Blood*. 2001;97:3117–22.
- [26] Sinha D, Marcinkiewicz M, Navaneetham D, Walsh PN. Macromolecular substrate-binding exosite on both the heavy and light chains of Factor XIa mediate the formation of the Michaelis Complex required for Factor IX activation. *Biochemistry*. 2007;46:9830–9.
- [27] Krishnaswamy S, Jones KC, Mann KG. Prothrombinase Complex Assembly. Kinetic Mechanism of Enzyme Assembly on Phospholipid Vesicles. *J Biol Chem*. 1988;263:3823–3834.
- [28] Mann KG. Prothrombin and thrombin. In: Colman R, Hirsh J, Marder V, Salzman E, editors. *Hemostasis and Thrombosis: Basic Principles and Clinical Practice*. 3rd ed. Philadelphia, PA: J.B. Lippincott Company; 1994. p. 184–199.
- [29] Greengard JS, Heeb MJ, Ersdal E, Walsh PN, Griffin JH. Binding of coagulation Factor XI to washed human platelets. *Biochemistry*. 1986;25:3884–90.
- [30] Monkovic DD, Tracy PB. Activation of human Factor V by Factor Xa and thrombin. *Biochemistry*. 1990;29:1118.

- [31] Mann KG. The assembly of blood clotting complexes on membranes. *TIBS*. 1987;12:229–233.
- [32] Rawala-Sheikh R, Ahmad SS, Ashby B, Walsh PN. Kinetics of coagulation Factor X activation by platelet-bound Factor IXa. *Biochemistry*. 1990;29:2606–11.
- [33] Nesheim ME, Tracy RP, Tracy PB, Boskovic DS, Mann KG. Mathematical Simulation of Prothrominase. *Methods Enzymol*. 1992;215:316–328.
- [34] Rosenberg RD, Bauer KA. The Heparin-antithrombin System: A Natural Anticoagulant Mechanism. In: Colman RW, Hirsh J, Marder VJ, Salzman EW, editors. *Hemostasis and Thrombosis: Basic Principles and Clinical Practice*. 3rd ed. Philadelphia, PA: J.B. Lippincott Company; 1994. p. 837–860.
- [35] Solymoss S, Tucker MM, Tracy PB. Kinetics of inactivation of membrane-bound Factor Va by activated protein C. Protein S modulates Factor Xa protection. *J Biol Chem*. 1988;263:14884–90.
- [36] Jesty J, Wun TC, Lorenz A. Kinetics of the Inhibition of Factor Xa and the Tissue Factor-Factor VIIa Complex by the Tissue Factor Pathway Inhibitor in the Presence and Absence of Heparin. *Biochemistry*. 1994;33:12686–12694.
- [37] Griffin JH. Control of Coagulation Reactions. In: Beutler E, Coller B, Lichtman M, Kipps T, Seligsohn U, editors. *Williams Hematology*. New York: McGraw Hill; 2001. p. 1435–1447.
- [38] Broze GJ, Miletich JP. Biochemistry and Physiology of Protein C, Protein S, and Thrombomodulin. In: Colman RW, Hirsh J, Marder VJ, Salzman EW, editors. *Hemostasis and Thrombosis: Basic Principles and Clinical Practice*. Philadelphia: Lippincott Company; 1994. p. 259–276.
- [39] Turitto VT, Baumgartner HR. Platelet Interaction with Subendothelium in Flowing Rabbit Blood: Effect of Blood Shear Rate. *Microvasc Res*. 1979;17:38–54.
- [40] Turitto VT, Weiss HJ, Baumgartner HR. The Effect of Shear Rate on Platelet Interaction with Subendothelium Exposed to Citrated Human Blood. *Microvasc Res*. 1980;19:352–365.
- [41] Gear ARL. Platelet adhesion, shape change, and aggregation: rapid initiation and signal transduction events. *Can J Physiol Pharmacol*. 1994;72:285–94.

## Chapter 4

# A mathematical model of coagulation under flow identifies factor V as a modifier of thrombin generation in hemophilia A

This chapter originally submitted on the BioArXiv as “Link, K.G., **Stobb, M.T.**, Sorrells, M.G., Bortot, M., Ruegg, K., Manco-Johnson, M.J., Di Paola, J.A., Sindi, S.S., Fogelson, A.L., Leiderman, K., Neeves, K.B. (2019). *A mathematical model of flow-mediated coagulation identifies factor V as a modifier of thrombin generation in hemophilia A.*” Reprinted in accordance with the Creative Commons Attribution 4.0 International License (<http://creativecommons.org/licenses/by/4.0/>) with some changes for continuity. The co-authors listed in this publication directed and supervised research which formed the basis for the dissertation. KGL and MTS contributed equally to this work.

### 4.1 Abstract

Hemophilia A is a bleeding disorder categorized as severe, mild, and moderate deficiencies in factor VIII (FVIII). Within these categories the variance in bleeding severity is significant and the origins unknown. The number of parameters that could modify bleeding are so numerous that experimental approaches are not feasible for considering all possible combinations. Consequently, we turn to a mathematical model of coagulation under flow to act as a screening tool to identify parameters that are most likely to enhance thrombin generation. We performed global sensitivity analysis on 110,000 simulations that varied coagulation factor levels by 50-150% of their normal values in humans while holding FVIII levels at 1%. These simulations identified low factor V (FV) levels as the strongest candidate, with additional enhancement when combined with high prothrombin levels. This prediction was confirmed in two experimental models: Partial FV inhibition boosted fibrin deposition in flow assays performed at  $100 \text{ s}^{-1}$  on collagen-tissue factor surfaces using whole blood from individuals with mild and moderate FVIII deficiencies. Low FV ( $\sim 50\%$ ) or partial FV inhibition also augmented thrombin generation in FVIII-inhibited or FVIII-deficient plasma in calibrated automated thrombography. These effects were amplified by

high prothrombin levels in both experimental models. Our mathematical model suggests a mechanism in which FV and FVIII compete to bind to factor Xa to initiate thrombin generation in low FV, FVIII-deficient blood. This unexpected result was made possible by a mechanistic mathematical model, providing an example of the potential of such models in making predictions in complex biological networks.

## 4.2 Introduction

Hemophilia A is a genetic bleeding disorder caused by a deficiency in coagulation factor VIII (FVIII), a protein in blood plasma necessary to generate stable blood clots. FVIII deficiency prevents sufficient generation of thrombin, the major enzyme of coagulation that plays a pivotal role in clot formation. The plasma concentration of FVIII defines clinical categories of hemophilia A as mild ( $> 5\%$ ), moderate (1-5%), or severe ( $<1\%$ ) but within these categories, individuals with similar plasma levels can have different bleeding phenotypes [1]. Some variations in bleeding phenotype can be assigned to the different mutations in the *F8* gene, or thrombophilic mutations, but a large portion remains unexplained[2, 3]. Plasma protein levels are potential modifiers of bleeding; in particular, the variability in coagulation factor levels is quite large, with the normal range generally regarded as 50-150% of the mean of the healthy population. We hypothesize that certain combinations of coagulation factor levels within this normal range could enhance thrombin generation in the context of FVIII deficiencies and thus reduce bleeding. Identifying such combinations using a reductionist approach alone is unlikely to succeed since clot formation is a complex, nonlinear process. In this study, we use a mechanistic mathematical model of flow-mediated coagulation as a screening tool to predict modifiers of thrombin generation in FVIII deficiency and verify these predictions with experimental models.

The coagulation reaction network shares many features with gene, metabolic, and protein networks, for which mathematical and computational approaches are essential to decipher behavior and predict system responses [4–6]. First, complex networks often display nonlinear responses due to the presence of positive and negative feedback loops. In the coagulation network, thrombin both enhances and inhibits its own production through different pathways. Second, the interactions between components of complex networks must be fully described to mechanistically explain emergent properties of the network itself. For example, our previous mathematical models of coagulation under flow showed that thrombin generation had a threshold dependence on the amount of exposed tissue factor (TF) [7–9], a prediction later validated in experiments [10]. Finally, complex networks are robust in that they maintain phenotypic stability in the face of perturbations. Even with the normal variability in coagulation factors levels, the healthy hemostatic response is quite robust, leading to clots that prevent bleeding while maintaining vessel patency. The robustness of the coagulation network response to perturbations under disease states such as hemophilia is unknown.

A powerful tool for analyzing the variability of a model network’s output is sensitivity analysis (SA); here, model inputs are altered, either one-at-a-time (local SA, LSA) or in combination (global SA, GSA), and the resulting influence on model outputs is studied [11]. In variance-based GSA methods, the variance in model output is decomposed and attributed to individual parameters and interactions between groups of parameters. One SA approach is to vary model parameters to identify those to which the model output

is the most sensitive. There are LSA studies that use this approach on mathematical models of coagulation in the absence of flow [12, 13]. Another approach is to use the model to make predictions about potential outcomes given variations in the input. For example, the inputs could represent variability in a disease state or to predict therapeutic outcomes or targets [14, 15]. We previously conducted a LSA and GSA to determine how variation ( $\pm 50\%$ ) in plasma levels of coagulation factors affected thrombin generation in a model of flow-mediated coagulation under healthy conditions [16]. Our analysis revealed low overall variance of thrombin output, which is in line with results from Danforth et al. [15]. Collectively, these results underscore the robustness of thrombin generation under healthy conditions.

In this study, we are interested in FVIII deficiencies and thus, we have fixed the FVIII level to be low in our mathematical model and performed a GSA by varying the remaining plasma protein levels. We used the GSA as an initial screening tool to search for combinations of plasma protein levels that either enhance or reduce thrombin generation in the context of FVIII deficiency. Combinations identified with the GSA to have the greatest effect were verified in whole blood flow assays and calibrated automated thrombography (CAT). This systems biology approach identified a potential mechanism where variations in FV levels within the normal range dramatically alter thrombin generation and fibrin formation in FVIII deficiencies.

#### 4.2.1 Brief overview of clotting

Blood clot formation involves the coupled processes of platelet aggregation and coagulation, which are triggered when blood is exposed to the subendothelium (SE). Platelet aggregation begins when platelets adhere to SE matrix proteins, become activated and form a platelet plug to arrest blood loss. Coagulation consists of a biochemical network that is initiated by TF, progresses by means of enzymatic reactions on activated platelet surfaces (APS) [17, 18], and culminates in thrombin generation. Thrombin activates platelets and converts the soluble fibrinogen into insoluble fibrin, which polymerizes to form a stabilizing mesh surrounding the platelet mass.

Coagulation proteins include inactive enzyme precursors (zymogens) factors VII, IX, X, XI and II (prothrombin) and the corresponding active enzymes factors VIIa, IXa, Xa, XIa, and IIa (thrombin), as well as the inactive/active cofactor pairs factors V/Va and VIII/VIIIa. Enzyme inhibitors include antithrombin (AT), tissue factor pathway inhibitor (TFPI), and activated protein C (APC). Thrombin generation occurs through the activity of three major cofactor/enzyme complexes, TF:FVIIa, FVIIIa:FIXa (tenase), and FVa:FXa (prothrombinase); each requires a suitable cellular surface on which to form, the SE for TF:FVIIa and APS for FVIIIa:FIXa and FVa:FXa. Coagulation proteins bind to specific binding sites on APS prior to forming platelet-bound complexes. We denote platelet-bound species with a prefix "plt", e.g., plt-FV. Below we use "plasma proteins" to refer collectively to zymogens, inactive cofactors, and inhibitors.

The backbone of the coagulation reaction network involves the following steps (see Fig. S1A) that can greatly amplify the initiating signal of TF exposure: TF:FVIIa activates FIX and FX on the SE; FIXa and FXa bind to APS; plt-FXa activates small amounts of plt-FV and plt-FVIII; plt-FVIIIa and plt-FIXa form tenase complexes on APS; plt-FVa and plt-FXa form prothrombinase complexes on APS; prothrombinase converts prothrombin into thrombin. The backbone is augmented with numerous feedback loops which are critical

to robust thrombin generation. For example, plt-Xa produced by tenase activates plt-VIII allowing more tenase to form; thrombin activates plt-FVIII and plt-FV allowing more tenase and prothrombinase to form. FVIII deficiencies reduce thrombin generation because less tenase forms on APS. Factor XII and blood-bourne sources of TF are not considered in our mathematical model.

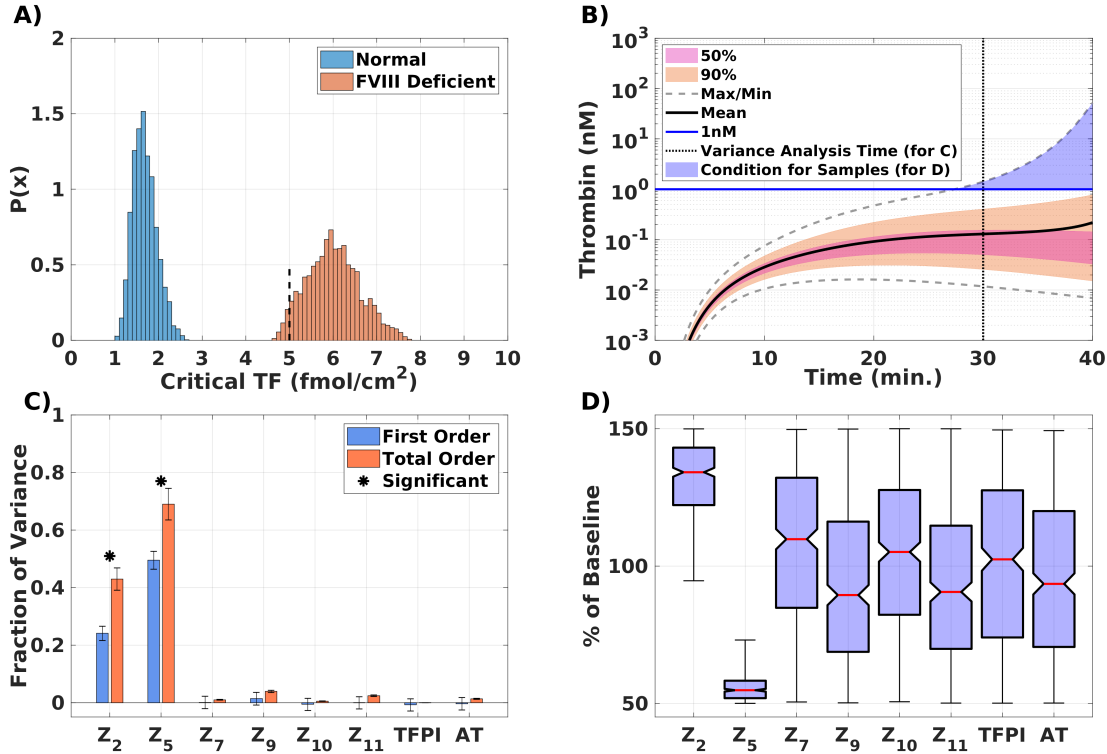


**Figure 4.1: Global sensitivity analysis for mathematical model of flow-mediated coagulation.** **A)** Critical TF distributions for normal and FVIII deficient plasma. Dashed black line at 5 fmol/cm<sup>2</sup> is the fixed TF for all further simulations. **B)** Thrombin concentration time series generated by uniformly and independently varying plasma protein levels  $\pm 50\%$  from normal (110,000 total simulations); mean (solid black line), boundaries that encompass 50% (pink), and 90% of the data (orange), and the maximum/minimum of the computed solutions (gray-dashed); blue line drawn at 1nM. **C)** First (blue) and total (orange) order Sobol indices are plotted as mean  $\pm$  standard deviation computed with 5,000 bootstrap samples of the original 110,000 simulations. **D)** Plasma zymogen and inhibitor levels distributions shown as box-and-whisker plots (mean in red, whiskers  $3IQR$ ), conditioned on achieving more than 1nM of total thrombin.

## Results

The mathematical model we use is presented in [9, 16] and is an extension of our earlier models [7, 8, 19]. The model includes all of the reactions depicted in Fig. S11, with the equations and parameter choices fully described in [9]. The inputs to this model are the TF level, plasma protein levels, platelet count, binding sites on APS, and flow rate; the available outputs are all model species' concentrations as a function of time.

### 4.2.2 Tissue factor density distributions for normal and FVIII-deficient plasma

Our previous studies revealed a critical TF level, where thrombin sharply transitioned between an attenuated and amplified response [7–9]. Under FVIII-deficient conditions and high TF, our model produces more than 1 nM of thrombin by 10 min, albeit at a decreased rate compared to normal FVIII levels [7]. Furthermore, it is known that individuals with FVIII deficiencies bleed mostly in regions of the body with low TF levels [20–22]. Taken together, these studies show that the TF level has an important influence on whether substantial thrombin is produced for any given values of plasma protein levels. Thus, to identify modifiers of hemophilia A, we first determine a range of critical TF levels so that minor decreases in that level result in little or no thrombin generation and minor increases result in substantial thrombin generation. As an initial screen, we varied the plasma protein levels between 50 and 150% of their physiologic levels for both normal and FVIII-deficient plasma (FVIII fixed to 1% or normal), using 2,500 Latin Hypercube samples [23]. For each of these parameter set samples, a bisection procedure was used to determine the minimum TF level required to achieve an amplified thrombin response, i.e., 1 nM thrombin by 40 min. The distribution of these values determines a critical range of TF levels over which the thrombin response is most sensitive to variations in plasma protein levels. In our model, thrombin that reaches 1 nM (indicated by a blue line in Fig. 4.1B) activates platelets and is then likely to continue to increase [7–9, 16].

Fig. 4.1A shows the TF distributions for the normal (blue) and FVIII-deficient (orange) plasma where the protein levels were varied between 50-150%. No overlap between the two distributions is observed, with normal and FVIII-deficient plasma having a TF range of [1.07, 2.62] fmol/cm<sup>2</sup> and [4.63, 7.78] fmol/cm<sup>2</sup>, respectively. These distributions suggest that a TF level of 5 fmol/cm<sup>2</sup>, near the left edge of the distribution for FVIII-deficient plasma, is a good choice for conducting further probes of plasma protein levels in a GSA, because for the majority, but not all, of the plasma protein combinations that we tested, little thrombin is produced. All further simulations in this study are performed with TF at 5 fmol/cm<sup>2</sup>.

### 4.2.3 GSA identifies FV as a modifier of thrombin generation in hemophilia A

We performed a GSA of thrombin generation by varying plasma protein levels using 110,000 samples in which each plasma protein level (except FVIII, which was fixed to 1%) was sampled uniformly and independently between 50-150% of normal. Quantiles of the thrombin concentration time-course are shown in Fig. 4.1B. While no simulation achieved more than 100 nM by 40 min, about 5% of the simulations eventually led to thrombin greater than 100 nM (not shown). We further distinguish simulations by those that led to 1 nM thrombin within 40 min and those that did not.

To assign fractions of the thrombin output variance observed in the quantiles of Fig. 4.1B, we performed a Sobol analysis [24]. Fig. 4.1C shows the first order (blue) and total order (orange) Sobol sensitivity indices for the thrombin concentration at 30 min. The first order indices represent the fraction of the variance attributable to that one parameter alone while the total order index indicates the fraction due to that parameter plus its interactions with other parameters. We see that the parameters, i.e., the plasma protein levels, that

had the most influence on the variance in thrombin at 30 min are FV and prothrombin (FII), which account for approximately 50% and 24% of the variance, respectively. In addition, approximately 19% of the model variance is explained by the interaction between prothrombin and FV, as indicated by the total order Sobol indices exceeding the first order indices.

Next, we characterized the  $\approx 5000$  simulations that led to 1 nM thrombin within 40 min (blue shaded region in Fig. 4.1B). Fig. 4.1D shows the distribution of all plasma proteins that correspond to those simulations. The majority of the plasma protein levels have medians close to their average and distributions that appear roughly uniform. This indicates that 1 nM thrombin is possible with any value of these plasma levels. The plasma FV and prothrombin levels were striking exceptions. Both have medians close to their extreme values and are distributed over a narrower range than the other plasma protein levels. Although the prothrombin distribution is skewed towards higher levels, it does extend below 100%, indicating that higher than normal prothrombin is not strictly necessary to achieve 1 nM thrombin. Conversely, every sample that achieved 1nM thrombin had plasma levels of FV that were strictly less than 75% of normal. Indeed, over 75% of the samples had a FV level less than 60% of normal. This indicates that FV levels on the low end of normal (close to 50%) are necessary to enhance thrombin generation in FVIII-deficient plasma stimulated with a low level of TF in this model.

#### 4.2.4 Exploration of Mechanism: The competition for FXa

We used our mathematical model to explore how lower FV can enhance thrombin production in FVIII-deficient plasma. Table S1 lists the variations in plasma levels of prothrombin and FV that we considered. Fig. 4.2A shows the time-course of thrombin for these four cases. In the two cases with low FV, substantial thrombin is produced and thrombin generation occurs earlier with a higher prothrombin level. Very little thrombin is produced with normal levels of FV. These results indicate that low FV is key to enhancing thrombin production and increasing prothrombin level alone does not. Fig. 4.2B-C show that the tenase concentration associated with low FV diverges from normal FV as early as 5 min, before the prothrombinase and thrombin curves diverge. Given that there is little thrombin at these early times, the differences in the tenase behavior suggest that early competition between plt-FVIII and plt-FV to bind to plt-FXa plays a significant role.

To see this competition, Fig. 4.2D-E shows the concentrations of plt-FVIII:FXa and plt-FV:FXa. The concentration of plt-FVIII:FXa is substantially higher for the low FV cases than for the normal FV cases, and for each FV level, there is very little difference (for at least 20 min) between the high and low prothrombin levels. To further demonstrate the importance of FV and FVIII competition for FXa, we adjust the kinetic rate constants for these reactions while setting the FV and FII concentrations to their baseline levels (see Fig. S2A-B). We found that: increasing only the rate of binding of plt-FVIII to plt-FXa leads to very low thrombin production; decreasing the rate of binding of plt-FV to plt-FXa by 50% and increasing the rate of binding of plt-FVIII to plt-FXa by 50% from their normal values, however, results in a 30-fold higher thrombin concentration at 40 min and thrombin generation reaches 1 nM at about 37 min. These results confirm that competition between plt-FV and plt-FVIII for plt-FXa influences the rescue of thrombin under FVIII-deficient conditions.

Thrombin activation of FV and FVIII, and APC binding to FVa and FVIIIa, may

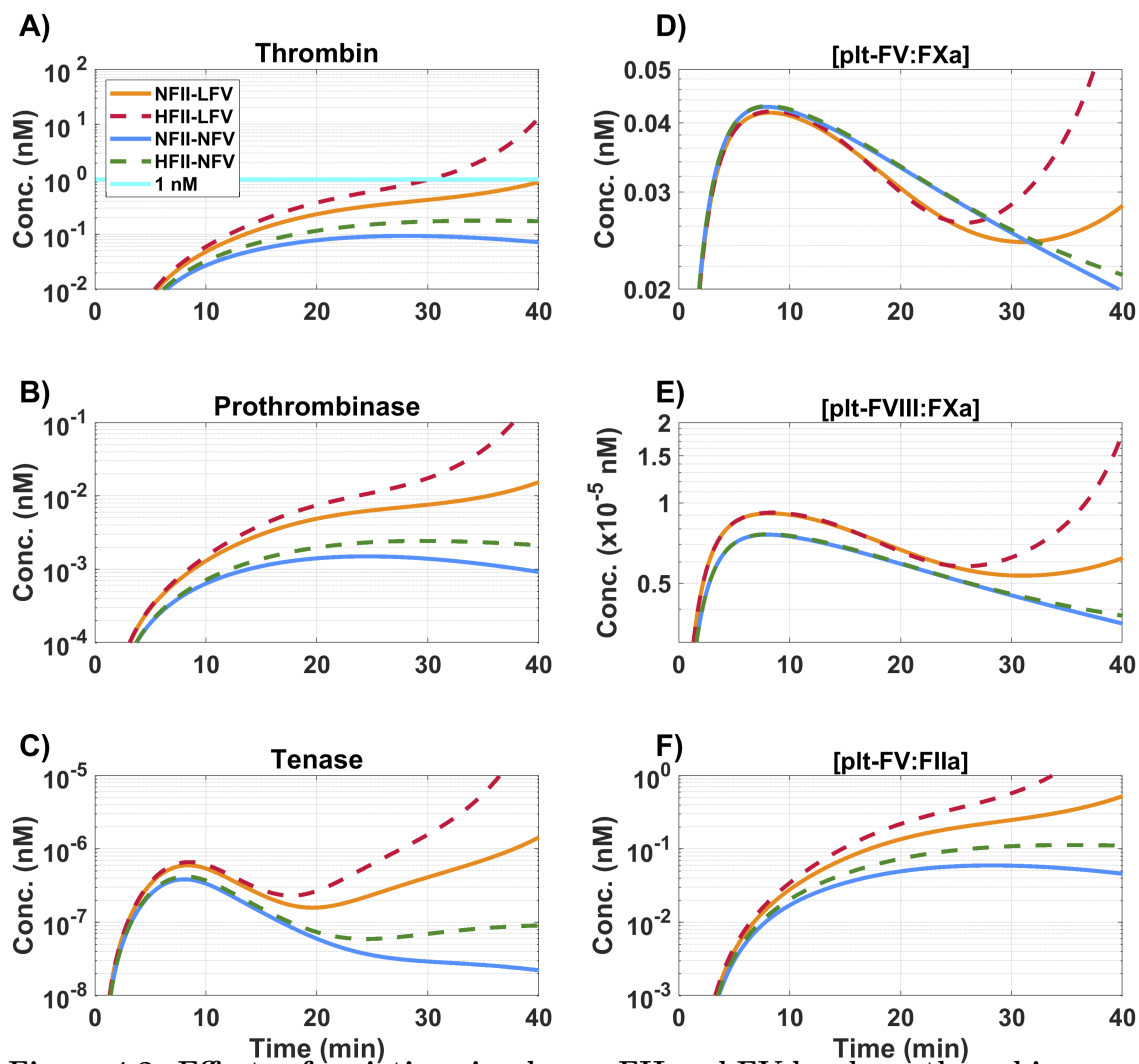


**Figure 4.2:** Effects of variations in plasma FII and FV levels on thrombin generation and the evolution of enzyme complexes in the mathematical model. “N” denotes 100%, “L” denotes 50%, and “H” denotes 150% of the respective baseline plasma level; “NFII” = 1400 nM, “NFV” = 10 nM. **A)** Total thrombin; **B)** prothrombinase (FVa:FXa); **C)** platelet tenase (FVIIIa:FIXa); **D)** FVIII:FXa complex on plt; **E)** FV:FXa complex on plt; **F)** FV:FIIa complex on plt; during a time course of 40 min. Description of labels found in Table S1.

also influence thrombin production in the low FV cases. To explore this, we performed simulations in which the binding rates for FV and FVIII to thrombin and for FVa and FVIIIa to APC were set to zero (Fig. S3A-F), and compared the results to those in Fig. 4.2A-F. We see that thrombin generation is initially increased in the low FV cases but is not sustained after 40 min (Fig. S3A). Tenase and prothrombinase follow a similar trend, where low FV produces higher concentrations initially but amplification of tenase and prothrombinase complex formation does not occur (Fig. S3B-C). Thus, thrombin-mediated activation of FV and FVIII is necessary to produce a significant thrombin response despite the lack of APC-mediated inhibition.

It is not intuitive how lowering FV plasma levels results in near-normal prothrombinase (see Fig. 4.2B) since FV is a precursor of a component of prothrombinase. In the low FV cases, despite decreased FXa-mediated activation of FV (Fig. 4.2D), the concentration of plt-FV bound to thrombin at 20 min is approximately 10-fold larger than that associated with normal FV cases (Fig. 4.2F). This is a direct result of the increased thrombin concentration shown in Fig. 4.2A. Thrombin feeds back by activating plt-FVIII and indirectly, plt-FIX via FXIa, to form more tenase (Fig. S4A-B). Increased tenase results in more plt-FXa, which binds to the thrombin-activated plt-FVa, leading to more prothrombinase and thus more thrombin, even with FVIII deficiency.

In summary, we used our mathematical model to identify where in the coagulation reaction network FV and FVIII most strongly interact. The coagulation network involves no direct reaction between FV and FVIII, but they compete for binding to FXa and thrombin. We confirmed that thrombin-mediated activation of FV and FVIII is essential to a substantial thrombin response. More importantly, the early divergence of thrombin and key complexes in low versus normal FV cases, even when thrombin-mediated activation of FV and FVIII is turned off, identifies the competition of FV and FVIII for FXa as the initiator of thrombin generation rescue in low FV, FVIII-deficient blood. Additional support for this hypothesis comes from simulations in which we isolated the reactions amongst plt-FV, plt-FVIII, and plt-FXa by varying their binding rates.

#### 4.2.5 Partial inhibition of FV enhances fibrin deposition in FVIII-deficient blood under flow

Whole blood microfluidic assays were performed at  $100 \text{ s}^{-1}$  on type I collagen-TF ( $1.09 \pm 0.2 \text{ fmol/cm}^2$ ). Blood from individuals with moderate and mild FVIII deficiencies was treated with exogenous prothrombin ( $50 \text{ }\mu\text{g/mL}$ ), an anti-FV antibody at a concentration that reduced FV activity to  $\sim 60\%$  in normal pooled plasma (Fig. S5), both exogenous prothrombin and anti-FV, or a vehicle control (Figs. 4.3, S6). In the vehicle and exogenous prothrombin cases, little to no fibrin was observed. Platelet adhered and nearly coated the surface over the 25 min experiment, but there were no large, multilayer platelet aggregates. Anti-FV alone supports fibrin formation in and around multilayer platelet aggregates, and when combined with prothrombin, the effect is even more pronounced with larger, platelet-fibrin thrombi forming. There was a significant increase in both the rate of and maximum accumulation of fibrin(ogen) with partial inhibition of FV. There were no significant differences in total platelet accumulation despite the morphological differences described above (Fig. S8). The FVIII levels in these samples were higher (3.0-8.5%) the day of the experiments than those considered in our mathematical model (1% FVIII) because

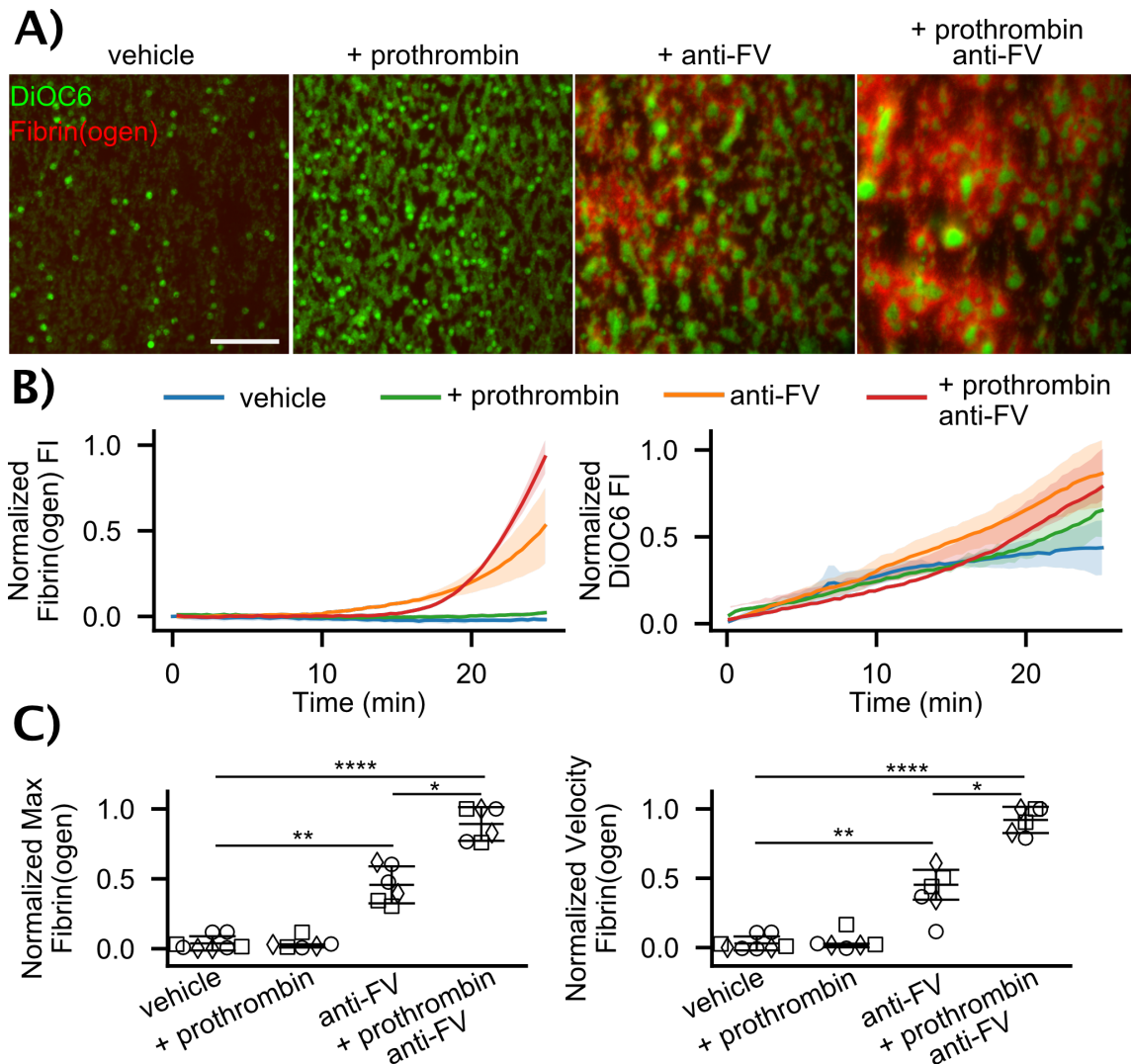


**Figure 4.3: Flow assays with whole blood from FVIII deficient individuals.** **A)** Representative images of DiOC6 labeled platelets and leukocytes and Alexa Fluor 555 labeled fibrin(ogen) on collagen-TF surfaces at  $100 \text{ s}^{-1}$  after 25 min for vehicle control,  $50 \mu\text{g/mL}$  exogenous prothrombin,  $100 \mu\text{g/mL}$  anti-FV, and exogenous prothrombin and anti-FV. Scale bar =  $50 \mu\text{m}$ . Individual fluorescent channels are found in Fig. S6. **B)** Representative fibrin(ogen) and platelet/leukocyte accumulation dynamics in terms of normalized fluorescent intensity (FI). **C)** Fibrin(ogen) normalized maximum fluorescence intensity and rate of deposition (normalized velocity) for FVIII levels of  $\bigcirc = 3.0\%$ ,  $\square = 7.5\%$ ,  $\diamond = 8.5\%$ . See SI and Fig. S7 for calculation of metrics. P-values represented as \*, \*\*, and \*\*\*\* for  $10^{-2}$ ,  $10^{-4}$ , and  $10^{-7}$ , respectively.

these individuals have mild to moderate FVIII deficiencies (SI Appendix). Nevertheless, the inhibition of FV clearly shows an increase in fibrin deposition in these experiments, and indirectly, thrombin generation.

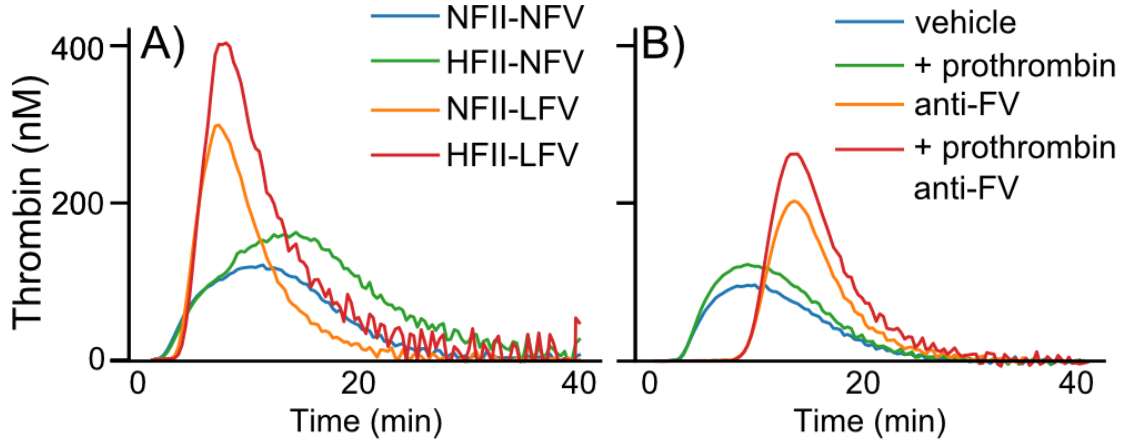


**Figure 4.4: Calibrated automated thrombography.** A) FII and FV levels were varied using immunodepleted plasmas and purified FII and FV in the presence of an anti-FVIII function blocking antibody. 'N', 'H', and 'L' corresponds to normal, high, and low levels of respective zymogen. B) FVIII deficient (<1%) plasma treated with vehicle control, 50  $\mu\text{g}/\text{mL}$  exogenous prothrombin, 100  $\mu\text{g}/\text{mL}$  anti-FV, and exogenous prothrombin and anti-FV. All assays conducted with 5 pM TF and phospholipids. Tables S3 and S4 contain the measured prothrombin, FV, and FVIII levels corresponding to each curve.

#### 4.2.6 Low FV and partial inhibition of FV enhances thrombin generation in FVIII-inhibited or FVIII-deficient plasma

We used calibrated automated thrombography (CAT) [25] to measure the effects of reducing FV levels or activity on thrombin generation dynamics in a clinical clotting assay. We altered zymogen concentrations to approximate the four conditions in Table S1 using mixtures of FV and prothrombin depleted plasmas, purified FV and prothrombin, and an anti-FVIII function blocking antibody used at a concentration that yields FVIII activity of <1% to simulate severe hemophilia A. Consistent with mathematical model predictions, Fig. 4.4A and Table S3 show that low FV (43%) increases the peak thrombin concentration, which is further enhanced when prothrombin (136%) is added. Similar trends, albeit with lower peak thrombin concentrations, were measured with FVIII deficient plasma using the same treatments as the flow assay experiments described in the previous section (Table S4). Fig. 4.4B shows results from an individual with severe FVIII-deficiency (<1%) and partial inhibition of FV (65% activity) increases thrombin peak concentration, with an even larger peak concentration when combined with high prothrombin (135%). Notably, there is an increased lag time for treatments including the anti-FV antibody in FVIII-deficient plasma. This observation could be due to the difference between inhibiting FVIII with an antibody compared to plasma deficient in FVIII.

### 4.3 Discussion

In this study, we showed that a mechanistic mathematical model of flow-mediated coagulation can identify important modifiers of network dynamics. We were motivated by observations of the variability in bleeding among individuals with hemophilia A with simi-

lar FVIII levels. We hypothesized that variations in coagulation plasma protein levels within the normal range could modify thrombin generation when FVIII is outside the normal range. We determined critical TF levels necessary for the model to produce 1 nM thrombin by 40 min; this was meant to represent a TF level where bleeding would be common in hemophilia A but where significant thrombin generation is still possible. Using GSA on the model at the specified TF level, we identified that FV levels at the low end of the normal range could push the coagulation system to generate a significant thrombin response. When this level of FV was combined with prothrombin levels at the high end of the normal range, thrombin generation was enhanced even further. This prediction was verified in a microfluidic model of thrombus formation on collagen-TF where fibrin accumulation was used as a proxy for thrombin generation, and in thrombin generation assays using immunodepleted plasma to match the plasma composition of the mathematical model and in plasma with a severe FVIII deficiency. Exploration with the model revealed a potential mechanism to explain these observations; a reduction in FV frees plt-FXa to activate plt-FVIII, leading to more tenase and more prothrombinase on APS, which ultimately boosts thrombin generation.

The modeling results in this paper depend on the assumption that plt-FXa can activate plt-FV and plt-FVIII. In our simulations, plt-FXa is the dominant activator of FV and FVIII before significant amounts of thrombin have been produced. The assumption that FXa can activate FV on an activated platelet's surface is based on data of Monkovic and Tracy [26] and studies using tick saliva protein [27]. In regards to activation of FVIII by FXa, there is in vitro evidence that FVIII bound to an APS can be activated by both thrombin and FXa [28, 29]. Because FVIII circulates in the plasma bound with von Willebrand factor (VWF) and while bound may be protected from activation by FXa [30, 31], some have suggested that FXa-mediated activation of FVIII occurs to a minimal extent in vivo. This protection may be mitigated because during clot formation vWF binds to APS and the FVIII attached to this vWF may redistribute to the APS, given that FVIII has similar affinities for VWF and phospholipid surfaces [32, 33]. Our results suggest that further biochemical studies of FXa's role in activating FVIII are needed.

An alternative view of the early stages of coagulation is that a trace amount of thrombin, produced on TF-bearing cells, is responsible for initial FV and FVIII activation [17, 34]. This view comes, in part, from experiments in a static cell-based model of coagulation [17] in which initial platelet activation itself seems to rely on this thrombin as there is no collagen exposure in that system. If translated to a situation of vascular injury under continued flow (a situation that our mathematical model and flow assay simulate), the trace thrombin would be produced on the vascular wall and could activate FVIII and FV in the plasma or on APS. Under flow conditions, even at the low shear rate of  $100 \text{ s}^{-1}$  used in our model simulations, this view is problematic. Our model predicts that  $\approx 99\%$  of the FXa and FIXa produced by TF:FVIIa on the vascular wall is quickly washed away by the flow and does not reach the surfaces of activated platelets [8]. The same would be true of any thrombin produced on the vascular wall and so, no more than 1% of any trace amounts of this thrombin would make it to activated platelets in order to carry out its putative activation of FV and FVIII there.

FV is contained in and secreted from platelet  $\alpha$ -granules, a mechanism that is incorporated into our model [7, 9]. Approximately 20% of the FV in blood is contained in the platelets [35]. Platelet FV comes from plasma FV that is endocytosed by megakaryocytes [36–38], thus we assume in the model that a percent change in FV plasma levels correlates

with an equal percent change in the platelet FV levels. However, it is unknown what the true correlation is between the two FV pools. Platelet FV is distinct from plasma FV due to modifications in megakaryocytes [39] and is more procoagulant than plasma FV [36, 40]. In our model both FV pools have the same biochemical characteristics. Future work is needed to tease out the relative roles of plasma and platelet FV in thrombin generation in the context of hemophilia A.

We are unaware of previous reports demonstrating a relationship between FVIII deficiencies, FV levels within the normal range, and thrombin generation. A mutation in a molecular chaperone that transports proteins from the endoplasmic reticulum to the Golgi results in a combined FV and FVIII deficiency [41]. This mutation causes low levels (5-30%) of both FV and FVIII. That situation is different than our findings where thrombin generation is modulated by FV levels within the normal range (50-150%) for FVIII deficiencies. There are reports of individuals with both a FVIII deficiency and a common variant of FV called FV Leiden (rs6025) [42]. FVa's endogenous inhibitor, APC, cannot bind to this variant, leading to a hypercoagulable state. Individuals with combined FVIII deficiency and FV Leiden have a milder bleeding phenotype [43], but this is distinct from the effect we show here where reduced FV levels allow for more FVIII binding to FXa on APS.

There are several potential implications for our findings. FV levels could be an inherent modifier of bleeding risk in combination with FVIII deficiency in hemophilia A. Studies of clinical bleeding in individuals with hemophilia A are needed to support this hypothesis. Our results also suggest that temporal changes in FV expression, such as those related to circadian rhythms or menstrual cycle, could influence bleeding risk. Finally, our study shows that a systems biology approach to coagulation may facilitate the discovery of previously unrecognized interactions between the several components of the system and may serve as a platform to study other highly complex clinical problems.

This work was supported in part by National Institutes of Health (R01 HL120728) and National Science Foundation (CBET-1351672)

## Bibliography

- [1] VS Blanchette, NS Key, LR Ljung, MJ Manco-Johnson, HM van den Berg, A Srivastava, Factor IX Subcommittee on Factor VIII, Rare Coagulation Disorders of the Scientific, Standardization Committee of the International Society on Thrombosis, and Hemostasis. Definitions in hemophilia: communication from the SSC of the ISTH. J Thromb Haemost, 12(11):1935–1939, 2014.
- [2] MD Carcao, HM van den Berg, R Ljung, ME Mancuso, PedNet, and the Rodin Study Group. Correlation between phenotype and genotype in a large unselected cohort of children with severe hemophilia A. Blood, 121(19):3946–52, S1, 2013.
- [3] M Franchini and PM Mannucci. Modifiers of clinical phenotype in severe congenital hemophilia. Thromb Res, 156:60–64, 2017.
- [4] T Schlitt and A Brazma. Current approaches to gene regulatory network modelling. BMC Bioinformatics, 8 Suppl 6:S9, 2007.
- [5] KA Janes and MB Yaffe. Data-driven modelling of signal-transduction networks. Nat Rev Mol Cell Biol, 7(11):820–828, 2006.
- [6] MA Oberhardt, BÅČÂÿ Palsson, and JA Papin. Applications of genome-scale metabolic reconstructions. Mol Syst Biol, 5:320, 2009.
- [7] A.L. Kuharsky and A.L. Fogelson. Surface-mediated control of blood coagulation: The role of binding site densities and platelet deposition. Biophys J, 80:1050–1074, 2001.
- [8] A.L. Fogelson and N. Tania. Coagulation under flow: The influence of flow-mediated transport on the initiation and inhibition of coagulation. Pathophysiol Haemost Thromb, 34:91–108, 2005.
- [9] Leiderman, K., W Chang, M Ovanesov, and A.L. Fogelson. Synergy between tissue factor and factor XIa in initiating coagulation. Arterioscl Thromb Vasc Biol, 36:2334–2345, 2016.
- [10] U. Okorie, W.S. Denney, M.S. Chatterjee, K.B. Neeves, and S.L. Diamond. Determination of surface tissue factor thresholds that trigger coagulation at venous and arterial shear rates: Amplification of 100 fM circulating tissue factor by flow. Blood, 111:3507–13, 2008.
- [11] Andrea Saltelli, Stefano Tarantola, Francesca Campolongo, and Marco Ratto. Sensitivity analysis in practice: a guide to assessing scientific models. John Wiley & Sons, 2004.
- [12] M.S. Chatterjee, W.S. Denney, H. Jing, and S.L. Diamond. Systems biology of coagulation initiation: Kinetics of thrombin generation in resting and activated human blood. PLoS Comput Biol, 6, 2010.
- [13] Christopher M Danforth, Thomas Orfeo, Kenneth G Mann, Kathleen E Brummel-Ziedins, and Stephen J Everse. The impact of uncertainty in a blood coagulation model. Math Med Biol, 26(4):323–336, 2009.

- [14] D. Luan, M. Zai, and J.D. Varner. Computationally derived points of fragility of a human cascade are consistent with current therapeutic strategies. PLoS Comp Bio, 3(7):e142, 2007.
- [15] Christopher M Danforth, Thomas Orfeo, Stephen J Everse, Kenneth G Mann, and Kathleen E Brummel-Ziedins. Defining the boundaries of normal thrombin generation: investigations into hemostasis. PloS One, 7(2):e30385, 2012.
- [16] Kathryn G Link, Michael T Stobb, Jorge Di Paola, Keith B Neeves, Aaron L Fogelson, Suzanne S Sindi, and Leiderman, Karin. A local and global sensitivity analysis of a mathematical model of coagulation and platelet deposition under flow. PloS One, 13(7):e0200917, 2018.
- [17] M. Hoffman and D.M. Monroe. A cell-based model of hemostasis. Thromb Haemost, 85:958–65, 2001.
- [18] D.M. Monroe and M. Hoffman. What does it take to make a perfect clot? Arterioscler Thromb Vasc Biol, 26:41–48, 2006.
- [19] A.L. Fogelson, Y.H. Hussain, and K. Leiderman. Blood clot formation under flow: The importance of factor XI depends strongly on platelet count. Biophys J, 102:10–18, 2012.
- [20] T A Drake, J H Morrissey, and T S Edgington. Selective cellular expression of tissue factor in human tissues. implications for disorders of hemostasis and thrombosis. Am J Pathol, 134(5):1087–1097, 1989.
- [21] Rebecca A Fleck, L Vijaya Mohan Rao, Samuel I Rapaport, and Nissi Varki. Localization of human tissue factor antigen by immunostaining with monospecific, polyclonal anti-human tissue factor antibody. Thromb Res, 59(2):421–437, 1990.
- [22] P H B Bolton-Maggs and K J Pasi. Haemophilias A and B. Lancet, 361(9371):1801–1809, 2003.
- [23] Jon C Helton and Freddie Joe Davis. Latin hypercube sampling and the propagation of uncertainty in analyses of complex systems. Reliab Eng Sys Safe, 81(1):23–69, 2003.
- [24] IM Sobol. Global sensitivity indices for nonlinear mathematical models and their monte carlo estimates. Math Comput Simulat, 55(1):271–280, 2001.
- [25] H C Hemker, P Giesen, R Al Dieri, V Regnault, E de Smedt, R Wagenvoord, T Lecompte, and S Béguin. Calibrated Automated Thrombin Generation Measurement in Clotting Plasma. Pathophysiol Haemost Thromb, 33(1):4–15, 2003.
- [26] D.D. Monkovic and P.B. Tracy. Activation of human Factor V by Factor Xa and thrombin. Biochemistry, 29:1118, 1990.
- [27] Tim J Schuijt, Kamran Bakhtiari, Sirlei Daffre, Kathleen DePonte, Simone JH Wielders, J Arnaud Marquart, Joppe W Hovius, Tom van der Poll, Erol Fikrig, Matthew W Bunce, et al. Factor Xa activation of factor V is of paramount importance in initiating the coagulation system: Lessons from a tick salivary protein. Circulation, 128(3):254–266, 2013.

- [28] F.H. Furby, M.C. Berndt, P.A. Castaldi, and J. Koutts. Characterization of calcium-dependent binding of endogenous factor VIII/von Willebrand factor to surface activated platelets. Thromb Res, 35:501–511, 1984.
- [29] P. Neuenschwander and J. Jesty. A comparison of phospholipid and platelets in the activation of human Factor VIII by thrombin and Factor Xa, and in the activation of Factor X. Blood, 72:1761–1770, 1988.
- [30] M-J. S.H. Donath, P.J. Lenting, J.A. van Mourik, and K. Mertens. The role of cleavage of the light chain at positions Arg1669 or Arg1721 in subunit interaction and activation of human blood coagulation Factor VIII. J Biol Chem, 270:3648–55, 1995.
- [31] J.A. Koedam, R.J. Hamer, N.H. Beeser-Visser, B.N. Bouma, and J.J. Sixma. The effect of von Willebrand factor on the activation of factor VIII by factor Xa. Eur J Biochem, 189:229–234, 1990.
- [32] E.L. Saenko, M. Shima, and A.G. Sarafanov. Role of activation of the coagulation FVIII in interaction with vWf, phospholipid, and functioning within the Factor Xase complex. Trends Cardiovas Med, 9:185–192, 1999.
- [33] J. Spaargaren, P.L.A. Giesen, M.P. Janssen, J. Voorberg, G.M. Willems, and J.A. van Mourik. Binding of blood coagulation Factor VIII and its light chain to phosphatidylserine/phosphatidylcholine bilayers as measured by ellipsometry. Biochem J, 310:539–545, 1995.
- [34] RM Camire and MHA Bos. The molecular basis of factor V and VIII procofactor activation. J Thromb Haemost, 7(12):1951–1961, 2009.
- [35] P.B. Tracy, L. L. Eide, E. J. Bowie, and K. G. Mann. Radioimmunoassay of factor V in human plasma and platelets. Blood, 60:59–63, 1982.
- [36] RM Camire, ES Pollak, K Kaushansky, and PB Tracy. Secretable human platelet-derived factor V originates from the plasma pool. Blood, 92(9):3035–3041, 1998.
- [37] BA Bouchard, JL Williams, NT Meisler, MW Long, and PB Tracy. Endocytosis of plasma-derived factor V by megakaryocytes occurs via a clathrin-dependent, specific membrane binding event. J Thromb Haemost, 3:541–551, 2005.
- [38] WR Gould, P Simioni, JR Silveira, D Tormene, M Kalafatis, and PB Tracy. Megakaryocytes endocytose and subsequently modify human factor V in vivo to form the entire pool of a unique platelet-derived cofactor. J Thromb Haemost, 3:450–456, 2005.
- [39] F Ayombil, S Abdalla, PB Tracy, and BA Bouchard. Proteolysis of plasma-derived factor V following its endocytosis by megakaryocytes forms the platelet-derived factor V/Va pool. J Thromb Haemost, 11(8):1532–1539, 2013.
- [40] D. D. Monkovic and P. B. Tracy. Functional characterization of human platelet-released Factor V and its activation by Factor Xa and thrombin., J Biol Chem, 265:17132–40, 1990.

- [41] WC Nichols, U Seligsohn, A Zivelin, VH Terry, CE Hertel, MA Wheatley, MJ Mousalli, HP Hauri, N Ciavarella, RJ Kaufman, and D Ginsburg. Mutations in the ER-Golgi intermediate compartment protein ERGIC-53 cause combined deficiency of coagulation factors V and VIII. Cell, 93(1):61–70, 1998.
- [42] W C Nichols, K Amano, P M Cacheris, M S Figueiredo, K Michaelides, R Schwaab, L Hoyer, R J Kaufman, and D Ginsburg. Moderation of hemophilia A phenotype by the factor V R506Q mutation. Blood, 88(4):1183–1187, 1996.
- [43] D H Lee, I R Walker, J Teitel, M C Poon, B Ritchie, J Akabutu, G D Sinclair, M Pai, J W Wu, S Reddy, C Carter, G Growe, D Lillicrap, M Lam, and M A Blajchman. Effect of the factor V Leiden mutation on the clinical expression of severe hemophilia A. Thromb Haemost, 83(3):387–391, 2000.

## 4.4 Supplement

### 4.4.1 Mathematical Model Description

The mathematical model used in this work is the same as that in [1, 2], which was an extension of our previous models [3–5]. A complete description of the model equations and parameter choices is presented in the supplement to [2]. Here, we give a brief overview of the model but refer the reader to these papers for more details.

The model includes the coagulation reactions shown in Fig. 4.5A. The reactions involve many coagulation proteins: inactive enzyme precursors (zymogens), active enzymes, and inactive and active cofactors. Active cofactors are not enzymes themselves but act to make the enzymes to which they are bound more effective than they would be alone. In Fig. 4.5A, the zymogens are FVII, FIX, FX, and FII (prothrombin) which have respective active enzymes FVIIa, FIXa, FXa, and FIIa (thrombin). The inactive/active cofactor pairs are FV/FVa, and FVIII/FVIIIa. Fig. 4.5A shows that many of the coagulation reactions occur only on a cellular surface, some on the subendothelium (SE) and others on an activated platelet’s surface (APS). There are three critical surface-bound enzyme-cofactor complexes: TF:FVIIa on the SE (“extrinsic tenase”) and FVIIIa:FIXa (“intrinsic tenase” which we refer to simply as tenase) and FVa:FXa (“prothrombinase”) on an APS. Their substrates (i.e., the proteins that the enzyme complexes activate) must also be bound to the cellular surface to become activated [6].

The mathematical model simulates the clotting response due to a small injury to a vessel wall. The response is monitored in a reaction zone (RZ) above a region where tissue factor (TF) in the SE is exposed to flowing blood (Fig. 4.5B). Within the RZ, coagulation protein concentrations are assumed to change due to transport into and out of the RZ and due to their involvement in the coagulation reactions depicted in Fig. 4.5A. Similarly, platelet concentrations change as platelets adhere to the injured wall, become activated, and as platelets are transported into and out of the RZ. The height of the RZ zone as well as the rate of platelet and protein transport into and out of the zone depend on the flow’s shear rate and on the species’ diffusivities. Each species in the RZ is assumed to be uniformly distributed (‘well-mixed’) and is described by its concentration, whose dynamics are tracked through an ordinary differential equation. Adjacent to the RZ, in the direction perpendicular to the flow, is an endothelial zone (Fig. 4.5C) with height equal to that of the reaction zone and width dependent on the flow shear rate and protein diffusion coefficients [4]. Each species in the endothelial zone is also assumed to be well-mixed.

Platelets are either (i) unactivated, unattached, and so free to move with the fluid, or (ii) activated, bound to the SE or to other activated platelets (APs), and therefore stationary. Platelet activation occurs by contact with the SE, by exposure to thrombin, or by contact with other APs. The last of these is used as a surrogate for activation by platelet-released ADP which we do not explicitly track in this model. We characterize coagulation proteins not only by their chemical identity but also by whether they are in the fluid, bound to the SE, or bound to an APS. Proteins bound to a surface are stationary whereas proteins in the plasma move with the fluid. During a transition from SE to APS, or vice versa, a protein is subjected to flow and thus might be carried downstream.

Our assumptions about protein interactions follow; for further discussion including citations to the literature see [1–5]. The reactions are all described using mass-action kinetics.

1. FVII and FVIIa can bind to TF on the SE. FXa can activate FVII in plasma and when FVII is bound to TF. FXa can bind to the TF:FVII complex directly from plasma without having to first bind the SE.
2. FIX and FX can be activated by the TF:VIIa complex on the SE; they bind to TF:VIIa directly from plasma. FX can also be activated by the FVIIIa:FIXa ('tenase') complex on an APS.
3. Prothrombin can be activated to thrombin on an APS by the FVa:FXa ('prothrombinase') complex.
4. FV and FVIII can be activated by FXa on an APS and by thrombin in plasma and on an APS.
5. FIX can be activated by FXIa in plasma and on an APS. FXI can be activated by thrombin in plasma and on an APS.
6. The model includes the chemical inhibitors antithrombin (AT), activated protein C (APC), and tissue factor pathway inhibitor (TFPI). Since the concentration of AT is high in plasma, we assume it acts in a first order manner to inactivate plasma FIXa, FXa, FXIa, and thrombin. APC can bind to fluid-phase and platelet-bound FVa and FVIIIa to permanently inactivate them with second-order kinetics, but cannot bind to FVIIIa in a tenase complex or to FVa in a prothrombinase complex. We assume that thrombin can diffuse from the reaction zone into the endothelial zone, bind to thrombomodulin (TM) there, and produce activated protein C (APC), which may then diffuse into the reaction zone. TFPI present in the plasma must first bind to FXa and then the complex TFPI:Xa must bind to the TF:VIIa complex to inhibit it.
7. The activity of the TF:VIIa complex decreases as platelet deposition on the injured tissue increases, *i.e.*, we assume that a platelet that adheres to the SE physically blocks the activity of the TF:VIIa complexes on the patch of SE to which the platelet has adhered.

An in-house FORTRAN program is used to set up the system of differential equations, to set parameter values, and to run the simulation. It uses the software package DLSODE [7] to solve the differential equations. Simulation sampling was carried out via a Python wrapper of the FORTRAN program. Unless stated otherwise, simulations were run on the MERCED cluster (NSF Grant No. ACI-1429783). Sensitivity analysis was conducted using MATLAB with in-house implementations from [8]. Graphical processing of simulation results was performed with MATLAB.

For each simulation, we specify the initial plasma concentrations of platelet and protein species, the rate constants for all reactions, the numbers of specific binding sites for coagulation factors on each APS, the dimensions of the injury, the flow velocity near the injured wall, the diffusion coefficients for all fluid-phase species, and the density of exposed TF. The outputs of the simulation are the concentration of every protein species in the reaction zone at each instant of time from initiation of the injury until the completion of the simulation, and the concentrations of platelets attached either directly to the SE or to other platelets.

#### 4.4.2 Global Sensitivity Analysis

Zymogen plasma levels were varied between 50 and 150% of normal using 2500 Latin Hypercube samples [9]. For each sample, a critical tissue factor level for bursting behavior, defined as achieving at least 1 nM of total thrombin by 40 minutes, was found with the bisection method. The resulting distribution of critical TF values gives the range and frequency of TF needed for the system to burst. Using a TF value below the minimum of the distribution will result in no burst, regardless of the input zymogens, whereas using a TF value above the maximum of the distribution will always generate a burst.

Global sensitivity analysis considers the impact of varying parameters simultaneously and uniformly over their full range of possible values, here values between 50% and 150% of baseline. As such, we consider the underlying system output to be a random variable over a probability space of parameter inputs, and quantify the sensitivity of a model output by its variance. We estimate the effects of parameter variations by using Monte Carlo sampling to explore the parameter space.

#### 4.4.3 Variations in Kinetic Rate Constants

We isolate the reactions amongst platelet-bound FV, FVIII, and FXa via variations in the association constants  $k_{FV:FXa}^+$ ,  $k_{FVIII:FXa}^+$  that dictate the concentrations of FV:FXa and FVIII:FXa complexes. Fig. S2A shows that increasing only the rate of binding of plt-FVIII to plt-FXa leads to increased but sub-nanomolar thrombin production. Decreasing the rate of binding of plt-FV to plt-FXa by 50% from its normal value alone, however, results in a five-fold higher thrombin concentration at 40 min and does not reach 1 nM thrombin concentration at 40 min. It is clear that lowering the association constant of plt-FV and plt-FXa results in high thrombin concentrations. Fig. S2B shows that when thrombin feedback (FV activation by thrombin) is turned off, there is significantly lower thrombin production in all cases. When the normal value of  $k_{FV:FXa}^+$  is lowered by 50%, there is high thrombin production for the first 12 minutes. Without thrombin feedback, the benefit of the increased platelet tenase formation is not amplified.

#### 4.4.4 Affect of APC & Thrombin-mediate FV/FVIII Activation

We further investigated the affects of turning off thrombin feedback (FV activation by thrombin) in our system in Fig. S3A-F. In Fig. S3A-C, production of thrombin, prothrombinase, and tenase is significantly lower than that in Fig. 2A-C. These results suggest that to achieve 1 nM thrombin concentration, thrombin must activate FV to amplify the system. Propagation of amplified tenase formation is not seen in Fig. S3C and therefore results in little prothrombinase and thrombin production. Fig. 2D-E reveal that the competition of plt-FV and plt-FVIII for plt-FXa is not entirely dependent on the thrombin feedback discussed above. In Fig. S3D-E, there are slight decreases in FV:FXa and FVIII:FXa concentrations in comparison to those in Fig. 2D-E and the result of low FV increasing the concentration of FVIII:FXa holds. Therefore, this mechanistic competition is robust to thrombin feedback on FV activation.

#### 4.4.5 Race to Tenase Formation

We have identified that increased tenase formation in the first 12 minutes as a result of lowering FV plasma levels is due to decreased competition for plt-FIXa. It is not clear how after 12 minutes, tenase formation amplifies in the low FV cases. To explore this mechanism, Fig. S4A-B show the concentrations of total plt-FIXa and plt-FVIIIa, rate of FIX activation on the subendothelium and rate of FIX activation on the platelet. We note that FIX activation on the subendothelium is facilitated by enzyme TF:VIIa. FIXa species on the platelet activate FIX after sufficient thrombin is present. We can see that in both the HFII-LFV and NFII-NFV cases, total plt-FIXa concentrations are very similar during the first 10 minutes of the simulation (see Fig. S4A). At approximately 13 minutes, total plt-FIXa concentration switches from decreasing to increasing in the HFII-LFV cases, in time with significant total plt-FVIIIa concentration. The increase in FIXa and FVIIIa concentrations results in increased tenase formation in comparison to that in the NFII-NFV case. We further investigate which mechanism contributes to the FIXa burst. By examining the evolution of the rates of FIX activation on the subendothelium and platelet in Fig. 4B, we can see that activation on the subendothelium largely contributes to FIX activation for the first 12 minutes and then activation on the platelet takes over, becoming the main location and source of FIXa.

#### 4.4.6 Materials

Recombinant human tissue factor (TF) purified from SF9 cells (# RTF-0300), anti-human factor V (AHV-5101, mouse, monoclonal, IgG1), human prothrombin (# HCP-0010), human factor V (HCV-0100) and plasma immunodepleted of factor V (FV-ID) or prothrombin (FII-ID) were from Haematologic Technologies Inc (Essex Junction, VT). L- $\alpha$ -Phosphatidylserine (PS, brain, porcine) and L- $\alpha$ -phosphatidylcholine (PC, egg, chicken) were from Avanti Polar Lipids (Alabaster, AL). Bio-Beads SM-2 (# 152-3920) were from Bio-Rad Laboratories (Hercules, CA). TF ELISA (# ab220653) was from Abcam, Inc (Cambridge, MA). Sodium deoxychoate was from Calbiochem (La Jolla, CA). HEPES-NaOH, NaCl, NaN<sub>3</sub>, and methanol were from Sigma Aldridge (St. Louis, MO). Type I collagen from equine tendon was from Chrono-log (Chrono-Par Collagen, Havertown, PA). Anti-mouse factor VIII (mouse monoclonal, IgG2ak) was from Green Mountain Antibodies (GMA-8015, Burlington, VT). Human fibrinogen was from Enzyme Research Laboratory (South Bend, IN). Pooled normal plasma was from George King Bio-medical (Overland Park, KS). Alexa Fluor 555 protein labeling kit was from Thermo-Fisher (A20174, Waltham, MA). DiOC6 was from Sigma Aldridge (318426, St. Louis, MO). HEPES buffered saline (HBS) contained 20 mM HEPES, 150 mM NaCl, and was titrated to a pH of 7.4. Recalcification buffer was HBS with 75 mM CaCl<sub>2</sub> and 37.5 mM MgCl<sub>2</sub>. Factor VIII deficient (<1%) plasma was from George King Bio-Medical (Overland Park, KS). Anti-human factor VIII (ab 61370) was obtained from Abcam Inc (Cambridge, MA). Round-bottom polystyrene 96-well plate (Immulon 2HB) were obtained from Thermo Scientific. All Calibrated Automated Thrombogram Assay (CAT Assay) reagents were obtained from Diagnostica Stago.

#### 4.4.7 Tissue factor vesicles

TF was reconstituted in 20:80 PS:PC vesicles using the protocol of Smith and Morrissey [10]. Briefly, PS:PC phospholipids were dissolved in methanol, combined at 20:80 molar ratio, lyophilized, and then resuspended in HBS and 15 mM sodium deoxycholate and 10  $\mu\text{g}$  of recombinant TF. The sodium deoxycholate was removed using Bio-Beads SM-2. The resultant phospholipid vesicles containing TF were sized by dynamic light scattering (Brookhaven Instruments, ZetaPALS) and determined to be  $64.29 \pm 0.44$  nm. The concentration of TF was determined by ELISA (Abcam, ab220653) to be 280 nM, giving a molar ratio of phospholipid:TF was 9285:1.

#### 4.4.8 Subject recruitment and blood collection

Subjects were recruited at the Hemophilia and Thrombosis Center of the University of Colorado Anschutz Medical Campus. The study and consent process received Institutional Review Board (IRB) approval from the University of Colorado Anschutz Medical Campus. Additionally, written and informed consent was obtained for all participants. Phlebotomy was conducted in accordance with the Declaration of Helsinki and under the Colorado Multiple IRB. Human whole blood was collected by venipuncture into 3.2% sodium citrate. Blood used for flow assays was treated with 1  $\mu\text{M}$  DiOC6 and 60  $\mu\text{g}/\text{mL}$  Alexa 555-fibrinogen (1:50 labeled:plasma fibrinogen). For specified assays, blood was incubated individually or with a combination of a anti-human FV function blocking antibody at a final concentration 100  $\mu\text{g}/\text{mL}$  and prothrombin at a final concentration of 50  $\mu\text{g}/\text{mL}$ . The anti-human FV antibody at 100  $\mu\text{g}/\text{mL}$  concentration yields the same activity as 60% of normal levels of FV in normal pooled plasma (Diagnostica Stago Compact Max) (Fig. 4.9). All incubation times were 15 min at 37°C.

#### 4.4.9 Subject clinical categorization

Blood from three individuals with FVIII deficiency were used in this study and are referred to as Sample 1, 2, and 3 in Table S4. FVIII levels were determined the day of sample collection using a one stage clotting assay as described in below in the Calibrated automated thrombograph section. At the time of diagnosis, these individuals had baseline FVIII levels of 12%, 14%, and 3% and bleeding scores [11] of 12, 7, and 12, respectively.

#### 4.4.10 Whole blood flow assays

Type I collagen and TF vesicles were co-patterned on glass slides (25 mm x 75 mm) in 4 mm spots using PDMS microwells (4 mm in diameter, 3 mm in height). The microwells were filled with 10  $\mu\text{L}$  of collagen (1 mg/mL) and incubated overnight at 4°C. Wells were then rinsed in triplicate with HBS and then 10  $\mu\text{L}$  of TF vesicle suspension was incubated for 1 h at room temperature followed by a triplicate rinse of HBS. Stock TF vesicles were diluted 100X with an HBS solution containing 1 mM PS:PC phospholipids to maintain the same concentration of phospholipids adsorbed to the surface. Microfluidic devices consisting of four channels (h x w x l; 50  $\mu\text{m}$  x 500  $\mu\text{m}$  x 10 mm) were fabricated using standard photolithography techniques with KMPR 1050 photoresist (MicroChem) on 3 inch silicon wafers. Channel dimensions were measured using a profilometer (Dektak 3030). The four channels were aligned over the collagen-TF spots and placed on the glass slide. Each channel

contains a 6 mm well that holds 100  $\mu\text{L}$  of fluid and an outlet connected to tubing (0.01 in. ID, 0.03 in. OD) which is connected to a 21 gauge needle attached to a 50  $\mu\text{L}$  glass syringe (Hamilton) on a programmable syringe pump (Harvard Apparatus, PhD Ultra). The microfluidic channels and tubing were blocked with 2% wt BSA in HBS for 1 hour. The HBS was removed from the inlet well and replaced with 90  $\mu\text{L}$  of whole blood, which was then recalcified with 10  $\mu\text{L}$  of recalcification buffer to yield final concentrations of 7.5 mM  $\text{CaCl}_2$  and 3.75 mM  $\text{MgCl}_2$ . Blood was perfused at a flow rate of 1.25  $\mu\text{L}/\text{min}$ , which corresponds to a wall shear rate on the bottom of the channel of 100  $\text{s}^{-1}$ .

#### 4.4.11 Determination of TF surface concentration

Stock TF vesicle suspensions were diluted 100X in HBS and patterned as described above on glass slides previously patterned with type I collagen. The TF suspension was patterned for 1 hr at room temperature and rinsed in triplicate with HBS. Pacific Blue labeled annexin V (BioLegend-640917) was incubated in the patterning wells for 15 min to label the patterned vesicles. The vesicles were enumerated using confocal microscopy (Olympus FV10i, 60X objective). These images were used to determine the phospholipid surface coverage, which was in turn used to calculate the TF surface concentration using the method described by Zhu et. al [12]. For this calculation, it was assumed that there were 14 active and accessible TF molecules per liposome. This number was estimated using the measured size of the liposomes (64 nm), the measured molar ratio of phospholipid:TF (9285:1), the estimated surface density of phospholipids on a liposome ( $5 \times 10^6/\mu\text{m}^2$ ) [13], and the assumption that one quarter of the TF molecules in the phospholipid would be exposed to whole blood and in the correct orientation (half of the TF molecules will be oriented with their extracellular domain facing into the interior of the liposome, and of those with their extracellular domain facing outward, half will be inaccessible to blood because they will be buried between the adsorbed liposome and the glass). From this method it was estimated that the TF surface concentration for the whole blood flow assays was approximately  $1.09 \pm 0.2$  fmol/cm<sup>2</sup>.

#### 4.4.12 Image Acquisition and Analysis

The kinetics of platelet and fibrin(ogen) accumulation were measured in each channel by epifluorescence microscopy (IX83 Olympus, 40X, NA=0.6) equipped with a motorized stage (Applied Scientific Instrumentation, Eugene, OR). Platelets labeled with DiOC6 and Alexa Fluor 555 labeled fibrin(ogen) were imaged at an excitation/emission wavelength of 470/535 nm and 560/607 nm respectively. The images were then analyzed using a custom routine developed in Python. Images of a given assay were read in using a Scipy module. The mean fluorescence intensity of a given image was calculated by taking the mean value of the pixels in each image. The mean of the first image where blood was perfused through the assay channel was used to determine the background noise of the fluorescence intensity values. This value was subtracted from all of the images of that given assay to account for background noise in the time series. The time of each image was also recorded using the known time interval between images of a given assay. Once obtaining mean fluorescence and time data from each assay, the maximum fluorescence intensity was calculated using the max function in Numpy, and the velocity was determined by fitting a line to the linear growth region of these fluorescence intensity versus time curves (Fig. 4.11). The mean time

series fluorescence, maximum, and velocity were then normalized by dividing each value by the maximum of that value for each donor.

#### 4.4.13 Calibrated automated thrombography

Pooled normal plasma was obtained from consenting normal healthy individuals ages 18-65. Donors had no personal history of significant bleeding or hormonal, anticoagulant, or anti-platelet medications. Factor levels were measured and confirmed to be within normal ranges. Plasma samples with varying FV and prothrombin levels were prepared using plasma immunodepleted for FV or prothrombin. To achieve FV or prothrombin concentrations above 100% of normal purified zymogens of interest were added. An anti-human FVIII antibody was used to model hemophilia A conditions. Thrombin generation was measured with the Calibrated Automated Thrombogram Assay (CAT Assay, Thromboscope BV, Maastricht, The Netherlands), which consisted of the Fluoroskan Ascent instrument (Thermo, Vantaa, Finland) coupled with the Thromboscope software (Diagnostica Stago Inc., Parsippany, NJ, USA). First, low standard PPP-Reagent containing 5 pM TF and phospholipid (20  $\mu$ L per well) was added to 96-well microtiter plates. For each well containing an experimental plasma sample, a calibrator assay well was included. The latter contained a known concentration of thrombin- $\alpha$ 2-macroglobulin complex in place of the PPP-Reagent. The calibrator is used to correct for inner filter effects and variation among individual plasmas. Each calibrator and sample were prepared in triplicate. Each sample (80  $\mu$ L) was added to the wells and placed in a plate reader at 37°C for 10 min. Thrombin generation was initiated by dispensing (20  $\mu$ L) of a buffer containing calcium ions (Fluor-substrate, Stago, US), previously prepared following manufacturer's instructions. Thrombin generation curves were registered with a Fluoroskan FL instrument (Thermo LabSystems, Helsinki, Finland). Fluorescence was detected at an excitation wavelength of 390 nm and emission at 460 nm every 20 seconds for 90 minutes. Data was recorded using Thromboscope software (Thromboscope BV, Maastricht, The Netherlands). Prothrombin and FV activities were measured with a modified prothrombin time assays and FVIII activity was measured using a modified activated partial thromboplastin time assay using calibration curves based on dilutions of normal pooled plasma and prothrombin, FV, and FVIII deficient plasma using the Compact Max (Diagnostica Stago) following manufacturer instructions. These activity assays have standard deviation of 10%.

#### 4.4.14 Statistical analysis

P-values between treatment groups in whole blood flow assays was calculated using Kruskal-Wallis analysis of the variance, followed by Dunn post hoc test to determine differences between pairs. Values outside of 150% of the interquartile range were deemed outliers and removed before performing the analysis of variance and post hoc tests.



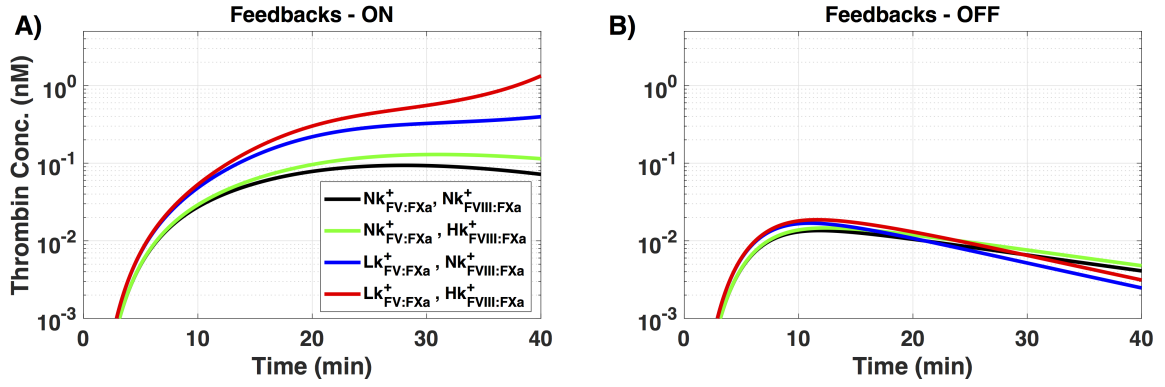


**Figure 4.6: Kinetic rate constant experiments where the rates of association of plt-FV with plt-FXa and plt-FVIII with plt-FXa increase or decrease by 50%. Thrombin generation in FVIII-deficient plasma **A**) with thrombin activation of FV; and **B**) without thrombin activation of FV. We denote thrombin activation of FV on the platelet as “thrombin feedback”.**

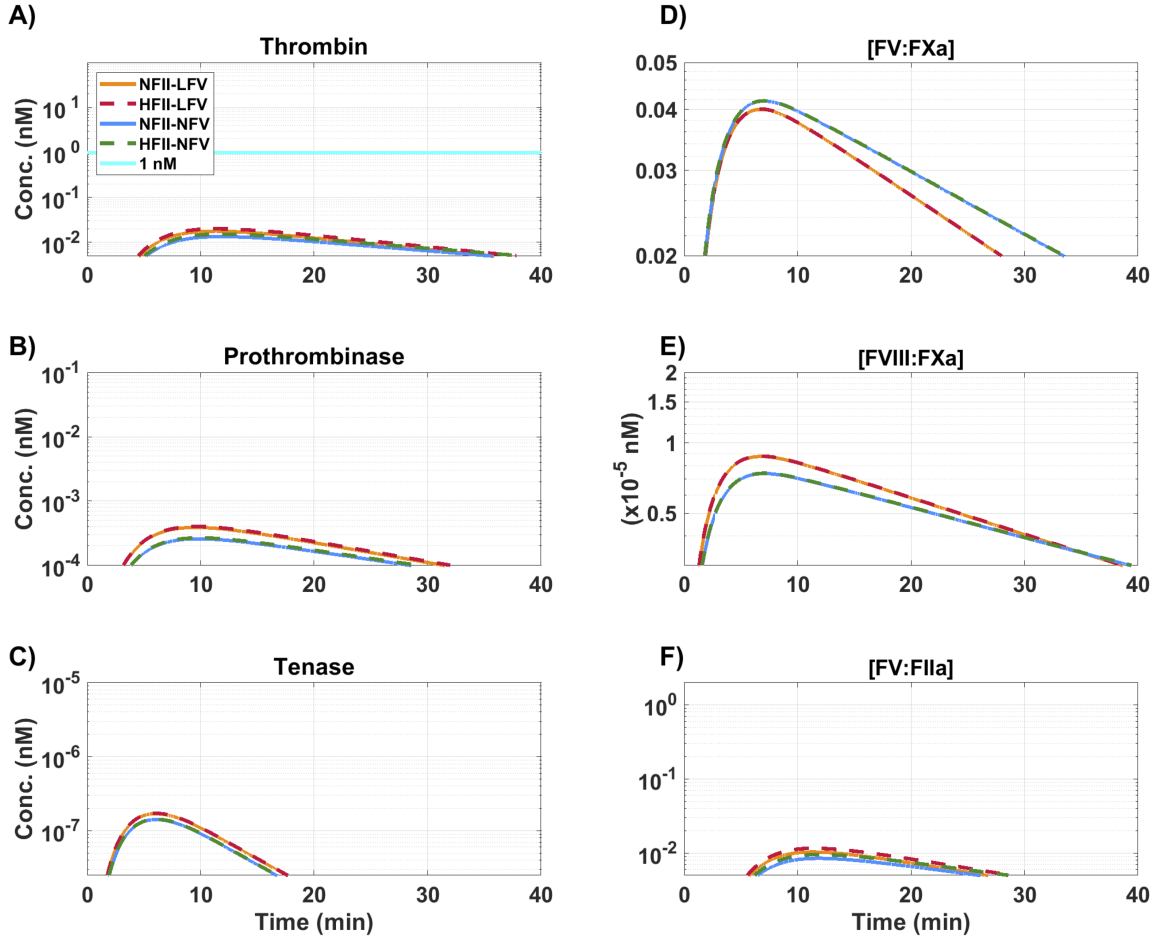


**Figure 4.7: Effects of variations in plasma FII and FV levels on intravascular thrombin generation and coagulation enzymes and complexes when thrombin activation of FV and FVIII as well as APC binding to FVa and FVIIIa are turned off.** “N” denotes 100%,”L” denotes 50%, and “H” denotes 150% of their respective baseline plasma level. **A)** Total thrombin; **B)** prothrombinase (FVa:FXa); **C)** plt. tenase (FVIIa:FIXa); **D)** FVIII:FXa complex; **E)** FV:FXa complex; **F)** FV:FIIa complex; during a time course of 40 minutes. Concentrations are in units of nM. Description of labels found in Table 1.

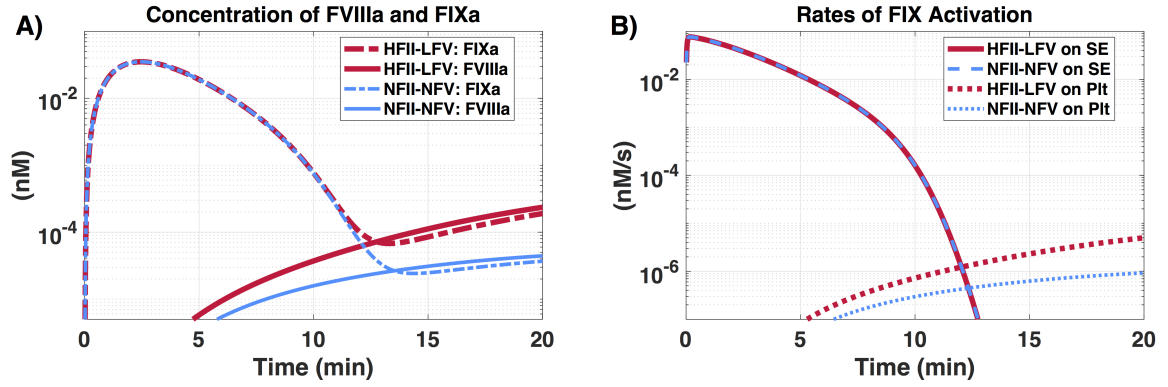


**Figure 4.8: Exploration of the race to platelet tenase production.** Evolution of **A)** concentration of total FIXa and FVIIIa on the platelet; **B)** rate of FIX activation on the subendothelium (SE); and **C)** rate of FIX activation on the platelet; in the HFII-LFV and NFII-NFV cases over 40 minutes.

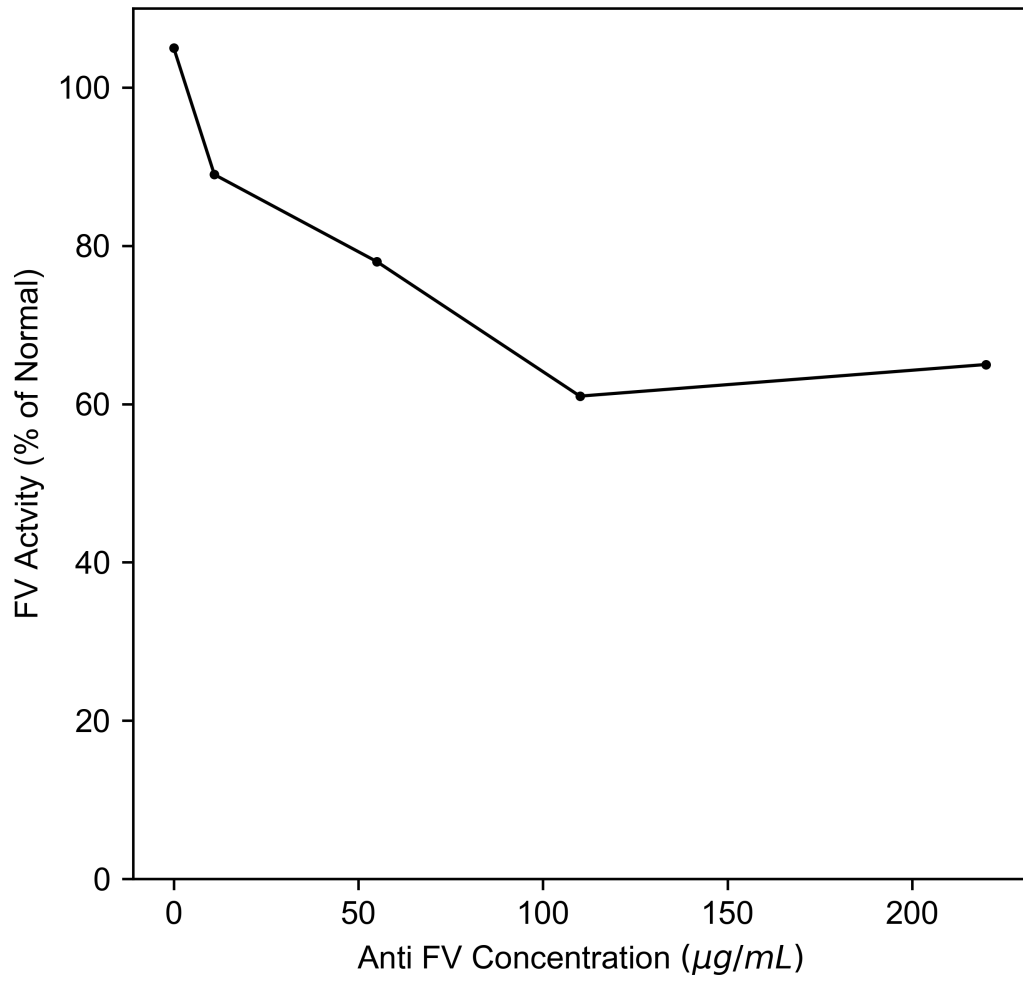


**Figure 4.9:** FV activity in pooled normal plasma as a function of anti-FV antibody concentration as measured in a modified prothrombin time assay.

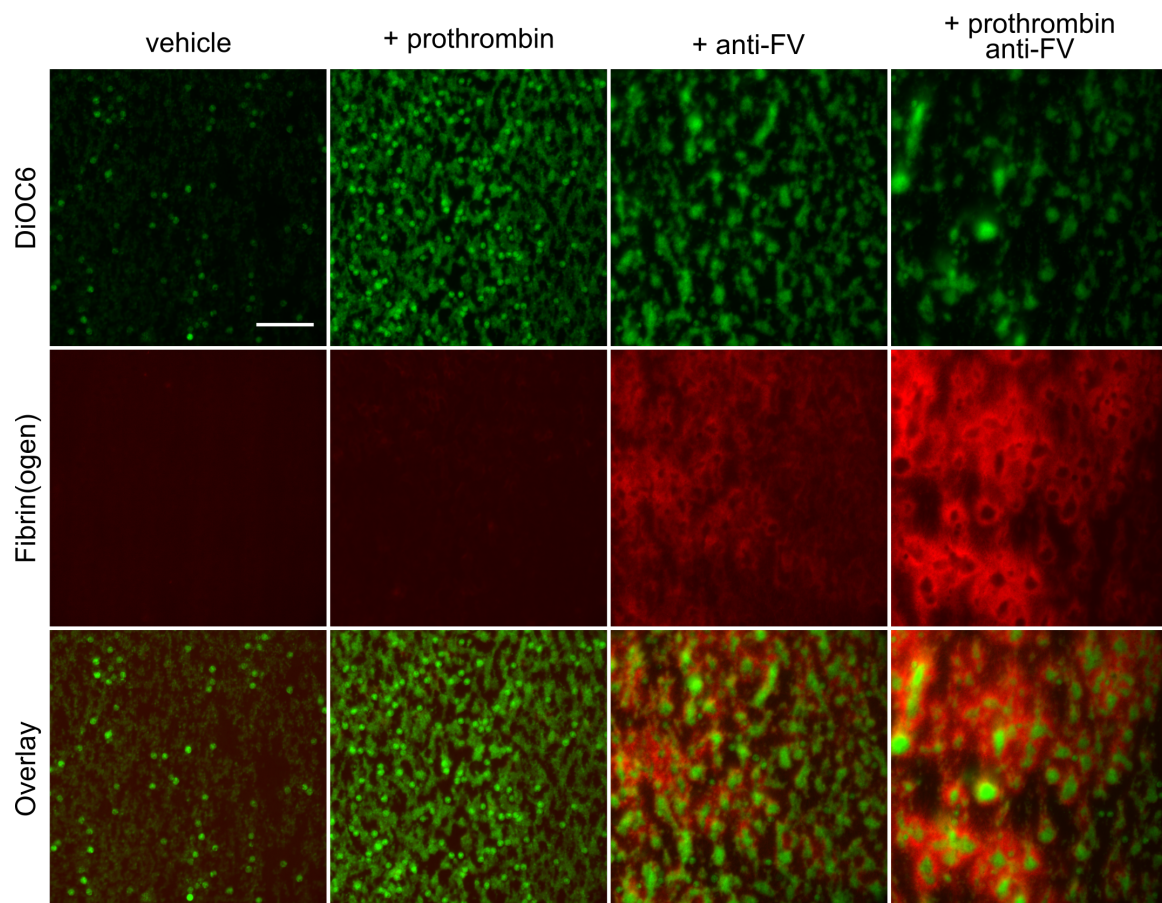


**Figure 4.10:** Representative images of DiOC6 labeled platelets and leukocytes and Alexa-555 labeled fibrin(ogen) formed in whole blood flow assays. Scale bar = 50  $\mu\text{m}$

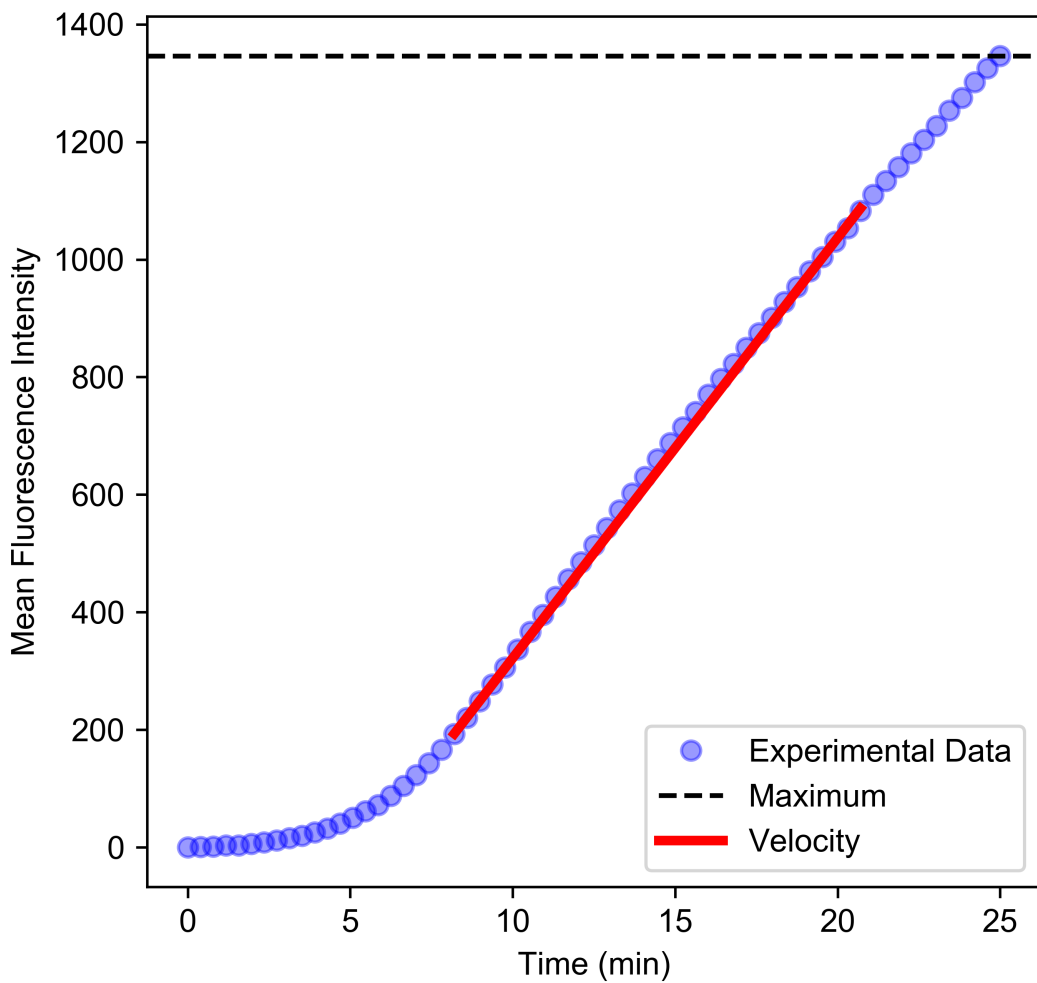


**Figure 4.11: Example of metrics fitted from fluorescence time series curves.** Maximum is determined using the max function in Numpy, and velocity is determined by fitting a line to the experimental data in the linear growth region of the fluorescence curve.

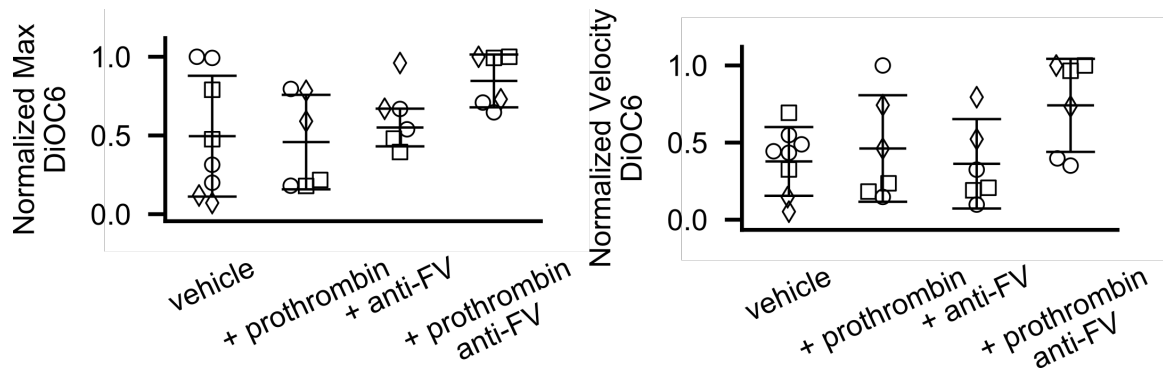


**Figure 4.12: DiOC6 normalized maximum fluorescence intensity and rate of deposition (normalized velocity) for FVIII levels of  $\circ$  = 3.0%,  $\square$  = 7.5%,  $\diamond$  = 8.5%. No significant difference was found between groups.**

**Table 4.1: Description of variations in FII and FV plasma levels.**

| Label    | Variation                           |
|----------|-------------------------------------|
| NFII-NFV | 100% FII (1400 nM), 100% FV (1 nM)  |
| NFII-LFV | 100% FII (1400 nM), 50% FV (0.5 nM) |
| HFII-NFV | 150% FII (2100 nM), 100% FV (1 nM)  |
| HFII-LFV | 150% FII (2100 nM), 50% FV (0.5 nM) |

**Table 4.2: Description of variations in FII and FV plasma levels and variations in association constants describing FV:FXa and FVIII:FXa complex formation.**

| Label                                | Value ( $s^{-1}M^{-1}$ )                                                |
|--------------------------------------|-------------------------------------------------------------------------|
| $Nk_{FV:FXa}^+$ , $Nk_{FVIII:FXa}^+$ | $k_{FV:FXa}^+ - 1 \times 10^8$ , $k_{FVIII:FXa}^+ - 5.1 \times 10^7$    |
| $Nk_{FV:FXa}^+$ , $Hk_{FVIII:FXa}^+$ | $k_{FV:FXa}^+ - 1 \times 10^8$ , $k_{FVIII:FXa}^+ - 7.65 \times 10^7$   |
| $Lk_{FV:FXa}^+$ , $Nk_{FVIII:FXa}^+$ | $k_{FV:FXa}^+ - 0.5 \times 10^8$ , $k_{FVIII:FXa}^+ - 5.1 \times 10^7$  |
| $Lk_{FV:FXa}^+$ , $Hk_{FVIII:FXa}^+$ | $k_{FV:FXa}^+ - 0.5 \times 10^8$ , $k_{FVIII:FXa}^+ - 7.65 \times 10^7$ |

**Table 4.3: Thrombin generation metrics for plasmas with normal prothrombin and FV levels (NFII-NFV), normal prothrombin and low FV (NFII-LFV), high prothrombin and normal FV (HFII-NFV), or high prothrombin and low FV (HFII-LFV) in the presence of a function blocking anti-FVIII antibody (12 nM).** Prothrombin and FV levels were altered using a combination of prothrombin and FV immunodepleted plasmas in combination with purified zymogens. Lag time, endogenous thrombin potential (ETP, analogous to area-under-curve), peak thrombin, and time to peak were measured by calibrated automated thrombogram (CAT) using 5 pM tissue factor and phospholipids. Data presented as mean  $\pm$  standard deviation of n=3

| <b>Label</b> | <b>Prothrombin<br/>(% normal)</b> | <b>FV<br/>(% normal)</b> | <b>FVIII<br/>(% normal)</b> | <b>Lag time<br/>(min)</b> | <b>ETP<br/>(nM min)</b> | <b>Peak thrombin<br/>(nM)</b> | <b>Time to peak<br/>(min)</b> |
|--------------|-----------------------------------|--------------------------|-----------------------------|---------------------------|-------------------------|-------------------------------|-------------------------------|
| NFII-NFV     | 93                                | 111                      | <1                          | 2.6 $\pm$ 0.1             | 1757 $\pm$ 110          | 120 $\pm$ 2                   | 11.3 $\pm$ 0.5                |
| NFII-LFV     | 117                               | 43                       | <1                          | 4.0 $\pm$ 0.1             | 2174 $\pm$ 19           | 298 $\pm$ 3                   | 7.3 $\pm$ 0.1                 |
| HFII-NFV     | 147                               | 115                      | <1                          | 3.0 $\pm$ 0.1             | 2876 $\pm$ 77           | 160 $\pm$ 3                   | 13.7 $\pm$ 0.2                |
| HFII-LFV     | 136                               | 43                       | <1                          | 4.3 $\pm$ 0.2             | 3417 $\pm$ 76           | 408 $\pm$ 2                   | 7.6 $\pm$ 0.1                 |

**Table 4.4: Thrombin generation metrics for commercial (George King) and patient derived FVIII deficient plasma (Samples 1, 2, and 3) in the presence of a vehicle control, FV partial inhibitor (anti-FV, 100  $\mu\text{g}/\text{mL}$ ), exogenous prothrombin (+prothrombin, 50  $\mu\text{g}/\text{mL}$ ), or both the anti-FV antibody and exogenous prothrombin (+prothrombin/anti-FV). Lag time, endogenous thrombin potential (ETP, analogous to area-under-curve), peak thrombin, and time to peak were measured by calibrated automated thrombogram (CAT) using 5 pM tissue factor and phospholipids.**

| Sample      | Label                | Prothrombin<br>(% normal) | FV<br>(% normal) | FVIII<br>(% normal) | Lag time<br>(min) | ETP<br>(nM min) | Peak<br>thrombin<br>(nM) | Time<br>to peak<br>(min) |
|-------------|----------------------|---------------------------|------------------|---------------------|-------------------|-----------------|--------------------------|--------------------------|
| George King | vehicle              | 103                       | 90               | <1                  | 2.6               | 1200            | 96                       | 8.6                      |
|             | anti-FV              | 99                        | 65               | <1                  | 8.9               | 1571            | 202                      | 12.9                     |
|             | +prothrombin         | 130                       | 95               | <1                  | 2.9               | 1498            | 121                      | 8.6                      |
|             | +prothrombin/anti-FV | 135                       | 66               | <1                  | 8.9               | 2115            | 263                      | 12.9                     |
| Sample 1    | vehicle              | 119                       | 98               | 8.5                 | 2.6               | 882             | 65                       | 9.2                      |
|             | anti-FV              | 112                       | 66               | 4.7                 | 8.6               | 805             | 102                      | 13.6                     |
|             | +prothrombin         | 134                       | 105              | -                   | 2.6               | 2320            | 201                      | 7.6                      |
|             | +prothrombin/anti-FV | 136                       | 68               | 5.6                 | 11.9              | 1662            | 155                      | 17.9                     |
| Sample 2    | vehicle              | 120                       | 138              | 7.5                 | 2.2               | 863             | 68                       | 9.6                      |
|             | anti-FV              | 96                        | 90               | 5.2                 | 4.5               | 811             | 129                      | 7.9                      |
|             | +prothrombin         | 141                       | 141              | 7.5                 | 1.9               | 2053            | 185                      | 7.2                      |
|             | +prothrombin/anti-FV | 124                       | 93               | 5.0                 | 8.9               | 1530            | 95                       | 15.9                     |
| Sample 3    | vehicle              | 122                       | 120              | 3.0                 | 3.2               | 498             | 32                       | 15.2                     |
|             | anti-FV              | 137                       | 84               | 1.9                 | 8.6               | 784             | 39                       | 15.6                     |
|             | +prothrombin         | 162                       | 129              | 3.1                 | 2.9               | 809             | 48                       | 12.2                     |
|             | +prothrombin/anti-FV | 138                       | 83               | 2.1                 | 9.9               | 1633            | 74                       | 17.2                     |

## Bibliography

- [1] Leiderman, K., W Chang, M Ovanesov, and A.L. Fogelson. Synergy between tissue factor and factor XIa in initiating coagulation. Arterioscl Thromb Vasc Biol, 36:2334–2345, 2016.
- [2] Kathryn G Link, Michael T Stobb, Jorge Di Paola, Keith B Neeves, Aaron L Fogelson, Suzanne S Sindi, and Leiderman, Karin. A local and global sensitivity analysis of a mathematical model of coagulation and platelet deposition under flow. PloS One, 13(7):e0200917, 2018.
- [3] A.L. Kuharsky and A.L. Fogelson. Surface-mediated control of blood coagulation: The role of binding site densities and platelet deposition. Biophys J, 80:1050–1074, 2001.
- [4] A.L. Fogelson and N. Tania. Coagulation under flow: The influence of flow-mediated transport on the initiation and inhibition of coagulation. Pathophysiol Haemost Thromb, 34:91–108, 2005.
- [5] A.L. Fogelson, Y.H. Hussain, and K. Leiderman. Blood clot formation under flow: The importance of factor XI depends strongly on platelet count. Biophys J, 102:10–18, 2012.
- [6] M. Hoffman and D.M. Monroe. A cell-based model of hemostasis. Thromb Haemost, 85:958–65, 2001.
- [7] A.C. Hindmarsh. ODEPACK, a systematized collection of ODE solvers. In R. S. Stepleman, editor, Scientific Computing, volume 1 of IMACS Trans Sci Comput, pages 55–64. North-Holland, Amsterdam, 1983.
- [8] Andrea Saltelli, Marco Ratto, Terry Andres, Francesca Campolongo, Jessica Cariboni, Debora Gatelli, Michaela Saisana, and Stefano Tarantola. Global sensitivity analysis: the primer. John Wiley & Sons, 2008.
- [9] Jon C Helton and Freddie Joe Davis. Latin hypercube sampling and the propagation of uncertainty in analyses of complex systems. Reliab Eng Sys Safe, 81(1):23–69, 2003.
- [10] S A Smith and J H Morrissey. Rapid and efficient incorporation of tissue factor into liposomes. Journal of thrombosis and haemostasis : JTH, 2(7):1155–1162, 2004.
- [11] F Rodeghiero, A Tosetto, T Abshire, DM Arnold, B Coller, P JAMES, C Neunert, and D Lillicrap. Isth/ssc bleeding assessment tool: A standardized questionnaire and a proposal for a new bleeding score for inherited bleeding disorders. Journal of thrombosis and haemostasis, 8:2063–2065, 2010.
- [12] S. Zhu, R. J. Travers, J. H. Morrissey, and S. L. Diamond. FXIa and platelet polyphosphate as therapeutic targets during human blood clotting on collagen/tissue-factor surfaces under flow. Blood, 126:1494–1502, 2015.
- [13] B. Alberts, A. Johnson, M. Raff, K. Roberts, J. Lewis, and P. Walter. Molecular Biology of the Cell. 4th edition, 2002.

## Chapter 5

# Conclusions & Future Work

### 5.1 Conclusions

Mathematical modeling of biological phenomena has been an important tool for understanding biological systems as evidenced by the numerous textbooks on the subject [1–3]. Understanding how uncertainty affects these models, both when estimating parameters and recording model output, leads to increased insights and more accurate predictions. With advanced computing power, we are able to efficiently handle model uncertainty and use our models more effectively.

This dissertation details my contributions to the field of mathematical biology, with a particular focus on models of blood coagulation. This work has been guided by two general questions:

1. Does the parametric uncertainty of a model explain the mismatch between a model and data?
2. Can we determine which uncertain parameters are most *important* in a complex and highly non-linear model?

My work in Chapter 2 addressed the first question, where we examined the model for a single chromogenic substrate cleaved by its target enzyme. The prototypical mathematical model for the kinetic reaction, incorporating parameter uncertainty, was a poor fit to the experimental data. This led me to propose a new model for the interaction, one which explicitly included inhibition with the reaction products. The improvement of fit for this new model was statistically significant, and moreover, correctly predicted the outcome of a validation experiment.

My work in Chapters 3 and 4 addressed the second question, where a known mathematical model for blood coagulation was deeply investigated for important parameters. In Chapter 3, both local and global approaches for uncertainty quantification were employed. They revealed that for certain classes of parameters, the two types of methods gave similar (and typically identical) results, however, other parameter classes required global sensitivity methods to reveal important interactions *between* parameters. In Chapter 4, the consequences of two previously determined parameters was examined closer under hemophilic conditions. The global sensitivity results directly lead to the hypothesis that higher FII levels and lower FV levels, but each still within the normal range, rescued the bleeding

response for hemophilia A. This hypothesis was then validated by two sets of independent lab experiments.

While progress has been made in each class of project, there remains several unanswered questions. My approaches detailed in Chapter 2-4 are highly generalizable and are able to be extended to further probe the systems. I next describe two ongoing applications in each project class and present preliminary results for each.

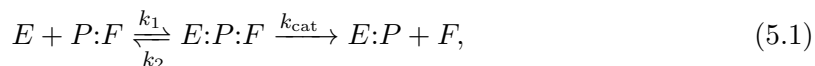
## 5.2 Full Progress Curves of Chromogenic Substrates Provide Evidence for Two Step Inactivation of FXa by AT

In examining the chromogenic substrate experiments for Chapter 2, it was noted that the standard model for FXa inactivation by antithrombin (AT) provided a poor match to the experimental data (see Figure 5.1). This model discrepancy appeared to be robust and present in all experiments involving AT. The process for parameter fitting detailed in Chapter 2 will be extended to include these more complex experiments that include AT. It was hypothesized that the standard one-step model for FXa inactivation by AT was incorrect and that a two-step model could more accurately fit the data.

I intend to determine if a two-step model actually has more support, in a process similar to Chapter 2, where the Null model uses one-step inactivation and the Alternative uses two-step. Both models would be fit using MCMC, directly allowing for the incorporation of parametric uncertainty, and the resulting fits compared.

### 5.2.1 Kinetic Schemes

As in Chapter 2, we assume potential kinetic schemes to describe the reactions between factor Xa, its chromogenic substrate, and AT. The first is the One-Step Inactivation scheme, which incorporates the previously demonstrated product inhibition between factor Xa and the chromogenic substrate, and assumes no reversible binding between factor Xa and AT:



Here, the enzyme  $E$  represents the activated coagulation protein, factor Xa, the substrate  $P:F$  is the intact chromogenic substrate Pefachrome-FXa, the products  $P$  and  $F$  are the peptide and the cleaved para-nitroaniline (pNA), respectively, and  $AT$  is antithrombin. Equation (5.2) is the inhibition from previously cleaved product, while Equation (5.3) is the one step-step enzyme inactivation. The parameter,  $\alpha$ , is the constant of proportionality that controls the ‘strength’ of the product inhibition. As demonstrated in Chapter 2,  $\alpha$  was estimated to be approximately 2.54.

An alternative description of the inactivation of factor Xa by AT allows for reversible binding before full inactivation occurs. Here the enzyme,  $E$ , is explicitly able to bind with

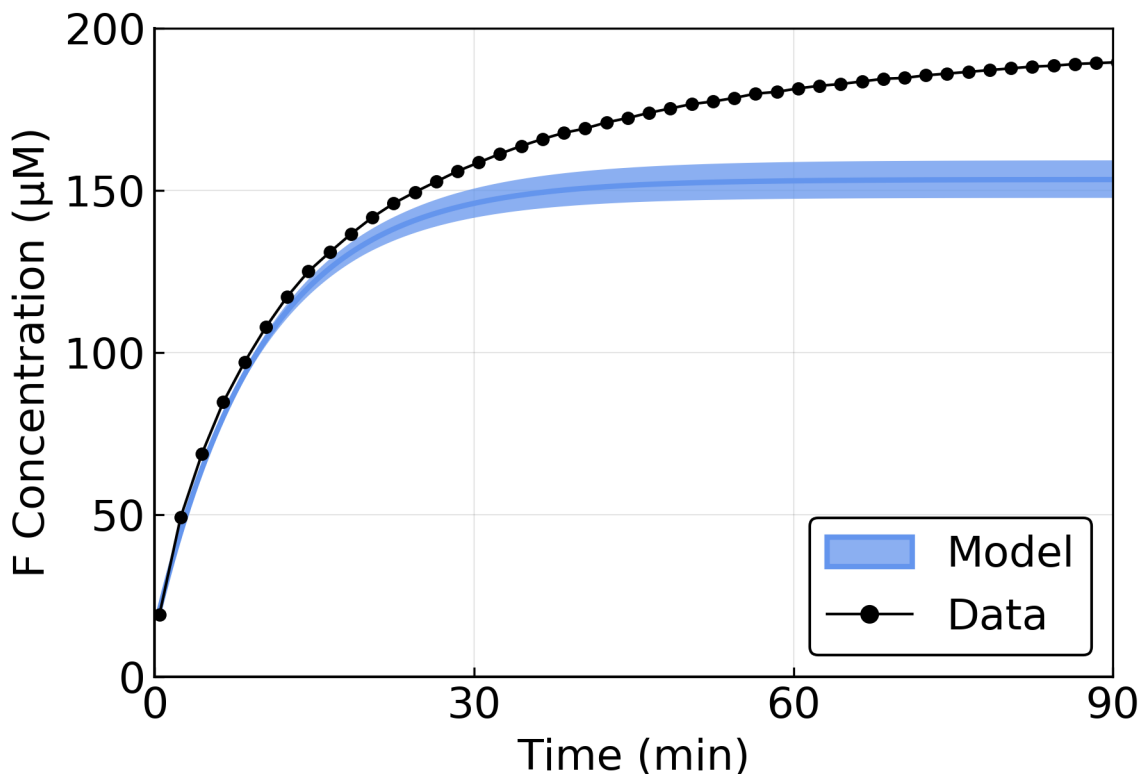
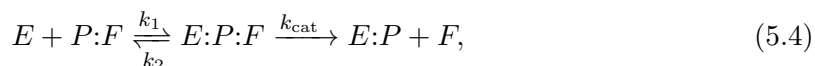


**Figure 5.1: Standard model for FXa inactivation by AT is a poor match to data.** The fitted model from Chapter 2, with product inhibition incorporated, and literature values for the inactivation rate, do not qualitatively match the data. The model predicts nearly complete inactivation by 30 minutes, while the experimental data continues to show active enzyme throughout.

AT but not become inactivated by it. This Alternative scheme is described as follows:



### One-Step Inactivation

Using the kinetic scheme given in Equation (5.1) and assuming Mass Action kinetics, a mathematical model for the cleavage of substrate in the presence of AT was developed, which directly incorporates uncertainty from pipetting error. We assume the same kinetic rates for the cleavage of substrate and fraction of hydrolyzed substrate estimated in Chapter 2 since the estimates were made using the same experimental setup and reagents; however, pipetting error would be unique for each replicate and must be individually determined. Uncertainty from pipetting error would be implemented by allowing the initial concentrations

of the CS, enzyme, and AT to vary as distributions. The ODE system from the One-Step Inactivation Model (Equations (5.1)-(5.3)) with these uncertainties incorporated becomes our Null Model:

$$\frac{d[E]}{dt} = -\mathbf{k}_1[E][P:F] + k_2[E:P:F] - \mathbf{k}_1[E][P] + \alpha k_2[E:P] - K_I[E][AT], \quad (5.7)$$

$$\frac{d[P:F]}{dt} = -\mathbf{k}_1[E][P:F] + k_2[E:P:F], \quad (5.8)$$

$$\frac{d[E:P:F]}{dt} = \mathbf{k}_1[E][P:F] - k_2[E:P:F] - k_{cat}[E:P:F], \quad (5.9)$$

$$\frac{d[E:P]}{dt} = k_{cat}[E:P:F] + \mathbf{k}_1[E][P] - \alpha k_2[E:P], \quad (5.10)$$

$$\frac{d[F]}{dt} = k_{cat}[E:P:F], \quad (5.11)$$

$$\frac{d[P]}{dt} = -\mathbf{k}_1[E][P] + \alpha k_2[E:P], \quad (5.12)$$

$$\frac{d[AT]}{dt} = -\mathbf{K}_I[E][AT], \quad (5.13)$$

$$\frac{d[E:AT]}{dt} = \mathbf{K}_I[E][AT]. \quad (5.14)$$

with initial conditions

$$[E]_0 = \mathbf{U}_p(E_0), \quad (5.15)$$

$$[P:F]_0 = (1 - U_h)\mathbf{U}_p(P:F_0), \quad (5.16)$$

$$[E:P:F]_0 = 0, \quad (5.17)$$

$$[E:P]_0 = 0, \quad (5.18)$$

$$[P]_0 = U_h\mathbf{U}_p(P:F_0), \quad (5.19)$$

$$[F]_0 = U_h\mathbf{U}_p(P:F_0), \quad (5.20)$$

$$[AT]_0 = \mathbf{U}_p(AT_0), \quad (5.21)$$

$$[E:AT]_0 = 0, \quad (5.22)$$

where bolded symbols represent distributions rather than single values. Specifically,  $\mathbf{k}_1$  is the rate of enzyme binding to substrate,  $\mathbf{K}_I$  is the kinetic parameter governing the inactivation of the enzyme, and  $\mathbf{U}_p(\cdot)$  are distributions for the initial enzyme, CS, and AT concentration due to pipetting error.  $U_h$  is the fraction of substrate hydrolyzed at the start of the experiment.

## Two-Step Inactivation

The Two-Step Inactivation Model consists of the ODEs that result from applying the law of mass action to the Two-Step scheme (Equations (5.4-5.6)), and incorporating uncertainty in the same way as above. The resulting model is similar to the above (Equations (5.7-5.14)),

with 3 equations changed (Equations (5.7), (5.13), and (5.14)) and one added:

$$\frac{d[E]}{dt} = -\mathbf{k}_1^I[E][P:F] + k_2[E:P:F] - \mathbf{k}_1[E][P] + \alpha k_2[E:P] - \mathbf{k}_1^I[E][AT] + \mathbf{k}_2^I[E:AT], \quad (5.23)$$

$$\frac{d[AT]}{dt} = -\mathbf{k}_1^I[E][AT] + \mathbf{k}_2^I[E:AT], \quad (5.24)$$

$$\frac{d[E:AT]}{dt} = \mathbf{k}_1^I[E][AT] - \mathbf{k}_2^I[E:AT] - \mathbf{K}_I[E:AT], \quad (5.25)$$

$$\frac{d[E:AT_I]}{dt} = \mathbf{K}_I[E:AT], \quad (5.26)$$

with the corresponding initial conditions

$$[E]_0 = \mathbf{U}_P(E_0), \quad (5.27)$$

$$[P:F]_0 = (1 - U_h)\mathbf{U}_P(P:F_0), \quad (5.28)$$

$$[E:P:F]_0 = 0, \quad (5.29)$$

$$[E:P]_0 = 0, \quad (5.30)$$

$$[P]_0 = U_h\mathbf{U}_P(P:F_0), \quad (5.31)$$

$$[F]_0 = U_h\mathbf{U}_P(P:F_0), \quad (5.32)$$

$$[AT]_0 = \mathbf{U}_P(AT_0), \quad (5.33)$$

$$[E:AT]_0 = 0, \quad (5.34)$$

$$[E:AT_I]_0 = 0, \quad (5.35)$$

where again bolded symbols represent distributions. This alternative model has all the same parameter distributions with the addition of  $\mathbf{k}_1^I$  and  $\mathbf{k}_2^I$ , which together controls the respective binding and unbinding of enzyme with AT.

## Preliminary Results

A Markov-Chain Monte Carlo process was used to estimate the parameters in the above models from experimental data (see Chapter 2 for details on the general methodology). Because reported values for the kinetic parameters we want to estimate vary widely in the literature, non-informative priors were used extensively (see Table 5.1). The posterior distributions for both the Null and Alternative model showed strong convergence using the Geweke test as previously described. The fit for the two trained models is shown in Figure 5.2, with samples taken from the full joint posterior distributions. The Null model is unable to accurately capture the qualitative shape of the data, even after extended model fitting. This is believed to be due to the fast rate of Xa inactivation, which is not evidenced in the data. However, the Alternative model, which allows for more free Xa to be available at later times, does obtain a strong match to data. The model selection tests presented in Chapter 2, Akaike's Information Criterion (AIC) and the Bayesian Information Criterion (BIC), show strong statistical support for the Alternative model, with  $AIC_{Null} - AIC_{Alt} = 432.9$  and  $BIC_{Null} - BIC_{Alt} = 422.5$ .

**Table 5.1: Model parameters and their distributions.** Prior and Posterior estimates of unknown parameters for both the One and Two-Step Inactivation models. \*Because there were several individual initial concentrations measured, we only report here the overall average pipetting error for all cases. †Estimated previously in Chapter 2.

| Parameter          | Prior                                        | Null<br>(mean±std)    | Alternative<br>(mean±std) |
|--------------------|----------------------------------------------|-----------------------|---------------------------|
| $k_{\text{cat}}$ † | Fixed at $78.7s^{-1}$                        | N/A                   | N/A                       |
| $k_1$              | $N(0.01, 0.005)nM^{-1}s^{-1}$                | $1.30e-3 \pm 1.77e-5$ | $6.92e-3 \pm 0.15$        |
| $k_2$              | Fixed at $(110.4e3 \cdot k_1 - 78.7) s^{-1}$ | N/A                   | N/A                       |
| $K_I$              | $N(2.0, 1.0)s^{-1}$                          | N/A                   | $1.06e-3 \pm 1.17e-4$     |
| $K_M^I$            | $N(1.35e6, 6.75e5)nM$                        | N/A                   | $5.67e2 \pm 57.58$        |
| $k_1^I$            | $N(1.0e-5, 5.0e-6)nM^{-1}s^{-1}$             | $2.13e-6 \pm 2.55e-8$ | $3.72e-6 \pm 2.92e-7$     |
| $k_2^I$            | Fixed at $(K_M^I \cdot k_1^I - K_I)s^{-1}$   | N/A                   | N/A                       |
| $U_h$ †            | Fixed at 5.1%                                | N/A                   | N/A                       |
| $\alpha$ †         | Fixed at 2.54                                | N/A                   | N/A                       |
| $Up(P:F_0)^*$      | $N(0\%, 1\%)$                                | $2.0\% \pm 0.9\%$     | $3.2e-3\% \pm 0.9\%$      |
| $Up(E_0)^*$        | $N(0.0\%, 1\%)$                              | $0.2\% \pm 1.0\%$     | $-6.1e-2 \pm 1.0\%$       |
| $Up(AT_0)^*$       | $N(0.0\%, 1\%)$                              | $1.2e-2 \pm 1.0\%$    | $-1.3e-3 \pm 1.0\%$       |

### Ongoing Work

Although we have compelling preliminary support for the two-step model, an independent, validating experiment needs to be designed and performed, where both models can be used to predict the results without additional parameter tuning. The outcome of this experiment would hopefully give strong evidence to the importance of the two-step inactivation.

## 5.3 Global Sensitivity of Coagulopathies

Chapters 3 and 4 demonstrated how GSA methods aid in identifying modifiers to hemophilia A. One natural extension of this work is to apply the same methods to other coagulopathies, such as hemophilia B and C. Each of these conditions is diagnosed by large deficiency in a specific clotting protein (see the Introduction 1.2.1 for more information) with hemophilia A being deficient in FVIII, hemophilia B in FIX, and hemophilia C in FXI. As shown in Chapter 4, the output of GSA allows for increased exploration of a model and the potential discovery of novel parameter combinations capable of rescuing the bleeding response.

In order to extend that analysis to other hemophilia cases with additional coagulation parameters being varied, such as the platelet characteristics from Chapter 3, the *normal ranges* of these parameters must first be determined. While the plasma levels of zymogens are known to vary by approximately 50%, no such information is available for platelet binding site numbers. To find these normal ranges, we first define a *normal thrombotic response* as one that obtains 1 nM of total thrombin between 3 and 10 minutes [4]. Next, the plasma levels (PL), platelet characteristics (PC), and fixed concentration of Tissue

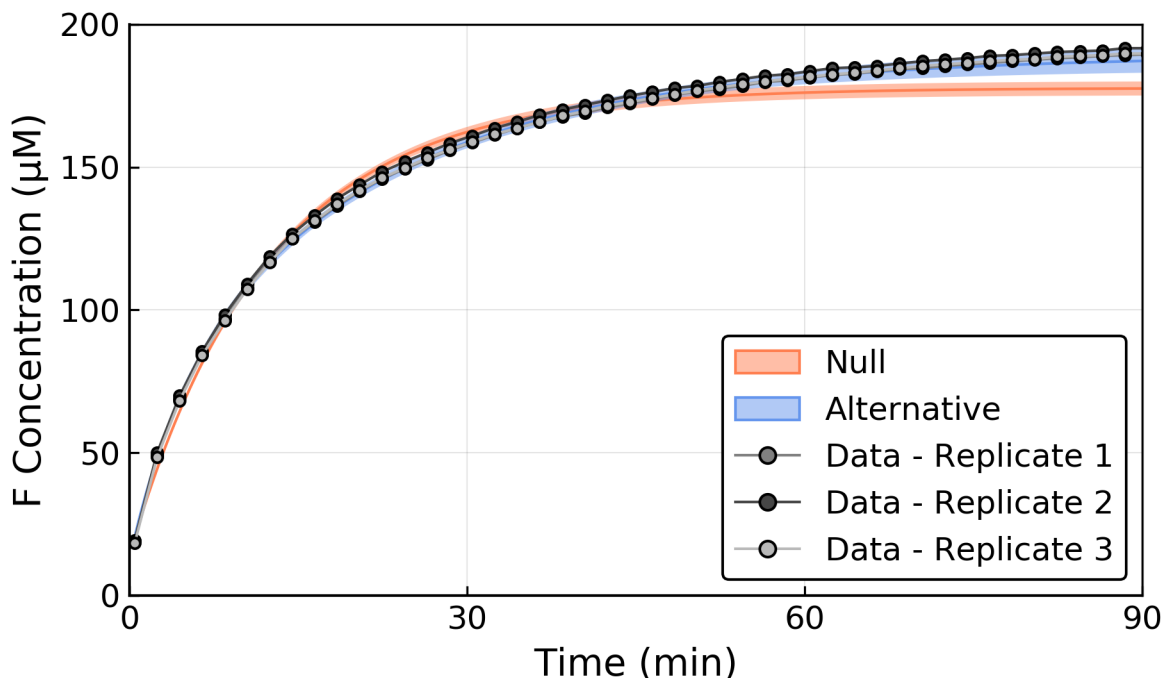


**Figure 5.2: Preliminary MCMC fits to data for the Null and Alternative AT inactivation models.** The Null (orange) and Alternative (Blue) models were fit to the data (Circles) using an MCMC procedure. The posterior distributions were sampled 1,000 times and used to construct 95% credibility intervals for the concentration of product at a fixed time (shaded regions).

Factor (TF) were simultaneously varied in the KFHL model under normal coagulation settings, with the plasma levels uniformly varying by  $\pm 50\%$ , the platelet characteristics between varying between  $\pm 1\%$  -  $\pm 65\%$ , and TF fixed between 1-30 fmol/cm<sup>2</sup>. For each combination of PC percentage and TF level, 5000 simultaneous samples were drawn and the number of normal thrombotic responses recorded. The sample sets were bootstrapped to obtain replicate data sets to construct confidence intervals. Figure 5.3 shows for each PC variation percentage the largest (blue) and smallest (red) TF level that obtained 99.5% normal responses (multiple dots show results from bootstrapping). By selecting a TF range of [5, 20]fmol/cm<sup>2</sup> and a PC variation percentage of  $\pm 20\%$ , we observe at least 99.5% normal responses from the simulations.

Preliminary work has already examined the effect of varying the PLs and PCs for models of normal and the three hemophilic blood cases, which only differ from normal by a single initial protein level. The variance in the time to 1 nM of total thrombin, a standard metric used in clotting assays (see Chapter 3 and 4 for more information), was analyzed using Sobol indices (see Figure 5.4), which apportions fractions of variance to individually varied parameters. The results show that the hemophilic cases obtain 1 nM of thrombin in vastly different ways. More investigation into these differences needs to be carried out, as well as looking at other clotting metrics, such as the thrombin concentration at a particular time.

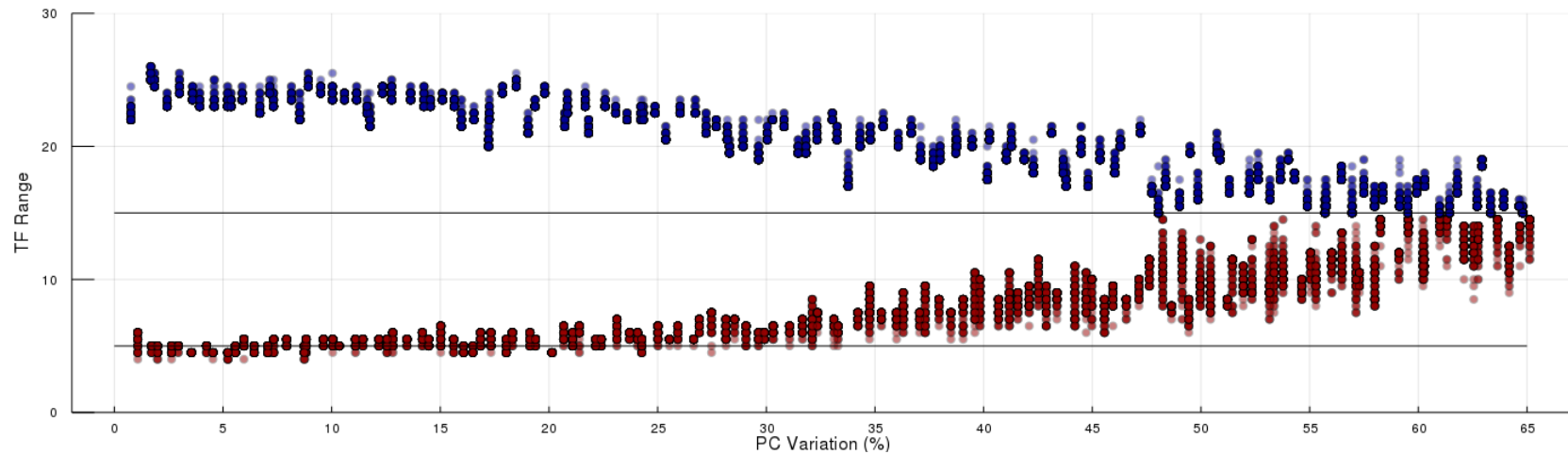


**Figure 5.3: Preliminary study varying Plasma Levels, Platelet Characteristics, and TF simultaneously.** Plasma levels (PL) of zymogens were varied  $\pm 50\%$ , platelet characteristics (PC) were varied at different percentage levels (x-axis), and TF varied between 1 and 30fmol/cm<sup>2</sup>(N=5,000 for each PC var % and fixed TF value). The minimum (red) and maximum (blue) TF levels that allowed 99.5% of samples to have a time to 1 nM of total thrombin between 3 and 10 minutes, *i.e.*, the metric for a normal response.

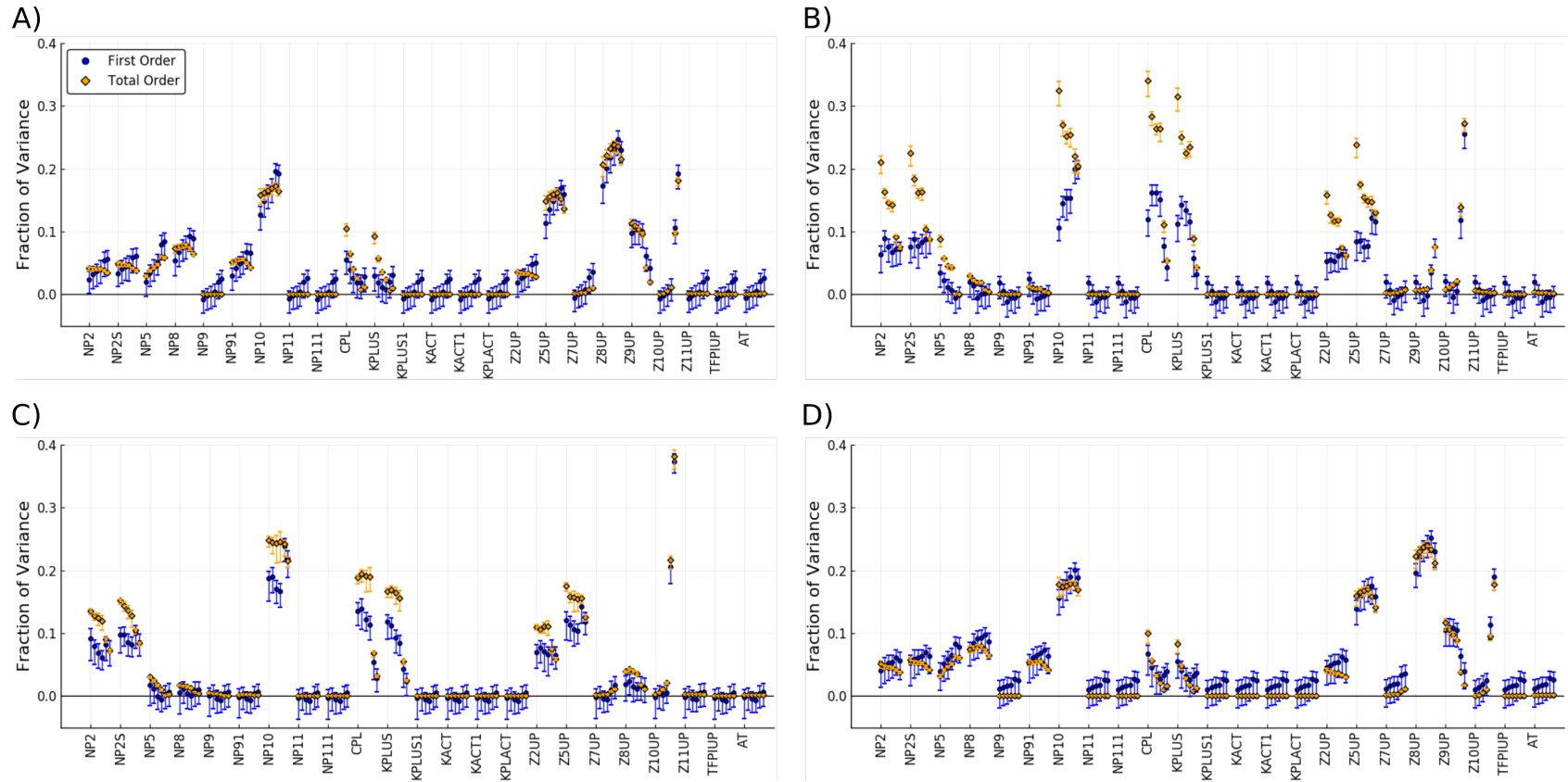


**Figure 5.4: Preliminary Sobol index results for the time to 1 nM of thrombin for hemophilic models.** The variance for the time to 1 nM of total thrombin was decomposed using Sobol indices where plasma protein levels and platelet characteristics were allowed to vary within a hypothetical normal range for normal (A), hemophilia A (B), hemophilia B (C), and hemophilia C (D) type blood.

## Bibliography

- [1] Nicholas F Britton. Essential mathematical biology. Springer Science & Business Media, 2012.
- [2] Leah Edelstein-Keshet. Mathematical Models in Biology. Random House, New York, 1988.
- [3] Gerda De Vries, Thomas Hillen, Mark Lewis, Johannes Müller, and Birgitt Schönfisch. A course in mathematical biology: quantitative modeling with mathematical and computational methods. SIAM, 2006.
- [4] Christopher M Danforth, Thomas Orfeo, Stephen J Everse, Kenneth G Mann, and Kathleen E Brummel-Ziedins. Defining the boundaries of normal thrombin generation: investigations into hemostasis. PloS One, 7(2):e30385, 2012.